Physics Reports 542 (2014) 1–132

Contents lists available at ScienceDirect

Physics Reports

journal homepage: www.elsevier.com/locate/physrep

# Optical wave turbulence: Towards a unified nonequilibrium thermodynamic formulation of statistical nonlinear optics

A. Picozzi [a,*], J. Garnier [b], T. Hansson [c], P. Suret [d], S. Randoux [d], G. Millot [a], D.N. Christodoulides [e]

[a] Laboratoire Interdisciplinaire Carnot de Bourgogne, Université de Bourgogne, CNRS-UMR 5027, Dijon, France
[b] Laboratoire de Probabilités et Modèles Aléatoires & Laboratoire Jacques-Louis Lions, Université Paris VII, 75205 Paris Cedex 13, France
[c] Department of Information Engineering, Università di Brescia, Brescia 25123, Italy
[d] Laboratoire de Physique des Lasers, Atomes et Molécules, CNRS, Université de Lille, France
[e] College of Optics/CREOL, University of Central Florida, Orlando, FL 32816, USA

ARTICLE INFO

*Article history:*
Accepted 26 February 2014
Available online 12 March 2014
editor: G. I. Stegeman

*Keywords:*
Optical wave turbulence
Incoherent solitons
Thermalization and condensation
NLS equation

ABSTRACT

The nonlinear propagation of coherent optical fields has been extensively explored in the framework of nonlinear optics, while the linear propagation of incoherent fields has been widely studied in the framework of statistical optics. However, these two fundamental fields of optics have been mostly developed independently of each other, so that a satisfactory understanding of statistical nonlinear optics is still lacking. This article is aimed at reviewing a unified theoretical formulation of statistical nonlinear optics on the basis of the wave turbulence theory, which provides a nonequilibrium thermodynamic description of the system of incoherent nonlinear waves. We consider the nonlinear Schrödinger equation as a representative model accounting either for a nonlocal or a noninstantaneous nonlinearity, as well as higher-order dispersion effects. Depending on the amount of nonlocal (noninstantaneous) nonlinear interaction and the amount of inhomogeneous (nonstationary) statistics of the incoherent wave, different types of kinetic equations are derived and discussed.

In the spatial domain, when the incoherent wave exhibits inhomogeneous statistical fluctuations, different forms of the (Hamiltonian) Vlasov equation are obtained depending on the amount of nonlocality. This Vlasov approach describes the processes of incoherent modulational instability and localized incoherent soliton structures.

In the temporal domain, the causality property inherent to the response function leads to a kinetic formulation analogous to the weak Langmuir turbulence equation, which describes nonlocalized spectral incoherent solitons. In the presence of a highly noninstantaneous response, this formulation reduces to a family of singular integro-differential kinetic equations (e.g., Benjamin–Ono equation), which describe incoherent dispersive shock waves. Conversely, a non-stationary statistics leads to a (non-Hamiltonian) long-range Vlasov formulation, whose self-consistent potential is constrained by the causality condition of the response function.

The spatio-temporal domain will be considered in the limit of an inertial nonlinearity. We review different theories developed to describe bright and dark spatial incoherent solitons experimentally observed in slowly responding nonlinear media: The coherent density method, the mutual coherence function approach, the modal theory and the Wigner–Moyal formulation.

* Corresponding author. Tel.: +33 380395979.
*E-mail address:* Antonio.Picozzi@u-bourgogne.fr (A. Picozzi).

http://dx.doi.org/10.1016/j.physrep.2014.03.002

When the incoherent wave exhibits homogeneous fluctuations, the relevant kinetic equation is the wave turbulence (Hasselmann) equation. It describes wave condensation and the underlying irreversible process of thermalization to thermodynamic equilibrium, as well as genuine nonequilibrium turbulent regimes. In this way different remarkable phenomena associated to wave thermalization are reviewed, e.g., wave condensation or supercontinuum generation in photonic crystal fibers, as well as different mechanisms of breakdown of thermalization. Finally, recent developments aimed at providing a wave turbulence formulation of Raman fiber lasers and passive optical cavities are reviewed in relation with condensation-like phenomena.



**Contents**

## 1. Introduction

### 1.1. From incoherent solitons to wave turbulence

The coherence properties of partially incoherent optical waves propagating in nonlinear media have been studied since the advent of nonlinear optics in the 1960s, because of the natural poor degree of coherence of laser sources available at that time (see, e.g., [1,2]). However, it is only recently that the dynamics of incoherent nonlinear optical waves received a renewed interest. The main motive for this renewal of interest is essentially due to the first experimental demonstration of incoherent solitons in photorefractive crystals [3,4]. The formation of an incoherent soliton results from the *spatial self-trapping* of incoherent light that propagates in a highly noninstantaneous response nonlinear medium [5,6]. This effect is possible because of the noninstantaneous photorefractive nonlinearity that averages the field fluctuations provided that its response time, $\tau_R$, is much longer than the correlation time $t_c$ that characterizes the incoherent beam fluctuations, i.e., $t_c \ll \tau_R$. The remarkable simplicity of experiments realized in photorefractive crystals has led to a fruitful investigation of the dynamics of incoherent nonlinear waves. Several theoretical approaches have been also developed to describe these experiments [7–10]. Subsequently, these different theoretical methods have been shown to be formally equivalent one to each other [11,12].

In this way, the field of incoherent optical solitons has become a blooming area of research, as illustrated by several important achievements, e.g., the existence of incoherent dark solitons [13,14], the modulational instability of incoherent waves [15–18], incoherent solitons in periodic lattices [19,20], in resonant interactions [21,22], in liquid crystals [23,24], in nonlocal nonlinear media [25–27], in spin waves [28], or spectral incoherent solitons in optical fibers [29,30]. Nowadays, statistical nonlinear optics constitutes a growing field of research covering various topics of modern optics, e.g., supercontinuum generation [31], filamentation [32], random lasers [33], or extreme rogue waves events [34–36].

From a broader perspective, statistical nonlinear optics is fundamentally related to fully developed turbulence [37,38], a subject which still constitutes one of the most challenging problems of theoretical physics [39,40]. In its broad sense, the kinetic wave theory provides a nonequilibrium thermodynamic description of developed turbulence. We schematically report in Fig. 1 a qualitative and intuitive physical insight into the analogy which underlies the kinetic wave approach and the kinetic theory relevant for a gas system. The wave turbulence theory occupies a rather special place on the road-map of modern science, at the interface between applied mathematics, fluid dynamics, statistical physics and engineering. It has potential applications and implications in a diverse range of subjects including oceanography, plasma physics and condensed matter physics. This review article is aimed at showing that the kinetic wave theory appears as the appropriate theoretical framework to formulate statistical nonlinear optics.

### 1.2. Panoramic overview

In the following we give a panoramic overview of the subjects covered by the review article. Note that these topics have been usually discussed separately in the literature within different contexts. As schematically depicted through Figs. 1–3, the review article provides a generalized description and classification of these topics on the basis of a unified kinetic wave formulation.

#### 1.2.1. Wave turbulence formulation: Thermalization and condensation

Consider the nonlinear propagation of a partially coherent optical wave characterized by fluctuations that are statistically homogeneous in space.[1] In complete analogy with a system of classical particles, the incoherent optical field evolves, owing to nonlinearity, towards a thermodynamic equilibrium state, as schematically illustrated in Fig. 1(a)–(b). A detailed theoretical description of the process of dynamical thermalization constitutes a difficult problem. However, a considerable simplification occurs when wave propagation is essentially dominated by linear dispersive effects, so that a weakly nonlinear description of the field becomes possible [37,39,40]. The weak- (or wave-)turbulence (WT) theory has been the subject of lot of investigations in the context of plasma physics [42,43], in which it is often referred to the so-called "random phase-approximation" approach [37,42–47]. This approach may be considered as a convenient way of interpreting the results of the more rigorous technique based on a multi-scale expansion of the cumulants of the nonlinear field, as originally formulated in

[1] Note that caution should be exercised when separating the description of statistically homogeneous and inhomogeneous random waves, since a homogeneous statistical wave can become inhomogeneous as a result of the incoherent MI (as discussed below in Sections 2–4), or the instability of the Zakharov–Kolmogorov spectrum as recently discussed in Ref. [41].

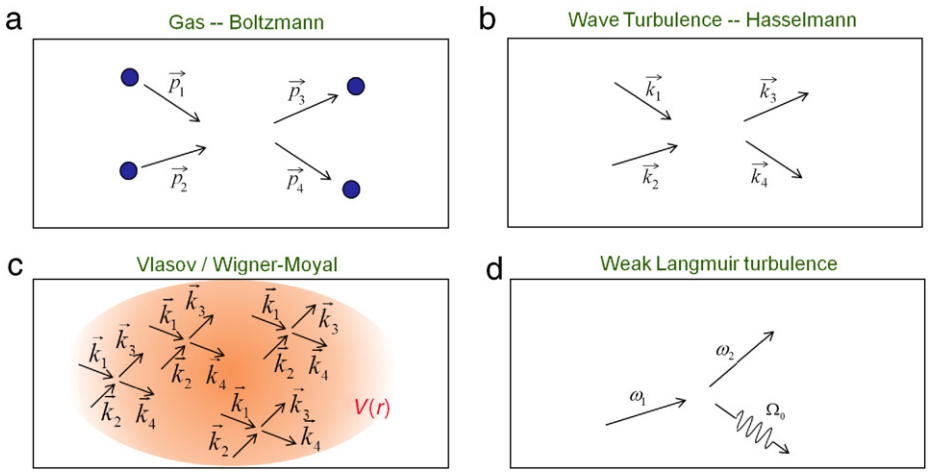


**Fig. 1.** Analogy between a system of classical particles and the propagation of an incoherent optical wave in a cubic nonlinear medium. (a) As described by the kinetic gas theory (Boltzmann kinetic equation), collisions between particles are responsible for an irreversible evolution of the gas towards thermodynamic equilibrium. (b) In complete analogy, the (Hasselmann) WT kinetic equation and the underlying four-wave mixing describe an irreversible evolution of the incoherent optical wave towards the thermodynamic Rayleigh–Jeans equilibrium state. (c) When the incoherent optical wave exhibits an inhomogeneous statistics, the four-wave interaction no longer takes place locally, i.e., the quasi-particles feel the presence of an effective self-consistent potential, $V(r)$, which prevents them from relaxing to thermal equilibrium. The dynamics of the incoherent optical wave turns out to be described by a Vlasov-like kinetic equation. (d) In the presence of a noninstantaneous nonlinear interaction, the causality condition inherent to the response function changes the physical picture: The nonlinear interaction involves a material excitation (e.g., molecular vibration in the example of Raman scattering). The dynamics of the incoherent optical wave turns out to be described by a kinetic equation analogous to the weak Langmuir turbulence equation. Note however that a highly noninstantaneous nonlinear response is no longer described by the weak Langmuir turbulence equation, but instead by the 'long-range' Vlasov-like equation (see Fig. 3).

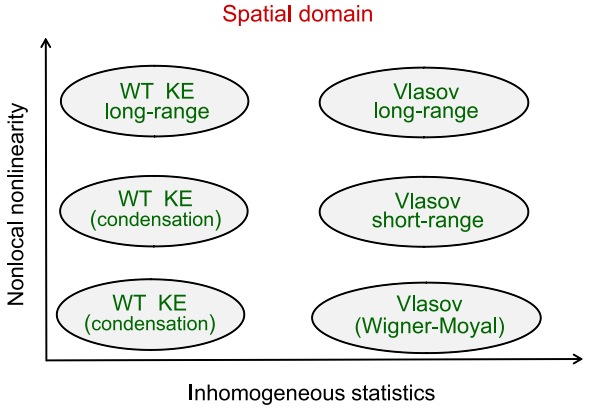


**Fig. 2.** Schematic illustration of the validity of the fundamental kinetic equations in the framework of a spatially nonlocal nonlinear response—the vertical arrow denotes the amount of nonlocality of the nonlinear interaction, while the horizontal arrow represents the amount of inhomogeneous statistics of the incoherent wave. When the incoherent wave is characterized by fluctuations that are statistically homogeneous in space, the relevant kinetic description is provided by the wave turbulence kinetic equation ('WT KE'), which describes in particular the processes of optical wave thermalization or condensation (see Section 5.1). When the incoherent wave exhibits an inhomogeneous statistics, the relevant kinetic description is provided by different variants of the Vlasov equation, whose self-consistent potential depends on the amount of nonlocality in the system (see Section 2). The Vlasov equation, or more generally the Wigner–Moyal formalism (see Section 4), describe in particular the phenomena of incoherent modulational instability and the formation of incoherent soliton states.

Refs. [48–50]. This theory has been reviewed in Ref. [51], and studied in more details through the analysis of the probability distribution function of the random field in Refs. [52–54,40]. In a loose sense, the so-called 'random phase approximation' may be considered as justified when phase information becomes irrelevant to the wave interaction due to the strong tendency of the waves to decohere. The random phases can thus be averaged out to obtain a weak turbulence description of the incoherent wave interaction, which is formally based on irreversible kinetic equations [37]. It results that, in spite of the formal reversibility of the equation governing wave propagation, the kinetic equation describes an irreversible evolution of the field to thermodynamic equilibrium. This equilibrium state refers to the fundamental Rayleigh–Jeans spectrum, whose tails are characterized by an equipartition of energy among the Fourier modes. The mathematical statement of such irreversible process relies on the $H$-theorem of entropy growth, whose origin is analogous to the Boltzmann's $H$-theorem relevant for gas kinetics. Note that the terminology 'wave turbulence' is often employed in the literature to denote the study

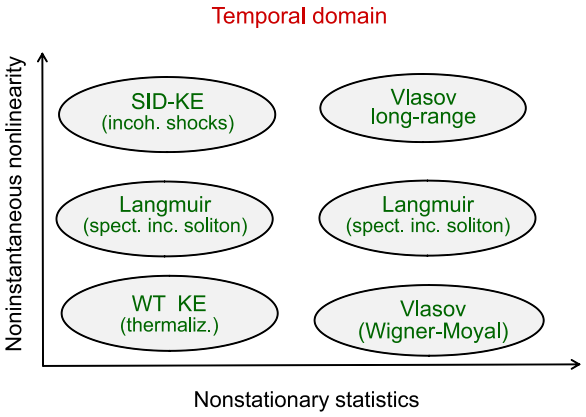


**Fig. 3.** Schematic illustration of the validity of the fundamental kinetic equations in the framework of a temporally noninstantaneous nonlinear response—the vertical arrow denotes the amount of noninstantaneous response of the nonlinearity, while the horizontal arrow represents the amount of non-stationary statistics of the incoherent wave. The diagram for the temporal domain reported here is similar to that reported in the spatial domain in Fig. 2. The essential difference between the spatial and the temporal domain relies on the fact that in the temporal domain the response function is constrained by the causality condition. It turns out that when the finite response time of the nonlinearity cannot be neglected, the relevant kinetic description is provided by an equation analogous to the weak Langmuir turbulence equation, irrespective of the nature of the fluctuations that may be stationary or non-stationary (see Section 3.2). This equation has been shown to describe non-localized spectral incoherent solitons. In the presence of a highly noninstantaneous nonlinear response and a stationary statistics of the incoherent wave, the weak Langmuir turbulence reduces to singular integro-differential kinetic equations ('SID-KE'), e.g., Benjamin–Ono equation, which describe incoherent dispersive shock waves. Conversely, when the wave exhibits a non-stationary statistics still in the presence of a highly noninstantaneous response, the dynamics is ruled by a 'temporal long-range' Vlasov equation, whose self-consistent potential is constrained by the causality condition of the noninstantaneous response function, which breaks the Hamiltonian structure of the Vlasov equation (see Section 3.3). The WT kinetic equation ('WT KE') turns out to be relevant for an instantaneous nonlinear response and a statistically stationary incoherent wave, as will be discussed in Sections 5.3–5.4, in particular in the framework of supercontinuum generation.

of wave systems governed by this type of irreversible kinetic equations, whose structure is analogous to the Boltzmann kinetic formulation (see, e.g., [37,47,40]). However, in many cases in this review the terminology 'wave turbulence' will be employed in a broader sense, which also includes different forms of nonequilibrium kinetic formalisms, such as the Vlasov or the weak Langmuir turbulence descriptions of a wave system (see Fig. 1). We remark that besides this *nonequilibrium* kinetic approach, the equilibrium properties of a random nonlinear wave may be studied on the basis of *equilibrium* statistical mechanics by computing appropriate partition functions [55–64]. In this way, the statistical properties of incoherent fields in random lasers have been analyzed by applying methods inherited from spin-glass theory [65,66]. It should also be noted that a statistical mechanics of a gas of soliton particles has been developed in the framework of integrable (NLS) equations [67,68].

In this article we will review different processes of optical wave thermalization on the basis of the WT theory, as well as some mechanisms responsible for its inhibition. In particular, we will see how the phenomenon of supercontinuum generation can be interpreted, under certain conditions, as a consequence of the natural thermalization of the optical field towards the thermodynamic equilibrium state. Furthermore, wave thermalization can be characterized by a self-organization process, in the sense that it is thermodynamically advantageous for the system to generate a large-scale coherent structure in order to reach the most disordered equilibrium state. A remarkable example of this counterintuitive phenomenon is provided by wave condensation [69–73], whose thermodynamic equilibrium properties are analogous to those of quantum Bose–Einstein condensation. Classical wave condensation can be interpreted as a redistribution of energy among different modes, in which the (kinetic) energy is transferred to small scales fluctuations, while an inverse process increases the power (i.e., number of 'particles') into the lowest allowed mode, thus leading to the emergence of a large scale coherent structure.

We note in this respect that the phenomenon of condensation has been recently extended to optical cavities in different circumstances [74–81], which raises important questions, such as e.g., the relation between laser operation and the phenomenon of Bose–Einstein condensation (see Section 7.1) [82]. From a different perspective, when a wave system is driven away from equilibrium by an external source, it no longer relaxes towards the Rayleigh–Jeans equilibrium distribution. A typical physical example of forced system can be the excitation of hydrodynamic surface waves by the wind. This corresponds to the generic problem of developed turbulence. In general, it refers to a system in which the frequency-scales of forcing and damping differ significantly. The nonlinear interaction leads to an energy redistribution among the frequencies (modes). A fundamental problem is to find the stationary spectrum of the system, i.e., the law of energy distribution over the different scales. The WT theory provides an answer to this vast issue under the assumption that the nonlinear interaction is weak—the so-called Kolmogorov–Zakharov spectra of turbulence [37]. An experiment aimed at observing these nonequilibrium stationary turbulent states in the context of optics has been reported in Ref. [83] (see Section 5.5, or Ref. [84] for a complete review). Beyond optics, we refer the interested reader to different comprehensive reviews concerning this vast area of research [37,51,47,39,40].

*1.2.2. Vlasov and Wigner–Moyal formulations: Incoherent solitons*

When the nonlinear material is characterized by a nonlocal or a highly-noninstantaneous response, the dynamics of the incoherent wave turns out to be essentially governed by an effective nonlinear potential $V(r)$. This potential is *self-consistent* in the sense that it depends itself on the averaged intensity distribution of the random field, as schematically illustrated in Fig. 1(c). Actually, the mechanism underlying the formation of an incoherent soliton state finds its origin in the existence of such self-consistent potential, which is responsible for a spatial self-trapping of the incoherent optical beam. From this point of view, the vary nature of incoherent optical solitons is analogous to the random phase solitons predicted in plasma physics a long time ago in the framework of the Vlasov equation [85–87]. This analogy with nonlinear plasma waves has been also exploited in optics in different circumstances [88–92], in particular in the framework of the Wigner–Moyal formalism [10,93,12,94,95], or to interpret the existence of a threshold in the incoherent modulational instability as a consequence of the phenomenon of Landau damping [96,10,17,97].

Incoherent spatial solitons can be also supported by a nonlocal spatial nonlinearity, instead of the traditional noninstantaneous nonlinearity inherent to the photorefractive experiments discussed above in Section 1.1. A nonlocal wave interaction means that the response of the nonlinearity at a particular point is not determined solely by the wave intensity at that point, but also depends on the wave intensity in the neighborhood of this point. Nonlocality thus constitutes a generic property of a large number of nonlinear wave systems [98–105], and the dynamics of nonlocal nonlinear waves has been widely investigated in this last decade [106–110]. In particular, in the highly nonlocal limit, i.e., in the limit where the range of the nonlocal response is much larger than the size of the beam, the propagation equation reduces to a linear and local equation with an effective guiding potential given by the nonlocal response function. The optical beam can thus be guided by the nonlocal response of the material, a process originally termed 'accessible soliton' [111,110,100,101]. In this highly nonlocal limit, it has been shown both theoretically and experimentally that a speckled beam can be guided and trapped by the effective waveguide induced by the nonlocal response [112,26].

More recently, the long-term evolution of a modulationally unstable homogeneous wave has been studied in the presence of a nonlocal response [27]. Contrarily to the expected soliton turbulence process where a coherent soliton is eventually generated in the midst of thermalized small-scale fluctuations [113,114,58,60,61], a highly nonlocal response is responsible for an *incoherent soliton turbulence* process [27]. It is characterized by the spontaneous formation of an incoherent soliton structure starting from an initially homogeneous plane-wave. A WT approach of the problem revealed that this type of incoherent solitons can be described in detail in the framework of a long-range Vlasov equation, which is shown to provide an accurate statistical description of the nonlocal random wave even in the *highly nonlinear regime* of interaction. We note that this Vlasov equation differs from the traditional Vlasov equation considered for the study of incoherent modulational instability and incoherent solitons in plasmas [115,86,87], hydrodynamics [116] and optics [10,91,92,90]. The structure of this Vlasov equation is in fact analogous to that recently used to describe systems of particles with long-range interactions [117]. For this reason we will term this equation 'long-range Vlasov' equation. It is important to underline that the long-range nature of a highly nonlocal nonlinear response prevents the wave system from reaching thermal equilibrium [27]. This fact can be interpreted intuitively in analogy with gravitational long-range systems and the Vlasov-like description of galaxies in the Universe [117].

*1.2.3. Weak Langmuir turbulence formulation: Spectral incoherent solitons and incoherent shocks*

When the incoherent wave propagates in a nonlinear medium whose non-instantaneous response time cannot be neglected (e.g., Raman effect in optical fibers), the dynamics turns out to be strongly affected by the causality property inherent to the nonlinear response function (see Fig. 1). The kinetic wave theory reveals in this case that the appropriate description is provided by a formalism analogous to that used to describe weak Langmuir turbulence in plasmas [29,118]. A major prediction of the theory is the existence of spectral incoherent solitons [29,119,30]. This incoherent soliton is of a fundamental different nature than the incoherent solitons discussed here above. In particular, it does not exhibit a confinement in the spatiotemporal domain, but exclusively in the frequency domain. For this reason this incoherent structure has been termed 'spectral incoherent soliton'. Indeed, because the optical field exhibits a stationary statistics, the soliton behavior only manifests in the spectral domain. Then contrarily to the expected thermalization process, the incoherent wave self-organizes into these incoherent soliton structures, which can thus be regarded as nonequilibrium and nonstationary stable states of the incoherent field.

As discussed here above in Section 1.2.2, the existence of a highly nonlocal response changes the dynamics of spatially incoherent nonlinear waves in a profound way. A natural question is to see how a highly noninstantaneous nonlinear response can change the dynamics of temporally incoherent waves. In this temporal long-range regime, the spectral dynamics of the field can exhibit incoherent shock waves [120]. They manifest themselves as an unstable singular behavior of the spectrum of incoherent waves, i.e., 'spectral wave-breaking'. Note that shock waves play an important role in many different branches of physics [121]. However, it should be underlined that, at variance with conventional coherent shock waves, which require the strong nonlinear regime, incoherent shocks develop into the highly incoherent regime of propagation, in which linear dispersive effects dominate nonlinear effects. The weakly nonlinear kinetic approach then reveals that these incoherent shocks are described, as a rule, by singular integro-differential kinetic equations, which involve the Hilbert transform as singular operator. In this way, the theory reveals unexpected links with the 3D vorticity equation in incompressible fluids [122], or the integrable Benjamin–Ono equation [123,124], which was originally derived

in hydrodynamics to model internal waves in stratified fluids [125,126], and recently considered in the context of quantum liquids and quantum Hall states [127,128].

#### 1.2.4. Breakdown of thermalization and the FPU problem

The relationship between formal reversibility and actual dynamics can be rather complex for infinite dimensional Hamiltonian systems like classical optical waves. In integrable systems, one may expect that the dynamics is essentially periodic in time, reflecting the underlying regular phase-space structure of nested tori. This recurrent behavior is broken in nonintegrable systems, where the dynamics is in general governed by an irreversible process of diffusion in phase space [129]. The essential properties of this irreversible evolution to equilibrium can be described by the wave turbulence theory, as discussed here above in Section 1.2.1.

It is instructive to discuss the phenomenology of nonlinear wave thermalization from a broader perspective. We recall in this respect the fundamental assumption of statistical mechanics that a closed system with many degrees of freedom ergodically samples all equal energy points in phase space. In order to analyze the limits of this assumption, Fermi, Pasta and Ulam (FPU) considered in the 1950's a one-dimensional chains of particles with anharmonic forces between them [130]. They argued that, owing to the nonlinear coupling, an initial state in which the energy is in the first few lowest modes would eventually relax to a state of thermal equilibrium where the energy is equidistributed among all modes on the average. However they observed that, instead of leading to the thermalization of the system, the energy transfer process involves only a few modes and exhibits a reversible behavior, in the sense that after a sufficiently (long) time the system nearly goes back to its initial state. This recurrent behavior could not be interpreted in terms of Poincaré recurrences, a feature which motivated an intense research activity. Fundamental mathematical and physical discoveries, like the Kolmogorov–Arnold–Moser theorem and the formulation of the soliton concept, have led to a better understanding of the Fermi–Pasta–Ulam problem, although it is by no means completely understood [130].

We should note that, in spite of the large number of theoretical studies, experimental demonstrations of FPU recurrences have been reported in very few systems. In particular, the FPU recurrences associated to modulational instability of the NLS equation have been experimentally studied in deep water waves [131], and, more recently, in magnetic feedback rings [132] and optical wave systems [133–137].

In relation with the FPU problem, we will discuss in this review some mechanisms which inhibit the irreversible process of optical wave thermalization towards the Rayleigh–Jeans distribution. We will focus the presentation on particular mechanisms which are described in detail by the WT kinetic equation. We will consider the concrete example of the one-dimensional NLS equation in the presence of higher-order dispersion effects. This generalized NLS equation is known to provide an accurate description of light propagation in photonic crystal fibers [138,139,31]. We will discuss three different mechanisms which inhibit optical thermalization [140–143]. The WT theory will be shown to provide an accurate description of this breakdown of thermalization. In particular, the WT theory reveals the existence of local invariants in frequency space, which lead to a novel family of equilibrium states of a different nature than the expected thermodynamic (Rayleigh–Jeans) equilibrium states. The inhibition of thermalization for the integrable NLS equation will also be considered in the framework of a generalized WT equation.

### 1.3. Organization of the manuscript

This review article is also aimed to render the mathematical tools of the kinetic theory accessible to a broad audience in the nonlinear physics community. A special effort is thus devoted to structure the article in a self-contained and pedagogical fashion. In order to start with a simple physical situation, we first consider in Section 2 the spatial evolution of the incoherent wave in a nonlocal Kerr environment. In this way, different variants of the Vlasov equation are derived, whose self-consistent potential depends on the amount of nonlocality in the system, as discussed above in Section 1.2.2. Then we consider in Section 3 the temporal evolution of an incoherent wave, in which the causality condition of the response function introduces the weak Langmuir turbulence formalism commented here above in Section 1.2.3. The general spatio-temporal problem is analyzed in Section 4 in the limit of a slowly responding (inertial) nonlinearity, which also provides an introduction to the Wigner–Moyal formalism. Section 5 is devoted to the analysis of the WT kinetic equation and the phenomena of wave thermalization and condensation or incoherent waves, as discussed above in Section 1.2.1. The mechanisms responsible for possible inhibitions of the thermalization process are presented in Section 6, in line with the FPU problem commented in Section 1.2.4. Section 7 discusses several important perspectives and open problems, in particular in relation with the study of optical turbulence in passive cavities and laser systems. We finally note that, although this review is essentially focused on theoretical formulations of the dynamics of incoherent nonlinear waves, we also briefly comment some major experimental observations in various different subsections.

## 2. Spatial domain

In this section we study the transverse spatial evolution of a partially coherent wave that propagates in a nonlocal nonlinear medium. We consider the case where the random wave exhibits fluctuations that are statistically inhomogeneous in space. As illustrated schematically in Fig. 2, the dynamics of the incoherent wave is described by different forms of the

Vlasov equation, whose self-consistent potential depends on the degree of nonlocality. The case of homogeneous statistics will be discussed in Section 5, in the framework of the WT kinetic equation. The presentation of this section is structured along the lines of Refs. [27,144].

### 2.1. Nonlocal response

#### 2.1.1. NLS model

A nonlocal nonlinear response of the medium is found in several wave systems such as, e.g., dipolar Bose–Einstein condensates [98], atomic vapors [99], nematic liquid crystals [100,101,145], photorefractive media [104], thermal susceptibilities [146,102,103], soft materials [147] and plasmas physics [105]. For this reason the impact of nonlocality on the dynamics of nonlocal nonlinear waves has been widely investigated [110], in particular through the analysis of MI [106], of dark solitons [109], of the role of disorder [148–151], or through the inhibition of collapse in multi-dimensional systems [107,108].

We consider here the standard form of the nonlocal NLS model equation describing wave propagation in nonlinear media that exhibit a nonlocal response

$$i\partial_z\psi + \alpha\nabla^2\psi + \gamma\psi \int U(\boldsymbol{x}-\boldsymbol{x}')\,|\psi|^2(z,\boldsymbol{x}')\,d\boldsymbol{x}' = 0, \tag{1}$$

where $\boldsymbol{x}$ denotes the position in the transverse plane of dimension $d$ and $\nabla^2$ denotes the corresponding transverse Laplacian ($\nabla^2 = \partial_x^2$ for $d = 1$, $\nabla^2 = \partial_x^2 + \partial_y^2$ for $d = 2$). The nonlocal response function $U(\boldsymbol{x})$ is a real and even function normalized in such a way that $\int U(\boldsymbol{x})\,d\boldsymbol{x} = 1$, so that in the limit of a local response ($U(\boldsymbol{x}) = \delta(\boldsymbol{x})$, $\delta(\boldsymbol{x})$ being the Dirac function), Eq. (1) recovers the standard local NLS equation. The parameters $\alpha = 1/(2k_L)$ and $\gamma$ refer to the linear and nonlinear coefficients, respectively, where $k_L = n2\pi/\lambda_L$, $n$ being the linear refractive index of the material and $\lambda_L$ the wavelength of the laser source. A positive (negative) value of $\gamma$ corresponds to a focusing (defocusing) nonlinear interaction. Besides the momentum, Eq. (1) conserves the power (or number of particles) $\mathcal{N} = \int |\psi(\boldsymbol{x})|^2 d\boldsymbol{x}$, and the Hamiltonian $\mathcal{H} = \mathcal{E} + \mathcal{U}$, where

$$\mathcal{E}(z) = \alpha \int |\nabla\psi(\boldsymbol{x},z)|^2\,d\boldsymbol{x} \tag{2}$$

denotes the linear (kinetic) contribution, and

$$\mathcal{U}(z) = -\frac{\gamma}{2}\iint |\psi(\boldsymbol{x},z)|^2\,U(\boldsymbol{x}-\boldsymbol{x}')\,|\psi(\boldsymbol{x}',z)|^2\,d\boldsymbol{x}\,d\boldsymbol{x}' \tag{3}$$

the nonlinear contribution to the total energy $\mathcal{H}$. We denote by $\sigma$ the spatial extension of $U(\boldsymbol{x})$, which characterizes the amount of nonlocality in the system. This length scale has to be compared with the healing length $\Lambda = \sqrt{\alpha/(|\gamma|\rho)}$, where $\rho = \mathcal{N}/L^d$ is the density of power (intensity), $L$ being the size of the periodic box in the numerical simulations. We recall that $\Lambda$ denotes the typical wavelength excited by the modulational instability of a homogeneous background in the limit of a local nonlinearity, $\sigma \to 0$. An other important length scale is the typical length $\Delta$ that characterizes the homogeneity of the statistics. It reflects the typical length scale over which the fluctuations of the incoherent wave can be considered as homogeneous in space.

*Homogeneous vs. inhomogeneous statistics*

The kinetic equation consists of an equation describing the evolution of the spectrum of the field during its propagation in the nonlinear medium. Note that, in the particular case in which diffraction effects can be neglected ($\alpha = 0$), an expression for the evolution of the second order correlation function can be obtained in explicit form, see Refs. [152,153].

As schematically described through Figs. 2 and 3, the structure of a kinetic equation depends on the nature of the statistics of the random wave. The statistics is said to be homogeneous (or stationary in the temporal domain), if the correlation function $B(\boldsymbol{x}_1,\boldsymbol{x}_2,z) = \langle\psi(\boldsymbol{x}_1,z)\psi^*(\boldsymbol{x}_2,z)\rangle$ only depends on the distance $|\boldsymbol{x}_1 - \boldsymbol{x}_2|$. In the following, the brackets $\langle.\rangle$ denote an average over the realizations of the initial noise of the random wave $\psi(\boldsymbol{x}, z = 0)$. In this section we consider the case where the statistics of the random wave is assumed to be inhomogeneous. We will see that the dynamics is ruled by different forms of the Vlasov equation, whose self-consistent potential depends on the degree of nonlocality [144].

### 2.2. Short-range Vlasov equation

We follow the standard procedure to derive an equation for the evolution of the autocorrelation function of the field, $B(\boldsymbol{x},\boldsymbol{\xi},z) = \langle\psi(\boldsymbol{x}+\boldsymbol{\xi}/2,z)\psi^*(\boldsymbol{x}-\boldsymbol{\xi}/2,z)\rangle$, with

$$\boldsymbol{x} = (\boldsymbol{x}_1+\boldsymbol{x}_2)/2, \qquad \boldsymbol{\xi} = \boldsymbol{x}_1 - \boldsymbol{x}_2. \tag{4}$$

Because of the nonlinear character of the NLS equation, the evolution of the second-order moment of the wave depends on the fourth-order moment. In the same way, the equation for the fourth-order moment depends on the sixth-order moment, and so on. One obtains in this way an infinite hierarchy of moment equations, in which the $n$th order moment depends

on the $(n+2)$th order moment of the field. This makes the equations impossible to solve unless some way can be found to truncate the hierarchy. This refers to the fundamental problem of achieving a closure of the infinite hierarchy of the moment equations [37,51,39,40]. A simple way to achieve a closure of the hierarchy is to assume that the field has Gaussian statistics. This approximation is justified in the weakly nonlinear regime, $L_d/L_{nl} \ll 1$ (or $|\mathcal{U}/\mathcal{E}| \ll 1$), where $L_d = \lambda_c^2/\alpha$ is the diffraction length, $\lambda_c$ being the coherence length, and $L_{nl} = 1/(|\gamma|\rho)$ is the characteristic length of nonlinear interaction.

*2.2.1. Nonlocal case*

Exploiting the property of factorizability of moments of Gaussian fields, one obtains the following closed equation for the evolution of the autocorrelation function

$$i\partial_z B(\boldsymbol{x},\boldsymbol{\xi},z) = -2\alpha\nabla_{\boldsymbol{x}}.\nabla_{\boldsymbol{\xi}}B(\boldsymbol{x},\boldsymbol{\xi},z) - \gamma P(\boldsymbol{x},\boldsymbol{\xi},z) - \gamma Q(\boldsymbol{x},\boldsymbol{\xi},z), \tag{5}$$

where

$$P(\boldsymbol{x},\boldsymbol{\xi}) = B(\boldsymbol{x},\boldsymbol{\xi})\int U(\boldsymbol{y})\big[N(\boldsymbol{x}-\boldsymbol{y}+\boldsymbol{\xi}/2) - N(\boldsymbol{x}-\boldsymbol{y}-\boldsymbol{\xi}/2)\big]d\boldsymbol{y}, \tag{6}$$

$$Q(\boldsymbol{x},\boldsymbol{\xi}) = \int U(\boldsymbol{y})\big[B(\boldsymbol{x}-\boldsymbol{y}/2+\boldsymbol{\xi}/2,\boldsymbol{y})B(\boldsymbol{x}-\boldsymbol{y}/2,\boldsymbol{\xi}-\boldsymbol{y}) - B(\boldsymbol{x}-\boldsymbol{y}/2,\boldsymbol{\xi}+\boldsymbol{y})B(\boldsymbol{x}-\boldsymbol{y}/2-\boldsymbol{\xi}/2,-\boldsymbol{y})\big]d\boldsymbol{y}, \tag{7}$$

and

$$N(\boldsymbol{x},z) \equiv B(\boldsymbol{x},\boldsymbol{\xi}=0,z) = \left\langle|\psi|^2\right\rangle(\boldsymbol{x},z) \tag{8}$$

denotes the averaged power of the field, which depends on the spatial variable $\boldsymbol{x}$ because the statistics of the field is *a priori* inhomogeneous. Note that we have omitted the $z$-label in Eqs. (6) and (7).

Eq. (5)–(7) is quite involved. To provide an insight into its physics we assume that the incoherent wave exhibits a quasi-homogeneous statistics, that is to say $\lambda_c$ (i.e. the length scale of the random fluctuations) is much smaller than the length scale of homogeneous statistics $\Delta$ (i.e. typically the size of the incoherent beam), $\varepsilon = \lambda_c/\Delta \ll 1$. We assume that the range of the response function is of the same order as the healing length, $\sigma \sim \Lambda$. Defining the local spectrum of the wave as the Wigner-like transform of the autocorrelation function,

$$n_{\boldsymbol{k}}(\boldsymbol{x},z) = \int B(\boldsymbol{x},\boldsymbol{\xi},z)\ \exp(-i\boldsymbol{k}.\boldsymbol{\xi})\,d\boldsymbol{\xi}, \tag{9}$$

and performing a multiscale expansion of the solution

$$B(\boldsymbol{x},\boldsymbol{\xi},z) = B^{(0)}\big(\varepsilon\boldsymbol{x},\boldsymbol{\xi},\varepsilon z\big) + O(\varepsilon), \tag{10}$$

we obtain in the first-order in $\varepsilon$ the following Vlasov-like kinetic equation (see Appendix A.1)

$$\partial_z n_{\boldsymbol{k}}(\boldsymbol{x},z) + \partial_{\boldsymbol{k}}\tilde{\omega}_{\boldsymbol{k}}(\boldsymbol{x},z).\partial_{\boldsymbol{x}}n_{\boldsymbol{k}}(\boldsymbol{x},z) - \partial_{\boldsymbol{x}}\tilde{\omega}_{\boldsymbol{k}}(\boldsymbol{x},z).\partial_{\boldsymbol{k}}n_{\boldsymbol{k}}(\boldsymbol{x},z) = 0. \tag{11}$$

The generalized dispersion relation reads

$$\tilde{\omega}_{\boldsymbol{k}}(\boldsymbol{x},z) = \omega(\boldsymbol{k}) + V_{\boldsymbol{k}}(\boldsymbol{x},z), \tag{12}$$

where $\omega(\boldsymbol{k}) = \alpha|\boldsymbol{k}|^2$ is the linear dispersion relation of the NLS equation (1), and the self-consistent potential reads

$$V_{\boldsymbol{k}}(\boldsymbol{x},z) = -\frac{\gamma}{(2\pi)^d}\int(1+\tilde{U}_{\boldsymbol{k}-\boldsymbol{k}'})\,n_{\boldsymbol{k}'}(\boldsymbol{x},z)\,d\boldsymbol{k}', \tag{13}$$

where $\tilde{U}(\boldsymbol{k}) = \int U(\boldsymbol{x})\exp(-i\boldsymbol{k}.\boldsymbol{x})\,d\boldsymbol{x}$ is the Fourier transform of $U(\boldsymbol{x})$ [$\tilde{U}(\boldsymbol{k})$ being real and even] and

$$N(\boldsymbol{x},z) = \frac{1}{(2\pi)^d}\int n_{\boldsymbol{k}}(\boldsymbol{x},z)\,d\boldsymbol{k} \tag{14}$$

is the averaged spatial intensity profile of the wave [see Eq. (8)].

*Properties of the Vlasov equation*

Several important properties of the Vlasov equation (11) result from its Poisson bracket structure. More specifically, the Vlasov equation can be recast in Hamiltonian form by means of the following Liouville's equation

$$d_z n_{\boldsymbol{k}}(z,\boldsymbol{x}) \equiv \partial_z n + \dot{\boldsymbol{x}}.\partial_{\boldsymbol{x}}n + \dot{\boldsymbol{k}}.\partial_{\boldsymbol{k}}n = 0, \tag{15}$$

where the variables $\boldsymbol{k}$ and $\boldsymbol{x}$ appear as canonical conjugate variables,

$$\dot{\boldsymbol{k}} = \partial_z\boldsymbol{k} = -\partial_{\boldsymbol{x}}\tilde{\omega}, \tag{16}$$

$$\dot{\boldsymbol{x}} = \partial_z\boldsymbol{x} = \partial_{\boldsymbol{k}}\tilde{\omega}, \tag{17}$$

where the generalized dispersion relation (12) plays the role of an effective Hamiltonian.

The Vlasov equation is a formally reversible equation, i.e., it is invariant under the transformation $(z, \boldsymbol{k}) \to (-z, -\boldsymbol{k})$. Moreover, it conserves the number of particles, $\mathcal{N} = (2\pi)^{-d} \iint n_{\boldsymbol{k}}(\boldsymbol{x}, z)\, d\boldsymbol{x}\, d\boldsymbol{k}$, the momentum $\mathcal{P} = (2\pi)^{-d} \iint \boldsymbol{k}\, n_{\boldsymbol{k}}(\boldsymbol{x}, z)\, d\boldsymbol{x}\, d\boldsymbol{k}$, and the Hamiltonian

$$\mathcal{H} = \frac{1}{(2\pi)^d} \iint \omega(\boldsymbol{k})\, n_{\boldsymbol{k}}(\boldsymbol{x})\, d\boldsymbol{x}\, d\boldsymbol{k} - \frac{\gamma}{2(2\pi)^{2d}} \iiint n_{\boldsymbol{k}_1}(\boldsymbol{x})\, \tilde{U}_{\boldsymbol{k}_1 - \boldsymbol{k}_2}\, n_{\boldsymbol{k}_2}(\boldsymbol{x}) d\boldsymbol{x}\, d\boldsymbol{k}_1\, d\boldsymbol{k}_2. \tag{18}$$

In addition, the Vlasov equations (11)–(13) also conserves the so-called Casimirs, $\mathcal{M} = \iint f[n]\, d\boldsymbol{x} d\boldsymbol{k}$, where $f[n]$ is an arbitrary functional of the distribution $n_{\boldsymbol{k}}(\boldsymbol{x}, z)$.

We remark that the effective potential (13) of the Vlasov equation also depends on the spatial frequency $\boldsymbol{k}$, which considerably complicates the study of the Vlasov equation. The dependence of the potential (13) on $\boldsymbol{k}$ is expected to introduce new dynamical behaviors which will be the subject of future investigations.

#### 2.2.2. Local limit

In the limit of a local interaction, $U(\boldsymbol{x}) \to \delta(\boldsymbol{x})$, the Vlasov equation derived here above recovers the traditional Vlasov equation, whose self-consistent potential (13) becomes $\boldsymbol{k}$-independent and reduces to

$$V(\boldsymbol{x}, z) = -2\gamma N(\boldsymbol{x}, z). \tag{19}$$

This type of Vlasov equation will be discussed more specifically in Section 4. It was considered in various different fields to study incoherent modulational instability and incoherent solitons in plasmas [115,86,87], hydrodynamics [116] and optics [10,91,92,90].

### 2.3. Long-range Vlasov equation

#### 2.3.1. Long-range response

Let us now consider a long-range nonlocal nonlinear response, $\sigma/\Lambda \gg 1$. Note that in this case the random field exhibits fluctuations whose spatial inhomogeneities are of the same order as the range of the nonlocal potential, $\sigma \sim \Delta$ (a feature illustrated by the incoherent solitons discussed in [27], whose typical size is determined by $\sigma$). The derivation of the long-range Vlasov equation is obtained by following a procedure similar to that for the short-range case ($\sigma \sim \Lambda$), except that we have to introduce the following scaling for the nonlocal potential

$$U(\boldsymbol{x}) = \varepsilon U^{(0)}(\varepsilon \boldsymbol{x}). \tag{20}$$

Note that the prefactor $\varepsilon$ is required by the normalization condition, $\int U(\boldsymbol{x}) d\boldsymbol{x} = \int U^{(0)}(\varepsilon \boldsymbol{x})\, d(\varepsilon \boldsymbol{x}) = 1$. Following the multiscale expansion technique, we derive in Appendix A.2 the Vlasov-like kinetic equation (11), with the effective dispersion relation

$$\tilde{\omega}_{\boldsymbol{k}}(\boldsymbol{x}, z) = \omega(\boldsymbol{k}) + V(\boldsymbol{x}, z), \tag{21}$$

and the long-range self-consistent potential

$$V(\boldsymbol{x}, z) = -\gamma \int U(\boldsymbol{x} - \boldsymbol{x}')\, N(\boldsymbol{x}', z)\, d\boldsymbol{x}'. \tag{22}$$

This effective potential then appears as a convolution of the nonlocal response with the intensity profile of the incoherent wave. Contrarily to the short-range potential, it does not depend on the spatial frequency $\boldsymbol{k}$. The long-range Vlasov equation conserves the number of particles, $\mathcal{N} = (2\pi)^{-d} \iint n_{\boldsymbol{k}}(\boldsymbol{x}, z)\, d\boldsymbol{x}\, d\boldsymbol{k}$, the momentum $\mathcal{P} = (2\pi)^{-d} \iint \boldsymbol{k}\, n_{\boldsymbol{k}}(\boldsymbol{x}, z)\, d\boldsymbol{x}\, d\boldsymbol{k}$, the Hamiltonian

$$\mathcal{H} = \frac{1}{(2\pi)^d} \iint \omega(\boldsymbol{k})\, n_{\boldsymbol{k}}(\boldsymbol{x}, z)\, d\boldsymbol{x}\, d\boldsymbol{k} + \frac{1}{2} \int V(\boldsymbol{x}, z) N(\boldsymbol{x}, z)\, d\boldsymbol{x}, \tag{23}$$

as well as the Casimirs, $\mathcal{M} = \iint f[n]\, d\boldsymbol{x} d\boldsymbol{k}$, where $f[n]$ is an arbitrary functional of the distribution $n_{\boldsymbol{k}}(\boldsymbol{x}, z)$. As will be discussed below in Section 2.3.5, the long-range Vlasov equation was considered in [27] to describe highly nonlocal spatial incoherent solitons.

#### 2.3.2. Validity of the long-range Vlasov equation

It is important to underline that, thanks to the long-range nonlocal response, the system exhibits a self-averaging property of the nonlinear response, $\int U(\boldsymbol{x} - \boldsymbol{x}')|\psi(\boldsymbol{x}', z)|^2 d\boldsymbol{x}' \simeq \int U(\boldsymbol{x} - \boldsymbol{x}') N(\boldsymbol{x}', z) d\boldsymbol{x}'$. Substitution of this property into the nonlocal NLS equation (1) thus leads to a closure of the hierarchy of the moment equations. More specifically, using statistical arguments similar as those in [91], one can show that, owing to the highly nonlocal response, the statistics of the incoherent wave turns out to be Gaussian. Then contrarily to a conventional Vlasov equation, whose validity is constrained by the assumptions of (i) weakly nonlinear interaction and (ii) quasi-homogeneous statistics, the long-range Vlasov equation provides an *exact* statistical description of the random wave $\psi(\boldsymbol{x}, z)$ in the highly nonlocal regime, $\varepsilon \ll 1$.

This property is corroborated by the fact that the Vlasov equation considered here is formally analogous to the Vlasov equation considered to study long-range interacting systems [117,154]. In this context, it has been rigorously proven that, in the limit of an infinite number of particles, the dynamics of *mean-field Hamiltonian systems* is governed by the long-range Vlasov equation [117]. Note however that the term 'long-range' used in Ref. [117] refers to a response function whose integral diverges, $\int U(\boldsymbol{x})\, d\boldsymbol{x} = +\infty$, while the response functions considered here refer to exponential or Gaussian shaped functions typically encountered in optical materials (see e.g., [110]).

*2.3.3. Highly nonlocal response: Linear limit*

In the limit of a highly nonlocal nonlinear interaction, the range of the response function can be much larger than the scale of inhomogeneous statistics, $\sigma \gg \Delta$. In this limit, the response function can be extracted from the convolution integral in the effective potential (22), which thus leads to

$$V(\boldsymbol{x}) = -\gamma \mathcal{N} U(\boldsymbol{x}). \tag{24}$$

It is interesting to note that in this limit, the response function plays the role of the effective potential. Accordingly, the Vlasov equation looses its self-consistent nonlinear character and thus reduces to a *linear* kinetic equation.

*Accessible (incoherent) solitons*

This highly nonlocal limit was originally explored by Snyder and Mitchell in Ref. [111], and has then been the subject of a detailed investigation in optics in the framework of the so-called 'accessible solitons' [100,101]. Indeed, the above approximation ($\sigma \gg \Delta$) can be performed starting from the original NLS equation (1), which is thus reduced to a *local and linear Schrödinger wave equation*,

$$i\partial_z \psi + \alpha \nabla^2 \psi + \gamma \mathcal{N} U(\boldsymbol{x}) \psi = 0. \tag{25}$$

This equation describes the evolution of an optical beam trapped in an effective waveguide structure whose profile is given by the nonlocal response function $U(\boldsymbol{x})$. Because this equation is linear, it does not describe modulational instability, or the generation of new frequency components. It is in this highly nonlocal limit that the incoherent solitons reported in Ref. [112,26,155] were studied. These incoherent solitons may thus be viewed as a random superposition of the linear eigenmodes of the potential $U(\boldsymbol{x})$, which are preserved during the linear propagation of the incoherent beam. We finally note that the Vlasov equation with the effective potential (24) can also be readily derived from the linear Schrödinger equation (25).

*2.3.4. Incoherent modulational instability*

Modulational (or Benjamin–Feir) Instability (MI) refers to the phenomenon in which an initially plane- (or continuous-) wave tends to break up spontaneously into periodic modulations while it propagates through a nonlinear medium. In the frequency domain, this phenomenon can be interpreted as a phase-matched partially degenerate four-wave mixing process in which an intense pump wave yields energy to a pair of weak sideband waves. In the following we shall see that an incoherent field that exhibits a homogeneous statistics may become modulationally unstable with respect to the growth of weakly statistical inhomogeneities, i.e., the incoherent field thus becomes statistically inhomogeneous [115,15,16,18].

The phenomenon of incoherent MI was originally described in the context of plasma physics [156,157]. More recently, incoherent MI has been the subject of a detailed investigation in the optical context with an inertial nonlinear response [15,16,10,17,158], a feature that will be discussed in Section 4.3 in more details. We present here the phenomenon of incoherent MI in the framework of the long-range Vlasov formalism, which provides an 'exact' description of the random nonlinear wave, as discussed here above in Section 2.3.2.

For the sake of simplicity, we limit the incoherent MI analysis to the one-dimensional case. We assume that the incident field exhibits a homogeneous statistics, except for small perturbations that depend on $x$ and $z$. Note that any homogeneous stationary distribution, $n_k^0$, is a solution of the Vlasov equation, that is, $\partial_z n_k^0 = 0$. We perturb this stationary solution according to $n_k(x,z) = n_k^0 + \delta n_k(x,z)$, with $|\delta n_k(x,z)| \ll n_k^0$, and linearize the Vlasov equation

$$\partial_z \delta n_k(x,z) + 2\alpha k \partial_x \delta n_k(x,z) + \frac{\gamma}{2\pi} \partial_k n_k^0 \int dx' \partial_x U(x-x') \int dk \delta n_k(x',z) = 0. \tag{26}$$

This equation can be solved by a Fourier–Laplace transform, $\tilde{\delta n}_k(K,\lambda) = \int_0^\infty dz \int_{-\infty}^{+\infty} dx\, \exp(-\lambda z - iKx)\, \delta n_k(x,z)$, which gives the dispersion relation

$$-1 = \frac{\gamma}{\pi} \alpha K^2 \tilde{U}(K) \int_{-\infty}^{+\infty} \frac{n_k^0}{(i\lambda - 2\alpha K k)^2}\, dk, \tag{27}$$

where $\tilde{U}(K) = \int U(x) \exp(-iKx)\, dx$. Assuming that the initial spectrum is Lorentzian-shaped, $n_k^0 = 2N_0 \Delta k/(k^2 + (\Delta k)^2)$ [i.e., $(2\pi)^{-1} \int n_k^0 dk = N_0$], Eq. (27) gives

$$\lambda(K) = -2\alpha \Delta k |K| + |K| \sqrt{2\alpha\gamma N_0 \tilde{U}(K)}, \tag{28}$$

where the incoherent MI gain reads $g_{\mathrm{MI}}(K) = 2\Re[\lambda(K)]$.

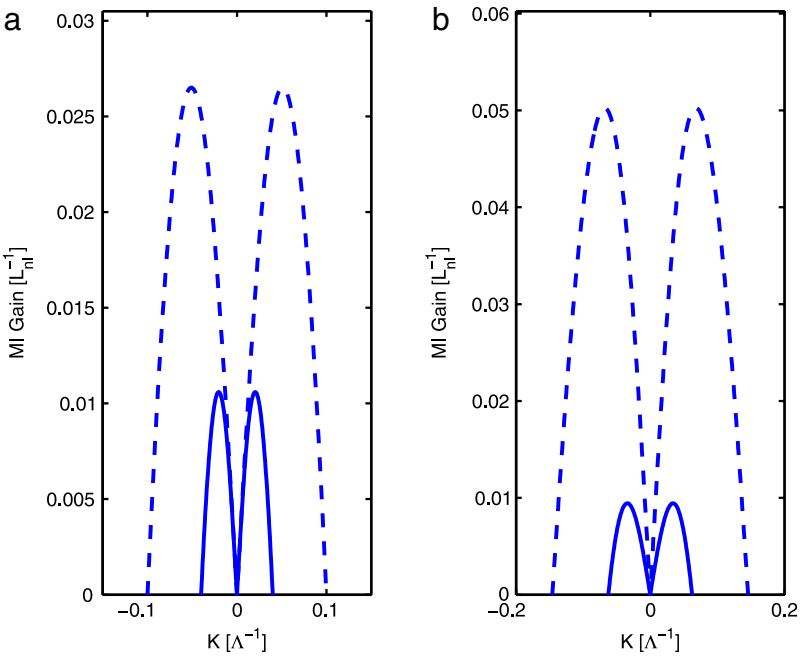


**Fig. 4.** Spatial incoherent MI: Plots of the MI gain given by Eq. (28), $g_{\rm MI}(K) = 2\Re[\lambda(K)]$, for an exponential response function, $U(x) = \exp(-|x|/\sigma)/(2\sigma)$: (a) $\sigma = 10\Lambda$ (dashed), $\sigma = 25\Lambda$ (continuous), for $\Delta k = 0.5\Lambda^{-1}$. (b) $\Delta k = 0.4\Lambda^{-1}$ (dashed), $\Delta k = 0.6\Lambda^{-1}$ (continuous), for $\sigma = 10\Lambda$.

First of all, we can note that incoherent MI requires a focusing nonlinearity, $\gamma > 0$, as for the usual coherent MI. However, contrary to coherent MI, a focusing nonlinearity is not a sufficient condition for the occurrence of incoherent MI. Indeed, we remark in the MI gain expression (28) the existence of a damping term, which introduces a threshold for incoherent MI [10,15,92]. Note that, the existence of a threshold for incoherent MI was shown to be formally related to the existence of an effective Landau damping [96,10,17,97]. In this way, the stabilizing effect of the partial coherence does not refer to a genuine dissipative damping, but rather a self-action effect analogous to Landau damping of electron plasma waves [159] that causes a redistribution of the spectrum $n_k(x, z)$. This effective damping effect significantly reduces the MI gain and the optimal MI frequency, $K_{\rm MI}$, as illustrated in Fig. 4. We note here that incoherent MI has been the subject of lot of interest, in relation with experiments performed in photorefractive inertial nonlinearities [17,160–162] (see Section 4.3), or in optical fiber systems [163–165,18].

It is interesting to note that in the limit of a local response ($\tilde{U}(K) = 1$), Eq. (28) reduces to a straight line. This leads to an unphysical result: The MI gain increases with the modulation frequency $K$. This pathology stems from the fact that the derivation of the Vlasov equation with a local nonlinearity is constrained by the assumption of *q*uasi-homogeneous statistics. However, as discussed above in Section 2.3.1, the assumption of quasi-homogeneous statistics is automatically satisfied in the presence of a long-range nonlocality. Accordingly, the incoherent MI gain curve (28) is bell-shaped, with a maximum growth-rate at some optimal frequency, $K_{\rm MI}$.

### *2.3.5. Incoherent solitons*

The Vlasov equation describes the evolution of the averaged spectrum of a random wave. Hence, a spatially localized and stationary solution of the Vlasov equation describes an incoherent soliton state. The mechanism underlying the formation of an incoherent soliton is schematically explained in Fig. 5. We consider here the case of bright solitons with a focusing nonlinearity ($\gamma > 0$), and again we limit the study to the pure one-dimensional situation. Let us consider the stationary Vlasov equation

$$2\alpha k\, \partial_x n_k^{st}(x) - \partial_x V(x)\, \partial_k n_k^{st}(x) = 0 \tag{29}$$

where the self-consistent potential is given by $V(x) = -\gamma \int U(x-x')\, N(x')\, dx'$ [see Eq. (22)]. Let us now recall an important observation originally pointed out in the seminal paper [85], namely the fact that the solution to Eq. (29) can be expressed as an arbitrary function of the effective Hamiltonian, $h = \alpha k^2 + V(x)$. To find an explicit analytical solution to Eq. (29), we make use of this observation by following the procedure outlined in Ref. [86]. In this work, Hasegawa obtained an analytical soliton solution of the Vlasov equation in the limit of a *local nonlinear interaction*, $U(x) = \delta(x)$. This solution has been recently generalized to a nonlocal interaction in Ref. [27]. The idea of the method is to argue that the 'particles' that constitute the soliton are trapped by the self-consistent potential $V(x)$ provided that their energy is negative, $h \leq 0$. This determines a specific interval of momenta for the trapped particles, $-k_c \leq k \leq k_c$, where $k_c = \sqrt{-V/\alpha}$ (note that $V < 0$ in the focusing

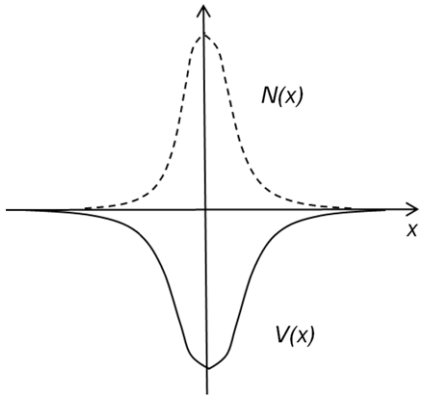


**Fig. 5.** Schematic representation of the self-trapping mechanism underlying the formation of an incoherent soliton solution of the Vlasov equation. A soliton forms when the optical beam induces an attractive potential $V(x) < 0$ (waveguide) owing to a focusing nonlinearity ($\gamma > 0$). In turn, the optical beam is guided in its own induced potential $V(x)$.

regime, see Fig. 5). According to Eq. (14), the intensity profile of the soliton solution thus reads $N(x) = (2\pi)^{-1} \int_{-k_c}^{+k_c} n_k^{st}(x)\, dk$. By means of a simple change of variables, this integral can thus be expressed in the form of a Fredholm equation

$$N = \frac{1}{2\pi} \int_V^0 \frac{n^{st}(h)}{\sqrt{h - V}} dh. \tag{30}$$

A solution to this equation can be obtained under the assumption that $U(x)$ and $N(x)$ are Gaussian-shaped [27]. Assuming $U(x) = (2\pi\sigma^2)^{-1/2} \exp[-x^2/(2\sigma^2)]$ and $N(x) = \mathcal{N}(2\pi\sigma_N^2)^{-1/2} \exp[-x^2/(2\sigma_N^2)]$, and making use of the Laplace convolution theorem, we have

$$n_k^{st}(x) = Q_\eta \left[c_\eta N^\eta(x) - \beta k^2\right]^{\frac{1}{\eta} - \frac{1}{2}}, \tag{31}$$

where

$$Q_\eta = \frac{2\pi \beta^{\frac{1}{2}} \Gamma(\eta^{-1} + 1)}{\Gamma(\eta^{-1} + 1/2)\Gamma(1/2) c_\eta^{1/\eta}}, \tag{32}$$

$\Gamma(x)$ being the Gamma function, and

$$c_\eta = \frac{(2\pi)^{\frac{\eta}{2} - \frac{1}{2}} \gamma \sigma_N^\eta}{\mathcal{N}^{\eta - 1} \sqrt{\sigma^2 + \sigma_N^2}}, \tag{33}$$

with

$$\eta = \frac{1}{1 + (\sigma/\sigma_N)^2}. \tag{34}$$

This analytical solution is self-consistent, in the sense that it verifies the condition (30), and it is straightforward to check by direct substitution that it is indeed a solution of (30).

*Local limit*

The fact that this solution generalizes the solution obtained by Hasegawa [86] becomes apparent by remarking that Eq. (31) can be expressed as

$$n^{st}(h) \sim (-h)^{\frac{1}{\eta} - \frac{1}{2}}. \tag{35}$$

In the limit of a local potential, $U(x) = \delta(x)$, the parameter $\eta \to 1$, and (35) recovers the solution $n^{st}(h) \sim \sqrt{-h}$ [86]. Note however that for a local nonlinearity [86], the analytical solution is valid for *any* form of the intensity distribution, $N(x)$, a property that was subsequently interpreted in the framework of a ray-optics approach [166]. Conversely, for a nonlocal nonlinearity, the analytical solution (31)–(34) refers to a Gaussian-shaped intensity profile.

*Vlasov simulations: Incoherent soliton turbulence*

The phenomena of incoherent MI and subsequent incoherent soliton formation can be visualized by means of a direct numerical integration of the long-range Vlasov equations (11) and (22). This is illustrated in Fig. 6, which reports the

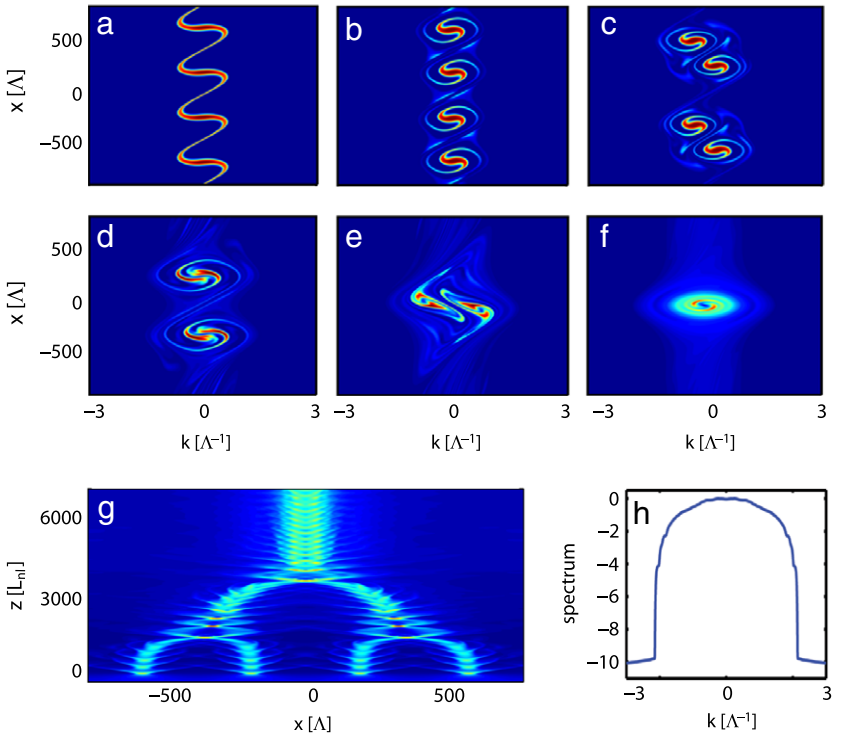


**Fig. 6.** Incoherent soliton turbulence: Numerical simulation of the long-range Vlasov equations (11) and (22), showing the evolution of the local spectrum, $n_k(x)$, during the propagation. The initial homogeneous spectrum exhibits incoherent MI: The four modulations excited by the initial condition lead to the generation of four incoherent structures, which slowly coalesce into two, and then into one incoherent soliton state. (a) $z = 300$, (b) $z = 1000$, (c) $z = 1500$, (d) $z = 3000$, (e) $z = 4000$, (f) $z = 10^4$ (in units of $L_{nl}$), $\sigma = 10^2\,\Lambda$. (g) Corresponding evolution of the spatial intensity profile, $N(x, z)$. (h) Corresponding spectrum $S(k, z_0)$ at $z_0 = 700L_{nl}$, in $\log_{10}$-scale.
*Source:* From Ref. [27].

evolution of the spectrum of the incoherent wave during its propagation. The simulation starts from a homogeneous spectrum, $n_k(x, z = 0) \simeq n_k^0$, which is periodically perturbed to seed the incoherent MI. Because of the nonlinear Hamiltonian flow, particles following different orbits travel at different angular speeds, a process known as 'phase-mixing'. Each MI-modulation thus starts spiraling in the phase-space $(x, k)$, which leads to the formation of four localized incoherent structures, which are mutually attracted and coalesce into two, and eventually into a single incoherent structure. Note that this process is analogous to the soliton turbulence scenario that occurs for *coherent* solitons [113], as discussed in Section 5.2.1. The phase-mixing then leads to a smoothing and homogenization of the perturbations on the incoherent structure, which thus slowly tend to relax towards a stationary incoherent soliton state. Note that the asymptotic evolution of inhomogeneous Vlasov states is a long standing mathematical problem (see, e.g., [167–169]).

## 3. Temporal domain

In this section we study the longitudinal temporal evolution of a partially coherent wave that propagates in a nonlinear medium characterized by a noninstantaneous response. As discussed in Section 1 through Fig. 3, the structure of the kinetic equation depends on the nature of the statistics of the field. The main difference with respect to the spatial nonlocal nonlinearity considered in the previous section relies on the fact that in the temporal case the response function is constrained by the causality condition. We will see below that a noninstantaneous nonlinearity leads to a kinetic description which is formally analogous to the weak Langmuir turbulence equation, irrespective of the nature of the fluctuations that may be either stationary or non-stationary. In the presence of a temporal long-range response and a stationary statistics of the incoherent wave, the weak Langmuir turbulence reduces to singular integro-differential kinetic equations (e.g., Benjamin–Ono equation) that describe incoherent dispersive shock waves. Conversely, when the wave exhibits a non-stationary statistics still in the presence of a highly noninstantaneous response, the dynamics is ruled by a non-Hamiltonian temporal version of the long-range Vlasov equation, whose self-consistent potential is constrained by the causality condition of the noninstantaneous response function. It is interesting to note that, in the temporal domain, the WT kinetic equation turns out to be only relevant for an instantaneous nonlinear response and a statistically stationary incoherent wave, as will be discussed in Section 5.4 in the framework, e.g., of supercontinuum generation.

In this section we first discuss the WT Langmuir equation in the framework of spectral incoherent solitons and incoherent shocks. Next we the present the temporal version of the long-range Vlasov equation through the description of incoherent

modulational instability and incoherent solitons. The presentation of this section is structured along the lines of Refs. [29,92,119,120,170,18].

### 3.1. Noninstantaneous response

#### 3.1.1. NLS model

A noninstantaneous nonlinear response of the medium arises in several problems of radiation–matter interaction [171]. A typical example in one dimensional systems is provided by the Raman effect in optical fibers, which finds its origin in the delayed molecular response of the material [138]. We consider the standard one-dimensional NLS equation accounting for a noninstantaneous nonlinear response function

$$i\partial_z\psi + \beta\partial_{tt}\psi + \gamma\psi\int_{-\infty}^{+\infty} R(t-t')\,|\psi|^2(z,t')\,dt' = 0, \tag{36}$$

where the response function $R(t)$ is constrained by the causality condition. In the following we use the convention that $t > 0$ corresponds to the leading edge of the pulse, so that the causal response will be on the trailing edge of a pulse, i.e., $R(t) = 0$ for $t > 0$ (obviously, the physical phenomena we are going to present do not depend on the choice of the convention). We will write the response function in the form $R(t) = H(-t)\bar{R}(-t)$, where $\bar{R}(t)$ is a smooth function from $[0,\infty)$ to $(-\infty,\infty)$, while the Heaviside $H(-t)$ ensures the causality property. As we will see, this convention will allow us to easily compare the dynamics of temporal incoherent solitons with the corresponding spatial dynamics discussed in Section 2. Because of the causality property, the real and imaginary parts of the Fourier transform of the response function

$$\tilde{R}(\omega) = \tilde{U}(\omega) + i\,g(\omega), \tag{37}$$

are related by the Kramers–Krönig relations, $\tilde{U}(\omega) = \frac{1}{\pi}\mathcal{P}\int\frac{g(\omega')}{\omega'-\omega}\,d\omega'$, and $g(\omega) = -\frac{1}{\pi}\mathcal{P}\int\frac{\tilde{U}(\omega')}{\omega'-\omega}\,d\omega'$, where $\mathcal{P}$ denotes the principal Cauchy value and $\tilde{R}(\omega) = \int R(t)\exp(i\omega t)dt$[note that $g(\omega) = -\mathrm{Im}\big(\int_0^\infty \bar{R}(t)\exp(i\omega t)dt\big)$]. We recall in particular that the real part $\tilde{U}(\omega)$ is an even function, which will be shown to lead to a conservative dynamics, in a way similar to the nonlocal potential $U(\boldsymbol{x})$ in the spatial domain. On the other hand, the imaginary part $g(\omega)$ is an odd function, which is known to play the role of a gain spectrum that leads to a spectral shift of the wave, a well-known feature in the example of the Raman effect in optical fibers [138]. The causality condition breaks the Hamiltonian structure of the NLS equation, so that Eq. (36) only conserves the total power ('number of particles') of the wave

$$\mathcal{N} = \int |\psi|^2(t,z)\,dt. \tag{38}$$

The typical temporal range of the response function $R(t)$ denotes the response time, $\tau_R$. In Eq. (36), $\beta$ denotes the (second-order) dispersion coefficient of the material, $\beta = -\frac{1}{2}\partial_\omega^2 k(\omega)$ [138]. We recall that $\beta > 0$ ($\beta < 0$) denotes the regime of anomalous (normal) dispersion—in this way the parameter $\beta$ plays the same role as the diffraction parameter $\alpha$ in the spatial case.

The dynamics is ruled by the comparison of the response time and the 'healing time', $\tau_0 = \sqrt{|\beta|/(|\gamma|\rho)}$, where, as discussed previously in the spatial case, $\rho = \mathcal{N}/T$ is the density of power (intensity), $T$ being the size of the numerical window. Moreover, as in the spatial case, the weakly nonlinear regime of interaction refers to the regime in which linear dispersive effects dominate nonlinear effects, i.e., $L_d/L_{nl} \ll 1$ where $L_d = t_c^2/|\beta|$ and $L_{nl} = 1/(|\gamma|\rho)$ refer to the dispersive and nonlinear characteristic lengths respectively, $t_c$ being the correlation time of the partially coherent wave.

### 3.2. Short-range: Weak Langmuir turbulence equation

Proceeding as in the spatial case we look for an equation describing the evolution of the auto-correlation function, $B(t,\tau,z) = \langle\psi(t-\tau/2,z)\psi^*(t+\tau/2,z)\rangle$. Exploiting the property of factorizability of moments of Gaussian fields, one obtains the following closed equation for the evolution of the autocorrelation function

$$i\partial_z B(t,\tau) = 2\beta\partial_{t\tau}^2 B(t,\tau) - \gamma P(t,\tau) - \gamma Q(t,\tau), \tag{39}$$

where we have omitted the $z$-label. The functions $P(t,\tau)$ and $Q(t,\tau)$ are

$$P(t,\tau) = B(t,\tau)\int R(\theta)\big[N(t-\theta-\tau/2) - N(t-\theta+\tau/2)\big]d\theta, \tag{40}$$

$$Q(t,\tau) = \int R(\theta)\big[B(t-\theta/2-\tau/2,-\theta)B(t-\theta/2,\tau+\theta) - B(t-\theta/2,\tau-\theta)B(t-\theta/2+\tau/2,\theta)\big]d\theta, \tag{41}$$

where

$$N(z,t) \equiv B(z,t,0) = \big\langle|\psi(z,t)|^2\big\rangle \tag{42}$$

denotes the averaged power of the field, which depends on time $t$ because the statistics of the field is *a priori* nonstationary.

We consider here the case of a noninstantaneous nonlinearity characterized by a short-range response time, i.e., the regime where the response time is of the same order as the 'healing time', $\tau_R \sim \tau_0$. We look for an equation for the averaged local spectrum defined by $n_\omega(t,z) = \int_{-\infty}^{+\infty} B(t,\tau,z)\,\exp(i\omega\tau)\,d\tau$. We proceed as in the spatial case discussed above in Section 2.2 and perform a multiscale expansion with

$$B(t,\tau,z) = B^{(0)}\big(\varepsilon t,\tau,\varepsilon z\big) + O(\varepsilon),$$

where $\varepsilon = t_c/\Delta$ is the ratio of the time correlation and the characteristic time of nonstationary fluctuations. However, contrarily to the spatial case, the response function is constrained by the causality condition in the temporal domain, an important property which completely changes the picture. It turns out that the relevant kinetic equation describing the evolution of the averaged spectrum of the wave is the WT Langmuir equation (see in Appendix A.3)

$$\partial_z n_\omega(t,z) = \frac{\gamma}{\pi}\, n_\omega(t,z) \int_{-\infty}^{+\infty} g(\omega-\omega')\, n_{\omega'}(t,z)\, d\omega', \tag{43}$$

where we recall that $g(\omega) = \Im[\tilde{R}(\omega)]$ is an odd function that refers to the imaginary part of the Fourier transform of the response function. In the spatial case this function vanishes simply because the response function $U(\boldsymbol{x})$ is a real and even function, and thus $\tilde{U}(\boldsymbol{k})$ is real and even too. As a matter of fact, the derivation of the short-range Vlasov equations (11)–(13) in the spatial case requires a first-order perturbation expansion in $\varepsilon$, whereas the WT Langmuir equation (43) is obtained at zero-th order (see Appendix A.3 for details). Then *the WT Langmuir equation originates in the causality property of the noninstantaneous response function* $R(t)$.

Note that several simplified forms of this kinetic equation have been the subject of a detailed study in the literature. A differential ('hydrodynamic') approximation of the integrodifferential equation (43) was derived for the first time by Kompaneets [172]. This Compton Fokker–Planck equation has been subsequently analyzed by several authors [173–175]. The complete integral kinetic equation (43) may be derived from the Zakharov equations [176], it can also be derived from the quantum version of the Boltzmann-like kinetic equation describing the nonlinear induced Compton scattering [177,175]. Under certain conditions, the WT Langmuir equation has been shown to reduce to the Korteweg–de Vries equation. This aspect will be discussed in detail in Section 3.2.2, in relation with the causality condition inherent to the nonlinear response function, $R(t)$.

*Stationary vs. nonstationary statistics*

The fact that the WT Langmuir equation (43) is relevant for an incoherent wave whose fluctuations are statistically stationary in time has been pointed out recently in the context of optics [29,119,30], as well as in previous works in the plasma context [118,178–183]. One would have expected that the description of a non-stationary statistics would naturally involve a Vlasov-like kinetic equation, as discussed above in the spatial case. However, *it turns out that the WT Langmuir equation (43) is also relevant for the description of a statistically non-stationary random wave*. In this respect, an initial condition, $n_\omega(t, z = 0)$, localized in both the spectral and temporal domains will exhibit a nontrivial deformation in the plane $(\omega, t)$— the temporal regions characterized by a high spectral amplitude will exhibit a fast spectral shift as compared to regions with a lower spectral amplitude. This aspect was discussed at a qualitative level in the optical experiment reported in Ref. [184].

*Properties of the WT Langmuir equation*

We briefly summarize here the essential properties of the kinetic equation (43) in the limit of a stationary statistics

$$\partial_z n_\omega(z) = \frac{\gamma}{\pi}\, n_\omega(z) \int_{-\infty}^{+\infty} g(\omega-\omega')\, n_{\omega'}(z)\, d\omega'. \tag{44}$$

We first note that this equation does not account for dispersion effects (it does not involve the parameter $\beta$), although the role of dispersion in its derivation is essential in order to verify the criterion of weakly nonlinear interaction, $L_d/L_{nl} \ll 1$. The fact that the dynamics ruled by the WT Langmuir equation does not depend on the sign of the dispersion coefficient has been verified by direct numerical simulations of the NLS equation (36) [119]. The kinetic equation (44) conserves the power of the field

$$N = \frac{1}{2\pi}\int n_\omega(z)\, d\omega. \tag{45}$$

Moreover, as discussed above for the Vlasov equation, the WT Langmuir equation (44) is a formally reversible equation [it is invariant under the transformation $(z,\omega) \to (-z,-\omega)$], a feature which is consistent with the fact that it also conserves the non-equilibrium entropy

$$S = \frac{1}{2\pi}\int \log[n_\omega(z)]\, d\omega. \tag{46}$$

*3.2.1. Spectral incoherent solitons*

The WT Langmuir equation admits solitary wave solutions [118,179,180,182,183]. This may be anticipated by remarking that, as a result of the convolution product in (44), the odd spectral gain curve $g(\omega)$ amplifies the low-frequency components of the wave at the expense of the high-frequency components, thus leading to a global red-shift of the spectrum.

*Continuous vs. discrete spectral incoherent solitons*

A physical insight into spectral incoherent solitons may be obtained by a qualitative analysis of the shape of the gain spectrum $g(\omega)$. To be concrete, we consider the useful example of a damped harmonic oscillator response $\bar{R}(t) = \frac{1+\eta^2}{\eta\tau_R}\sin(\eta t/\tau_R)\exp(-t/\tau_R)$, which has been normalized in such a way that $\int R(t)dt = 1$. The parameter $\eta$ denotes the ratio between the response time $\tau_R$ and the time related to the resonant frequency, $\omega_R \simeq \eta/\tau_R$. We reported in Fig. 7 two examples of gain spectra $g(\omega)$ that correspond to different ratios of the response times, $\eta = 1$ (a), and $\eta = 32/12.2 \simeq 2.6$ (d). The latter case (d) is of particular interest since it corresponds to the example of the Raman response in silica optical fibers, i.e., $\tau_R = 32$ fs, $\tau_R/\eta = 12.2$ fs [138]. We report in Fig. 7(c) and (f) the corresponding evolutions of the optical spectra obtained by integrating numerically the NLS equation (36). The initial condition is an incoherent wave characterized by a Gaussian spectrum with $\delta$-correlated random spectral phases, so that the initial wave exhibits stationary fluctuations. The Gaussian spectrum is superposed on a background of small noise of averaged intensity $n_0 = 10^{-5}$. This is important in order to sustain a steady soliton propagation, otherwise the soliton undergoes a slow adiabatic reshaping so as to adapt its shape to the local value of the noise background. The spectral width of the initial Gaussian spectrum has been chosen of the same order as $\omega_R$, i.e., of the same order as the maximum gain frequency of $g(\omega)$. In this way the initial spectrum 'feels' the whole spectral gain curve $g(\omega)$.

As illustrated in Fig. 7(c), the spectrum of the wave splits into two components during the propagation: A continuous spectral incoherent soliton emerges from the initial condition, while the remaining energy is characterized by a small-amplitude field, which essentially evolves linearly as a radiation-like part. This soliton behavior refers to the *continuous* spectral incoherent soliton. Conversely, as the parameter $\eta$ increases, we see in Fig. 7(f) that the continuous spectral incoherent soliton is unstable, and relaxes at $z \sim 60L_{nl}$ towards a *discrete* soliton behavior, which is subsequently conserved for very long propagation distances.

The fact that a continuous spectral incoherent soliton may become discrete during its evolution may easily be interpreted through a qualitative analysis of the gain curve $g(\omega)$. Indeed, a comparison of Fig. 7(a) and (d) clearly shows that the gain curve becomes narrower and more peaked as $\eta$ is increased, i.e., as the resonant frequency $\omega_R$ gets much larger than the spectral bandwidth of the gain curve, $\omega_R \gg \Delta\omega$. As a result, the red-shift of the wave spectrum becomes discrete, because the leading edge of the low-frequency tail of the spectrum exhibits a much higher gain as compared to the mean gain of the whole front of the spectrum. The remarkable result is that the global spectral red-shift exhibits a genuine discrete soliton-like behavior: The discrete soliton propagates with a constant velocity in frequency space for arbitrary long distances, without emitting any apparent radiation.

Note that the optical field associated to spectral incoherent solitons exhibits a stationary statistics. This is illustrated in Fig. 7(b) and (e), which report typical temporal intensity profiles associated to the continuous and the discrete solitons considered in Fig. 7(c) and (f). Then the soliton behavior of these incoherent structures does not manifest in the temporal domain, but exclusively in the spectral domain.

*Role of the background noise level*

The relative intensity of the background noise with respect to the average power of the wave plays an important role in the dynamics of discrete spectral incoherent solitons. Indeed, the *continuous* spectral incoherent soliton is known to become narrower (i.e., of higher amplitude) as the intensity of the background noise decreases. Accordingly, a transition from the continuous to the discrete spectral incoherent soliton occurs as the relative intensity of the background noise is decreased: As the spectral soliton becomes narrower than $\omega_R$, the leading edge of the tail of the spectrum will be preferentially amplified, thus leading to the formation of a discrete spectral incoherent soliton. This is confirmed by the numerical simulations reported in Fig. 8, which illustrates the evolution of the spectrum of the field during the propagation for different values of the background noise intensity.

In order to test the validity of the WT Langmuir theory, we reported in Fig. 8 a direct comparison with the NLS approach. The numerical simulations of the NLS equation (36) involving a stochastic function $\psi(t, z)$ have been realized with the same parameters and the same initial conditions as those of the WT Langmuir equation (44). We underline that an excellent agreement has been obtained between them, without using any adjustable parameter. This good agreement has been obtained with a reasonable value of the weakly nonlinear parameter, $L_d/L_{nl} \sim 0.02$.

*Strong background noise: Incoherent spectral oscillations*

We finally note that if the background noise level increases in a significant way and becomes of the same order than the amplitude of the spectral soliton, the incoherent wave enters a novel regime [185]. This regime is characterized by an oscillatory dynamics of the incoherent spectrum which develops within a spectral cone during the propagation. Such spectral dynamics exhibits a significant spectral blue shift, which is in contrast with the expected Raman-like spectral red shift. In the presence of a strong noise background, the Langmuir WT equation (44) can be linearized, so that an explicit

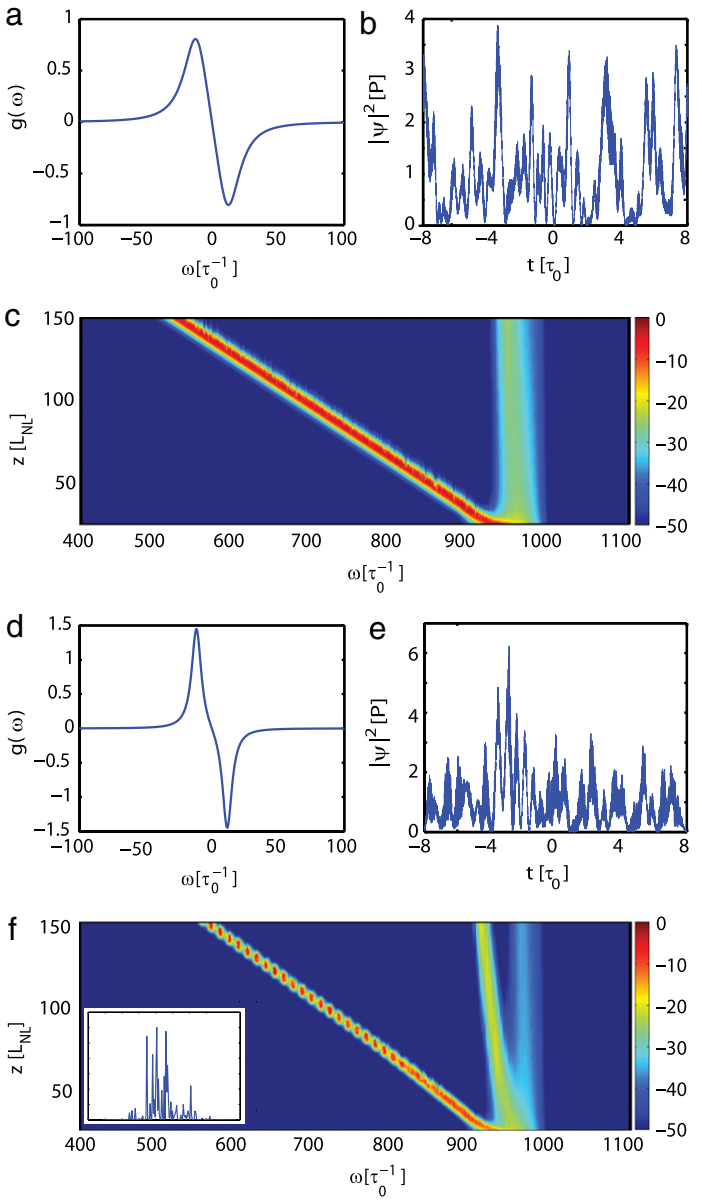


**Fig. 7.** Continuous vs. discrete spectral incoherent solitons: Influence of the gain spectrum $g(\omega)$ on the dynamics of spectral incoherent solitons. Gain spectra $g(\omega)$ for $\eta = 1$ (a), and $\eta = 2.6$ (d), corresponding to a damped harmonic oscillator (Raman-like) response function (see the text). Evolutions of the spectra of the field, $|\tilde{\psi}|^2(z, \omega)$ (in dB-scale), obtained by solving numerically the NLS equation (36) for $\eta = 1$ (c), and $\eta = 2.6$ (f). The inset in (f) represents the spectrum of the field at $z_0 = 88L_{nl}$. Temporal intensity profile $|\psi|^2(z_0, t)$ for $\eta = 1$ (b), and $\eta = 2.6$ (e) at $z_0 = 88L_{nl}$, showing that the optical field is not localized in the time domain (the random wave exhibits a stationary statistics). Note that the dots in the discrete spectral incoherent soliton in (f) are separated by (the Raman-like spectral shift) $\omega_R$ in frequency space ($\beta\gamma < 0$).
*Source:* From Ref. [119].

analytical expression for the spectral evolution of the incoherent wave can be obtained, in quantitative agreement with the simulations of the NLS equation [185].

*Spectral incoherent solitons: Analytical solution*

The WT Langmuir equation admits soliton solutions. More precisely, it is possible to compute the width and velocity of the soliton given its peak amplitude $n_m$ in the regime $n_m \gg n_0$, where $n_0$ denotes the spectral amplitude of the background noise. This was done in Ref. [182] for the particular case where the gain spectrum $g(\omega)$ is the derivative of a Gaussian. As discussed below in Section 3.2.2, this kind of gain spectrum is not relevant to optical waves. However, this solution can be generalized for a generic form of the gain spectrum $g(\omega)$ [92].

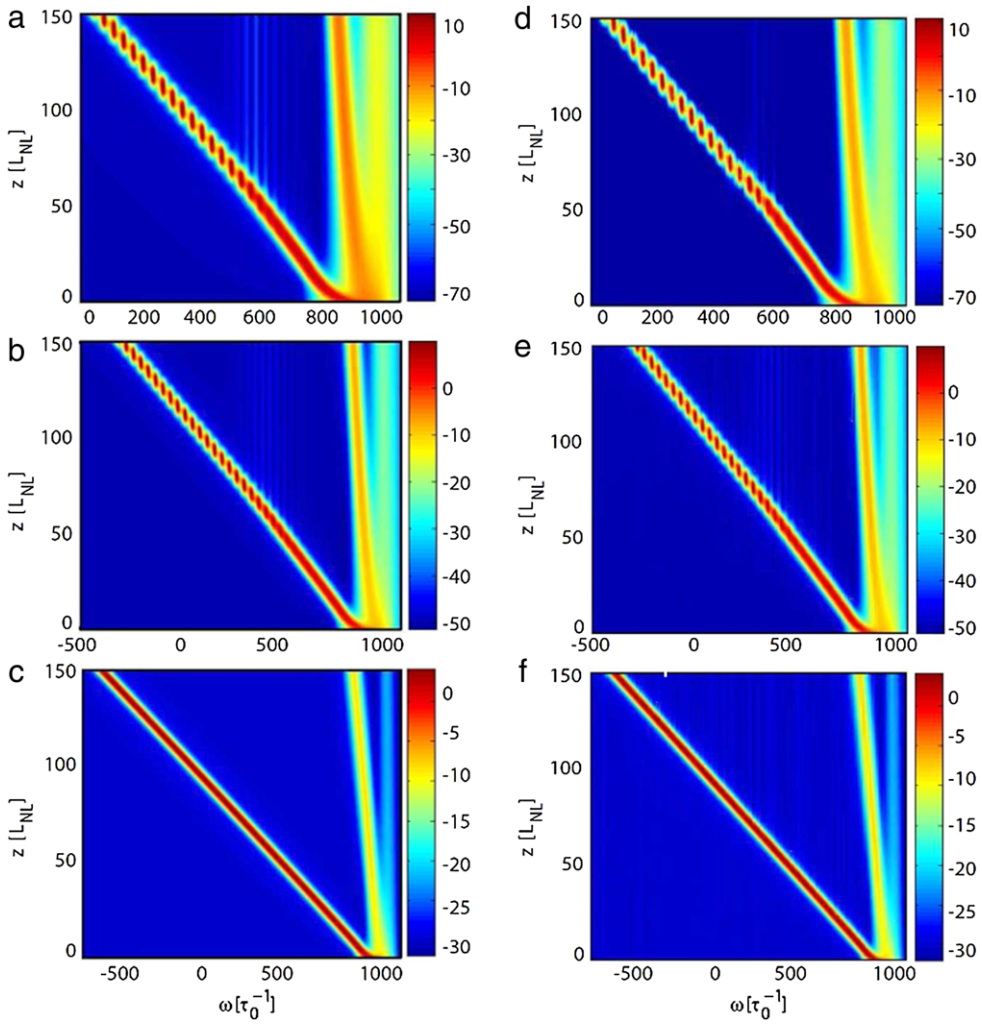


**Fig. 8.** Transition from discrete to continuous spectral incoherent soliton. Left column (a)–(c): Evolution of the non-averaged spectrum of the optical field, $|\tilde{\psi}|^2(z,\omega)$ (in dB-scale), obtained by integrating numerically the NLS equation (36) for three different values of the noise background, $n_0 = 10^{-7}$ (a), $n_0 = 10^{-5}$ (b), $n_0 = 10^{-3}$ (c). Right column (d)–(f): Corresponding evolution of the averaged spectrum, $n(z,\omega)$ (in dB-scale), obtained by solving the Langmuir WT Eq. (44): The comparison reveals a quantitative agreement, without using adjustable parameters. We considered $\eta = 2.6$ in the Raman-like gain spectrum $g(\omega)$ ($\beta\gamma < 0$).
*Source:* From Ref. [119].

We introduce the antiderivative of the spectral gain

$$G(\omega) = -\int_{\omega}^{\infty} g(\omega')d\omega'. \tag{47}$$

The gain spectrum $g(\omega)$ is characterized by its typical gain amplitude $g_i$ and its typical spectral width $\omega_i$. Regardless of the details of the gain curve $g(\omega)$, $g_i$ and $\omega_i$ can be assessed by two characteristic quantities, namely the gain slope at the origin $\partial_\omega g(0)$ and the total amount of gain $G(0) = -\int_0^\infty g(\omega)d\omega$. Note that, by integration by parts, we have $g(\omega) = -\frac{\bar{R}(0)}{\omega} + \frac{1}{\omega^2}\int_0^\infty \bar{R}^{(2)}(t)\ \sin(\omega t)\, dt$, where $\bar{R}^{(2)}(t)$ is the second time derivative of $\bar{R}(t)$. This shows that $G(0)$ is finite if and only if $\bar{R}(0) = 0$. A dimensional analysis allows us to express $g_i$ and $\omega_i$ in terms of these two quantities

$$g_i = \frac{1}{\sqrt{2}}\Big[-\partial_\omega g(0)\Big]^{1/2}\Big[-\int_0^\infty g(\omega)d\omega\Big]^{1/2}, \qquad \omega_i = \sqrt{2}\frac{\Big[-\int_0^\infty g(\omega)d\omega\Big]^{1/2}}{\Big[-\partial_\omega g(0)\Big]^{1/2}}. \tag{48}$$

With these definitions, the function $G(\omega)$ can be written in the following normalized form

$$G(\omega) = g_i\omega_i h\Big(\frac{\omega}{\omega_i}\Big),$$

where the dimensionless function $h(x)$ verifies $h(0) = 1$, $h'(0) = 0$, and $h''(0) = -2$. Proceeding as in [182], the profile of the soliton in the regime $n_m \gg n_0$ is of the form [92]:

$$\log\Big(\frac{n_\omega(z)}{n_0}\Big) = \log\Big(\frac{n_m}{n_0}\Big) h\Big(\frac{\omega - Vz}{\omega_{\rm i}}\Big),$$
$$n_\omega(z) - n_0 = \big(n_m - n_0\big) \exp\Big[-\log\Big(\frac{n_m}{n_0}\Big)\frac{(\omega - Vz)^2}{\omega_{\rm i}^2}\Big], \tag{49}$$

where the velocity of the soliton is

$$V = -\frac{n_m - n_0}{\log^{3/2}\big(\frac{n_m}{n_0}\big)} \frac{\gamma g_{\rm i}\omega_{\rm i}^2}{\sqrt{\pi}}, \tag{50}$$

and its full width at half maximum is

$$\omega_{\rm sol} = \frac{2\log^{1/2} 2}{\log^{1/2}\big(\frac{n_m}{n_0}\big)}\omega_{\rm i}. \tag{51}$$

The structure of discrete spectral incoherent solitons can also be interpreted with an analytical soliton solution of the *d*iscretized WT Langmuir equation derived in Ref. [180]. In this way, discrete frequency bands of the soliton are modeled as coupled Dirac $\delta$-functions in frequency space ($\delta$-peak model). However, the simulations show that, when injected as initial condition into the WT Langmuir equation with a Raman-like gain spectrum, the analytical soliton solution rapidly relaxes during the propagation towards a discrete spectral incoherent solution [119]. This property reveals the incoherent nature of discrete spectral incoherent solitons. It also distinguishes these discrete structures from the cascaded Raman soliton solutions reported in Refs. [186–188] or their recent generalizations [189–191], which involve several phase-locked Raman lines. Since these Raman solitons are inherently coherent localized structures, they are of a different nature than discrete spectral incoherent solitons.

We finally note that the emergence of continuous and discrete spectral incoherent solitons has been identified experimentally owing to the Raman effect in photonic crystal fibers in the context of supercontinuum generation (see Section 5.4.5).

### 3.2.2. Korteweg–de Vries limit

Let us consider the case of a highly noninstantaneous nonlinear response of the material. This case is interesting because, as the response time $\tau_R$ increases, the typical bandwidth of the gain spectrum $g(\omega)$ decreases, and can thus become much smaller than the spectral bandwidth of the incoherent wave. Assuming furthermore that the wave spectrum evolves in the presence of a strong noise background, it can be shown that the WT Langmuir equation reduces to the Korteweg–de Vries (KdV) equation. This aspect was already discussed in Ref. [180]. Here we provide a rigorous derivation of the KdV equation from the WT Langmuir equation.

We start from the WT Langmuir equation (44) and introduce the small parameter $\varepsilon = \Delta\omega_g/\Delta\omega \ll 1$, where we recall that $\Delta\omega_g$ is the bandwidth of the spectral gain curve $g(\omega)$ and $\Delta\omega$ the bandwidth of the incoherent wave. The incoherent wave is assumed to evolve in the presence of a high level of constant spectral noise background of amplitude $n_0$. In this way the gain curve can be written $g(\omega) = g^{(0)}(\omega/\varepsilon)$ and we look for the spectrum in the form

$$n_\omega(z) = n_0 + \tilde{n}_\omega(z),$$

with $\tilde{n}_\omega(z) = \varepsilon^2\tilde{n}_\omega^{(0)}(\varepsilon^2 z) + O(\varepsilon^4)$. In these conditions a multiscale expansion shows that $\tilde{n}_\omega$ satisfies the Korteweg–de Vries equation (see Appendix A.4)

$$\partial_z\tilde{n}_\omega(z) - \frac{\gamma n_0 g_1}{\pi}\partial_\omega\tilde{n}_\omega(z) = \frac{\gamma g_1}{\pi}\tilde{n}_\omega(z)\partial_\omega\tilde{n}_\omega(z) + \frac{\gamma n_0 g_3}{6\pi}\partial_\omega^3\tilde{n}_\omega(z), \tag{52}$$

where

$$g_1 = -\int_{-\infty}^{+\infty}\omega g(\omega)d\omega, \qquad g_3 = -\int_{-\infty}^{+\infty}\omega^3 g(\omega)d\omega.$$

The soliton solutions of this integrable equation have been used to interpret the formation of jets in the frequency space in the study of weak Langmuir turbulence [180]. Note however that the KdV equation considered in [180] differs substantially from Eq. (52). In particular, it is important to note that the validity of the KdV equation (52) is constrained by the convergence of the integrals $g_1$ and $g_3$, i.e., the gain spectrum must decay as or faster than $g(\omega) \sim 1/\omega^5$ as $\omega \to \pm\infty$. However, in general, a response function does not lead to such rapidly decaying spectral gains. To comment on this aspect, we first remark that, because of the causality condition of the response function $R(t)$, its Fourier transform *necessarily decays algebraically at*

*infinity*.[2] In the example of the damped harmonic oscillator response the spectral gain decays as $g(\omega) \sim 1/\omega^3$, while for a purely exponential response $g(\omega) \sim 1/\omega$. A decay as or faster than $g(\omega) \sim 1/\omega^5$ happens if and only if $\bar{R}(0) = \bar{R}^{(2)}(0) = 0$, which thus requires a quite artificial expression of the response function $\bar{R}(t)$. We also remark in Eq. (52) that $g_1 = \pi \bar{R}^{(1)}(0)$ and $g_3 = -\pi \bar{R}^{(3)}(0)$.

Actually, the reduced KdV equation is relevant in plasmas because a different physics is considered in this context. In many cases, the kernel function that plays the role of $g(\omega)$ has been approximated by the derivative of a Gaussian in plasma [118]. For instance, when one considers stimulated Compton scattering, photons are scattered from thermalized electrons, and $g(\omega)$ can be approximated by the derivative of a Maxwellian [182]. In this case $g(\omega)$ does not decay algebraically. This discussion reveals that the KdV equation does not appear as the appropriate reduced equation of the WT Langmuir equation in the context of optics.

### 3.2.3. Singular integro-differential kinetic equations: Incoherent shock waves

In this section we present the procedure which allows one to derive appropriate reduced kinetic equations from the WT Langmuir equation in the long-range limit, i.e., the limit of a highly noninstantaneous nonlinear response. As discussed here above, the causality condition leads to a gain spectrum $g(\omega)$ that decays algebraically at infinity, a property which introduces singularities into the convolution operator of the WT Langmuir equation (44). The mathematical procedure consists in accurately addressing these singularities (for details see Appendix A.5). It reveals that, as a general rule, a singular integro-differential operator arises systematically in the derivation of the reduced kinetic equation [120]. The resulting singular integro-differential kinetic equation then originates in the causality property of the nonlinear response function.

These singular integro-differential kinetic equations find a direct application in the description of dispersive shock waves, i.e., shock waves whose singularity is regularized by dispersion effects instead of dissipative (viscous) effects [121]. Dispersive shock waves have been constructed mathematically [192] and observed in ion acoustic waves [193] long ago, though it is only recently that they emerged as a general signature of singular fluid-type behavior in areas as different as Bose–Einstein condensed atoms [193–197], nonlinear optics [198,199,102,103,200–206], oceanography [207], quantum liquids [127,128], nonlinear chains [208] or granular materials [209], and electrons [210]. We remark that dispersive shock waves have been also recently studied in the presence of structural disorder of the nonlinear medium [211,200,203].

These previous studies on dispersive shock waves have been discussed for coherent, i.e., deterministic, amplitudes of the waves. Through the analysis of the WT Langmuir equation, we will see that incoherent waves can exhibit dispersive shock waves of a different nature that their coherent counterpart. They manifest themselves as a wave breaking process ("gradient catastrophe") in the spectral dynamics of the incoherent field [120]. Contrary to conventional shocks which are known to require a strong nonlinear regime, these incoherent shocks develop into the weakly nonlinear regime. This WT kinetic approach also reveals unexpected links with the 3D vorticity equation in incompressible fluids [122], or the integrable Benjamin–Ono equation [123,124], which was originally derived in hydrodynamics [125,126] and recently considered in the field of quantum liquids [127,128].

#### *Damped harmonic oscillator response: Incoherent shocks*

*(a) Without background*

The derivation of singular integro-differential kinetic equations has been developed for a general form of the response function (see the Supplemental of Ref. [120]). Here we illustrate the theory by considering two physically relevant examples of response functions, which, respectively, induce and inhibit the formation of incoherent shock waves.

Let us first consider the example of the damped harmonic oscillator response, $\bar{R}(t) = \frac{1+\eta^2}{\eta\tau_R} \sin(\eta t/\tau_R) \exp(-t/\tau_R)$. Fig. 9 reports a typical evolution of the spectrum of the incoherent wave obtained by numerical simulations of the NLS equation (36). As discussed above in Section 3.2.1, when the spectral bandwidth of the initial wave is of the same order as the gain bandwidth, $\Delta\omega \sim \Delta\omega_g$ ($t_c \sim \tau_R$), the field rapidly evolves towards a spectral incoherent soliton. Considering the highly incoherent limit, $\Delta\omega \gg \Delta\omega_g$ ($t_c \ll \tau_R$), one would expect that the initial broad spectrum would split into several spectral incoherent solitons of typical width $\sim\Delta\omega_g$. However, the initial broad spectrum exhibits a global collective deformation on a spectral scale much larger than $\Delta\omega_g$, which means that the system exhibits a kind of 'long-range interaction in frequency space'. The behavior of the system then changes in a significant way when $t_c \ll \tau_R$: The low-frequency front of the spectrum exhibits a pronounced self-steepening, whose spectral wave breaking is ultimately regularized by the development of large amplitude and rapid spectral oscillations.

To describe the properties of these incoherent dispersive shock waves, we derive a singular integro-differential equation from the WT Langmuir equation [120]. The convolution integral in Eq. (44), $N_\omega = \int_{-\infty}^{+\infty} g(\omega - u)\, n_u\, du$, can be written in the

[2] The algebraic decay of $g(\omega)$ is determined by the smoothness of the response function $\bar{R}(t)$ at 0. If $\bar{R}(t)$ can be expanded $\bar{R}(t) = \sum_{j\geq 0} \frac{t^j}{j!} \bar{R}^j(0)$ as $t \to 0^+$, then $g(\omega)$ can be expanded as $\sum_{j\geq 0}(-1)^{j+1}\omega^{-2j-1}\bar{R}^{(2j)}(0)$ as $\omega \to \pm\infty$. If $\bar{R}(0) \neq 0$ (e.g., exponential response), then $g(\omega) \sim 1/\omega$. If $\bar{R}(0) = 0$ but $\bar{R}^2(0) \neq 0$ (e.g. damped oscillator), then $g(\omega) \sim 1/\omega^3$. If $\bar{R}(0) = \bar{R}^{(2)}(0) = 0$, then $g(\omega)$ decays at least as $1/\omega^5$.

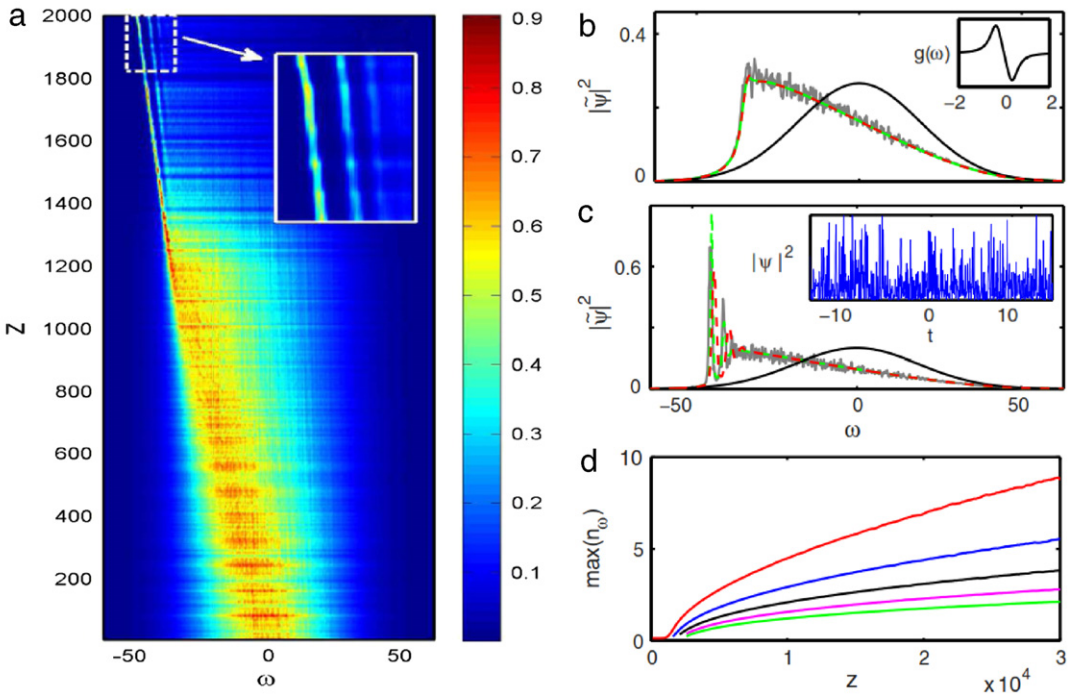


**Fig. 9.** Incoherent dispersive shock waves with a damped harmonic oscillator (Raman-like) response function: (a) Numerical simulation of the NLS equation (36): The stochastic spectrum $|\tilde{\psi}|^2(\omega, z)$ develops an incoherent shock at $z \simeq 1200L_{nl}$ ($\tau_R = 3\tau_0$, $\eta = 1$). Snapshots at $z = 1040L_{nl}$ (b), $z = 1400L_{nl}$ (c): NLS (36) (gray) is compared with WT Langmuir equation (44) (green), singular kinetic equation [Eq. (56)] (dashed-red), and initial condition (solid black). (d) First five maxima of $n_\omega$ vs. $z$ in the long-term post-shock dynamics: The spectral peaks keep evolving, revealing the non-solitonic nature of the incoherent dispersive shock wave. Insets: (b) Gain spectrum $g(\omega)$, note that $\Delta\omega_g$ is much smaller than the initial spectral bandwidth of the wave [black line in (b)]. (c) Corresponding temporal profile $|\psi(t)|^2$ showing the incoherent wave with stationary statistics. (For interpretation of the references to color in this figure legend, the reader is referred to the web version of this article.)
*Source:* From Ref. [120].

following form without approximations (see Appendix A.5)

$$N^0_\omega = \frac{\pi\eta}{\tau_R}\partial_\omega n_\omega - \frac{\pi\eta}{\tau_R^2}\mathcal{H}\partial^2_\omega n_\omega + \frac{1}{\tau_R^3}\int_0^\infty \left[\partial^3_\omega n_{\omega+\frac{u}{\tau_R}} + \partial^3_\omega n_{\omega-\frac{u}{\tau_R}}\right] G_\eta(u)du, \tag{53}$$

where $N_\omega = (1+\eta^2)N^0_\omega/(\eta\tau_R)$. We have defined for $u > 0$

$$G_\eta(u) = \int_u^\infty \left(F_\eta(v) - \frac{\eta}{v}\right) dv, \tag{54}$$

and

$$F_\eta(u) = \frac{\pi\eta}{2} - \frac{1}{2}\left[v\ \arctan(v) - \frac{1}{2}\log(1+v^2)\right]_{u-\eta}^{u+\eta}. \tag{55}$$

The operator $\mathcal{H}$ refers to the Hilbert transform,

$$\mathcal{H}f(\omega) = \frac{1}{\pi}\mathcal{P}\int_{-\infty}^{+\infty}\frac{f(\omega-u)}{u}du,$$

where we recall that $\mathcal{P}$ denotes the Cauchy principal value. Considering the limit $\tau_R/\tau_0 \gg 1$ in Eq. (53), we obtain the singular integro-differential kinetic equation

$$\tau_R^2\partial_z n_\omega = \gamma(1+\eta^2)\left(n_\omega\partial_\omega n_\omega - \frac{1}{\tau_R}n_\omega\mathcal{H}\partial^2_\omega n_\omega\right). \tag{56}$$

This kinetic equation describes the essence of incoherent dispersive shock waves: The leading-order Burgers term describes the formation of the shock, which is subsequently regularized by the nonlinear dispersive term involving the Hilbert operator.

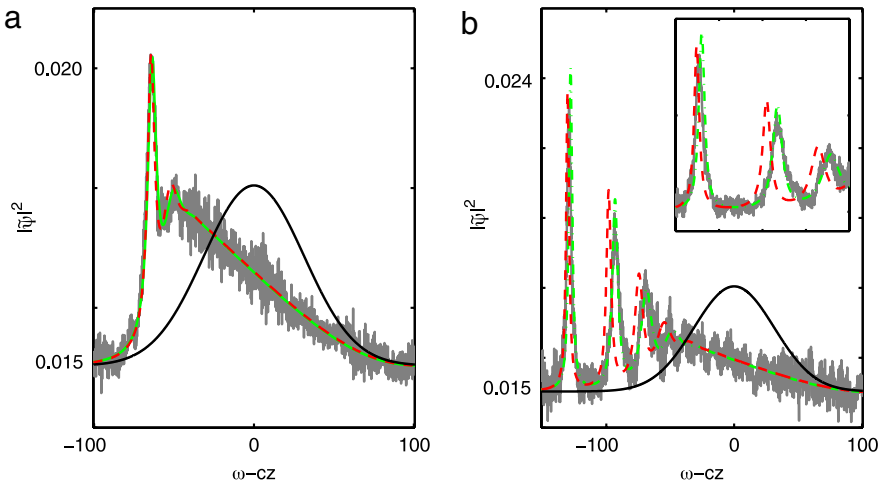


**Fig. 10.** Incoherent dispersive shocks with a Raman-like response function in the presence of a spectral background noise: The shock is regularized by the emission of incoherent Benjamin–Ono solitons. NLS (36), gray; WT Langmuir equation (44), green; Benjamin–Ono equation (57), dashed-red; initial condition (dark). ($\tau_R = 5\tau_0$, $\eta = 1$, (a) $z = 3 \times 10^5$, (b) $z = 7 \times 10^5$ in units of $L_{nl}$). The inset in (b) shows a zoom on the first three spectral peaks.
*Source:* From Ref. [120].

*(b) With background: Benjamin–Ono kinetic equation*

When the incoherent wave evolves in the presence of a significant background spectral noise, $n_\omega(z) = n_0 + \tilde{n}_\omega(z)$, a scale expansion of the convolution operator (53) with $\tilde{n}_\omega(z) \sim n_0/\tau_R$, leads to the singular integro-differential kinetic equation

$$\tau_R^2 \partial_z \tilde{n}_\omega - \gamma(1+\eta^2) n_0 \partial_\omega \tilde{n}_\omega = \gamma(1+\eta^2)\left(\tilde{n}_\omega \partial_\omega \tilde{n}_\omega - \frac{1}{\tau_R} n_0 \mathcal{H} \partial_\omega^2 \tilde{n}_\omega\right). \tag{57}$$

The second term in the lhs of this equation can be removed by a change of Galilean reference frame in frequency space, with 'velocity' $c = -\gamma(1+\eta^2) n_0/\tau_R^2$. Eq. (57) then recovers the integrable Benjamin–Ono equation, which admits soliton solutions and an infinite number of conserved quantities [124,123]. We just give here the simpler conserved quantities $N = \int \tilde{n}_\omega \, d\omega$, $Q = \int \tilde{n}_\omega^2 \, d\omega$, and the Hamiltonian structure

$$\tau_R^2 \partial_z \tilde{n}_\omega = \left(\frac{\delta H}{\delta \tilde{n}_\omega}\right)_\omega \tag{58}$$

with

$$H = \gamma(1+\eta^2) \int \left(\frac{n_0}{2}\tilde{n}_\omega^2 + \frac{1}{6}\tilde{n}_\omega^3 - \frac{n_0}{2\tau_R}\tilde{n}_\omega \mathcal{H} \partial_\omega \tilde{n}_\omega\right) d\omega. \tag{59}$$

The Benjamin–Ono equation was originally derived to model internal waves in stratified fluids [125,126]. Here, it provides the deterministic description of the averaged spectral dynamics of incoherent waves. Then the incoherent shock in Fig. 10 is regularized by the emission of genuine *incoherent BO solitons* in the stochastic wave spectrum.

A quantitative agreement (without adjustable parameters) has been obtained between the numerical simulations of the singular kinetic equations (56) and (57) and those of the WT Langmuir equation (44) for large values of $\tau_R/\tau_0$, consistently with the scaling expansion underlying the derivation of singular integro-differential kinetic equations. A remarkable agreement is also obtained for moderate values of $\tau_R/\tau_0$. The singular kinetic equations (56) and (57) thus provide a detailed deterministic description of the incoherent shocks observed in the simulations of the NLS (36) with a stochastic function $\psi(z, t)$, as illustrated by the good agreement between the corresponding simulations in Figs. 9–12.

*Exponential response: Inhibition of incoherent shocks*

*(a) Without background*

Contrarily to what one may expect from the reduced KdV equation (52), the formation of dispersive shocks does not constitute a generic feature of the WT Langmuir equation (44). We will illustrate this by considering the example of a purely exponential response function, $\bar{R}(t) = \exp(-t/\tau_R)/\tau_R$. In the limit $\tau_R/\tau_0 \gg 1$, the singular kinetic equation reads (see Appendix A.5)

$$\tau_R \partial_z n_\omega = -\gamma n_\omega \mathcal{H} n_\omega - \frac{\gamma}{\tau_R} n_\omega \partial_\omega n_\omega + \frac{\gamma}{2\tau_R^2} n_\omega \mathcal{H} \partial_\omega^2 n_\omega. \tag{60}$$

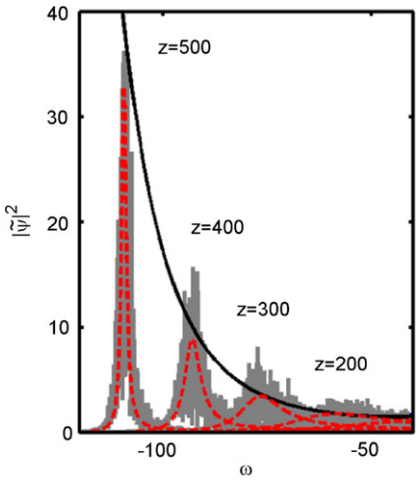


**Fig. 11.** Inhibition of incoherent shocks with an exponential response function. Without background spectral noise the spectrum exhibits a collapse-like behavior: NLS (36), gray; singular kinetic equation (60), dashed-red ($\tau_R = 5\tau_0$). The dark continuous line denotes the theoretical behavior $\sim 1/[z^2 n^0(\omega = \tilde{c}z)]$, with $\tilde{c} = -\gamma N/\tau_R$, predicted from the first term of Eq. (60) and the corresponding analytical solution (61).
*Source:* From Ref. [120].

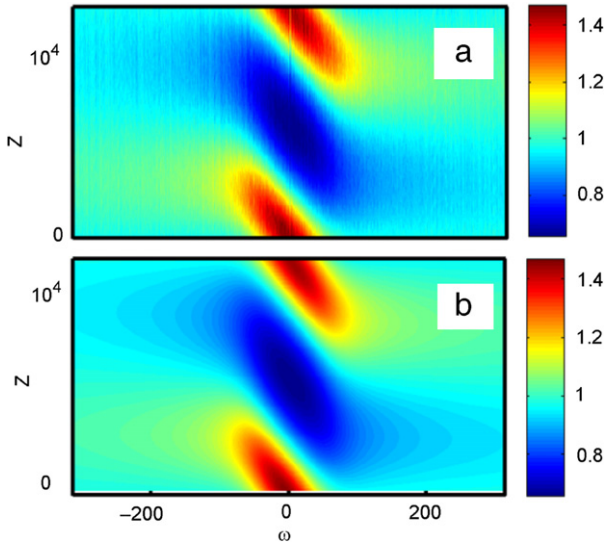


**Fig. 12.** Inhibition of incoherent shocks with an exponential response function. Instead of the collapse-like behavior (see Fig. 11), the presence of a background noise turns the dynamics periodic: NLS simulation of Eq. (36) (a), plot of the analytical solution (63) (b), $\tau_R = 2\tau_0$.
*Source:* From Ref. [120].

Note that the second-order Burgers term produces a shock towards the high-frequency components ($\omega > 0$), so that the leading-order term is the only one liable to produce a shock.

On the other hand, the second perturbative Burgers term produces a shock towards the high-frequency components ($\omega > 0$), so that the first term is the only one liable to produce a shock. Interestingly, the first term of (60) was considered as a one-dimensional model of the vorticity formulation of the 3D Euler equation of incompressible fluid flows [122]. In this work, the authors found an explicit analytical solution to the equation $\tau_R \partial_z n_\omega = -\gamma n_\omega \mathcal{H} n_\omega$. For a given initial condition $n_\omega(z = 0) = n^0_\omega$ the solution has the form

$$n_\omega(z) = \frac{4n^0_\omega}{\left(2 + (\gamma z/\tau_R)\mathcal{H} n^0_\omega\right)^2 + (\gamma z/\tau_R)^2 (n^0_\omega)^2}. \tag{61}$$

There is blow up if and only if there exists $\omega$ such that $n^0_\omega = 0$ and $\mathcal{H} n^0_\omega < 0$. Then the blow up distance $z_c$ is given by $z_c = -2\tau_R/[\gamma \mathcal{H} n^0_{\omega=\omega_0}]$, where $\omega_0$ is such that $n^0_{\omega_0} = 0$. If the initial condition is Lorentzian: $n^0_\omega = \frac{2N_0\sigma}{\sigma^2+\omega^2}$ with

$N_0 = (2\pi)^{-1}\int n^0_\omega d\omega$, then the solution propagates with constant shape and constant velocity

$$n_\omega(z) = \frac{2N_0\sigma}{\sigma^2 + (\omega - \tilde{c}z)^2},$$

with $\tilde{c} = -N_0\gamma/\tau_R$. However, if the initial condition decays faster than a Lorentzian, the spectrum exhibits a collapse-like dynamics, which is ultimately arrested by a small background noise. In this process, the spectrum moves at velocity $\tilde{c}$, while its peak amplitude increases according to $\sim 4\tau_R^2/[\gamma^2 z^2 n^0(\omega = \tilde{c}z)]$. This property is confirmed by the simulations of the NLS equation, as illustrated in Fig. 11.

*(b) With background*

This collapse-like behavior changes in a profound way when the incoherent wave evolves in the presence of a significant spectral background. A scale expansion of the convolution operator in the WT Langmuir equation (44) with $n_\omega(z) = n_0 + \tilde{n}_\omega(z)$ and $\tilde{n}_\omega(z) \sim n_0/\tau_R$ (see Appendix A.5), leads to the singular kinetic equation

$$\tau_R\partial_z\tilde{n}_\omega = -\gamma(n_0 + \tilde{n}_\omega)\mathcal{H}\tilde{n}_\omega - \frac{\gamma}{\tau_R}(n_0 + \tilde{n}_\omega)\partial_\omega\tilde{n}_\omega + \frac{\gamma n_0}{2\tau_R^2}\mathcal{H}\partial^2_\omega\tilde{n}_\omega. \tag{62}$$

Since $n_0 \gg \tilde{n}_\omega(z)$, the spectral dynamics of the incoherent wave is dominated by the first linear term in the rhs of (62), which admits the following analytical solution,

$$\tilde{n}_\omega(z) = \cos\big(\gamma n_0 z/\tau_R\big)\tilde{n}^0_\omega - \sin\big(\gamma n_0 z/\tau_R\big)\mathcal{H}\tilde{n}^0_\omega, \tag{63}$$

where $\tilde{n}^0_\omega = \tilde{n}_\omega(z = 0)$ refers to the initial condition. This periodic behavior of the incoherent spectrum has been found in quantitative agreement with the simulations of the whole singular kinetic equation (62), as well as with those of the WT Langmuir equation (44) and the NLS equation (36), as illustrated in Fig. 12.

### 3.3. Long-range: Non-Hamiltonian Vlasov equation

In the previous Section 3.2.3 we have considered the role of long-range temporal responses for an incoherent wave characterized by a stationary (homogeneous) statistics. Here we will study statistically nonstationary random waves in the presence of a highly noninstantaneous nonlinear response. We will see that the dynamics of the incoherent wave is ruled by a long-range Vlasov-like kinetic equation, whose self-consistent potential is constrained by the causality condition of the response function, which breaks the Hamiltonian structure of the Vlasov equation.

In analogy with the study of long-range responses in the spatial domain (Section 2), we study here a long-range noninstantaneous response $R(t)$ in the regime $\tau_R/\tau_0 \gg 1$. We assume that the response function has the form $R(t) = \varepsilon R^{(0)}(\varepsilon t)$ and we look for the autocorrelation function in the multiscale form $B(t, \tau, z) = B^{(0)}(\varepsilon t, \tau, \varepsilon z) + O(\varepsilon)$, with $B^{(0)}(\varepsilon t, \tau, \varepsilon z) = (2\pi)^{-1}\int n^{(0)}_\omega(\varepsilon t, \varepsilon z)\exp(-i\omega\tau)\, d\omega$. In these conditions, we derive in Appendix A.6 the temporal version of the long-range Vlasov equation

$$\partial_z n_\omega(t, z) + \partial_\omega\tilde{k}_\omega(t, z)\,\partial_t n_\omega(t, z) - \partial_t\tilde{k}_\omega(t, z)\,\partial_\omega n_\omega(t, z) = 0, \tag{64}$$

where the generalized dispersion relation reads

$$\tilde{k}_\omega(t, z) = k(\omega) + V(t, z), \tag{65}$$

with $k(\omega) = \beta\omega^2$ and the effective potential

$$V(t, z) = -\gamma\int R(t - t')N(t', z)\, dt'. \tag{66}$$

The intensity profile of the incoherent wave is $N(t, z) = B(t, \tau = 0, z) = (2\pi)^{-1}\int n_\omega(t, z)\, d\omega$. Eq. (64) conserves

$$\mathcal{N} = (2\pi)^{-1}\iint n_\omega(t, z)d\omega dt, \tag{67}$$

and more generally $\mathcal{M} = \iint f[n]d\omega dt$ where $f[n]$ is an arbitrary functional of $n$.

*Non-Hamiltonian structure of the Vlasov equation*

Because of the causality property of $R(t)$, Eq. (64) is no longer Hamiltonian. However, one can decompose the Vlasov equations (64)–(66)into a Hamiltonian contribution and a non-conservative contribution. Indeed, according to the

decomposition given in (37), $\tilde{R}(\omega) = \tilde{U}(\omega) + ig(\omega)$, the response function splits into the sum of an even contribution, $U(t)$, and an odd contribution, $G(t)$, i.e., $R(t) = U(t) + G(t)$, where

$$U(t) = \frac{1}{2\pi} \int \tilde{U}(\omega)\ \exp(-i\omega t)\, d\omega, \tag{68}$$

$$G(t) = \frac{i}{2\pi} \int g(\omega)\ \exp(-i\omega t)\, d\omega. \tag{69}$$

Accordingly, the Vlasov equation (64) can be written in the following form

$$\partial_z n_\omega(t,z) + \partial_\omega k_\omega(t,z)\, \partial_t n_\omega(t,z) - \partial_t V_U(t,z)\, \partial_\omega n_\omega(t,z) = \partial_t V_G(t,z)\, \partial_\omega n_\omega(t,z), \tag{70}$$

where $V_U(t,z) = -\gamma \int U(t-t')N(t',z)\, dt'$ and $V_G(t,z) = -\gamma \int G(t-t')N(t',z)\, dt'$. The lhs of Eq. (70) thus refers to a conservative Vlasov equation, while the rhs of (70) may be viewed as a non-conservative 'collision' term, which leads to a spectral shift of the wave. More precisely, it can be shown that the total Hamiltonian, $\mathcal{H} = \frac{1}{2\pi} \iint k(\omega)\, n_\omega(t,z)\, dt d\omega + \frac{1}{2} \int V(t,z) N(t,z)\, dt$, evolves according to

$$\partial_z \mathcal{H}(z) = -\frac{\beta}{\pi} \int \partial_t V_G(t,z) \int \omega n_\omega(t,z)\, d\omega\, dt. \tag{71}$$

It becomes apparent that $\mathcal{H}$ becomes a conserved quantity in the spatial case (see Section 2.2.1), where the odd contribution to the response function vanishes, $G(t) = 0$, so that $V_G(t,z) = 0$. The spectral shift of a wave-packet can be determined through the analysis of the total momentum, $\mathcal{P}(z) = (2\pi)^{-1} \iint \omega n_\omega(t,z)\, dt\, d\omega$, which is related to the barycenter of the spectrum, $\langle\omega\rangle = \mathcal{P}/\mathcal{N}$. An equation for the momentum can easily be obtained from the Vlasov equation (70)

$$\partial_z \mathcal{P}(z) = \int V_G(t,z)\, \partial_t N(t,z)\, dt, \tag{72}$$

which confirms that only the non-conservative potential contribution, $V_G(t,z)$, leads to a spectral shift. Remarking furthermore that $G(t)$ can expressed in terms of the response function, $G(t) = \frac{1}{2}\big[R(t) - R(-t)\big]$, it becomes easy to see that a focusing (defocusing) nonlinearity leads to a spectral red-shift, $\partial_z \mathcal{P} < 0$ (blue-shift, $\partial_z \mathcal{P} > 0$). We can remark that this dependence of the spectral shift on the sign of the nonlinearity is also apparent in the WT Langmuir [see Eqs. (43) or (44)]. Note that a spectral blue-shift induced by a defocusing delayed nonlinearity is known to occur, e.g., in plasma [32,212], in which, however, the total power of the wave is no longer conserved.

It is also interesting to analyze the position of the wave-packet in the time domain, $\mathcal{T}(z) = (2\pi)^{-1} \iint t\, n_\omega(t,z)\, dt\, d\omega$, which is related to the barycenter by $\langle t\rangle = \mathcal{T}/\mathcal{N}$. The evolution of $\mathcal{T}(z)$ can easily be obtained from the Vlasov equation (70)

$$\partial_z \mathcal{T}(z) = 2\beta \mathcal{P}(z), \tag{73}$$

so that $\mathcal{T}(z) = \mathcal{T}(0) + 2\beta \int_0^z \mathcal{P}(z')\, dz'$. Accordingly, propagation in the normal (anomalous) dispersion regime in the presence of a focusing (defocusing) nonlinearity leads to an acceleration of the wave-packet towards $t > 0$. Eq. (73) also reveals that there is a close relation between the spectral shift and the temporal shift of a wave-packet. This can easily be interpreted by remarking that a spectral shift combined with group-velocity dispersion leads to an acceleration of the wave-packet. These aspects will be discussed in detail in Section 3.3.4 through the analysis of the dynamics of incoherent soliton states.

We finally remark that, in spite of this spectral shift of the incoherent wave given in Eq. (72), the Vlasov equations (64)–(66) predicts the existence of a genuine incoherent MI in the temporal domain [18], a property that will be discussed in Section 3.3.3.

### 3.3.1. Instantaneous limit

To be complete, we briefly comment here the limit of an instantaneous response function. Making use of the assumptions that the incoherent wave exhibits a quasi-stationary statistics and that it evolves into the weakly nonlinear regime, one obtains the traditional form of the Vlasov equation (64) with the self-consistent potential

$$V(t,z) = -2\gamma N(t,z). \tag{74}$$

This self-consistent potential is nothing but the temporal counterpart of the spatial potential discussed above in Section 2.2.2 in the limit of a purely local nonlinear response. In particular, the factor 2 in the effective potential (74) has the same origin as in Eq. (19).

### 3.3.2. Highly noninstantaneous response: Linear limit

The limit of a highly noninstantaneous response function corresponds to the temporal counterpart of the highly nonlocal limit discussed above in the spatial case (see Section 2.3.3). Indeed, in the limit $\tau_R \gg \Delta$, the response function can be

extracted from the convolution integral in the effective potential (66), which thus leads to the temporal Vlasov equation (64) with the potential

$$V(t) = -\gamma \mathcal{N} U(t). \tag{75}$$

As for the highly nonlocal limit, the temporal response function $U(t)$ plays the role of the effective potential, so that the Vlasov equation recovers a linear kinetic equation. We remark that the dynamics of *coherent* optical waves in a highly noninstantaneous response nonlinear medium has been recently explored theoretically in Ref. [213], in the framework of gas- or liquid-filled photonic crystal fibers. By deriving a linear Schrödinger wave equation analogous to that discussed above in Eq. (25) in the spatial domain, the authors of Ref. [213] predicted that a highly noninstantaneous responding medium can support the existence of coherent soliton solutions. These soliton solutions are the temporal counterpart of the so-called 'accessible solitons' in the spatial case [111,100,101].

### 3.3.3. Incoherent modulational instability

According to the Vlasov equation derived here above, we will see that the incoherent wave exhibits an incoherent MI in the presence of a highly non-instantaneous nonlinear response, i.e., $\tau_R/\tau_0 \gg 1$. This result seems to be completely analogous to the spatial case considered in Section 2.3.4. However, contrary to the spatial case, we will see that, because of the causality condition of the response function, temporal incoherent MI can also take place in the *normal* dispersion regime.

Let us note that this result of temporal incoherent MI is in some sense an unexpected result. Indeed, as discussed in detail above in this section in the framework of the WT Langmuir formalism, one would expect that a statistically stationary incoherent wave exhibit a spectral red-shift during its propagation. This is a well-known fact when one considers the example of the Raman effect in optical fibers. However, we will see that a *highly* noninstantaneous response leads to a genuine process of incoherent MI of the wave, which is characterized by the growth of two symmetric MI bands within the spectrum of the incoherent wave.

Proceeding in a way completely analogous to the spatial incoherent MI, we linearize the Vlasov equation with $n_\omega(t,z) = n^0_\omega + \delta n_\omega(t,z)$. Then assuming a Lorentzian-shaped initial spectrum, $n^0_\omega = 2N_0\Delta\omega/(\omega^2+(\Delta\omega)^2)$ [i.e., $N_0 = (2\pi)^{-1}\int n^0_\omega d\omega$], one obtains

$$\lambda(\Omega) = -2\Delta\omega|\beta\Omega| + |\Omega|\sqrt{2\beta\gamma N_0 \tilde{R}(\Omega)}, \tag{76}$$

where the incoherent MI gain reads $g_{\mathrm{MI}}(\Omega) = 2\Re[\lambda(\Omega)]$. This expression of MI gain is formally analogous to the expression considered in the spatial case in Eq. (28). However, because of the causality property of the response function $R(t)$, its Fourier transform is complex, $\tilde{R}(\omega) = \tilde{U}(\omega) + ig(\omega)$. Recalling that $\tilde{U}(\omega)$ is even and $g(\omega)$ odd, the MI gain $g_{\mathrm{MI}}(\Omega)$ is always even, which means that incoherent MI is characterized by the growth of two symmetric sidebands. Another consequence of the fact that $\tilde{R}(\omega)$ is complex is that incoherent MI can also occur in the normal dispersion regime, i.e., for $\gamma\beta < 0$. This is illustrated in Fig. 13, which reports the incoherent MI gains in the anomalous and normal dispersion regimes. In this example we considered a damped harmonic oscillator response, $\bar{R}(t) = \frac{1+\eta^2}{\eta\tau_R}\sin(\eta t/\tau_R)\exp(-t/\tau_R)$, with the value of $\eta = 2.6$ corresponding to the Raman effect in optical fibers. We remark that the MI gain curves are of a different nature in the normal dispersion regime as compared to the usual MI gain in the anomalous dispersion regime. In particular, in the normal dispersion regime, incoherent MI develop within a narrow spectral band, a feature that may favor the formation of temporal incoherent solitons (see Section 3.3.4).

*Difference with incoherent MI in instantaneous response nonlinear media*

To conclude this discussion on temporal incoherent MI, we underline its fundamental different nature with respect to incoherent MI considered in *instantaneous* response Kerr media [165]. In the limit $\tau_R \to 0$, incoherent MI can only take place if the spectral width of the incoherent wave is smaller than the MI frequency, $\Delta\omega \ll \omega_{\mathrm{MI}}$ [165]. This means that temporal modulations associated to MI are more rapid than the time correlation, $t_c \gg \tau_0$, i.e., MI modulations take place within each individual fluctuation of the incoherent wave. This is in contrast with the MI spectral gains reported in Fig. 13, in which the optimal MI frequency gets much smaller than the spectral bandwidth, $\omega_{\mathrm{MI}} \ll \Delta\omega$ as the nonlinearity becomes noninstantaneous (i.e., as $\tau_R$ increases). This means that incoherent MI manifests itself by a slow modulation of the whole random wave profile, i.e., the modulation frequency is smaller than the spectral bandwidth, $\omega_{\mathrm{MI}} \ll \Delta\omega$. This feature has been confirmed by the numerical simulations of the NLS equation (36) and the corresponding long-range Vlasov equation (64) in Ref. [18].

### 3.3.4. Incoherent solitons in normal dispersion

In this section we study temporal incoherent solitons in highly noninstantaneous response nonlinear media by considering the temporal version of the long-range Vlasov equations (64)–(66). We will see that, contrarily to the usual temporal soliton, which is known to require a focusing nonlinearity with anomalous dispersion, a highly noninstantaneous nonlinear response leads to incoherent soliton structures which require the inverted situation. In the focusing regime (and

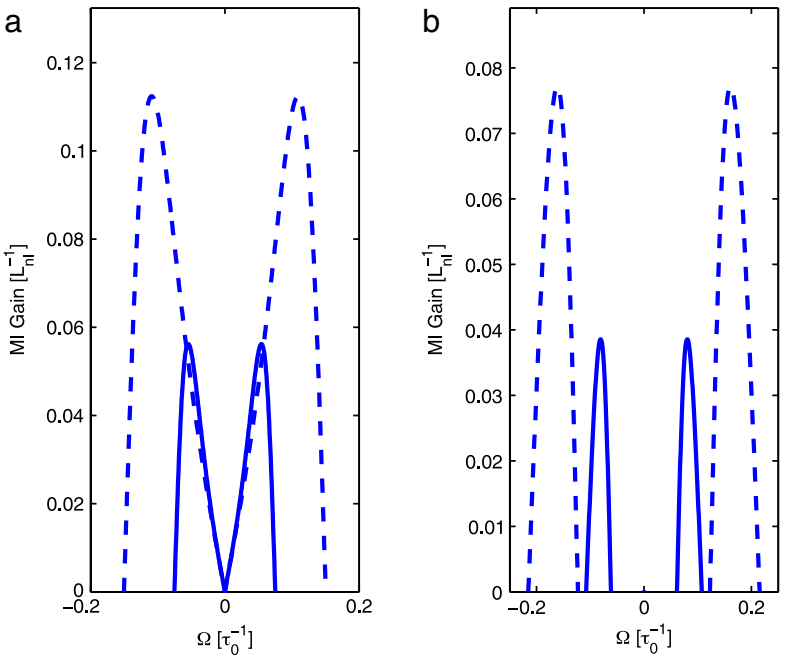


**Fig. 13.** Temporal incoherent MI: Contrarily to the spatial case, incoherent MI occurs in both normal and anomalous dispersion regimes. Plots of incoherent MI gains given by Eq. (76). (a) Anomalous dispersion regime ($\beta\gamma > 0$): $\tau_R = 20\tau_0$ (continuous), $\tau_R = 40\tau_0$ (dashed); (b) normal dispersion regime ($\beta\gamma < 0$): $\tau_R = 20\tau_0$ (dashed), $\tau_R = 40\tau_0$ (continuous). In both cases $\Delta\omega = 0.5\tau_0^{-1}$.

anomalous dispersion) the incoherent wave-packet experiences an unlimited spreading, whereas in the defocusing regime (still with anomalous dispersion) the incoherent wave-packet exhibits a self-trapping [170]. These counterintuitive results are explained in detail by the long-range Vlasov equations (64)–(66).

*Numerical simulations*

In order to make the comparison with spatial nonlocal effects easier, we assume that the wave propagates in the anomalous dispersion regime ($\beta > 0$), so that the diffraction parameter $\alpha$ in Eq. (1) plays the same role as the dispersion parameter $\beta$ in equation (36), and we consider separately the focusing ($\gamma > 0$) and defocusing ($\gamma < 0$) regimes of interaction. We report in the left columns of Figs. 14 and 15 the evolutions of the spectrograms of an initial super-Gaussian incoherent wave-packet which has been obtained by integrating numerically the NLS equation (36). The corresponding spectral and temporal FWHM are $\Delta_\omega = 1.257$ and $\Delta_t = 200$, respectively. In Fig. 14, $z$ is in units of $L_{nl} = 1/(|\gamma|\rho)$, where $\rho = \mathcal{N}/T$, $T$ being the size of the numerical temporal window, as introduced in Section 3.1.1. Note however that, since the initial condition is localized in time (non-stationary statistics), $L_{nl}$ no longer denotes the familiar nonlinear length scale. We considered in Fig. 14 a Gaussian-like response function, $\bar{R}(t) = t^2 \exp[-t^2/(2\tau_R^2)]/(\tau_R^3\sqrt{\pi/2})$, while similar results are obtained with an exponential-shaped response function. As we will see, the prefactor $t^2$ plays a role in the formation of incoherent solitons. It also avoids discontinuities in the derivative of $R(t)$ at $t = 0$, which is important in order to accurately simulate the Vlasov equation (64).

We remark in Fig. 14 that in the focusing regime ($\gamma > 0$), the incoherent wave-packet exhibits a delocalization process characterized by an unlimited temporal spreading of the pulse and a slow process of spectral broadening. In contrast with this dispersive behavior, in the defocusing regime ($\gamma < 0$, see Fig. 15) the incoherent wave-packet exhibits a phenomenon of self-trapping, which is very robust and thus preserved for long propagation distances. In the example of Fig. 15 the incoherent soliton loses less than 0.1% of its power while it propagates over a propagation distance of more than $z = 10^3 L_{nl}$. As thoroughly discussed in this section, the spectral shift of the optical wave simply results from the causality property of the response function, and manifests itself as a red- (blue-)shift in the focusing (defocusing) nonlinear regime, a feature that has been discussed through Eq. (72). We will see below that, as a result of group-velocity dispersion, this spectral-shift leads to an acceleration of the incoherent wave-packet, which in turn is responsible for its self-trapping.

*Vlasov interpretation*

This phenomenon of incoherent self-trapping is explained in detail by the long-range Vlasov equation. We report in the right columns of Figs. 14 and 15 the simulations of the Vlasov equation (64) starting from the same initial condition as the NLS equation (36). We underline that a quantitative agreement is obtained between the NLS and Vlasov simulations without using adjustable parameters, which corroborates the fact that the 'long-range' Vlasov equation (64) provides an

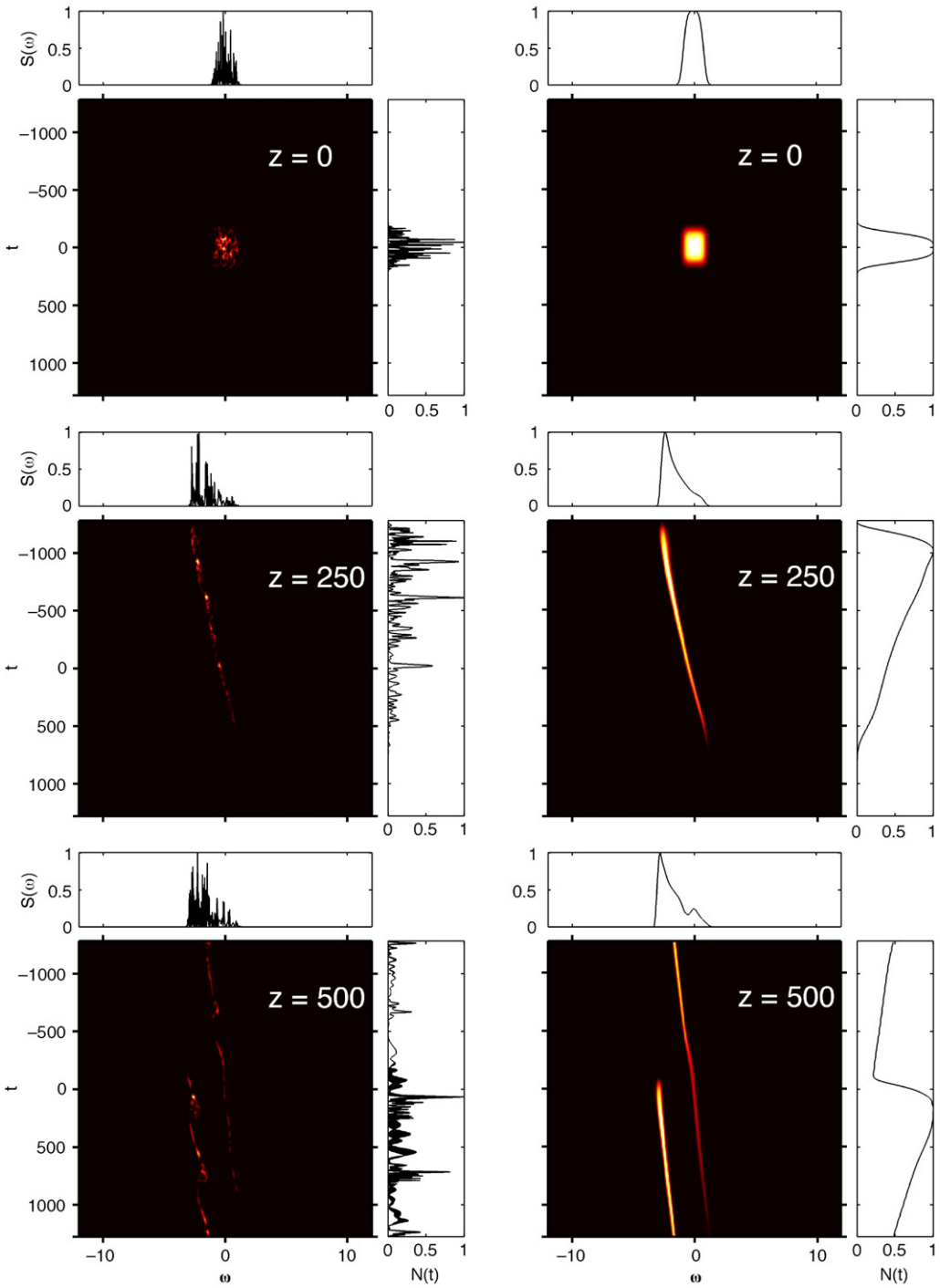


**Fig. 14.** Spreading of a localized initial incoherent wave-packet: Numerical simulations of the NLS equation (36) (left column) and of the Vlasov equations (64)–(66) (right column) with a focusing nonlinearity in the anomalous dispersion regime, $\beta\gamma > 0$ [$\tau_R = 200\tau_0$, $z$ is in units of $L_{nl}$]. The temporal numerical window is $T = 2560\tau_0$, $t$ and $\omega$ are in units of $\tau_0$ and $\tau_0^{-1}$, respectively.
*Source:* From Ref. [170].

'exact' statistical description of the random nonlinear wave, as discussed above in Section 2.3.2. Fig. 16 reveals that, after a transient ($z \sim 300L_{nl}$), the wave-packet adopts an invariant profile characterized by a linear spectral shift, which in turn induces a constant IS acceleration (parabolic trajectory) in the temporal domain. More specifically, let us denote by $\alpha_0$ the soliton velocity in frequency space—the parameter $\alpha_0$ will appear to have a specific meaning below in Eq. (81). As discussed above through Eq. (72), the momentum evolves linearly as $\mathcal{P}(z) = \mathcal{N}\alpha_0 z$. Then Eq. (73) explicitly shows that,

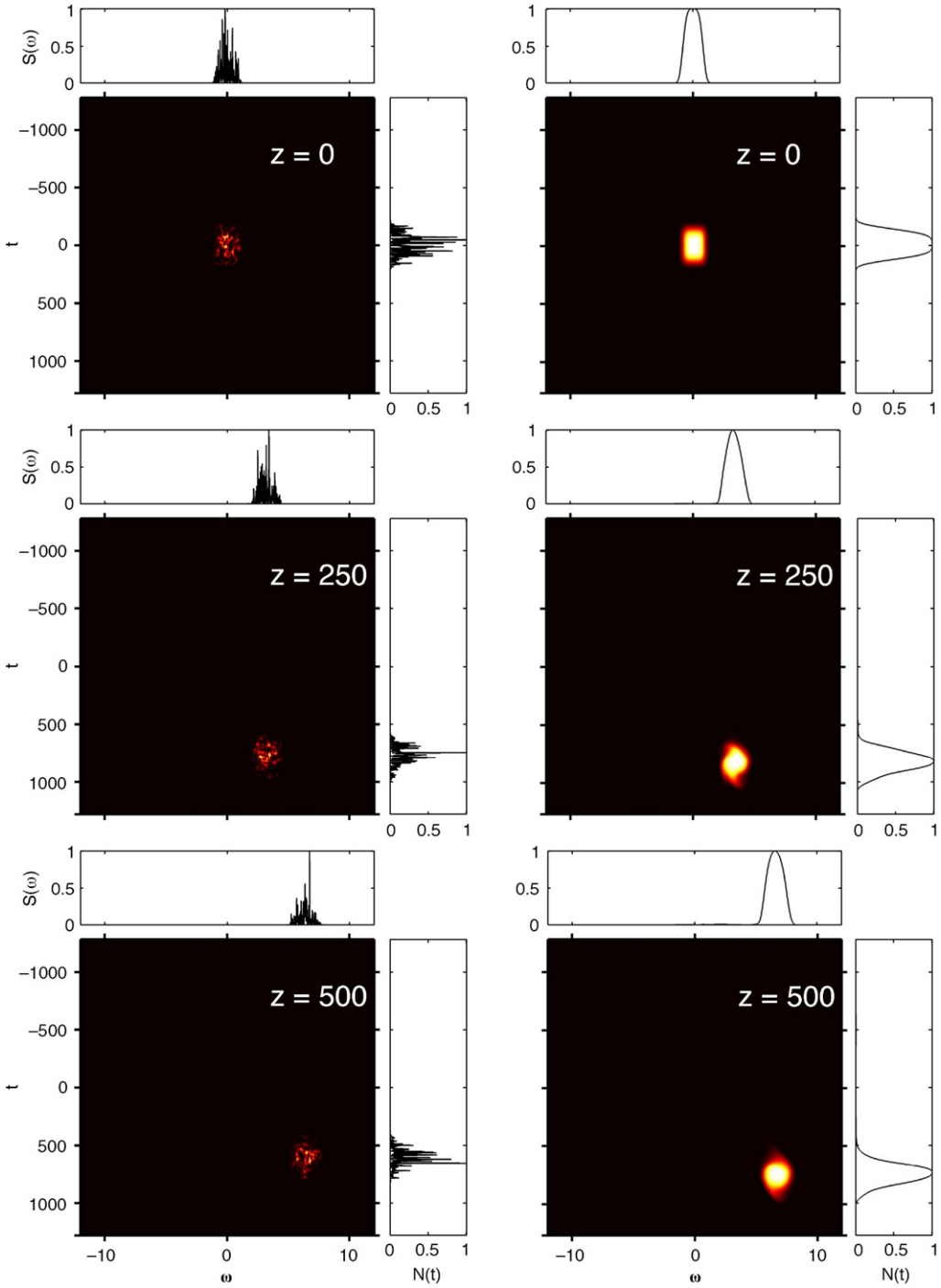


**Fig. 15.** Temporal incoherent solitons: Numerical simulations of the NLS equation (36) (left column) and of the Vlasov equations (64)–(66) (right column) with a defocusing nonlinearity, in the anomalous dispersion regime—parameters and initial conditions are the same as in Fig. 14, except that we are now in the defocusing regime ($\beta\gamma < 0$). After a transient ($z \sim 300L_{nl}$), the incoherent wave-packet evolves into an incoherent soliton state (see Fig. 16). *Source:* From Ref. [170].

when combined with group-velocity dispersion, this linear spectral shift induces an acceleration of the incoherent soliton in the temporal domain given by Eq. (73)

$$\mathcal{T}(z) = \mathcal{T}(0) + \beta\mathcal{N}\alpha_0 z^2. \tag{77}$$

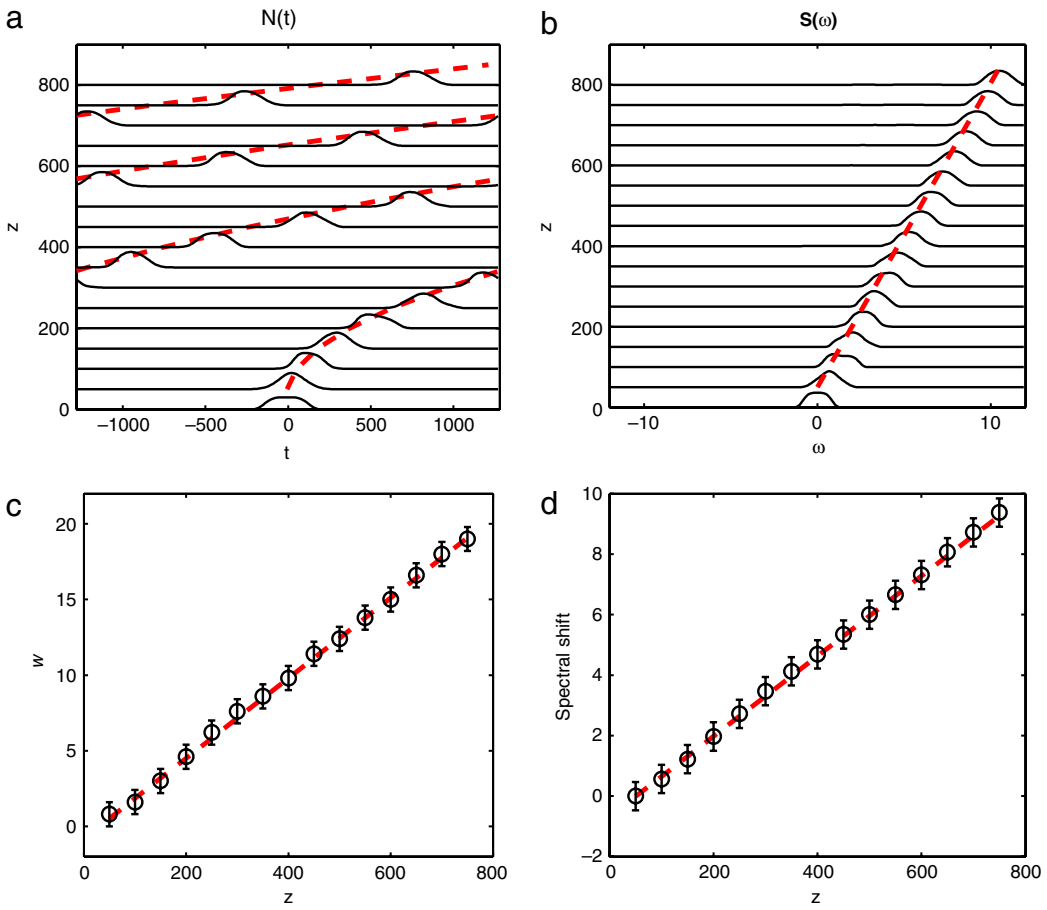


**Fig. 16.** Constant acceleration of temporal incoherent solitons: Parabolic trajectory of the intensity profile $N(t,z) = (2\pi)^{-1}\int n_\omega(t,z)d\omega$ (a), and evolution of the spectral profile $S(\omega,z) = \int n_\omega(t,z)dt$ (b), corresponding to the simulation of the Vlasov equation (64) reported in Fig. 15 (right column). The linear increase of the incoherent soliton velocity $w$ (constant acceleration) (c), results from the linear spectral shift of the incoherent soliton (d): The slope of the dashed red line in (c) is twice the corresponding slope in (d), as expected from the group-velocity dispersion law, $\partial_\omega k(\omega) = 2\beta\omega$ (note that $\beta = 1$ when $k$ and $\omega$ are expressed in units of $L_{nl}^{-1}$ and $\tau_0^{-1}$ respectively). $z$, $t$, $\omega$ are in units of $L_{nl}$, $\tau_0$, $\tau_0^{-1}$, respectively.
*Source:* From Ref. [170].

Both phenomena of linear spectral shift and constant acceleration of the incoherent soliton are clearly visible in the numerical simulations, as illustrated in Fig. 16.

*Temporal vs. spatial incoherent solitons*

To discuss the mechanism underlying the formation of the incoherent soliton, it is instructive to comment first an analogy with a *n*onlocal spatial response. Contrary to temporal effects, nonlocal spatial effects are not constrained by the causality condition, so that the spatial response function $U(x)$ is even. Assuming that the beam intensity is approximately symmetric ($N(x)$ is even), then the self-consistent potential $V(x) = -\gamma U * N$ is also even. Then as discussed above in Section 2.3.5, in the focusing regime ($\gamma > 0$), the optical beam induces an attractive potential $V(x) < 0$, so that the beam is guided by its own induced potential. Conversely, in the defocusing regime ($\gamma < 0$) the repelling potential leads to the expected beam spreading. This is illustrated schematically in Fig. 17(a)–(b), in which the beam intensity $N(x)$ has been obtained by integrating the spatial Vlasov equation with a Gaussian response function $U(x)$ (see Ref. [27] for details).

*Vlasov approach: Noninertial reference frame*

As a result of the causality property of $R(t)$, the self-consistent potential $V(t)$ is shifted towards $t < 0$ in the temporal domain (see Fig. 17(c)–(d)). Moreover, as commented above through Fig. 16, the spectral-shift of the wave-packet, with spectral velocity $\alpha$, leads to a constant acceleration of the IS. It thus proves convenient to study the dynamics of the wave-packet in its own accelerating reference frame

$$\xi = z, \qquad \tau = t - \alpha\beta z^2, \qquad \Omega = \omega - \alpha z. \tag{78}$$

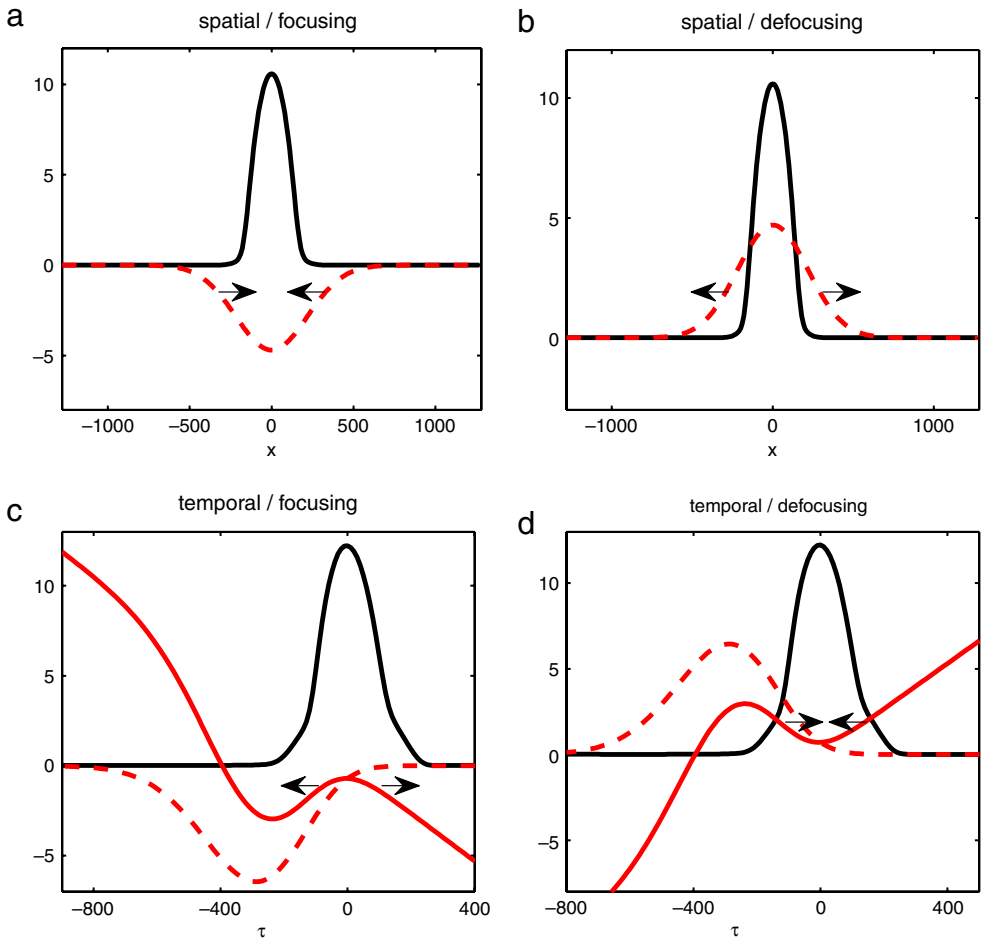


**Fig. 17.** Mechanism underlying the formation of temporal incoherent solitons: Intensity profile $N(x)$ (continuous dark line) and corresponding self-consistent potential $V(x) = -\gamma U * N$ (dashed red line), in the case of a spatial nonlocal nonlinearity in the focusing (a), and defocusing (b), regimes. Intensity profile $N(\tau)$ obtained by integrating numerically the Vlasov equation (79) (continuous dark line), corresponding self-consistent potential $V(\tau) = -\gamma R * N$ (dashed red line), and effective potential $V_{\rm eff}(\tau)$ [Eq. (80)] (continuous red line) in the accelerating reference frame, in the case of a temporal noninstantaneous nonlinearity in the focusing (c), and defocusing (d), regimes. The arrows indicate the 'particle motions' in the effective self-consistent potentials $V_{\rm eff}(\tau)$: The non-inertial fictitious force inhibits (c) (induces (d)) the self-trapping in the defocusing (focusing) regime.
*Source:* From Ref. [170].

In this non-inertial reference frame the Vlasov equation (64) reads

$$\partial_\xi n_\Omega(\tau,\xi) + 2\beta\Omega\,\partial_\tau n_\Omega(\tau,\xi) - \partial_\tau V_{\rm eff}(\tau,\xi)\,\partial_\Omega n_\Omega(\tau,\xi) = 0. \tag{79}$$

This equation remarkably *reveals the existence of an effective self-consistent potential*

$$V_{\rm eff}(\tau,\xi) = V(\tau,\xi) + \alpha\tau, \tag{80}$$

where $V(\tau,\xi) = -\gamma\int_{-\infty}^{+\infty} R(\tau-\tau')\,N(\tau',\xi)\,d\tau'$ just refers to the self-consistent potential of the original Vlasov equation (64) written with the new variables (78). The linear part of the potential in (80) finds its origin in the fictitious force which results from the non-inertial nature of the reference frame. It is this fictitious force which prevents the IS structure from dispersing towards the direction of increasing $\tau$. Note that this force is analogous to the effective gravity mimicked by an elevator, an analogy that was commented in Ref. [214].

This fictitious force due to the accelerating reference frame explains both phenomena of self-trapping with a defocusing nonlinearity, as well as the inhibition of self-trapping with a focusing nonlinearity. Let us first discuss the defocusing regime. Recalling that the potential is induced by the wave-packet itself, an IS can only form provided that *the self-induced potential* $V_{\rm eff}(\tau)$ *has a local minimum at the pulse center, i.e., at* $\tau = 0$ *in the accelerating reference frame of the IS*. Contrary to the spatial case (Fig. 17(a)), it seems that this condition cannot be satisfied in the temporal case, since the causality condition shifts the potentials towards $\tau < 0$. However, in the defocusing regime, a local minimum can be restored at $\tau = 0$ thanks to the fictitious force due to the non-inertial reference frame, as illustrated in Fig. 17(d). More precisely, one can Taylor expand the effective potential $V_{\rm eff}(\tau) = a + (b+\alpha)\tau + c\tau^2 + \mathcal{O}(\tau^3)$ at $\tau = 0$, where $b < 0$ in the defocusing regime and $c > 0$

if the nonlinear response is slow enough (see Fig. 17(d)). In these conditions the particular choice $\alpha_0 = -b$ guarantees that $V_{\rm eff}(\tau)$ has a local minimum at $\tau = 0$ (see Fig. 17(d)). In other words, *the system spontaneously selects the amount of spectral shift,*

$$\alpha_0 = -\partial_\tau V\,|_{\tau=0}, \tag{81}$$

*and hence the amount of soliton acceleration, $2\beta\alpha_0$, in such a way that the effective self-consistent potential $V_{\rm eff}(\tau)$ admits a local minimum at $\tau = 0$.* This is confirmed by the numerical simulations of the Vlasov equation (79) reported in Fig. 17(d), in which the value of $\alpha_0 = 0.01325$ used to plot $V_{\rm eff}(\tau) = V(\tau) + \alpha_0\tau$ has been determined from the spectral shift measured in Fig. 16(d).

Note however that the potential barrier in the negative $\tau$ axis is characterized by a limited depth, so that highly energetic particles can overcome such barrier to escape from the localized incoherent soliton. Then depending on the initial condition and on the particular form of the response function, the phenomenon of incoherent self-trapping can be more or less efficient. In particular, if one assumes $N(t)$ approximately Gaussian with variance $\Delta^2$ and $\bar{R}(t) \sim t^\nu \exp[-t^2/(2\tau_R^2)]$, the condition $c > 0$ reads $\tau_R > \Delta/\sqrt{\nu}$. This indicates that, as $\nu$ decreases, incoherent solitons are no longer generated, a feature that has been confirmed by the numerical simulations of the NLS equation (36).

Let us now discuss the focusing regime, which is characterized by a red-shift of the wave-packet, $\alpha < 0$. Following the same reasoning as above and remarking that we now have $b > 0$ and $c < 0$, the choice $\alpha_0 = -b$ still leads to an extremum of $V_{\rm eff}(\tau)$ at $\tau = 0$. However, contrary to the defocusing regime, this extremum refers to a local maximum, as illustrated in Fig. 17(c). Note that, in order to clearly differentiate the focusing and defocusing regimes, the incoherent soliton profile $N(\tau)$ of Fig. 17(d) has been used in Fig. 17(c) to calculate $V(\tau)$ and $V_{\rm eff}(\tau)$ in the focusing case. Actually, in the focusing regime, there is no value of $\alpha$ such that $V_{\rm eff}(\tau)$ has a local minimum at $\tau = 0$. The local maximum around $\tau = 0$ then plays the role of a repelling potential, which explains the temporal broadening of the incoherent pulse: The 'unstable particles' located near by $\tau = 0$ are either attracted towards the local minimum at $\tau < 0$, or either pushed towards $\tau > 0$ by the non-inertial force (see Fig. 17(c)).

### 3.3.5. Spectral long-range interaction due to a highly noninstantaneous response

As discussed above in this section through the WT Langmuir formalism, one may expect that the spectral dynamics of an incoherent wave should be described by the (Raman-like) spectral gain curve, $g(\omega)$. This is indeed what happen when one deals with a short-range interaction, $\tau_R \sim \tau_0$. In particular, the typical bandwidth of $g(\omega)$, say $\Delta\omega_g \sim 1/\tau_R$, denotes the characteristic interaction range in frequency space. However, as described by the long-range Vlasov formalism, the spectral dynamics of incoherent waves is no longer captured by the spectral gain function $g(\omega)$ in the presence of a highly noninstantaneous response of the nonlinearity. Indeed, a long-range interaction in the temporal domain, $\tau_R \gg \tau_0$, should lead to a short-range interaction in frequency space, $\Delta\omega_g \sim 1/\tau_R \ll 1/\tau_0$. Conversely, we will see here below that a long-range interaction in the time domain implies a long-range interaction in the spectral domain, i.e., an interaction whose spectral range is of order $\Delta\omega_{int} \sim 1/\tau_0 \gg \Delta\omega_g$ [215].

This spectral long-range behavior can easily be discussed through a qualitative analysis of the temporal Vlasov equation. Let us denote by $\Delta\omega_{int}$ and $\Delta t \sim \tau_R$ the typical spectral and temporal widths of an incoherent wave-packet, such as e.g., an incoherent soliton. We consider a typical (soliton-like) evolution in which linear and nonlinear effects [i.e., second and third terms in (64)], are of the same order of magnitude: $2\beta\omega\partial_t n_\omega(t,z) \sim \partial_t V \partial_\omega n_\omega(t,z)$, or $\Delta\omega_{int}^2 \sim |V|/|\beta| = |\gamma/\beta| R * N$, where $*$ denotes the temporal convolution product. To qualitatively assess the potential $V(t)$, it proves convenient to rescale the functions by introducing the small parameter $\varepsilon = 1/\tau_R \ll 1$, $R(t) = \varepsilon R_0(\varepsilon t)$ and $N(t) = \rho T \varepsilon N_0(\varepsilon t)$, where the numerical temporal window $T$ scales as $1/\varepsilon = \tau_R$. We have $|V|(t) \sim |\gamma|\rho R_0 * N_0$. Introducing the reduced time, $\tilde{t} = t/\tau_R$, we have $\int N_0(\tilde{t})d\tilde{t} = 1$ and $\int R_0(\tilde{t})d\tilde{t} = 1$, so that the typical amplitudes and widths of $R_0(\tilde{t})$ and $N_0(\tilde{t})$ are now of order one, which thus readily gives $\Delta\omega_{int}^2 \sim 1/\tau_0^2$. In other terms we have

$$\frac{\Delta\omega_{int}}{\Delta\omega_g} \sim \frac{\tau_R}{\tau_0} \gg 1, \tag{82}$$

which means that *the typical spectral width of the wave-packet (incoherent soliton) is $\tau_R/\tau_0$ larger than the spectral width of the gain curve $g(\omega)$.* We remark that such broad spectral width of the wave-packet is clearly visible in the numerical simulation reported in Fig. 15, where the typical spectral bandwidth of the incoherent soliton is of the order $\Delta\omega_{int} \simeq 1/\tau_0 \gg \Delta\omega_g$. Note that this reasoning does not involve the spectral gain function $g(\omega)$, nor the causality property of $R(t)$, so that the spectral long-range interaction appears as a property inherent to the long-range Vlasov formalism, i.e., it also applies to the spatial version of the long-range Vlasov equation considered in Section 2.3.

This qualitative analysis reveals that temporal incoherent solitons considered in the previous Section 3.3.4 exhibit a spectral long-range interaction, a feature confirmed by the numerical simulations reported in Ref. [215]. More specifically, incoherent solitons exhibit a non-mutual phase insensitive interaction, which can be either attractive or repulsive depending on their relative initial distance [215]. This anomalous interaction originates in the combined effects of the causality condition of the nonlinear response function and their constant acceleration in the temporal domain. We refer the interested reader to Ref. [215] for more details regarding the interaction of temporal incoherent solitons.

We conclude this section by remarking that optical hollow-core fibers and waveguides (see, e.g., [216]) turn out to be ideal test beds for the experimental verifications of the predictions related to highly-noninstantaneous nonlinearities, such as incoherent MI, incoherent solitons or shock waves. This is thanks to the easily tailorable non-instantaneous response via the well-known Raman effect, as well as other recently investigated mechanisms involving liquid-cores or photo-ionizable noble gases and surface plasmon polaritons [217–224].

## 4. Spatio-temporal domain: Inertial nonlinearity

In the previous two sections we considered separately the spatial and temporal coherence properties of an optical wave that propagates in a nonlinear Kerr medium that exhibits a nonlocal and a noninstantaneous response, respectively. A generalized WT theory of the spatio-temporal coherence properties of the optical wave which unifies the previous formalisms still needs to be developed. In this section we discuss an important example of such a spatio-temporal generalization that has been the subject of lot of interest in the past after the pioneering experimental studies of incoherent optical solitons, as discussed in Section 1.1.

### 4.1. Averaged NLS equation

We consider the *spatial coherence properties* of an optical beam that propagates in a Kerr medium characterized by a response which is local in the spatial domain, but very slow in the temporal domain. In the following this nonlinearity will be termed 'inertial'. An immediate generalization of the NLS equations considered in the previous two sections reads

$$i\partial_z\psi + \alpha\nabla^2\psi + \gamma\psi \int R(t-t')\,|\psi(z,\boldsymbol{x},t')|^2\,dt' = 0. \tag{83}$$

The first assumption is that the coherence time is much shorter than the nonlinear response time, $t_c \ll \tau_R$. As a consequence, the medium averages out the fast oscillations of the incoherent wave. Then the nonlinear index of refraction depends only on the locally time-averaged intensity, which is equal by ergodicity to the local statistical average of the intensity, $\int R(t-t')\,|\psi(z,\boldsymbol{x},t')|^2\,dt' \simeq \int R(t-t')\,\left\langle|\psi|^2\right\rangle(z,\boldsymbol{x},t')\,dt'$. Notice that this reasoning is analogous to that discussed in the framework of a nonlocal nonlinearity in the presence of a long-range interaction (see Section 2.3.2). Furthermore, assuming that the pulse duration of the incoherent wave is much longer than the nonlinear response time, we have $\left\langle|\psi|^2\right\rangle(z,\boldsymbol{x},t') \simeq \left\langle|\psi|^2\right\rangle(z,\boldsymbol{x},t)$, for $|t-t'| \leq \tau_R$. In this way, the spatio-temporal NLS equation (83) reduces to the following averaged NLS equation

$$i\partial_z\psi + \alpha\nabla^2\psi + \gamma\left\langle|\psi|^2\right\rangle\psi = 0. \tag{84}$$

We remind an important property of this averaged NLS equation, namely that it preserves Gaussian statistics under nonlinear evolution [91]. This property is consistent with the fact that the averaged NLS equation (84) does not lead to an infinite hierarchy of moment equations. In other terms, thanks to the inertial nonlinearity, we do not need additional assumptions to achieve a closure of the hierarchy, which is automatically satisfied through the averaging of the nonlinear term in (84). This considerably simplifies the theoretical developments we are going to present, whose validity is no longer restricted to the weakly nonlinear regime inherent to the WT theory.

In this section we will study the coherence properties of an optical wave governed by averaged NLS equations of the form (84). The presentation will also points out some recent developments related e.g., to dynamic solutions of the Vlasov and Wigner–Moyal equations (see Section 4.5). The interested reader can find previous reviews on this vast subject in Ref. [5,6].

### 4.2. Theoretical methods and their equivalence

As discussed below in Section 4.7, the self-trapping of a partially coherent beam was first experimentally demonstrated by M. Segev's group in 1996 using an inertial photorefractive nonlinearity [3]. The experimental observation of partially coherent solitons spurred much research activity and led within a few years to the development of several theoretical formalisms for modeling the evolution and dynamics of partially coherent beams. The first formalism to be developed was the coherent density theory [9], which was later followed by the self-consistent multimode theory [8], the mutual coherence function approach [225] and the Wigner transform method [10]. All of these formalisms show good agreement with experimentally observed results and were later shown to provide equivalent descriptions of the partially coherent field [11,12].

Closed form analytical soliton solutions of these localized incoherent states were first demonstrated to exist for saturable media of the logarithmic type, which admits self-similar solutions with a Gaussian intensity profile. Soliton families were later also identified in other types of media using the self-consistent multimode approach. The equivalence of the different formalisms has been found to hold for a general inertial nonlinearity, regardless of character, as long as the nonlinear response is a function of the averaged intensity. The theoretical formalisms are therefore not restricted to different kinds of saturable media but can be used for studying any type of inertial nonlinear media where the nonlinearity is an arbitrary function of the noninstantaneous intensity, with the inertial Kerr medium being the simplest case.

Each of the different formalisms have their own evolution equations and display their own particular properties with certain advantages and disadvantages, e.g. being more suited for describing the evolution of partially coherent fields or for identifying soliton families. One of the main differences between the formalisms lies in how the initial field is determined for given initial conditions of the source. All formalisms may in some sense be considered as nonlinear generalizations of previous methods for linear propagation and the choice of the most suitable representation of the partially coherent field depends on the physical problem to be investigated.

It has been found that the 1D nonlinear evolution equations governing partially coherent wave propagation in inertial Kerr type media, are in fact integrable using the method of inverse scattering [226]. This has important implications for the stability of partially coherent soliton solutions since it is well known that integrable solutions will interact elastically so that solitons will retain their identity even after collisions. The integrability of the evolution equations implies moreover the existence of an infinite number of invariant quantities associated with the field, with the first three corresponding to conservation laws for energy, momentum and Hamiltonian, and enables the explicit analytical construction of partially coherent solitons solutions, see [227,228].

Below we will separately present each of the four main theoretical formalisms used for describing self-trapping of optical beams and the propagation of partially coherent fields in inertial nonlinear media. The presentation demonstrates both the equivalence of the different formalisms and shows how each approach can be derived starting from the averaged NLS equation (84).

#### 4.2.1. Mutual coherence function approach

The mutual coherence function approach [225] describes the evolution of the autocorrelation function in the presence of an inertial nonlinearity. This formalism is in some sense the simplest theory that can be obtained from the NLS equation (84). However, due to the difficulties involved in solving its corresponding evolution equation, it was historically not the first formalism to be used in the description of self-trapping of partially coherent optical beams, although it was used as early as 1974 to treat incoherent beams in a cubic medium [7]. We recall that the mutual coherence function is defined as the autocorrelation of the field envelope

$$B(\boldsymbol{x}_1, \boldsymbol{x}_2, z) = \langle \psi(\boldsymbol{x}_1, z)\psi^*(\boldsymbol{x}_2, z)\rangle, \tag{85}$$

and gives a measure of the correlation between different points of the beam. The coherence properties are easily extracted from the mutual coherence function by normalizing it to obtain the complex correlation function, defined as

$$\mu(\boldsymbol{x}_1, \boldsymbol{x}_2, z) = \frac{B(\boldsymbol{x}_1, \boldsymbol{x}_2, z)}{\sqrt{B(\boldsymbol{x}_1, \boldsymbol{x}_1, z)B(\boldsymbol{x}_2, \boldsymbol{x}_2, z)}} = \frac{B(\boldsymbol{x}_1, \boldsymbol{x}_2, z)}{\sqrt{N(\boldsymbol{x}_1, z)N(\boldsymbol{x}_2, z)}}, \tag{86}$$

where $N(\boldsymbol{x}, z) = B(\boldsymbol{x}, \boldsymbol{x}, z) = \langle|\psi|^2\rangle(\boldsymbol{x}, z)$ is the beam intensity. This function takes on values belonging to the interval $|\mu(\boldsymbol{x}_1, \boldsymbol{x}_2), z| \leq 1$, with $\mu(\boldsymbol{x}_1, \boldsymbol{x}_1, z) = 1$ indicating that the field is perfectly correlated and fully coherent. Another frequently used measure of the coherence is the correlation length $\lambda_c$ which is obtained using the complex correlation function via

$$\lambda_c(\boldsymbol{x}, z) = \left(\int |\mu(\boldsymbol{x}, \boldsymbol{x}', z)|^2 \, d\boldsymbol{x}'\right)^{1/d}. \tag{87}$$

The evolution equation for the mutual coherence function is obtained by following the procedure outlined in Section 2.1. Starting from the NLS equation (84), one readily obtains

$$i\partial_z B + \alpha\left(\nabla^2_{\boldsymbol{x}_1} - \nabla^2_{\boldsymbol{x}_2}\right)B + \gamma\left[N(\boldsymbol{x}_1, z) - N(\boldsymbol{x}_2, z)\right]B = 0. \tag{88}$$

As discussed above in Section 4.1, this equation is exact for an inertial nonlinearity since the application of averaging on the already time-averaged intensity does not result in additional higher-order moments, which permits a closure of the moment hierarchy without additional assumptions about the statistics of the field.

The evolution equation (88) is however complicated to solve in the general case, even using numerical methods, since it involves both derivatives of the correlation function and the intensity taken at two different points. An important simplification occurs by introducing the set of independent spatial variables defined in Eq. (4). The evolution equation for the correlation function $B(\boldsymbol{x}, \boldsymbol{\xi}, z) = \langle \psi(\boldsymbol{x} + \boldsymbol{\xi}/2, z)\psi^*(\boldsymbol{x} - \boldsymbol{\xi}/2, z)\rangle$ then reads

$$i\partial_z B + 2\alpha\nabla_{\boldsymbol{x}} \cdot \nabla_{\boldsymbol{\xi}} B + \gamma\left[N(\boldsymbol{x} + \boldsymbol{\xi}/2, z) - N(\boldsymbol{x} - \boldsymbol{\xi}/2, z)\right]B = 0. \tag{89}$$

The mutual coherence function approach has been applied to study self-similar soliton solutions in logarithmically saturable media [225,229] and also to investigate the MI of partially coherent optical waves [15].

We shall later see that the mutual coherence function $B(\boldsymbol{x}, \boldsymbol{\xi}, z)$ forms a Fourier pair together with the Wigner distribution function. The mutual coherence function approach has been the method of choice used to establish the equivalence between the different formalisms [11,12], and is frequently used as an intermediate function in order to extract the coherence properties of the field.

*4.2.2. Coherent density theory*

The coherent density formalism was the first theory to be applied to the description of incoherent soliton self-trapping and propagation of partially coherent beams in inertial nonlinear media [11,9]. The coherent density can be understood as a decomposition of the partially coherent field into an infinite set of coherent components that are weighted with respect to the angular power spectrum and are incoherently coupled with one another. We will now consider the derivation of this formalism following the presentation given in Ref. [230].

The decomposition of the field takes the form of a projection onto an orthogonal basis $\varphi$

$$\psi(\boldsymbol{x}, z) = \int C(\boldsymbol{\theta})\varphi(\boldsymbol{x}, \boldsymbol{\theta}, z)\, d\boldsymbol{\theta}. \tag{90}$$

The most familiar such decomposition is the Fourier transform where the basis functions take the form $\varphi(\boldsymbol{x}, \boldsymbol{\theta}, z) = \exp(i\boldsymbol{\theta} \cdot \boldsymbol{x})$.

From the definition of the mutual coherence function Eq. (85) we see that it can be expressed using the newly introduced basis functions as

$$B(\boldsymbol{x}_1, \boldsymbol{x}_2, z) = \int\int A(\boldsymbol{\theta}_1, \boldsymbol{\theta}_2)\varphi(\boldsymbol{x}_1, \boldsymbol{\theta}_1, z)\varphi^*(\boldsymbol{x}_2, \boldsymbol{\theta}_2, z)\, d\boldsymbol{\theta}_1 d\boldsymbol{\theta}_2, \tag{91}$$

with the correlation properties for the general case given by the function $A(\boldsymbol{\theta}_1, \boldsymbol{\theta}_2) = \langle C(\boldsymbol{\theta}_1)C^*(\boldsymbol{\theta}_2)\rangle$. By diagonalizing this function so that $A(\boldsymbol{\theta}_1, \boldsymbol{\theta}_2) = J(\boldsymbol{\theta}_1)\delta(\boldsymbol{\theta}_1 - \boldsymbol{\theta}_2)$, where $J(\boldsymbol{\theta})$ is the angular power spectrum, we find that Eq. (91) simplifies to

$$B(\boldsymbol{x}_1, \boldsymbol{x}_2, z) = \int J(\boldsymbol{\theta})\varphi(\boldsymbol{x}_1, \boldsymbol{\theta})\varphi^*(\boldsymbol{x}_2, \boldsymbol{\theta})\, d\boldsymbol{\theta}. \tag{92}$$

If we now introducing an auxiliary function $f(\boldsymbol{x}, \boldsymbol{\theta}, z) = \sqrt{J(\boldsymbol{\theta})}\varphi(\boldsymbol{x}, \boldsymbol{\theta}, z)\exp(i\boldsymbol{\theta} \cdot \boldsymbol{x} - i\boldsymbol{\theta}^2 z/2)$ we arrive at a modified version of the Van Cittert–Zernike theorem [231] where the mutual coherence function is expressed as

$$B(\boldsymbol{x}_1, \boldsymbol{x}_2, z) = \int f(\boldsymbol{x}_1, \boldsymbol{\theta}, z)f^*(\boldsymbol{x}_2, \boldsymbol{\theta}, z)\exp[i\boldsymbol{\theta} \cdot (\boldsymbol{x}_1 - \boldsymbol{x}_2)]\, d\boldsymbol{\theta}. \tag{93}$$

The function $f(\boldsymbol{x}, \boldsymbol{\theta}, z)$ is known as the coherence density function and its governing equation is obtained by substituting its definition $\varphi(\boldsymbol{x}, \boldsymbol{\theta}, z) = \left(f(\boldsymbol{x}, \boldsymbol{\theta}, z)/\sqrt{J(\boldsymbol{\theta})}\right)\exp(-i\boldsymbol{\theta} \cdot \boldsymbol{x} + i\boldsymbol{\theta}^2 z/2)$ into Eq. (90) whose evolution is in turn determined by the NLS equation (84). The resulting evolution equation for the coherent density function is then found to take the form of a modified NLS equation

$$i\left(\frac{\partial f}{\partial z} + \theta \cdot \nabla f\right) + \alpha\nabla^2 f + \gamma N(\boldsymbol{x}, z)f = 0, \tag{94}$$

where the intensity is given by the integral relation $N(\boldsymbol{x}, z) = B(\boldsymbol{x}, \boldsymbol{x}, z) = \int |f|^2\, d\boldsymbol{\theta}$. Eq. (94) is thus an integro-differential equation. This equation is the closest in form to the ordinary nonlinear Schrödinger equations for the different formalisms. Thus it can easily be simulated numerically using standard split-step Fourier methods, making it well suited for studying the dynamical evolution of partially coherent beams [232]. The first analytical solutions of partially coherent solitons were also obtained using this formalism for the case of a saturable nonlinearity of the logarithmic type, which allows exact soliton solutions having a Gaussian intensity profile and a Gaussian angular power spectrum [233]. This method has been also used to study beam collapse in Ref. [234].

The difficulty with this method lies in determining the initial coherent density function for given source conditions. This can be accomplished by inverting the relation Eq. (93), which is generally non trivial unless the stochastic variation is spatially homogeneous [11]. The source conditions can in this case be written as the product of the source angular power spectrum and a complex modulation function i.e. $f(\boldsymbol{x}, \boldsymbol{\theta}, z = 0) = \sqrt{J(\boldsymbol{\theta})}M(\boldsymbol{x})$, since

$$\psi(\boldsymbol{x}, z = 0) = M(\boldsymbol{x})\int C(\boldsymbol{\theta})\exp(i\boldsymbol{\theta} \cdot \boldsymbol{x})\, d\boldsymbol{\theta}, \tag{95}$$

and $\langle C(\boldsymbol{\theta}_1)C^*(\boldsymbol{\theta}_2)\rangle = J(\boldsymbol{\theta}_1)\delta(\boldsymbol{\theta}_1 - \boldsymbol{\theta}_2)$. The initial coherent density function can alternatively be constructed by using the above procedure, i.e. starting with the orthogonal decomposition Eq. (90) and diagonalizing the matrix $A(\boldsymbol{\theta}_1, \boldsymbol{\theta}_2)$, see Ref. [230] for examples.

*4.2.3. Modal theory*

The self-consistent multimode theory has frequently been the method of choice for investigating partially coherent soliton solutions [8]. The idea behind the model theory is conceptually similar to the coherent density theory but relies on a decomposition of the partially coherent field into a discrete rather than continuous set of coherent modes that are mutual orthogonal to one another. The eigenmodes in the multimode theory are also defined to be uncorrelated with one another which implies that they interact incoherently, with each mode seeing a superposition of the total averaged intensity due to the inertial nonlinearity.

The self-consistent multimode theory can, following Ref. [230], be derived analogously to the coherent density theory by making a discrete expansion of the field using a set of basis functions $\varphi_n$

$$\psi(\boldsymbol{x}, z) = \sum_n c_n \varphi_n(\boldsymbol{x}, z). \tag{96}$$

The basis functions of the expansion equation (96) are related to the mutual coherence function by the relation

$$B(\boldsymbol{x}_1, \boldsymbol{x}_2, z) = \langle \psi(\boldsymbol{x}_1, z)\psi^*(\boldsymbol{x}_2, z)\rangle = \sum_{mn} A_{nm}\varphi_n(\boldsymbol{x}_1, z)\varphi_m^*(\boldsymbol{x}_2, z), \tag{97}$$

which follows directly from the definition of the mutual coherence function Eq. (85). The Hermitian matrix $A_{nm} = \langle c_n c_m^*\rangle$ is known as the correlation matrix and the summation on the right hand side can be significantly simplified if the basis functions are chosen to be orthogonal to one another, in which case the correlation matrix is diagonal.

This is exploited in the self-consistent multimode theory which relies on using a set of orthogonal basis functions in the expansion equation (96), that is also known as a Karhunen–Loeve expansion [231]. The mutual coherence function is then given by

$$B(\boldsymbol{x}_1, \boldsymbol{x}_2, z) = \sum_n \lambda_n \varphi_n(\boldsymbol{x}_1, z)\varphi_n^*(\boldsymbol{x}_2, z), \tag{98}$$

with $\lambda_n = \langle |c_n|^2\rangle$ being the modal occupancy coefficient, corresponding to the eigenvalue of the correlation matrix. The basis functions of the self-consistent multimode theory are the concomitant set of orthogonal eigenfunctions, that can be found by solving the following Fredholm integral equation

$$\lambda_n \varphi_n(\boldsymbol{x}, z = 0) = \int B(\boldsymbol{x}, \boldsymbol{x}', 0)\varphi_n(\boldsymbol{x}', 0)\, d\boldsymbol{x}', \tag{99}$$

that is obtained from Eq. (98) by multiplying it with $\varphi_n(\boldsymbol{x}_2, 0)$ and using the orthogonality condition.

Since the field in Eq. (96) is given by a weighted sum one find that the eigenmodes of the self-consistent multimode theory will evolve according to an NLS equation similar to Eq. (84), i.e.

$$i\partial_z \varphi_n + \alpha\nabla^2\varphi_n + \gamma N(\boldsymbol{x}, z)\varphi_n = 0, \tag{100}$$

with the intensity provided by the relation

$$N(\boldsymbol{x}, z) = B(\boldsymbol{x}, \boldsymbol{x}, z) = \sum_n \lambda_n |\varphi_n|^2(\boldsymbol{x}, z). \tag{101}$$

The eigenmodes will remain orthogonal to one another during propagation given that they were so initially. The difficulties with using this method lies mainly in determining how the input eigenfunctions will excite the incoherent soliton modes. The eigenmodes, for given initial conditions, can either be obtained by solving the integral equation (99) or by beginning with an arbitrary basis as in Eq. (96) and diagonalizing the correlation matrix $A_{mn}$ using a unitary transformation, see [230].

The self-consistent multimode theory is particularly well suited for identifying and studying the existence of incoherent soliton families, as has been demonstrated both for logarithmic and Kerr nonlinearities [235,236]. Besides the requirement that the nonlinearity should be of the inertial type in order to respond only to the smooth averaged intensity profile, it can intuitively be understood that when a partially coherent beam propagates through a nonlinear medium it will induce a multimode waveguide in that medium. This waveguide can allow soliton formation, if it is self-consistent with that required for self-trapping of the optical beam.

Let us finally underline that a generalization of the modal and mutual coherence theories, which accounts for the contribution of pronounced intensity fluctuations of, e.g., white-light sources, has been developed in Ref. [237]. When such fluctuations are significant, the generalized theory shows that the properties of partially coherent solitons in saturable nonlinear media can be qualitatively different from those predicted by the conventional modal theory [237].

#### 4.2.4. Wigner–Moyal approach

The Wigner transform method has its origins in quantum mechanics and is the most recent of the formalisms to be developed [10,238,239,12,94]. The Wigner distribution function $n_{\boldsymbol{k}}(\boldsymbol{x}, z)$ was introduced in Section 2.2 as the Fourier transform of the mutual coherence function according to

$$n_{\boldsymbol{k}}(\boldsymbol{x}, z) = \int B(\boldsymbol{x}, \boldsymbol{\xi}, z)e^{-i\boldsymbol{k}\cdot\boldsymbol{\xi}}d\boldsymbol{\xi} = \int \langle \psi(\boldsymbol{x} + \boldsymbol{\xi}/2, z)\psi^*(\boldsymbol{x} - \boldsymbol{\xi}/2, z)\rangle e^{-i\boldsymbol{k}\cdot\boldsymbol{\xi}}d\boldsymbol{\xi}, \tag{102}$$

and

$$B(\boldsymbol{x}, \boldsymbol{\xi}, z) = \frac{1}{(2\pi)^d}\int n_{\boldsymbol{k}}(\boldsymbol{x}, z)e^{i\boldsymbol{k}\cdot\boldsymbol{\xi}}\, d\boldsymbol{k}, \tag{103}$$

where we remind that $d$ denotes the dimensionality for the transverse coordinates. It is possible to obtain an exact evolution equation for the Wigner transform for the case of an inertial nonlinearity with closure of the evolution equation for the mutual coherence function. The evolution equation can most easily be obtained from the evolution equation for the mutual coherence function Eq. (89) by multiplying it with $\exp(-i\boldsymbol{k}\cdot\boldsymbol{\xi})$ and integrating over $\boldsymbol{\xi}$. The diffraction term is partially integrated using $\nabla_{\boldsymbol{\xi}} \to -i\boldsymbol{k}$ which yields

$$\partial_z n_{\boldsymbol{k}}(\boldsymbol{x},z) + 2\alpha\boldsymbol{k}\nabla_{\boldsymbol{x}} n_{\boldsymbol{k}}(\boldsymbol{x},z) = i\gamma \int \left[N(\boldsymbol{x}+\boldsymbol{\xi}/2) - N(\boldsymbol{x}-\boldsymbol{\xi}/2)\right] B(\boldsymbol{x},\boldsymbol{\xi}) e^{-i\boldsymbol{k}\cdot\boldsymbol{\xi}} d\boldsymbol{\xi}. \tag{104}$$

The intensity terms in the nonlinearity are handled by Taylor expanding them around the mean position $\boldsymbol{x}$ to enable the $\boldsymbol{\xi}$ dependence to be replaced by $\boldsymbol{\xi} \to i\nabla_{\boldsymbol{k}}$. The result is an integro-differential equation known as the Wigner–Moyal equation

$$\partial_z n_{\boldsymbol{k}}(\boldsymbol{x},z) + 2\alpha\boldsymbol{k}\cdot\nabla_{\boldsymbol{x}} n_{\boldsymbol{k}}(\boldsymbol{x},z) + 2\gamma N(\boldsymbol{x},z) \sin\left(\frac{1}{2}\overleftarrow{\nabla_{\boldsymbol{x}}}\cdot\overrightarrow{\nabla_{\boldsymbol{k}}}\right) n_{\boldsymbol{k}}(\boldsymbol{x},z) = 0, \tag{105}$$

with the intensity given by the integral relation

$$N(\boldsymbol{x},z) = \langle|\psi|^2\rangle(\boldsymbol{x},z) = \frac{1}{(2\pi)^d}\int n_k(\boldsymbol{x},z)\, d\boldsymbol{k}. \tag{106}$$

The trigonometric sine function in the nonlinear term is an operator that is defined by its Taylor series expansion, and where the arrows indicate the direction of application of the gradient operators. There are thus an infinite number of nonlinear terms in the full Wigner–Moyal equation. However, in the limit of a quasi-homogeneous statistics (see Section 2), the condition $\Delta\boldsymbol{k}\cdot\Delta\boldsymbol{x} \gg 2\pi$ holds, where $\Delta\boldsymbol{k}$ is the local width of the Wigner spectrum and $\Delta\boldsymbol{x}$ is the local width of the intensity. Then it is convenient to truncate the infinite series after the second-order ('paraxial approximation'), and the resulting evolution equation simplifies to the following Vlasov equation

$$\partial_z n_{\boldsymbol{k}}(\boldsymbol{x},z) + 2\alpha\boldsymbol{k}\cdot\nabla_{\boldsymbol{x}} n_{\boldsymbol{k}}(\boldsymbol{x},z) + \gamma\nabla_{\boldsymbol{x}} N(\boldsymbol{x},z)\cdot\nabla_{\boldsymbol{k}} n_{\boldsymbol{k}}(\boldsymbol{x},z) = 0. \tag{107}$$

This Vlasov equation almost coincides with the Vlasov equation derived in the limit of a local nonlinearity in Section 2.2.2, where the so-called self-consistent potential now reads $V(\boldsymbol{x},z) = -\gamma N(\boldsymbol{x},z)$. Note however the presence of a factor 2 in the expression of the self-consistent potential in Eq. (19). In Section 2.2.2, such a factor of 2 was shown to originate from the closure of the hierarchy of moments equations and the underlying expansion of the fourth-order moment into two products of second-order moments. As commented in Section 4.1, the inertial nonlinearity leads to an automatic closure of the hierarchy through the averaged NLS equation (84), which explains the absence of the factor 2 in front of the nonlinear term in the Vlasov equation (107).

The Wigner–Moyal approach can easily seen to be equivalent to the other formalisms by virtue of the definition of the spectrum $n_{\boldsymbol{k}}(\boldsymbol{x},z)$, as the Fourier transform of the mutual coherence function [12]. The Wigner–Moyal formalism has been applied, in particular, to study incoherent MI [238,17].

### 4.3. Incoherent modulational instability

Incoherent MI has already been discussed in the spatial (Section 2.3.4) and temporal Section 3.3.3 domains in the presence of a long-range nonlinear response. In the presence of an inertial nonlinearity, incoherent MI was first considered theoretically in [15] using the mutual coherence formalism, and subsequently demonstrated experimentally in [16]. In the following we consider the MI process described by the Wigner formalism in one spatial dimension [10,239,238]. A similar treatment using the mutual coherence function approach can be found in [15,240]. The coherent continuous wave solution of the Wigner–Moyal equation (105) is homogeneous in space and is given by $n_k^0 = 2\pi N_0\delta(k)$, which satisfies the intensity relation $(2\pi)^{-1}\int n_k^0\, dk = N_0$ (see Section 2.3.4). This continuous wave solution generalizes to $k$ dependent function for a partially coherent wave, where the width in $k$-space of the Wigner distribution function can be seen as a measure of the degree of coherence. To analyze incoherent MI we proceed in a way similar to Section 2.3.4. We consider the stability of the background Wigner distribution with respect to plane wave perturbations of the form

$$n_k(x,z) = n_k^0 + n_{k,1}\exp(\lambda z + iKx), \tag{108}$$

where we assume that the perturbation amplitude $n_{k,1} \ll n_k^0$. Linearizing the Wigner–Moyal equation (105) around the steady-state solution we find that the perturbation satisfies the equation

$$i(2\alpha kK - i\lambda)n_{k,1} + \frac{\gamma}{\pi}N_1(x,z)\sin\left(\frac{\overleftarrow{iK}}{2}\cdot\overrightarrow{\partial_k}\right) n_k^0 = 0 \tag{109}$$

with $N_1(x,z) = \int n_{k,1}\, dk$, and where we have used that the background intensity is independent of $x$.

A general dispersion relation for the background distribution is obtained by dividing the above expression by the factor $(2\alpha kK - i\lambda)$ before integrating over $k$, while utilizing that the action of the sine operator on the background distribution

can be written as the difference of the Wigner function taken at two different points in a way similar to the derivation of the Wigner–Moyal equation. The dispersion relation is then found to take the form

$$1+\frac{\gamma}{4\pi\alpha}\int\frac{n_k^0(k+K/2)-n_k^0(k-K/2)}{K(k-i\lambda/(2\alpha K))}\,dk=0. \tag{110}$$

It should be emphasized that the above dispersion relation is valid for arbitrary background distributions $n_k^0$, and consists of both a principal value and a residue contribution. Eq. (110) is a generalization of the corresponding dispersion relation for the Vlasov (geometric optics) limit, which is found either by considering the second-order expansion of the sine operator or equivalently by taking the limit $K\to 0$, in which case it reduces to

$$1+\frac{\gamma}{4\pi\alpha}\int\frac{dn_k^0/dk}{(k-i\lambda/(2\alpha K))}\,dk=0. \tag{111}$$

By means of an integration by parts, this dispersion relation recovers the dispersion relation obtained in Section 2.3.4, provided that one takes the limit of a local nonlinearity in Eq. (27), i.e., $\tilde{U}(k)=1$.

Closed form solutions of the dispersion relation (110) cannot easily be found for the most common background distributions since the residue integral of e.g. a Gaussian distribution diverges as $z\to i\infty$. However, as discussed in Section 2.3.4, a closed form solution can be obtained for a Lorentzian distribution of the form $n_k^0=2N_0\frac{\Delta k}{k^2+(\Delta k)^2}$, where the spectral width $\Delta k$ is related to the coherence length. Eq. (110) can then be explicitly evaluated as [15,10]

$$\lambda(K)=-2\alpha\Delta k|K|+|K|\sqrt{2\alpha\gamma N_0-\alpha^2K^2}. \tag{112}$$

Note that in the long-wavelength limit, $K\to 0$, this expression of incoherent MI growth-rate coincides with that obtained in Section 2.3.4, provided that one considers the limit of a local nonlinearity in Eq. (28), i.e., $\tilde{U}(k)=1$. Then in complete analogy with incoherent MI considered in Section 2.3.4, Eq. (112) shows that the MI growth rate is affected by the coherence properties of the field, with a decrease in coherence leading to a damping of the MI growth rate. Indeed, Eq. (112) shows that a threshold exists such that the MI can be suppressed entirely if the partial coherence is large enough. This is in marked contrast with the coherent case that is obtained in the limit of $\Delta k\to 0$, which is always unstable.

It is important to note that the above analysis applies only to the initial linear stage of the instability growth and that the instability will eventually saturate as the amplitude of the perturbation becomes appreciable. This saturation phenomena has been found to lead to a redistribution of the background Wigner distribution function which is described by a quasi-linear diffusion process [241,158]. The effects of higher-orders of dispersion on the incoherent MI has also been studied using the Wigner formalism [17]. It was found that the third-order dispersion does not affect the MI growth rate similarly to the coherent case, however, the influence of fourth-order dispersion depends on its sign and relative magnitude as compared to second-order dispersion term, a feature which leads either to an enhancement or to a weakening of the instability growth rate.

### 4.4. Incoherent solitons

#### 4.4.1. Bright incoherent solitons

Soliton solutions can be thought of as behaving as distinguishable entities not only because they exist as a balance between diffraction(-dispersion) and nonlinearity, but also because they interact elastically, and are able to remain as stationary solutions even after collisions. It was by no means obvious before the mid 90s that partially coherent solitons could exist. However, much interest in these new objects followed after the experimental demonstrations of self-trapping of partially coherent beams and soliton formation in biased photorefractive media, leading both to the development of different formalisms and investigations of soliton properties [242]. The early works naturally focused on providing descriptions of the experimental observations and considered primarily saturable media with a nonlinearity proportional to $1/(1+I(x,z))$, where $I(x,z)$ is the intensity [8]. An other work focused on a logarithmic approximation $\log(1+I(x,z))\approx\log I(x,z)$, which is analytically convenient since it allows explicit solutions having a Gaussian intensity profile to be found [235].

A partially coherent beam of light will exhibit stronger diffraction effects than its coherent counterpart of the same width. Random phase fluctuations across a partially coherent beam will additionally lead to a speckled intensity pattern that would have generated filaments and fragmented the beam had the nonlinearity been instantaneous and not inertial. Therefore the necessary conditions for self-trapping and soliton formation are that the nonlinearity is stronger than for the coherent case and that the response time of the medium $\tau_R$ must be much longer than the characteristic timescale for the random phase fluctuations $t_c$, so that the medium responds only to the smooth averaged intensity profile of the beam and not to the instantaneous speckle pattern. The beam must additionally be able to induce its own waveguide by changing the refractive index profile through the intensity dependent nonlinearity and this waveguide must in turn be stationary so that the beam self-consistently traps itself.

The multimode formalism introduced above in Section 4.2.3 has frequently been used for studying the existence and coherence properties of partially coherent solitons. In this formalism a soliton is thought of as populating multiple modes that are mutually incoherent with one another and where the total intensity is the incoherent superposition of the intensities

from the individual modes. Each mode is thus able to support a completely coherent field with the partial coherence arising from the incoherent interaction of multiple modes. The existence of soliton solutions for an arbitrary nonlinearity can be investigated in an iterative manner using the modal theory by starting from an arbitrary intensity profile and solving the multimode equations to obtain guided modes. The modes which are thus obtained are then used to construct a new intensity profile which is once again used to obtain the modes that are guided, and the whole process is repeated until convergence is obtained and the intensity profile remains stationary. This procedure was first applied numerically to construct the existence range for bimodal solution in a saturable medium, see [8].

We will now illustrate a similar procedure by using the multimode theory to construct a one dimensional partially coherent bright soliton solution for an inertial nonlinear Kerr medium. This particular solution was derived by Carvalho et al. in [236]. The starting point is to assume that the evolution equation for the multimode theory Eq. (100) has a self-consistent solution with an intensity profile that generalizes the coherent soliton solution so that $N(x,z) = N_0^2\mathrm{sech}^2(x/x_0)$, with $N_0^2$ being the peak intensity and $x_0$ the soliton width. The eigenmodes $\varphi_m$ should thus satisfy the following linear equation

$$i\partial_z\varphi_m + \alpha\partial_x^2\varphi_m + \gamma N_0^2\mathrm{sech}^2(x/x_0)\varphi_m = 0. \tag{113}$$

To find a stationary solution of this equation one looks for a solution similar to the coherent NLS soliton by using the ansatz $\varphi_m = u_m(x)\exp(i\beta_m z)$, where $\beta_m$ is a mode dependent phase-constant. Eq. (113) will then simplify to an ordinary differential equation for each mode

$$\alpha d_x^2 u_m + \left(\gamma N_0^2\mathrm{sech}^2(x/x_0) - \beta_m\right)u_m = 0. \tag{114}$$

This equation can be rewritten in a different form by introducing the transformation $s = \tanh(x/x_0)$ and defining $\hat{\beta}_m = \beta_m x_0^2/(2\alpha)$ and $q = \gamma N_0^2 x_0^2/\alpha$, in which case one finds the following familiar equation for the associated Legendre functions

$$(1-s^2)d_s^2 u_m + 2s d_s u_m + \left(q - \frac{2\hat{\beta}_m^2}{1-s^2}\right)u_n = 0. \tag{115}$$

The solution of this equation that satisfies the physical boundary conditions which require the field to vanish at infinity is given by $u_m(s) = P_n^m(\tanh(x/x_0))$ where $P_n^m$ are the associated Legendre functions for $q = n(n+1)$ with $m \le n$ an integer and $\hat{\beta}_m = m^2/2$. Note that these functions form a suitable basis since they satisfy the orthogonality condition on the interval $[-1, 1]$ where the argument $s$ takes its values.

For the solution to be consistent the spatial width $x_0$ will need to be related to the number of guided modes $n$ and the peak intensity $N_0^2$ as $x_0 = \sqrt{\frac{\alpha n(n+1)}{\gamma N_0^2}}$, which agrees with the coherent soliton width for the coherent case $n = 1$ and shows that the spatial width increases with an increase of the incoherence, i.e. the number of guided modes $n$. It should be noted that this solution only exists for a discrete set of widths, corresponding to integer $n$, which is an artifact of the assumed intensity dependence. The general solution has a more complicated shape than the assumed symmetric sech-squared intensity profile unless the above condition is satisfied [227].

If the soliton solution is self-consistent it must also satisfy the intensity relation equation (101), which requires finding modal coefficients $c_m$ so that the relation

$$N(x,z) = \sum_m \langle|c_m|^2\rangle[P_n^m(\tanh(x/x_0))]^2 = N_0^2\mathrm{sech}^2(x/x_0), \tag{116}$$

is satisfied.

The lowest order solution with $m = 1$ is found to be given by $\varphi_1 = N_0 P_1^1(\tanh(x/x_0))$ and corresponds to the coherent bright soliton which involves only a single mode. The case $m = 2$ which involves two modes is the first partially coherent solution and is given by $\varphi_1 = (N_0/9)P_2^1(\tanh(x/x_0))$ and $\varphi_2 = (N_0/9)P_2^2(\tanh(x/x_0))$. Expression for higher-order solutions can be found in [236].

The coherence properties of the soliton solutions can be investigated by calculating the complex coherence function Eq. (86), which takes the form

$$\mu(x_1,x_2,z) = \sum_{m=1}^{n}\frac{\langle|c_m|^2\rangle P_n^m(\tanh(x_1/x_0))P_n^m(\tanh(x_2/x_0))}{\mathrm{sech}(x_1/x_0)\mathrm{sech}(x_2/x_0)}. \tag{117}$$

An example of the coherence function for the case $n = 2$ is shown in Fig. 18. This function is identical to unity for the coherent soliton solution but has a more complicated structure when the solution is partially coherent. A common feature of this function is that there is a large degree of coherence far from the center of the beam. The reason for this is that fact that each mode is coherent with itself but incoherent with the other modes. There are several different modes that contribute to the field close to the center, thus resulting in a lowering of the degree of coherence. However, only the highest order mode will contribute towards the edges, which implies that the coherence in this region will be large.

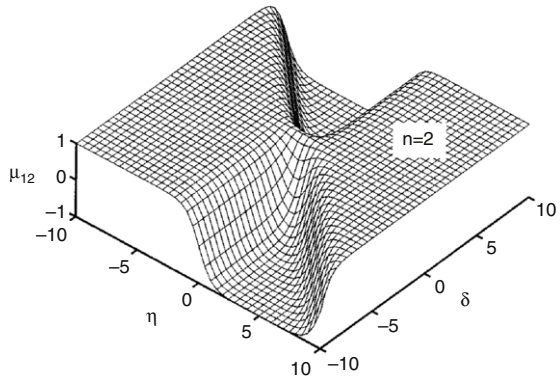


**Fig. 18.** Spatial coherence function given by Eq. (117) for the bright incoherent soliton solution with $n = 2$ as a function of $\eta = (x_1 + x_2)/2$ and $\delta = x_1 - x_2$.
*Source:* From Ref. [236].

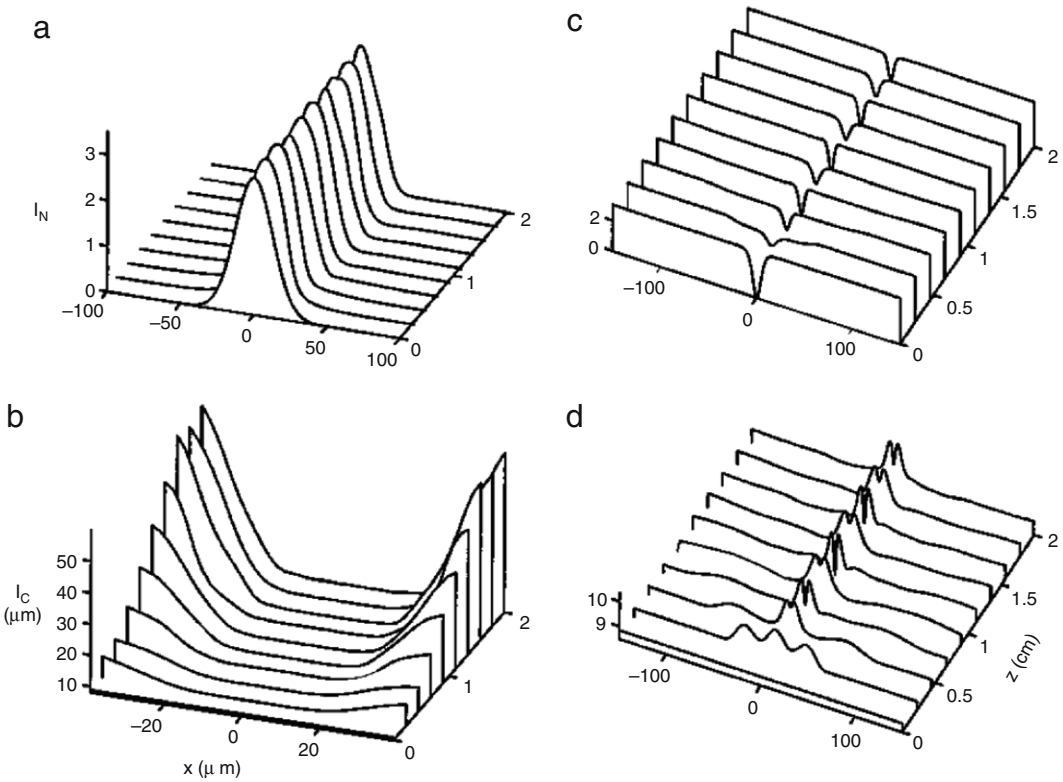


**Fig. 19.** Coherence properties of incoherent bright and dark solitons: Propagation of (a) bright incoherent soliton, (b) coherence length $l_c$ of this bright soliton, (c) dark incoherent soliton, (d) coherence length of this dark soliton.
*Source:* From Ref. [232].

### *4.4.2. Dark incoherent solitons*

Not only bright but also dark solitons have been found to exist in the presence of partially coherence. Dark solitons were originally predicted from numerical simulations using the coherent density method [232]. Incoherent dark solitons display certain properties which differ from their coherent counterparts. A distinct property of these incoherent structures is that they are always gray, meaning that their intensity never reaches zero at the center. The grayness of the soliton is a function of its incoherence with the ordinary dark (black) soliton representing the coherent limit. Partially coherent dark solitons have also been found to be very sensitive to the initial conditions and particularly to the phase shift at the center of the beam. For instance, a phase shift of $\pi$ at the center is needed for a single soliton to appear, while a continuous phase will give birth to two separating solitons [232]. An example showing the propagation of both bright and dark incoherent solitons is shown in Fig. 19 together with plots of their coherence lengths.

We will now consider the construction of one dimensional dark incoherent solitons in inertial Kerr media using a variant of the self-consistent multimode approach. This method of solution, see [13], differs somehow from that considered above for the bright incoherent soliton case but is still relying on the idea that the intensity induces a stationary waveguide in the material through the nonlinearity. This waveguide supports both bound states and radiation modes which together make up the dark incoherent soliton solution and that must additionally satisfy the self-consistency condition of being able to produce its own waveguide through its intensity profile.

We first make the assumption that the intensity profile of the dark incoherent soliton can be written as

$$N(x,z) = N_0^2\left[1-\epsilon^2\mathrm{sech}^2(x/x_0)\right] \tag{118}$$

where $N_0^2$ is the background intensity, $x_0$ is the soliton width and the parameter $\epsilon^2 \leq 1$ determines the amount of grayness, with the limit $\epsilon = 1$ corresponding to the coherent dark soliton case.

We will expect that the electric field $E(x,z)$ of the beam should satisfies a Helmholtz's equation

$$\nabla^2 E + k_0^2 n^2 E = 0 \tag{119}$$

with the refractive index for the self-defocusing nonlinearity given by $n^2 = n_0^2 - n_2 N$. Looking for a stationary solution for the electric field of the form $E = U(x)\exp(i\beta z)$ we thus find that the mode function $U$ satisfies

$$d_s^2 U + \left[g + f\,\mathrm{sech}^2(s)\right]U = 0 \tag{120}$$

where $s = x/x_0$, $g = [k_0^2(n_0^2 - n_2N_0^2) - \beta^2]x_0^2$ and $f = k_0^2 n_2 \epsilon^2 N_0^2 x_0^2$. This equation will have bound states whenever $g = -q^2$ is negative which occurs for $\beta^2 > k_0^2(n_0^2 - n_2N_0^2)$, and will similarly have radiation modes whenever $g = Q^2$ is positive. We limit ourselves to consider the case when $f = 2$ which implies that the soliton width $x_0^2 = 2/(k_0^2 n_2 \epsilon^2 N_0^2)$. For this case there will be only a single bound mode corresponding to $g = -q^2 = 1$, which takes the form $U_b = \mathrm{sech}(s)$. However there will also be a continuum of both even and odd radiation modes satisfying Eq. (120) with $g = Q^2$ and given by $U_e = Q\cos(Qs) - \tanh(s)\sin(Qs)$ and $U_o = Q\sin(Qs) + \tanh(s)\cos(Qs)$. The total electric field for the dark beam can therefore be written as superposition of these modes

$$E = c_b U_b(s)\exp(i\beta_b z) + \int_0^\infty [c_e(Q)U_e(s) + c_o(Q)U_o(s)]\exp(i\beta_r(Q)z)\,dQ \tag{121}$$

with $c_m$ denoting the modal coefficients. The different modes should be uncorrelated with one another for incoherent excitations, except for the autocorrelations which we define as $\langle |c_b|^2\rangle = A^2$ and $\langle c_e(Q)c_e^*(Q')\rangle = \langle c_o(Q)c_o^*(Q')\rangle = D(Q)\delta(Q-Q')$. This implies that the intensity $N \propto \langle |E|^2\rangle$ can be written as

$$N(s) = A^2\mathrm{sech}^2(s) + \int_0^\infty D(Q)[Q^2 + \tanh^2(s)]\,dQ. \tag{122}$$

With the function $D(Q)$ being a distribution function that characterizes the population of the radiation modes.

For the solution to be self-consistent the intensity must agree with the ansatz Eq. (118), requiring that

$$N_0^2 = \int_0^\infty D(Q)(Q^2+1)\,dQ, \qquad A^2 = \int_0^\infty D(Q)[1-\epsilon^2(Q^2+1)]\,dQ. \tag{123}$$

This solution shows that dark incoherent solitons do indeed exist in inertial media and that they consist of both a set of bound modes as well as a continuum of radiation modes. The gray nature of the incoherent dark soliton is found to be due to the presence of even bound states and radiation modes. It should be noted that the soliton solution is not unique since the radial-mode distribution function $D(Q)$ is arbitrary. Assuming e.g. that $D(Q) = D_0\exp(-Q/Q_0)$ allows Eq. (123) to be evaluated explicitly with the result $D_0 = N_0^2/(Q_0(2Q_0^2+1))$ and $A^2 = N_0^2(1/(2Q_0^2+1) - \epsilon^2)$. The width $Q_0$ is found to be related to the correlation length of the soliton at its tail, i.e. as $s \to \pm\infty$. Expressions for a higher-order solution with two bound modes ($f = 6$) can be found in Ref. [13].

#### 4.4.3. Antidark solitons

Another class of incoherent solitons that are present in self-focusing inertial nonlinear media is that of antidark solitons [243,244]. The antidark solitons can be seen as bright soliton solutions that sit on top of a constant but nonvanishing background. Antidark solitons cannot be observed for instantaneous nonlinear Kerr media governed by the ordinary nonlinear Schrödinger equation since the continuous wave background is modulationally unstable. However, due to the presence of a threshold for the MI when the nonlinearity is noninstantaneous one finds that antidark solitons are possible for inertial nonlinear media given that the background is sufficiently incoherent to suppress the instability. The antidark solitons are, similarly to the dark incoherent solitons considered above, composed of both a discrete set of bound states and a continuum of even and odd radiation modes, and are the only stationary solutions for a self-focusing nonlinearity that has a non-zero intensity everywhere.

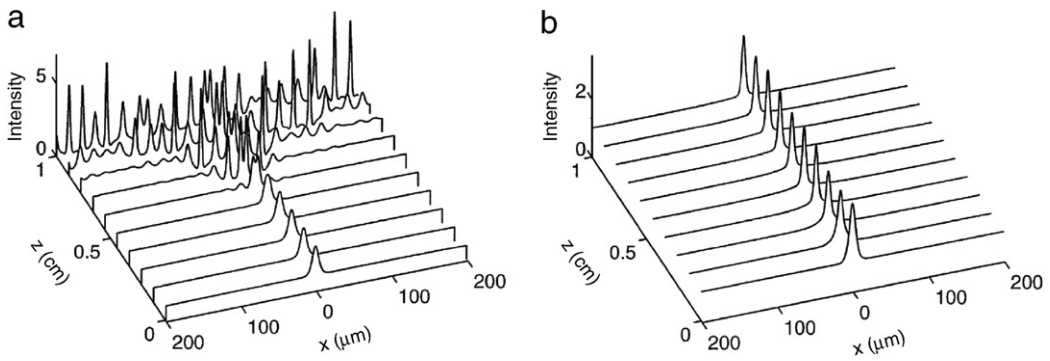


**Fig. 20.** (a) Propagation of an unstable multicomponent antidark soliton when the background is coherent. (b) Intensity evolution of a partially incoherent antidark soliton when initially $\lambda_c \approx 5.5$ mm. For both cases, the initial intensity FWHM of the beam is 10 mm, $\epsilon^2 = 2$, $n_2 N_0 = 6.1552 \times 10^{-4}$, $n_0 = 2.3$, and $\lambda_0 = 0.5$ μm.
*Source:* From Ref. [244].

The antidark soliton can be analyzed in a manner similar to that considered for the incoherent dark soliton solution. Assuming that the intensity profile takes the form

$$N(x, z) = N_0^2 \left[1 + \epsilon^2 \mathrm{sech}^2(x/x_0)\right], \tag{124}$$

we find that the mode function $U$ again satisfies Eq. (120) but with $g = [k_0^2(n_0^2 + n_2 N_0^2) - \beta^2]x_0^2$, while $s = x/x_0$ and $f = k_0^2 n_2 \epsilon^2 N_0^2 x_0^2$ remains the same. Considering once again the case of $f = 2$ we find as before that there is only a single bound mode $U_b = \mathrm{sech}(s)$ and a continuum of even and odd radiation modes satisfying $g = Q^2$, viz. $U_e = Q\cos(Qs) - \tanh(s)\sin(Qs)$ and $U_o = Q\sin(Qs) + \tanh(s)\cos(Qs)$.

Assuming the correlations of the modal functions to have the same functional dependence as before we see that Eq. (122) still hold but the second of the self-consistency equations (123) will need to be modified due the difference in sign in the intensity of Eq. (124). The new solution will instead satisfy the relations

$$N_0^2 = \int_0^\infty D(Q)(Q^2 + 1)\, dQ, \qquad A^2 = \int_0^\infty D(Q)[1 + \epsilon^2(Q^2 + 1)]\, dQ. \tag{125}$$

These results shows that antidark solitons do exist and that there is no upper limit to the incoherence of the background, thus making it possible to increase the incoherence to a point above which the MI will be suppressed in order to allow the antidark soliton to propagate as a stable entity in a self-focusing inertial medium. (See Fig. 20.)

### *4.5. Dynamic solutions of the Vlasov and Wigner–Moyal equations*

The evolution equations of the different formalisms for treating partial coherence are generally difficult to solve explicitly. Exceptions to this have been found for the integrable Kerr nonlinearity and when the analytically simplifying saturable logarithmic nonlinearity is considered. Exact soliton solutions were first found in a closed form for this approximate and special type of nonlinearity [233]. In this section we will present a different type of analytical solution to the Wigner–Moyal equation in the form of a dynamical self-similar paraboloid with a parabolic intensity profile. This solution is similar to the Gaussian solutions for the logarithmic nonlinearity in the sense that all higher-order derivatives in the nonlinear terms vanish identically beyond the second-order so that the evolution is effectively governed by a Vlasov type equation. We restrict the analysis to one spatial dimension were the Vlasov equation takes the form

$$\partial_z n_k(x, z) + 2\alpha k \partial_x n_k(x, z) + \gamma \partial_x N(x, z) \partial_k n_k(x, z) = 0. \tag{126}$$

We first note that if Eq. (126) is considered as a linear equation for $n_k = n_k(x, z)$ with the intensity $N(x, z) = \frac{1}{2\pi}\int n_k(x, z)\, dk$ held constant, then it will also be satisfied by any integer power $n_k^q$ of this solution. It is thus possible to make an additive ansatz for a solution

$$n_k^q = a(z) + b(z) f_2(x) + c(z) g_2(k) + d(z) f_1(x) g_1(k), \tag{127}$$

where $f_2(x)$, $g_2(k)$, $f_1(x)$ and $g_1(k)$ are unknown functions of the spatial coordinate $x$ and the conjugate variable $k$ while $a$, $b$, $c$ and $d$ are coefficient functions dependent on the evolution variable $z$. This ansatz generalizes the stationary solution of the Vlasov equation which must be a function of the Hamiltonian invariant, as discussed explicitly in the case of the long-range Vlasov equation in Section 2.3.5. Specifically, one has $n_k(x, z) = \Phi(\alpha k^2 - \gamma N(x, z))$, with the self-consistency requirement provided by the intensity relation [238]. Following the same procedure with a separable multiplicative ansatz one can also

produce the dynamic soliton solution for a logarithmic saturable nonlinearity, c.f. [162]. Substituting the ansatz Eq. (127) into Eq. (126) leads to the following expression:

$$a'(z) + b'(z)f_2(x) + c'(z)g_2(k) + d'(z)f_1(x)g_1(k) + 2\alpha b(z)f_2'(x)k + 2d(z)f_1'(x)kg_1(k) + \gamma c(z)\partial_x N(x,z)g_2'(k) + \gamma d(z)\partial_x N(x,z)f_1(x)g_1'(k) = 0. \tag{128}$$

By considering which combinations of terms depend on each independent variable one can further subdivided this expression into four separate equations

$$a'(z) = 0, \tag{129}$$

$$b'(z)f_2(x) + \gamma d(z)\partial_x N(x,z)f_1(x)g_1'(k) = 0, \tag{130}$$

$$c'(z)g_2(k) + 2\alpha d(z)f_1'(x)kg_1(k) = 0, \tag{131}$$

$$d'(z)f_1(x)g_1(k) + 2\alpha b(z)f_2'(x)k - \gamma c(z)\partial_x N(x,z)g'(k) = 0. \tag{132}$$

For this system to have a dynamical solution we must have $a(z) = a_0 = \text{const.}, f_2(x) \propto x^2, g_2(k) \propto k^2, f_1(x) \propto x, g_1(k) \propto k$ and $\partial_x N(x,z) \propto x$. The solution thus takes the form

$$n_k^q = a_0 - b(z)x^2 - c(z)k^2 + d(z)xk, \qquad N(x,z) = e(z) - f(z)x^2 \tag{133}$$

with the coefficient functions satisfying

$$b'(z) - 2\gamma d(z)f(z) = 0, \qquad c'(z) - 2\alpha d(z) = 0, \qquad d'(z) - 4\alpha b(z) + 4\gamma c(z)f(z) = 0. \tag{134}$$

One may easily find that this system has an invariant of the form $4b(z)c(z) - d^2(z) = C_0 = \text{const.}$, that will be helpful in simplifying the remaining calculations and reduce the number of independent parameters.

Since the Wigner function must decay to zero at infinity we make the assumption that the solution is defined only where the Wigner function is positive and that the solution is identical to zero otherwise. This allows a continuous solution to be constructed, even though the derivatives are discontinuous at the boundary. This requirement is however necessary to ensure a physically reasonable solution. It remains to satisfy the intensity relation

$$N(x,z) = \frac{1}{2\pi}\int n_k(x,z)\,dk = \frac{1}{2\pi}\int \left(a_0 - b(z)x^2 - c(z)k^2 + d(z)xk\right)^{1/q} dk = e(z) - f(z)x^2. \tag{135}$$

To simplify the evaluation of this integral we note that $a_0 - b(z)x^2 - c(z)k^2 + d(z)xk = a_0 - \frac{(4b(z)c(z)-d^2(z))}{4c}x^2 - c(z)\left(k - \frac{d(z)}{2c(z)}x\right)^2 = a_0 - \frac{C_0}{4c}x^2 - c\left(k - \frac{c'(z)}{4\alpha c(z)}x\right)^2$, which shows that the solution depends only on the parameter function $c(z)$ and its derivative. The limits of the integration are given by the condition that the argument of the inner function is zero, i.e. $k = \frac{c'(z)}{4\alpha c(z)}x \pm \sqrt{\frac{1}{c}\left(a_0 - \frac{C_0}{4c(z)}x^2\right)}$. By considering that the highest power of $k$ in the integrand goes as $k^{2/q}$ and that the integration limit gives $k \propto x$, enables one to deduces that $q = 2$. Assuming $c(z)$ to be positive will then allow the integral to be evaluated as

$$N(x,z) = \frac{a_0}{4\sqrt{c(z)}}\left(1 - \frac{C_0}{4a_0c(z)}x^2\right) = I_0(z)\left(1 - \frac{x^2}{L^2(z)}\right). \tag{136}$$

To relate the function $c(z)$ and the different constant in this expression to physical quantities, instead of $e(z)$ and $f(z)$, it is convenient to define the beam width function $L(z) = 2\sqrt{a_0c(z)/C_0}$ and the peak intensity $I_0(z) = \frac{a_0^{3/2}}{2\sqrt{C_0}L(z)}$. It is also convenient to introduce a constant parameter $\Lambda = 4\alpha\sqrt{a_0/C_0}$ which has been found to characterize the degree of coherence [245]. The full solution can then be written as

$$n_k(x,z) = \sqrt{8\alpha\frac{L(z)I_0(z)}{\Lambda}\left(1 - \frac{x^2}{L^2(z)}\right) - \frac{L^2(z)}{\Lambda^2}\left(2\alpha k - \frac{L'(z)}{L(z)}x\right)}, \tag{137}$$

defined where the argument is positive and with the evolution of the beam width function satisfying

$$\frac{d^2L(z)}{dz^2} = \frac{8\alpha I_0(z)\Lambda}{L^2(z)}\left(1 - \gamma\frac{L(z)}{2\Lambda}\right). \tag{138}$$

We emphasize that this is an exact dynamical solution of both the Vlasov equation (126) and the full Wigner–Moyal Eq. (105), by virtue of the fact that the nonlinearity truncates after the second order.

The solution (137) was analyzed in [245] where it was found that the nonlinear focusing effect is generally counteracted by the incoherence while the defocusing effect is enhanced. The paraboloid solution was found to reduce to a previously known approximate parabolic solution in the coherent limit of high field intensity. The beam width function $L(z)$ governed by Eq. (138) was, for a focusing nonlinearity, further shown to either oscillate between two limits or to monotonically approach an asymptotic value at a rate depending on the degree of coherence.

### 4.6. Subsequent developments

In this section we briefly comment several important developments of the theoretical approaches discussed above.

#### 4.6.1. Extension to nonlocal nonlinearities

The theory of incoherent solitons in inertial nonlinear media has been extended to account for a nonlocal nonlinearity. The main motivation for these studies was the experimental observation of incoherent solitons in nematic liquid crystals [23,24]. Besides their strong noninstantaneous saturable Kerr-like nonlinearity, liquid crystals are known to exhibit a nonlinear response which is also inherently spatially nonlocal, because the molecular reorientation induced by a light beam in a particular place will affect the orientation of molecules far beyond this point. In this way, different theoretical approaches have been developed to study incoherent solitons with a nonlocal and inertial nonlinearity. On the one hand, the mutual coherence function approach has been extended by considering the particular example of a nonlocal logarithmic nonlinearity [246]. Analytical formulas for the evolution of the beam parameters and conditions for the formation of nonlocal incoherent solitons are thus derived. On the other hand, the self-consistent multimode theory has been applied to the coupled equations governing wave propagation with the orientational nonlinearity of the nematic crystal taken into account [247]. A family of partially coherent soliton solutions is obtained, which is characterized by a relation between the power of the optical beam and the number of guided modes. The complex coherence factors are also obtained in closed form. We also note that incoherent surface solitons in a noninstantaneous and nonlocal nonlinear medium have been demonstrated theoretically and experimentally [248]. These incoherent surface waves are located at the interface between a nonlinear medium with long-range nonlocality and a linear dielectric medium.

#### 4.6.2. Extension to white light

An other important generalization of the previous studies is the extension of the theory of incoherent solitons and MI to the propagation of both spatially and temporally incoherent light [4]. It should be noted that, owing to the slowly responding nonlinearity, the temporal dynamics the incoherent wave is averaged out by the inertial nonlinearity, as discussed above in Section 4.1. In other words, the induced nonlinear index of refraction is unable to follow fast phase fluctuations of incoherent light but responds only to the time-averaged intensity, $\langle I\rangle$, which is independent of time, $\partial_t \langle I\rangle = 0$ – the time average being taken over the response time of material, $\tau_R$. The four different formalisms discussed above can thus be extended by including a dependence of the relevant functions (coherent density function, modal functions, or mutual coherence functions) on the frequency $\omega$ – though the equations governing the evolutions of such functions do not involve temporal dynamics. It should also be underlined that a generalized theory accounting for the contribution of pronounced intensity fluctuations of white-light-like sources has been developed in Ref. [237].

On the basis of these extensions of the four theoretical formalisms, white-light incoherent solitons [249,250] and white-light incoherent MI [251] have been theoretically predicted and observed experimentally [252,4]. In this way, characteristic features of the temporal power spectrum and the spatiotemporal coherence properties of white-light solitons have been described. For instance, the spatial intensity profile of light within some specific frequency interval $[\omega, \omega + d\omega]$ is wider (less localized) at lower frequencies and narrower at higher frequencies. Furthermore, the spatial correlation distance (across the soliton) is always larger for lower frequencies and shorter for higher frequencies [249]. Regarding white-light MI, it was shown that the frequency spectrum directly affects the strength of the MI gain, and can destabilize or stabilize the beam. The MI then appears as a collective effect, where all the temporal frequencies participate in the formation of the MI pattern by self-adjusting their respective contributions [251].

#### 4.6.3. Extension to periodic lattices

Nonlinear systems with inherent periodicity are abundant in nature and examples can be found in such diverse fields as biology, chemical physics, nonlinear optics, Josephson-junctions or Bose–Einstein condensates. Soliton solutions in periodic media have been widely studied and we refer the reader to the recent comprehensive reviews for details [253,254,6]. Actually, nonlinear waveguide arrays have been mostly treated with the coupled mode theory, where the dynamics is well approximated by the discrete NLS equation [255]. In a more general approach, the Floquet–Bloch theory is used to analyze a continuous differential equation with a periodic potential term. The main feature of wave propagation in periodic systems is the interference of waves reflected by the lattice – a property which is responsible for the richness of the dynamics in periodic media. These interference effects obviously depend on the coherence properties of the waves. However, in nonlinear periodic lattices, most studies have been essentially limited to the dynamics of coherent waves. This is justified provided that the coherence length of the waves is much larger than the characteristic dimension of the system (e.g., the lattice spacing). However, when the two length scales become comparable, the interference effects affect the interplay between the statistical (coherence) properties of the waves and the lattice periodicity.

This regime of incoherent nonlinear wave evolution in periodic media was studied theoretically [19], and subsequently experimentally [20], in the limit of a slowly responding (i.e., inertial) nonlinearity. The authors considered the NLS equation in the presence of a periodic potential along the direction of propagation of the wave. By making use of the modal expansion theory discussed above for the homogeneous case, the authors have constructed incoherent soliton states. These incoherent solitons are characterized by an intensity profile, a power spectrum, and coherence properties which conform to the

periodicity of the lattice. Subsequent theoretical studies predicted the existence of incoherent gap solitons in waveguide arrays, i.e., gap solitons constructed from partially spatially incoherent light [256,257]. The experimental observation of these entities has then been reported in Ref. [258]. It should be underlined that incoherent MI and white-light solitons in periodic lattices have been also investigated with an inertial nonlinearity [259,260].

#### 4.6.4. Pattern formation in cavities

The dynamics of incoherent optical waves in an optical system with feedback is the subject of growing interest in recent years, in relation with the phenomena of optical wave thermalization and condensation in passive optical cavities or in different kinds of laser systems. These aspects will be discussed in more detail in Section 7. Here we briefly comment on some interesting works in optical cavities which are closely related to the spatio-temporal inertial nonlinearity discussed in this Section 4.

The spatial dynamics of a partially coherent wave circulating in a passive cavity that exhibits an inertial nonlinearity has been studied both theoretically [261] and experimentally [262–264]. The system consists of a passive ring cavity of length $L_c$, containing a nonlinear medium of length $L \ll L_c$. The light wave coupled into the cavity is partially incoherent, with a 'temporal' coherence length, $\lambda_c$, much shorter than the cavity length, $L \ll \lambda_c \ll L_c$. The cavity is characterized by a low-finesse, a property which is in contrast to the passive cavity considered in Section 7.3. The response time of the nonlinearity is much longer than (i) the characteristic time of phase fluctuations across the beam and (ii) the average time of phase fluctuations between the beams from different cycles.

The main result of these studies was to show that, in spite of the spatial incoherence of the optical wave, the optical cavity exhibits pattern formation dynamics. The slowly responding (inertial) nonlinearity is the key physical mechanism responsible for the pattern formation in this incoherent cavity. By making use of the mutual coherence function formalism discussed above, a stability analysis of a uniform intensity beam in the cavity was performed in [261]. It was shown that the pattern formation process is always associated with two consecutive thresholds, which are determined by the degree of spatial coherence, the strength of the nonlinearity, and the cavity feedback parameter. At the first threshold the beam becomes unstable, as the nonlinear self-focusing overcomes the diffusive tendency of spatially incoherent light. The second threshold occurs when the nonlinear gain overcomes the loss in a single pass. The first threshold does not depend on the cavity boundary conditions, a property which is in contrast with coherent cavities [265,266], whereas the second threshold is an inherent feature of the cavity.

#### 4.6.5. Interaction between incoherent solitons

The interaction between incoherent solitons has been studied within various contexts. An important case is the 1D interaction of partially coherent solitons in Kerr type inertial nonlinear media, which has been investigated using the self-consistent multimode theory [267], for which the governing system of equations can be written in the form of a Manakov system of integrable NLS equations [268]. This allows partially coherent solitons to be analytically found, and understood not only as linear mode solutions of their own self-induced multimode waveguides, but as multisoliton complexes made up of individual, but incoherently interacting, coherent soliton solutions for each mode. The partially coherent solitons does not even have to be symmetric like the bright soliton solutions considered in Section 4.4.1 but can have a more general shape, which depends both on free parameters for each component and on the number of modes involved, and are nevertheless able to propagate as stationary intensity profiles. It has been found both theoretically and experimentally that partially coherent solitons can change their shape during collisions while still remaining as stationary solitons even after the collision, see [267,269]. An example of this is shown by the collision of a symmetric and an asymmetric partially coherent soliton in Fig. 21, where the two partially coherent solitons consist of two modes each. It should be emphasized that this collision occurs elastically, without the emission of any radiation, due to the integrability of the inertial Kerr type model.

Besides the inverse scattering transform, different methods have been also developed to study the richness of the problem associated with the interaction of incoherent solitons. From a general point of view, if one considers the incoherent nature of the soliton interaction, one might expect the interaction to be phase-insensitive and thus always attractive [270,271,6]. However, theoretical work revealed that incoherent solitons can exhibit a phase-sensitive interaction. This phase-sensitive interaction can be understood from the point of view of the modal theory. Each mode will experience an incoherent and thus attractive interaction with the other mode and will separately conserve mode energy. However, if two partially coherent solitons populate the same modes then the different components of each mode will be able to interact coherently with one another. This coherent interaction can be either attractive or repulsive depending on the relative phase between the components. The character of the overall interaction, which depends on the complicated combined interaction of all components both within and between the different modes, can therefore also be attractive or repulsive. In Ref. [272], the authors showed both theoretically and experimentally that the interaction dynamics of two closely spaced solitons that are made incoherent as a whole is fundamentally different from the case when the solitons are mutually coherent. It was shown that the interaction strength and the associated interaction length can be controlled by the amount of incoherence in the solitons. The interaction can change from attractive to repulsive near a certain threshold in the coherence parameter. In a subsequent theoretical study [273], it was shown that the problem of interaction of partially incoherent soliton stripes can be transformed into a form equivalent to that of (coherent) vector soliton interaction, where however the state of polarization corresponds to and is determined by the incoherence properties of the solitons. A variational approach was used to study

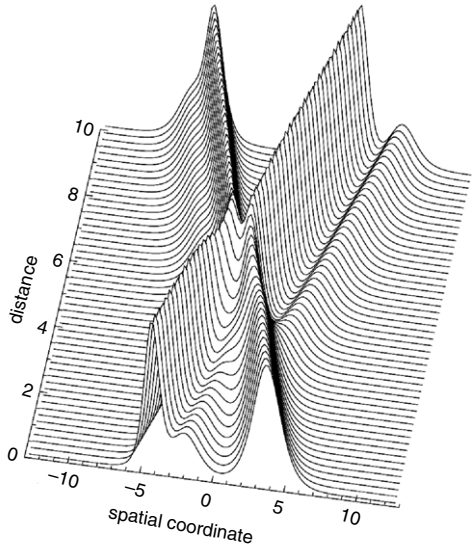


**Fig. 21.** Collision of a symmetric and an asymmetric partially coherent soliton consisting of two linear modes.
*Source:* From Ref. [267].

the interaction dynamics and analytical expressions for the change in the soliton parameters were obtained. These showed among other the variation of the relative distance between the solitons, with the possibility of a change from attractive to repulsive interaction at a certain critical degree of incoherence. The analysis revealed that the interaction may even change several times between attractive and repulsive and vice versa as the degree of incoherence of the solitons increases.

Also notice that the interaction of nonlocal incoherent spatial solitons in strongly nonlocal Kerr media has been investigated numerically [274]. The role of important parameters, such as the relative phase, the separation, the extent of nonlocality and the input power, has been found to be very similar to the case of nonlocal coherent soliton interactions. Interactions of incoherent white-light solitons in the presence of a logarithmic saturable nonlinearity has been also investigated [275], revealing that all the frequencies participate in the interaction (see Section 4.6.2).

We finally remark that the interaction of elliptic incoherent solitons has been also investigated. Contrarily to conventional 2D coherent solitons which are known to be always circular in isotropic self-focusing nonlinear materials, incoherent solitons can exhibit an elliptic structure provided that their correlation function is anisotropic [276]. During a collision event of two such elliptic incoherent solitons, their intensity ellipse rotates, and at the same time as their centers of gravity tend to revolve around each other. This type of elliptic incoherent solitons has been observed experimentally in Ref. [277].

### *4.7. Experiments*

Although this review article focuses on the theoretical formulations of the dynamics of incoherent nonlinear waves, we will here also briefly comment on some major experimental results, and refer the reader to the following review for a more complete discussions [5]. As discussed in the Introduction Section 1, the remarkable simplicity of experiments performed in photorefractive nonlinear crystals allowed for a fruitful investigation of the dynamics of incoherent nonlinear optical waves in the presence of an inertial nonlinearity. Most of these experimental works were conducted by M. Segev and his collaborators [5].

#### *4.7.1. Incoherent solitons*

*Bright incoherent solitons*

The first experimental demonstration of self-trapping of partially coherent light and the generation of a partially coherent spatial soliton was performed by Mitchell et al. [3] in 1996 (see Figs. 22–23). This experiment showed that by imposing random phase fluctuations onto a two-dimensional continuous wave beam it could self-trap and then propagates through a biased nonlinear photorefractive crystal without changing its width. As already discussed in Section 1, a key requirement for the existence of partially coherent solitons is that the nonlinearity is inertial, i.e. slowly responding. The experiment was cleverly designed to make use of the photorefractive nonlinearity of a Strontium–Barium–Niobate (SBN) crystal which allowed both the strength and the response time of the nonlinearity to be controlled by the application of an external voltage and by the beam intensity, respectively. Photorefractive crystals have properties that enables them to exhibit a very long response time for low intensities, allowing them to respond on a timescale which is long with respect to the random phase fluctuations of the beam, and thus fulfilling the requirement of being sensitive only to the smooth averaged intensity profile. The photorefractive nonlinearity relies on the optical excitation of electrons in the lit region of the medium into the

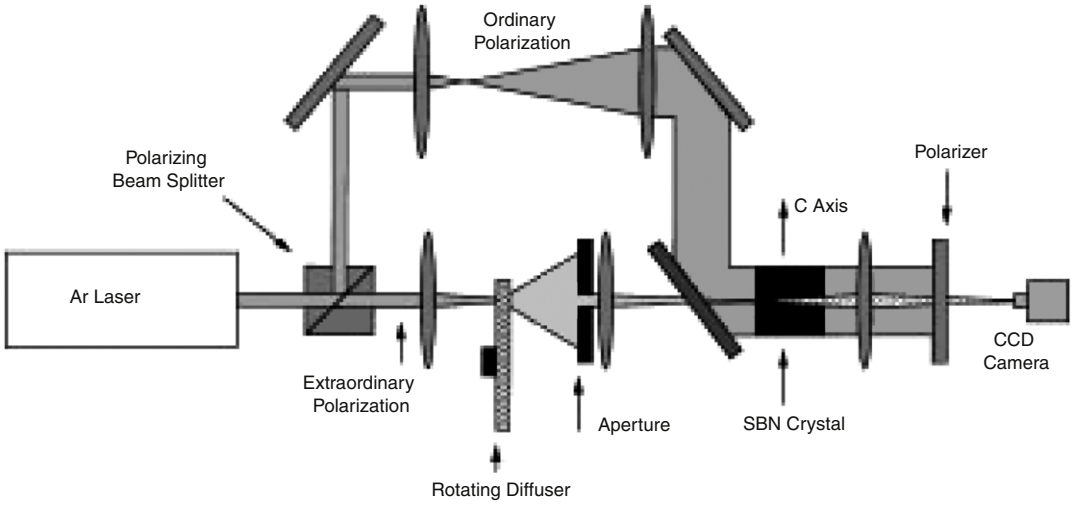


**Fig. 22.** Experimental setup for the observation of bright incoherent solitons. See the text for more details on the experiment.
*Source:* From Ref. [3].

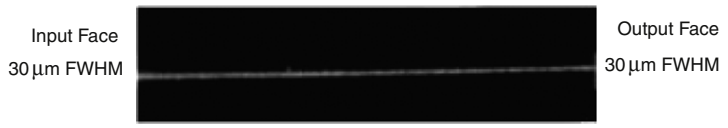


(a) Self-trapped beam.


(b) Regular diffracting beam.

**Fig. 23.** Photographs of the beam self-trapped by the nonlinearity (above) and the normally diffracting beam in its linear regime of propagation (below). The setup used in the experiment is reported in Fig. 22.
*Source:* From Ref. [3].

conduction band, which locally increases the conductivity. As a consequence there will be a larger voltage drop in the dark regions as compared to the lit regions in the medium, with a concomitant space-charge field of greater magnitude. This space-charge field will in turn cause a change in the refractive index through the electro-optic (Pockels') effect, with the refractive index change being proportional to the position dependent field, which will effectively manifest itself as a graded index waveguide.

A bright self-trapped soliton beam should maintain a constant width while propagating through the medium, with the nonlinear self-focusing effect being exactly balanced by diffractive broadening. In the experiment [3] a partially coherent beam was launched into the photorefractive crystal with an initial width of 30 μm at the input face (see Fig. 22). This beam would have broadened to a width of 102 μm after propagating through the 6 mm long crystal in the absence of a nonlinear self-focusing effect. This large amount of diffractive broadening is a direct consequence of the incoherent nature of the beam, since a fully coherent beam of the same initial width would broaden to only 36 μm when propagating through the same medium. Self-trapping was achieved after applying a voltage of 550 V to electrodes that were attached parallel to the direction of polarization of the beam and separated by 6 mm. The result was a non-diffracting, self-trapped, beam that had the same width at the output face as at the input, as illustrated in Fig. 23. The partial coherence of the spatial beam was imposed by scattering it off a rotating diffuser, which produced random phase fluctuations and associated intensity speckles on a time scale associated with the mechanical rotation (about 1 μs). The crystal medium had a response time that was slow enough that the nonlinearity could be considered to be inertial, and thereby respond only to the smooth time averaged intensity of the beam and not to the instantaneous speckle pattern.

*Experiments in nematic liquid crystals*

It is important to note that, besides photorefractive nonlinear crystals, the existence of incoherent bright solitons [23,24] and subsequently incoherent MI [278], has been also demonstrated in nematic liquid crystals. We refer the reader to the above three articles for details (also see the review [145]). As discussed above in Section 4.6.1, besides their strong

noninstantaneous saturable Kerr-like nonlinearity, liquid crystals are known to exhibit a nonlinear response which is also spatially nonlocal as a result of the molecular reorientation. This motivated different extensions of the theoretical methods developed to describe incoherent solitons (see Section 4.6.1).

*White light solitons*

Soon after the first experimental demonstration of self-trapping of partially coherent light beams followed another demonstration of self-trapping of a white light beam from an incandescent source by Mitchell et al. [4] in 1997. The source used was a quartz–tungsten–halogen incandescent bulb that generated white light with a temporal coherence time in the order of a few femtoseconds. Since this light source was already incoherent there was no need to impose any additional incoherence onto the beam, and the rotating diffuser was consequently left out of the experimental setup. The light from the bulb was spectrally filtered to a wavelength range of 380–720 nm and collimated to a beam before entering the photorefractive SBN crystal used as the nonlinear medium. The input beam had a width of 14 $\mu$m and would have diffracted to 82 nm after propagating through the 6 mm long crystal in the absence of self-focusing. This should be compared to its coherent counterpart which would have diffracted to only 35 $\mu$m at a wavelength of 380 nm or to 63 $\mu$m at a wavelength of 720 nm, respectively. The application of 600 V to the electrodes resulted similarly to the previous experiment in the self-trapping of the beam at a width of 12 $\mu$m. This experiment clearly shows that the presence of a coherent (laser) light source is not required for soliton formation as long as the nonlinear medium is of the inertial type allowing other types of light sources such as e.g. incandescent bulbs or LEDs to be used instead. We also note that, as discussed above in Section 4.6.2, white-light incoherent MI has been theoretically predicted [251] and observed experimentally [252], as well as white-light solitons in periodic lattices [259].

*Dark incoherent solitons*

Incoherent dark solitons have also been experimentally observed. A 1998 experiment [14] provided the first experimental demonstration of self-trapping of a dark notch in a spatial light beam that was partially incoherent. Dark incoherent wavepackets were observed both in the form of one dimensional dark stripes and two dimensional dark holes, that were self-trapped to form dark solitons (see Fig. 24). The experimental setup was similar to the one described above that was used to observe bright incoherent solitons. A biased photorefractive crystal was used but with the polarization of the applied electric field reversed to provide a self-defocusing instead of a self-focusing effect. The initial input profile for the one dimensional case consisted of a dark notch in a broad partially coherent background. The initial width of the notch was 18 $\mu$m which would have diffracted to 38 $\mu$m after propagating 11.7 nm through the crystal in the absence of the self-defocusing nonlinear effect which could be controlled by the applied voltage. The notch was self-trapped to preserve its initial width by applying a voltage of $-440$ V across the transverse dimension of the beam using electrodes separated by 5.3 nm. The experimental results confirmed the theoretical predictions that incoherent dark solitons are always gray [13,279], and that a larger degree of incoherence requires a higher intensity for self-trapping to occur. The need for a slowly responding nonlinearity was moreover demonstrated since the beam was found to fragment due to the stationary speckle pattern when the rotation of the diffuser was stopped and the crystal was allowed to reach its steady-state response. The extension to two dimensional beams was further considered with the demonstration of self-trapping of a dark soliton hole using a vortex-type beam [14].

An incoherent dark soliton also gives rise to interesting behaviors when it interacts with a bright soliton. Indeed, similar to the case of bright solitons, a dark soliton also changes the refractive index of the medium and thus induces a graded-index waveguide. In this way, it was shown that a coherent light beam can be guided through the waveguide created by an incoherent dark soliton [280]. Another interesting study revealed that the degree of coherence of a bright incoherent soliton can be strongly affected through its interaction with a dark coherent (or incoherent) spatial soliton [281]. Indeed, during the nonlinear interaction of the dark and bright beams, only a part of the incoherent bright beam is trapped (guided) by the dark beam, thus leading to the formation of a sharp intensity spike. In this region, the correlation length of the incoherent bright beam increases by at least two orders of magnitude. This constitutes a remarkable simple mechanism for increasing in a significant way the coherence of a localized incoherent optical beam.

*Influence of the initial phase profile*

The impact of the initial phase profile at the beam center of an incoherent dark stripe has been shown to play an unexpected and remarkable role on the propagation dynamics [279,282]. Experimental results show that an initial phase shift at the center of the stripe is essential for the evolution of dark incoherent solitons. If the phase jumps by $\pi$, a single gray incoherent soliton emerges. Conversely, if the phase is continuous across the input dark stripe, then two gray incoherent solitons emerge but they separate from each other with propagation [282]. Note that this behavior is similar to that occurring for coherent dark solitons [283]. The dynamics of these incoherent dark entities are associated with strong "phase-memory" effects that are otherwise absent in the linear regime.

### *4.7.2. Incoherent modulational instability*

Modulational instability of a partially coherent beam has been also experimentally observed, as illustrated in Fig. 25. In a 2000 experiment Kip et al. [16] showed that the nonlinearity does indeed has to exceed a threshold depending on the coherence properties of the beam in order for MI to occur, in accordance with theoretical predictions. The experiment used the by now familiar setup with a photorefractive SBN crystal as the nonlinear medium. The extraordinary polarization was used as a signal beam while the ordinary polarization was used as the background and served to tune the saturation of

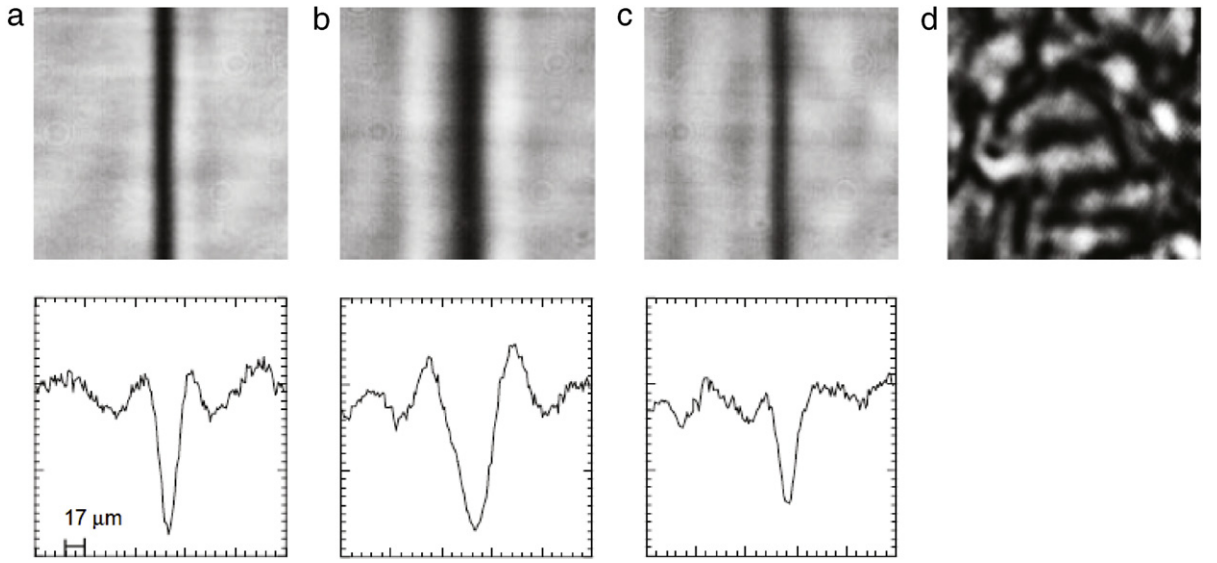


**Fig. 24.** Self-trapping of a dark stripe carried by a partially spatially incoherent beam. Shown are photographs and beam profiles of (a) the input beam, (b) diffracted output beam, and (c) the self-trapped output beam. The last photograph (d) shows the output beam in the presence of nonlinearity when the diffuser is stationary, illustrating the fragmentation of an incoherent dark stripe in an instantaneous self-defocusing medium.
*Source:* From Ref. [14].

the photorefractive nonlinearity. The incoherence was imposed by passing the beam through a rotating diffuser and the intensity profile at the output face was captured on a CCD camera. The experiment showed that the MI caused the optical beam to disintegrate above a certain threshold depending on the coherence properties, and resulted in the formation of one dimensional spatial filaments. A further increase of the strength of the nonlinearity resulted in a second transition and the formation of a two dimensional array pattern of self-ordered spots. The distance between the adjacent filaments and spots were much longer than the correlation length of the beam. The experiment demonstrated that both one and two dimensional spatial patterns can form spontaneously from noise for partially coherent waves in inertial nonlinear media due to the MI process, which is a known precursor to soliton formation. The experiment showed good agreement when compared with the one dimensional theory, predicting among others the dominant spatial frequency with the largest growth rate [240]. We note that induced incoherent MI has been also investigated experimentally in [284].

The possibility of suppressing MI using partial incoherence has been exploited in different circumstances. For instance, it has been used to form stable one dimensional soliton stripes in inertial bulk Kerr media [285,286]. Normally these stripes are unstable in the coherent case in the other spatial dimension. However, one may consider a stripe that is fully coherent in the self-trapping dimension, but partially incoherent and uniform in the other transverse dimension. Owing to incoherent MI suppression, such stripes become transversely stable when the amount of incoherence is above a certain threshold.

Following a similar idea, incoherent antidark solitons have been studied theoretically and experimentally [244]. The idea that bright solitons can exist on top of a nonvanishing background received lot of interest in the literature, see, e.g., [287–289]. As discussed above in Section 4.4.3, the instability of antidark solitons is usually triggered by the MI of the coherent background needed to confine the bright part of the antidark soliton. However, this MI can be suppressed owing to an incoherent background. In this way, incoherent antidark solitons have been shown to propagate in a stable fashion, provided that the spatial coherence of their background is reduced below the incoherent MI threshold [244].

## 5. Wave turbulence approach

In the previous Sections 2–3 we considered the Vlasov and WT Langmuir equations which are quadratic nonlinear equations whose derivations refer to a first-order closure of the hierarchy of moments equations. These kinetic equations are formally reversible and describe, in particular, the spontaneous formation of incoherent soliton structures. Let us now consider the following two limits. (i) In the spatial domain the limit of homogeneous statistics of a broadband incoherent wave, so that the Vlasov equation becomes irrelevant, as commented through Fig. 2 in Section 1. (ii) In the temporal domain the limit of stationary statistics and instantaneous response of the nonlinearity, so that the WT Langmuir equation becomes irrelevant, as commented through Fig. 3. In both limits, we thus need to close the hierarchy of the moments equations to the second-order. The analysis reveals that in this case the appropriate formalism for the description of the random wave is provided by the Hasselmann WT kinetic equation, which is a cubic nonlinear equation.

In this section we discuss the WT kinetic equation in the spatial and the temporal domains. In the spatial domain, we present the WT formalism in both the waveguide configuration (in a 'trapping potential') and in infinite space through the

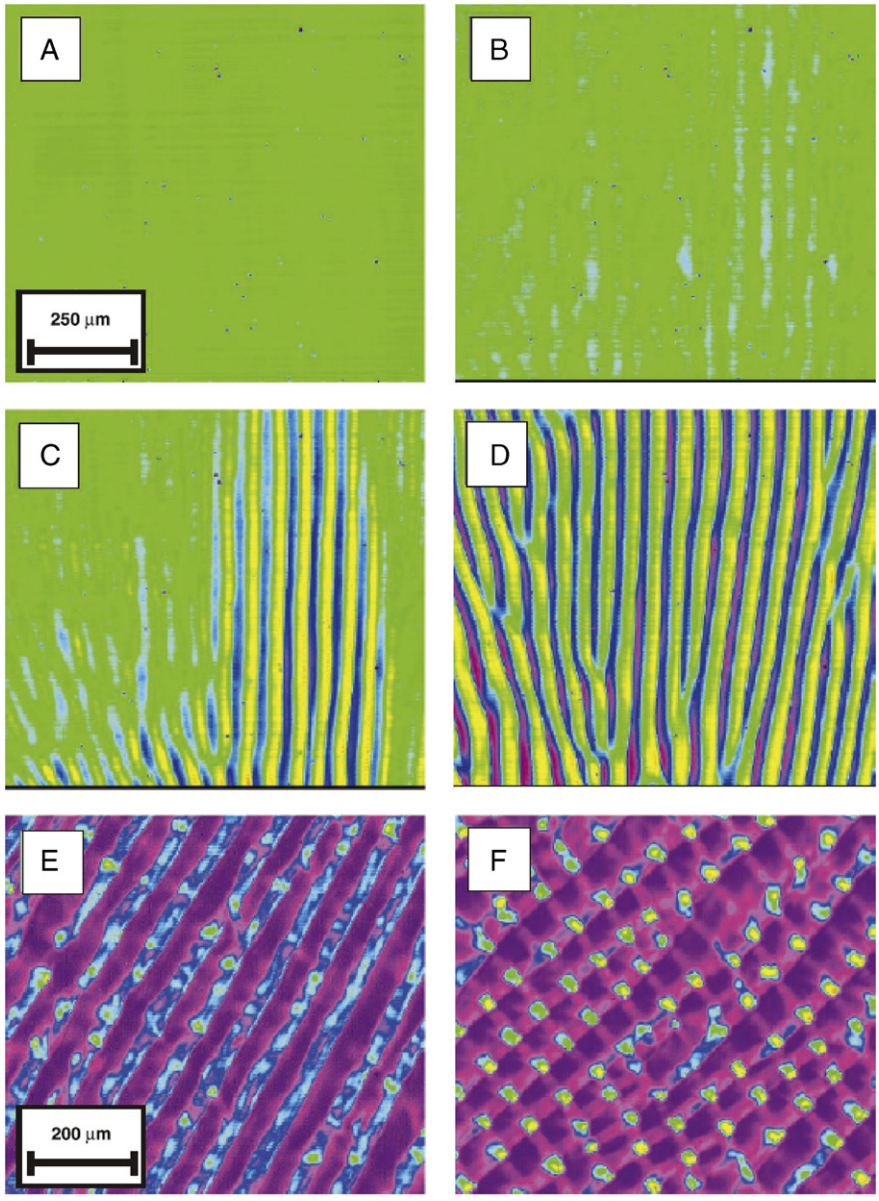


**Fig. 25.** Experimental observation of incoherent MI: The intensity structure of a partially spatially incoherent beam at the output plane of the nonlinear crystal. The sample is illuminated homogeneously with partially spatially incoherent light with a coherence length of 17.5 μm. The displayed area is 1.0 by 1.0 mm (A through D) and 0.8 by 0.8 mm (E and F), respectively. The size of the nonlinear refractive index change of the crystal is successively increased from (A) to (F). The plots (B through D) show the cases just below threshold (no features), at threshold (partial features), and just above threshold (features throughout) for 1D incoherent MI that leads to 1D filaments. Far above this threshold, the 1D filaments become unstable (E) and become ordered in a regular 2D pattern (F).
*Source:* From Ref. [16].

phenomena of optical wave thermalization and condensation (Section 5.2). In the temporal domain, the one-dimensional WT kinetic equation is discussed in the framework of a phenomenon of velocity-locking (Section 5.3), and more generally in the context of supercontinuum generation (Section 5.4).

### *5.1. Hasselmann wave turbulence kinetic equation*

#### *5.1.1. Wave turbulence in a waveguide*

The WT description of a random wave has been essentially developed in the ideal situation in which the random wave is supposed 'infinitely extended in space', an assumption that may be considered as justified when its correlation length is much smaller than the size of the whole beam. However, the propagation of an incoherent localized beam is

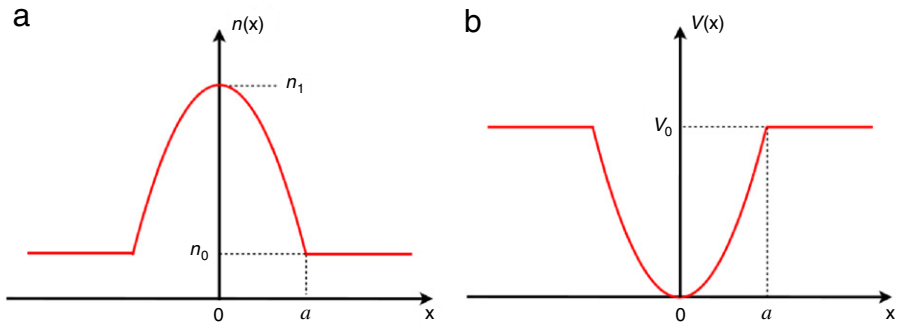


**Fig. 26.** Refractive index profile $n(x)$ of an optical waveguide (graded-index fiber) (a), and corresponding confining potential $V(x)$ in the NLS Eq. (139) (b). The finite depth of the potential, $V_0$, introduces an effective frequency cut-off for the classical wave problem. The existence of an inhomogeneous (e.g., parabolic) potential reestablishes wave condensation in the thermodynamic limit in 2D, in analogy with quantum Bose–Einstein condensation.

eventually affected by incoherent diffraction, which inevitably affects the processes of thermalization and condensation. In the following we derive the WT kinetic equation by considering the propagation of the incoherent beam in an optical waveguide. In the guided configuration, incoherent diffraction is compensated by a confining potential, thus allowing to study the thermalization and the condensation of the optical field over large propagation distances. Accordingly, we consider the NLS equation with a confining potential $V(\boldsymbol{x})$ and we formulate a WT description of the random wave into the basis of the eigenmodes of the waveguide (i.e., potential's eigenmodes), instead of the usual plane-wave Fourier basis relevant to statistically homogeneous random waves [$V(\boldsymbol{x}) = 0$] [290].

The NLS equation with a confining potential $V(\boldsymbol{x})$ reads

$$i\partial_z\psi = -\alpha\nabla^2\psi + V(\boldsymbol{x})\psi - \gamma|\psi|^2\psi. \tag{139}$$

Note that in this section we deal essentially with a defocusing nonlinearity, $\gamma < 0$ (so as to ensure the stability of the homogeneous plane-wave solution, i.e., condensate). We recall that this NLS equation conserves the power of the optical field, $N = \int |\psi|^2\, d\boldsymbol{x}$. The NLS equation also conserves the total energy (Hamiltonian) $H = E + U$, which has a linear contribution,

$$E = \int \alpha|\nabla\psi|^2\, d\boldsymbol{x} + \int V(\boldsymbol{x})|\psi|^2\, d\boldsymbol{x}, \tag{140}$$

and a nonlinear contribution,

$$U = -\frac{\gamma}{2}\int |\psi|^4\, d\boldsymbol{x}. \tag{141}$$

The potential $V(\boldsymbol{x})$ models the waveguide in which the optical beam propagates. For instance, if one considers a multimode optical fiber, the waveguide potential exhibits a revolution symmetry with respect to the axis of propagation of the beam. Then a direct correspondence exists between $V(|\boldsymbol{x}|)$ and the transverse refraction index profile of the waveguide. For a graded-index multimode fiber, we have $V(|\boldsymbol{x}|) = q|\boldsymbol{x}|^2$ if $|\boldsymbol{x}| \leq a$ and $V(|\boldsymbol{x}|) = V_0$, if $|\boldsymbol{x}| \geq a$, where $q = V_0/a^2$ [290]. This potential is schematically illustrated in Fig. 26. In this way the finite depth of the potential $V_0 < \infty$ introduces an effective frequency cut-off for the classical wave. This is due to the fact that the nonlinear coupling among bounded and unbounded modes is negligible, because of the poor spatial overlap of the corresponding modes.[3]

*Basic considerations*

We assume that the initial random field $\psi(\boldsymbol{x}, z = 0)$ can be expanded into the orthonormal basis of the eigenmodes of the linearized NLS equation [Eq. (139) with $\gamma = 0$],

$$\psi(\boldsymbol{x}, z = 0) = \sum_m c_m(z = 0)\, u_m(\boldsymbol{x}), \tag{142}$$

where the index $\{m\}$ labels the two numbers $(m_x, m_y)$ needed to specify the mode that $u_m(\boldsymbol{x})$ refers to. The modal coefficients are random variables uncorrelated with one another, $\langle c_m(z = 0)c_n^*(z = 0)\rangle = n_m(z = 0)\,\delta^K_{n,m}$, $\delta^K_{n,m}$ being the Kronecker's

[3] The efficiency of the generation of unbounded modes ($\omega \leq V_0$) is several orders of magnitude smaller than the conversion efficiency between bounded modes ($\omega \leq V_0$), so that their excitations can be neglected [for details see appendix 4 in [290]].

symbol. We remark that this formalism is also known as the Karhunen–Loeve expansion.[4] The eigenmodes $u_m(\boldsymbol{x})$ are orthonormal, $\int u_m(\boldsymbol{x})\, u_n^*(\boldsymbol{x})\, d\boldsymbol{x} = \delta^K_{n,m}$, and satisfy the 'stationary' (i.e., $z$-independent) Schrödinger equation

$$\beta_m u_m(\boldsymbol{x}) = -\alpha\nabla^2 u_m(\boldsymbol{x}) + V(\boldsymbol{x}) u_m(\boldsymbol{x}), \tag{143}$$

with the corresponding eigenvalues $\beta_m$.

As it propagates through the waveguide the incoherent field $\psi(\boldsymbol{x}, z)$ can be represented as a superposition of modal waves with random coefficients $c_m(z)$, which denotes the respective modal occupancy:

$$\psi(\boldsymbol{x}, z) = \sum_m c_m(z)\, u_m(\boldsymbol{x})\, \exp(-i\beta_m z). \tag{144}$$

In the linear regime of propagation $\gamma = 0$, we have $c_m(z) = c_m(z = 0)$. In the nonlinear regime, we will follow in the next section the procedure of the random phase approximation underlying the WT theory [37,47]. In particular, the modal occupancies $c_m(z)$ are still random variables uncorrelated with one another, $\langle c_m(z) c_n^*(z)\rangle = n_m(z)\, \delta^K_{n,m}$. The modal occupancies $n_m(z)$ satisfy a coupled system of nonlinear equations that we shall describe below.

The average local power of the field is $\langle|\psi(\boldsymbol{x}, z)|^2\rangle = \sum_m n_m(z)\, |u_m(\boldsymbol{x})|^2$, and a spatial integration over $\boldsymbol{x}$ gives the total average power of the beam

$$N = \sum_m n_m(z), \tag{145}$$

which is a conserved quantity. The parameter $n_m(z)$ thus denotes the amount of power in the mode $\{m\}$. It can be obtained by projecting the field $\psi(\boldsymbol{x}, z)$ on the corresponding eigenmode $u_m(\boldsymbol{x})$,

$$n_m(z) = \left\langle \left| \int \psi(\boldsymbol{x}, z)\, u_m^*(\boldsymbol{x})\, d\boldsymbol{x} \right|^2 \right\rangle = \langle |c_m(z)|^2\rangle . \tag{146}$$

Wave condensation takes place when the fundamental mode becomes macroscopically populated, i.e., when $n_0 \gg n_m$ for $m \neq 0$ [291,292].

In the same way, by substituting the modal expansion of the incoherent field $\psi(\boldsymbol{x}, z)$ into the expression of the linear energy (140), one obtains

$$E(z) = \sum_m E_m(z) = \sum_m n_m(z)\, \beta_m. \tag{147}$$

The total linear energy is the sum of the modal energies weighted by the corresponding modal occupancy $n_m(z)$.

*Wave turbulence kinetic equation in a waveguide*

We now study the influence of a weak nonlinear coupling among the modes, so that the modal occupancies defined by (146) depend on $z$, $n_m(z)$. This weakly nonlinear regime precisely corresponds to the regime investigated numerically in Section 5.2.4. Substituting the modal expansion (144) into the NLS Eq. (139), one obtains

$$i\partial_z a_m = \beta_m a_m - \gamma \sum_{p,q,s} W_{mpqs} a_p a_q^* a_s \tag{148}$$

where $a_m(z) = c_m(z)\, \exp(-i\beta_m z)$, and the fourth-order tensor is defined by the overlap integral

$$W_{mpqs} = \int u_m^*(\boldsymbol{x}) u_p(\boldsymbol{x}) u_q^*(\boldsymbol{x}) u_s(\boldsymbol{x})\, d\boldsymbol{x}. \tag{149}$$

Eq. (148) conserves the total power $N = \sum_m |a_m|^2$ and the Hamiltonian

$$H = \sum_m \beta_m |a_m|^2 - \frac{\gamma}{4} \sum_{m,p,q,s} \left( W_{mpqs} a_m^* a_p a_q^* a_s + W_{mpqs}^* a_m a_p^* a_q a_s^* \right). \tag{150}$$

Starting from Eq. (148) and following the procedure of the random phase approximation [37,47], we derive in the Appendix A.7 the irreversible kinetic equation governing the nonlinear evolution of the modal occupancies. For this purpose, we take the continuum limit of the discrete sum over the modes $\{m\}$, which is justified when one deals with a large number of modes, i.e., $V_0/\beta_0 \gg 1$. The substitution of the discrete sums by continuous integrals also refers to the so-called

[4] In the Karhunen–Loeve expansion, $\{u_m(\boldsymbol{x})\}$ are eigenfunctions of the integral equation, $\int B(\boldsymbol{x}_1, \boldsymbol{x}_2)\, u_m(\boldsymbol{x}_2)\, d\boldsymbol{x}_2 = n_m\, u_m(\boldsymbol{x}_1)$, where $n_m$ are the corresponding eigenvalues and $B(\boldsymbol{x}_1, \boldsymbol{x}_2, z) = \langle \psi(\boldsymbol{x}_1, z)\, \psi^*(\boldsymbol{x}_2, z)\rangle$ is the correlation function. The modal expansion of the correlation function reads $B(\boldsymbol{x}_1, \boldsymbol{x}_2) = \sum_m n_m\, u_m(\boldsymbol{x}_1)\, u_m^*(\boldsymbol{x}_2)$. In the quantum context, the correlation function is known as the one-body density matrix, which allows one to define the concept of long-range order (see e.g., Chap. 2 in [291], or Chap. 1 in [292]).

'semiclassical description of the excited states' [292]. Its validity implies that the relevant excitation energies contributing to the discrete sum are much larger than the level spacing $\beta_0$, i.e., the spreading of the modal occupancies is much larger than $\beta_0$. In Appendix A.7 we derive the following kinetic equation governing the irreversible evolution of the modal occupancies

$$\partial_z \tilde{n}_{\boldsymbol{\kappa}}(z) = \frac{4\pi\gamma^2}{\beta_0^6}\iiint d\boldsymbol{\kappa}_1 d\boldsymbol{\kappa}_2 d\boldsymbol{\kappa}_3 \delta(\tilde{\beta}_{\boldsymbol{\kappa}_1}+\tilde{\beta}_{\boldsymbol{\kappa}_3}-\tilde{\beta}_{\boldsymbol{\kappa}_2}-\tilde{\beta}_{\boldsymbol{\kappa}})|\tilde{W}_{\boldsymbol{\kappa}\boldsymbol{\kappa}_1\boldsymbol{\kappa}_2\boldsymbol{\kappa}_3}|^2 \tilde{n}_{\boldsymbol{\kappa}}\tilde{n}_{\boldsymbol{\kappa}_1}\tilde{n}_{\boldsymbol{\kappa}_2}\tilde{n}_{\boldsymbol{\kappa}_3}\left(\tilde{n}_{\boldsymbol{\kappa}}^{-1}+\tilde{n}_{\boldsymbol{\kappa}_2}^{-1}-\tilde{n}_{\boldsymbol{\kappa}_1}^{-1}-\tilde{n}_{\boldsymbol{\kappa}_3}^{-1}\right) + \frac{8\pi\gamma^2}{\beta_0^2}\int d\boldsymbol{\kappa}_1 \delta(\tilde{\beta}_{\boldsymbol{\kappa}_1}-\tilde{\beta}_{\boldsymbol{\kappa}})|\tilde{U}_{\boldsymbol{\kappa}\boldsymbol{\kappa}_1}(\tilde{\mathbf{n}})|^2(\tilde{n}_{\boldsymbol{\kappa}_1}-\tilde{n}_{\boldsymbol{\kappa}}), \tag{151}$$

where

$$\tilde{U}_{\boldsymbol{\kappa}\boldsymbol{\kappa}_1}(\tilde{\mathbf{n}}) = \frac{1}{\beta_0^2}\int d\boldsymbol{\kappa}'\, \tilde{W}_{\boldsymbol{\kappa}\boldsymbol{\kappa}_1\boldsymbol{\kappa}'\boldsymbol{\kappa}'}\,\tilde{n}_{\boldsymbol{\kappa}'}. \tag{152}$$

The functions with a tilde refer to the natural continuum extension of the corresponding discrete functions, i.e., $\tilde{n}_{\boldsymbol{k}}(z) = n_{[\boldsymbol{k}/\beta_0]}(z)$, $\tilde{\beta}_{\boldsymbol{\kappa}} = \beta_{[\boldsymbol{\kappa}/\beta_0]}$, $\tilde{W}_{\boldsymbol{\kappa}\boldsymbol{\kappa}_1\boldsymbol{\kappa}_2\boldsymbol{\kappa}_3} = W_{[\boldsymbol{\kappa}/\beta_0][\boldsymbol{\kappa}_1/\beta_0][\boldsymbol{\kappa}_2/\beta_0][\boldsymbol{\kappa}_3/\beta_0]}$ and so on, where $[x]$ denotes the integer part of $x$.

The kinetic equation (151) and (152) differs from the conventional WT kinetic equation in several respects. First, we remark the presence of the new second term in Eq. (151). Note that this term vanishes when the occupation of a mode depends only on its energy $\tilde{\beta}$. Actually, this term enforces an isotropization of the mode occupancies amongst the modes with the same modal energy. Another important property of the kinetic equation (151) is the presence of the function $\tilde{W}_{\boldsymbol{\kappa}\boldsymbol{\kappa}_1\boldsymbol{\kappa}_2\boldsymbol{\kappa}_3}$ in the collision term. We will discuss this term through the analysis of some particular examples of waveguide configurations.

We finally note that the idea to expand the solution of the NLS equation with potential $V(\boldsymbol{x})$ into the basis of the linearized equation has been applied in different contexts. This approach makes sense in the weakly nonlinear regime since the coupling terms between the mode amplitudes due to the cubic nonlinearity are small. If the cubic nonlinearity becomes strong then the relevance of this basis to expand the solution is questionable and it could be interesting to extend this WT approach by considering another type of nonlinear eigenmodes. The effect of the nonlinearity on the stationary eigenmodes was discussed in the particular case of a parabolic trapping potential in Ref. [293], in relation with a similar approach used earlier in the theory of the dispersion-managed optical solitons [294,295].

*Application to specific examples*

The kinetic equation (151) and (152) is general and, in principle, relevant to different types of waveguide configurations. We briefly comment this aspect by considering different concrete examples.

We first comment the parabolic potential relevant to graded-index multimode fibers. It is also known to play an important role in experiments involving weakly interacting Bose gases [292]. In the ideal parabolic limit ($V_0 \to \infty$), $u_m(\boldsymbol{x})$ refer to the normalized Hermite–Gaussian functions with corresponding eigenvalues $\beta_m = \beta_{m_x,m_y} = \beta_0(m_x+m_y+1)$,

$$u_{m_x,m_y}(x,y) = \kappa(\pi m_x!\, m_y!\, 2^{m_x+m_y})^{-1/2} H_{m_x}(\kappa x)\, H_{m_y}(\kappa y)\, \exp[-\kappa^2(x^2+y^2)/2], \tag{153}$$

where $\kappa = (q/\alpha)^{1/4}$. In the continuum limit, we have $\tilde{\beta}_{\boldsymbol{\kappa}} = \kappa_x + \kappa_y + \beta_0$. This expression plays the role of a generalized *anisotropic* dispersion relation, whose wave vector reads $\boldsymbol{\kappa} = \beta_0(m_x, m_y)$. The parabolic potential will be discussed in more detail below, in relation with wave condensation in a waveguide in Section 5.2.4.

An other example that can easily be illustrated is the circular waveguide of radius $R$, whose index of refraction is supposed to be constant for $|\boldsymbol{x}| < R$ ('step-index' waveguide). We assume the waveguide to be of infinite depth for simplicity. The field can be expanded into the orthonormal basis of the Bessel functions, $\psi(\boldsymbol{x}, z) = \sum_{l,s} c_{l,s}(z) u_{l,s}(\boldsymbol{x}) \exp(-i\beta_{l,s}z)$, with

$$u_{l,s}(\boldsymbol{x}) = \frac{1}{\sqrt{\pi R^2 J_{l+1}^2(x_{l,s})}} J_l(x_{l,s}|\boldsymbol{x}|/R)\exp(il\theta), \tag{154}$$

where $J_l(|\boldsymbol{x}|)$ is the Bessel function of the first kind, $x_{l,s}$ is the $s$th zero of $J_l(|\boldsymbol{x}|)$, and $(|\boldsymbol{x}|, \theta)$ are the polar coordinates. With these notations, the eigenvalues read $\beta_{l,s} = \alpha x_{l,s}^2/R^2$. In a similar way as above, the passage to the continuum limit can be done by defining the wave vector $\boldsymbol{\kappa} = \beta_{0,1}(l, s)$, which thus leads to the kinetic equation for the evolution of $\tilde{n}_{\boldsymbol{\kappa}}(z)$. Note that with this parametrization of the wave vectors $\boldsymbol{\kappa}$ the density of states $\rho(\beta)$ is uniform.

We finally show that Eq. (151) recovers the traditional WT equation when the field is expanded into the usual plane-wave basis with periodic boundary conditions

$$u_{m_x,m_y}(\boldsymbol{x}) = \frac{1}{L}\exp[2i\pi(m_x x + m_y y)/L], \tag{155}$$

where $L$ stands for the box size and $\boldsymbol{k} = \frac{2\pi}{L}(m_x, m_y)$ the usual wave-vector. This expansion is relevant to the homogeneous problem, i.e., in the absence of the confining potential [$V(x) = 0$]. It models the evolution of the random wave in the presence of a box-shaped confining potential, $V(\boldsymbol{x})$, whose frequency cutoff, $k_c = \pi/dx$ mimics the finite depth of the waveguide,

$V_0 \sim \alpha k_c^2$. With this plane-wave modal expansion, one obtains $|\tilde{W}_{\boldsymbol{\kappa}\boldsymbol{\kappa}_1\boldsymbol{\kappa}_2\boldsymbol{\kappa}_3}|^2 = \frac{(2\pi)^2}{L^6}\delta(\boldsymbol{k}_1+\boldsymbol{k}_3-\boldsymbol{k}_2-\boldsymbol{k})$. Because of the Dirac $\delta$-function, the second term in the kinetic equation (151) vanishes, which thus leads to the standard form of the WT kinetic equation

$$\partial_z \tilde{n}_{\boldsymbol{k}}(z) = \mathrm{Coll}[\tilde{n}_{\boldsymbol{k}}], \tag{156}$$

with the collision term

$$\mathrm{Coll}[\tilde{n}_{\boldsymbol{k}}] = \kappa_0\gamma^2 \iiint d\boldsymbol{k}_1\, d\boldsymbol{k}_2\, d\boldsymbol{k}_3 \delta\left(\omega_{k_1}+\omega_{k_3}-\omega_{k_2}-\omega_k\right)\, \delta(\boldsymbol{k}_1+\boldsymbol{k}_3-\boldsymbol{k}_2-\boldsymbol{k})\, \mathcal{Q}(\tilde{\mathbf{n}}), \tag{157}$$

where $\kappa_0 = 4\pi/(2\pi)^2$,[5] the dispersion relation is $\omega(k) = \alpha k^2$, and

$$\mathcal{Q}(\tilde{\mathbf{n}}) = \tilde{n}_{\boldsymbol{k}}\tilde{n}_{\boldsymbol{k}_1}\tilde{n}_{\boldsymbol{k}_2}\tilde{n}_{\boldsymbol{k}_3}\left(\tilde{n}_{\boldsymbol{k}}^{-1}+\tilde{n}_{\boldsymbol{k}_2}^{-1}-\tilde{n}_{\boldsymbol{k}_1}^{-1}-\tilde{n}_{\boldsymbol{k}_3}^{-1}\right). \tag{158}$$

As discussed in the Introduction, this kinetic equation can be derived by making use of a rigorous mathematical technique based on a multi-scale expansion of the cumulants of the nonlinear wave, as originally formulated in Refs. [48–50], and recently studied in more details through the analysis of the probability distribution function of the random field [52–54,40].

It is interesting to note that in the 1D case, the degenerate phase-matching conditions lead to a vanishing collision term in Eq. (157). This aspect will be discussed in detail in Section 6.3 through the WT analysis of the 1D integrable NLS equation. Notice that the presence of a nonlocal nonlinearity also leads to a vanishing collision term in 1D — though contrary to the integrable NLS case, the hierarchy of the moments equations can be closed to the next order in the presence of nonlocality. Instead of the usual four-wave resonant interaction [Eq. (156)], one obtains in this case a six-wave resonant interaction process. We refer the reader to Ref. [84] for a detailed discussion of this interesting six-wave nonlinear dynamics.

### *5.1.2. Thermalization and nonequilibrium Kolmogorov–Zakharov stationary states*

We will describe the essential properties of the WT kinetic equation by considering the standard version of the homogeneous WT kinetic equation, i.e., Eq. (156)–(158) [with $V(\boldsymbol{x}) = 0$], while the influence of the potential trap will be discussed in Section 5.2.4. Note that, to avoid cumbersome notations, in the following we drop the tilde notation adopted here above [in particular we substitute the notation $\tilde{n}_{\boldsymbol{\kappa}}(z)$ with the standard notation $n_{\boldsymbol{k}}(z)$]. We will also generalize the presentation of the results to a spatial dimension $d = 2$ or $d = 3$ in the framework of the dimensionless NLS equation

$$i\partial_z\psi = -\nabla^2\psi + a|\psi|^2\psi. \tag{159}$$

For $d = 2$, the spatial variable has been normalized with respect to the healing length $\Lambda = (\alpha L_{nl})^{1/2}$ (see Section 2). In the same way, for $d = 3$ the additional temporal variable has been normalized with respect to the healing time $\tau_0 = (|\beta|L_{nl})^{1/2}$ (see Section 3). The variables can be recovered in real units through the transformation: $z \to zL_{nl}$, $t \to t\tau_0$, $\boldsymbol{x} \to \boldsymbol{x}\Lambda$, $\psi \to \psi\sqrt{\rho}$, where we recall that $\rho = N/L^d$ denotes the wave intensity (see Section 2). Note that in this section we deal essentially with a defocusing nonlinearity, so as to ensure the stability of the homogeneous plane-wave solution ('condensate'). The parameter $a = -\mathrm{sign}(\gamma)$ then denotes the sign of the nonlinearity, $a > 0$ ($a < 0$) for a defocusing (focusing) nonlinearity. We keep in mind that for $d = 3$ the Laplacian operator in Eq. (159) accounts for both diffraction and dispersion effects, $\nabla^2 = \partial_{xx} + \partial_{yy} + \partial_{tt}$, where we implicitly assumed that the wave propagates in the anomalous dispersion regime, so that chromatic dispersion acts in the same way as diffraction effects, and thus ensures the stability of the monochromatic plane-wave solution in the defocusing regime [171].

#### *Thermodynamic Rayleigh–Jeans spectrum*

The WT kinetic equation has a structure analogous to the celebrated Boltzmann's equation, which is known to describe the evolution of a dilute classical gas far from the equilibrium state [296]. For this reason the kinetic equation (156) exhibits properties similar to those of the Boltzmann's equation. It conserves the total power (or quasi-particle number) of the field

$$N = L^d \int n_{\boldsymbol{k}}(z)\, d\boldsymbol{k}, \tag{160}$$

the momentum

$$\boldsymbol{P} = L^d \int \boldsymbol{k} n_{\boldsymbol{k}}(z)\, d\boldsymbol{k}, \tag{161}$$

and the kinetic (linear) energy

$$E = L^d \int \omega(\boldsymbol{k})\, n_{\boldsymbol{k}}(z)\, d\boldsymbol{k}. \tag{162}$$

[5] Note that the coefficient $\kappa_0$ depends on the definition adopted for the Fourier transform. For instance, considering the definition, $\psi(\boldsymbol{k}, z) = (2\pi)^{-d/2}\int \psi(\boldsymbol{x}, z)\, \exp(-i\boldsymbol{k}.\boldsymbol{x})d\boldsymbol{x}$, one obtains $\kappa_0 = 4\pi/(2\pi)^{2d}$.

Let us remark that Eq. (156) does not conserve the total energy $H$, but only its linear contribution $E$. This results from the fact that the nonlinear energy has a negligible contribution in the perturbation expansion procedure of the kinetic theory ($|U/E| \ll 1$).

In analogy with the Boltzmann's equation, the kinetic wave equation is not reversible with respect to the propagation distance $z$. The irreversible character of Eq. (156) is expressed by the $H$-theorem of entropy growth, $dS/dz \geq 0$, where the nonequilibrium entropy reads

$$S(z) = L^d \int \log[n_{\boldsymbol{k}}(z)]\, d\boldsymbol{k}. \tag{163}$$

As in standard statistical mechanics, the thermodynamic equilibrium state is determined from the extremum of entropy, subject to the constraint of conservation of kinetic energy (162), momentum (161) and power (160). The method of the Lagrange multipliers thus gives the thermodynamic Rayleigh–Jeans equilibrium distribution

$$n_{\boldsymbol{k}}^{eq} = \frac{T}{\omega(k) - \boldsymbol{k}.\boldsymbol{v} - \mu}. \tag{164}$$

The parameters $T$, $\mu$ and $\boldsymbol{v}$ are in principle arbitrary and refer to the temperature, chemical potential and mean velocity, by analogy with thermodynamics. We underline that there exist a one-to-one correspondence between $(T, \mu, \boldsymbol{v})$ and the conserved quantities $(E, N, \boldsymbol{P})$. This means that the evolution of the wave is described in the framework of the microcanonical statistical ensemble, in contrast with the conventional canonical treatment using a thermal bath [292]. Note that the equilibrium distribution (164) yields an exactly vanishing collision term (156), $\mathrm{Coll}[n^{eq}] = 0$. This means that once the spectrum has reached the equilibrium distribution (164), it no longer evolves during the propagation, $\partial_z n_{\boldsymbol{k}} = 0$.

In many cases the equilibrium distribution is spherically symmetric and the Rayleigh–Jeans distribution takes the following simplified form

$$n_k^{eq} = \frac{T}{\omega(k) - \mu}. \tag{165}$$

This equilibrium spectrum is Lorentzian-shaped and the chemical potential characterizes the correlation length of the field at equilibrium, $\lambda_c^{eq} \sim 1/\sqrt{-\mu}$. However, we will see later that the Lagrange multiplier associated to momentum conservation plays an essential role for the study of multiple interacting wave-packets (e.g., the vector NLS equation), or in the presence of higher-order dispersion effects that lead to an asymmetric supercontinuum equilibrium spectrum (see Sections 5.3–5.4).

*Hyperbolic dispersion relation*

As discussed here above through the normalized NLS Eq. (159), we have assumed in this section that the incoherent wave propagates in the regime of anomalous dispersion. Dispersion and diffraction effects then act in the same way and the spatiotemporal spectrum exhibits a symmetric spatio-temporal structure reflecting the symmetric roles of space and time. The situation is different in the normal dispersion regime, since in this case temporal dispersion and spatial diffraction act in opposite ways and compensate each other for those frequencies lying along specific lines. This confers a hyperbolic structure to the dispersion relation, a property that gives rise to a rich spatiotemporal dynamics of both coherent (e.g., nonlinear $X$-waves) [297–301], and partially coherent optical fields [302–305]. The corresponding equilibrium spectrum is expected to exhibit a spatio-temporal $X$-shape. This property has been only briefly discussed in Ref. [306] (see also [307]) and deserves to be analyzed in more details in future works.

*Nonequilibrium Kolmogorov–Zakharov stationary spectra*

As discussed in the Introduction Section 1.2.1, the process of thermalization is physically relevant when one considers a Hamiltonian wave system, which can be considered as an 'isolated' system. Conversely, when one considers a dissipative system which is driven far from equilibrium by an external source, then it no longer relaxes towards the Rayleigh–Jeans equilibrium distribution (164). A typical physical example of forced system could be the excitation of hydrodynamic surface waves by the wind. In general, the frequency-scales of forcing and damping differ significantly. The nonlinear interaction leads to an energy redistribution among the frequencies and an important problem is to find the stationary spectra of the system.

V.E. Zakharov was the first to realize that the kinetic equation of weak-turbulence theory also admits nonequilibrium stationary solutions [308,37]. Contrary to the Rayleigh–Jeans equilibrium distribution, these stationary solutions carry a non-vanishing flux of conserved quantities, i.e., the energy and the particle fluxes. Such nonequilibrium stationary distributions are the analogue of the Kolmogorov spectra of hydrodynamic turbulence proposed by Kolmogorov in his theory in 1941. Zakharov used a clever set of 'conformal transformations' to show that the kinetic equation admits finite flux spectra as exact stationary solutions.

The formation of these nonequilibrium stationary solutions requires the existence of a permanent forcing or damping in the system, a feature that has been widely studied theoretically [37,40,39] (also see [309,310]), and experimentally, e.g., for surface waves [311], spin waves [312], surface tension waves [313], capillary waves [314,315], or elastic waves [316–318]. In optics, an experiment aimed at observing these nonequilibrium stationary spectra has been reported in [83] and reviewed

in [84]. In this case, the optical system is forced at the entry of the nonlinear medium ($z = 0$), and the formation of the nonstationary spectrum was observed in the transient propagation of the optical wave. Actually, in optics the propagation length $z$ plays the role of time, so that the observation of a permanent nonequilibrium stationary state would require a forcing and a damping at any $z$. This situation is rather artificial in optics, so that, so far, Kolmogorov–Zakharov spectra did not play a major role in nonlinear optics experiments. For this reason, we will not discuss such nonequilibrium stationary states and refer the reader to Refs. [37,51,40] for details. For concreteness, we just give here the expressions of the nonequilibrium stationary solutions

$$n_{\boldsymbol{k}}^{Q} = C_Q \frac{Q^{1/3}}{k^{\alpha_Q}} \tag{166}$$

$$n_{\boldsymbol{k}}^{P} = C_P \frac{P^{1/3}}{k^{\alpha_P}} \tag{167}$$

where $Q$ and $P$ are the particle and energy fluxes in frequency space and $C_P$, $C_Q$ are prefactors. These solutions are exact stationary solutions of the WT kinetic equation (156). The exponents $\alpha_Q$ and $\alpha_P$ depend on the scaling of the dispersion relation and on the explicit nonlinearities. Considering the particular example of the NLS equation (159), one obtains $\alpha_Q = d - 2/3$ and $\alpha_P = d$, where $d$ denotes the spatial dimension.

It is interesting to note that the process of relaxation to a stationary spectrum can be described by means of self-similar solutions of the WT kinetic equation. In substance, the non-stationary solution describes a self-similar front that propagates in frequency-space and which leaves a quasi-stationary state in its wake. This self-similar relaxation solution can be obtained for both equilibrium and nonequilibrium Kolmogorov–Zakharov stationary solutions of the kinetic equation. We refer the reader to Refs. [46,319–321] for more details concerning the properties of these self-similar solutions. So far, these non-stationary solutions have not been exploited in the context of optical waves.

As discussed here above through the optical experiment reported in Ref. [84], Kolmogorov–Zakharov stationary spectra can also play a role in the description of the transient evolution of unforced systems, i.e., isolated (Hamiltonian) systems. For instance, the nonequilibrium formation of a condensate can be regarded as an inverse cascade of particles from large to small frequency components, i.e., towards $\boldsymbol{k} = 0$. We remind that, as described by the WT theory, in the weakly nonlinear regime such inverse cascade occurs irrespective of the sign of the nonlinearity, i.e., focusing or defocusing regime. However, once the system enters the nonlinear regime in which small frequency components become highly populated, then the system behaves in completely different fashion depending on the sign of the nonlinearity. In the defocusing regime the coherent homogeneous wave is stable and the inverse cascade eventually leads to wave condensation (see next Section 5.2). Conversely, in the focusing regime MI leads either to the formation of soliton-like structures, or collapse singularities [322], depending on the spatial dimension $d$. As a matter of fact, the understanding of the dynamics of large scale coherent structures in a turbulent environment is still the subject of lot of interest. In this respect, we will see how a strong condensate coherent structure modifies the nature of the WT interaction in Section 5.2.2, while the interaction of solitons in a sea of incoherent fluctuations will be discussed in Section 5.2.1 in the framework of soliton turbulence. The role of different types of coherent structures, such as quasi-solitons and collapsing filaments, will be commented in Section 7.4.1.

### 5.1.3. Long range: Slowing down of thermalization

We have seen in Section 2 that a long-range nonlocal nonlinearity introduces interesting novel dynamical features. Here we show that the natural process of wave thermalization slows down in a significant way in the presence of a highly nonlocal nonlinearity [144]. This fact may be interpreted in analogy with gravitation and astrophysics, in which it is well-known that the long-range gravitational potential dramatically affect the natural process of thermalization of the system (see, e.g., [117]).

The starting point is the NLS equation (1) accounting for a nonlocal nonlinearity. Following the standard procedure [37,51], one obtains the WT kinetic equation

$$\partial_z n_{\boldsymbol{k}} = \frac{\gamma^2 \kappa_0}{\alpha} \iiint \mathcal{Q}(n_{\boldsymbol{k}}, n_{\boldsymbol{k}_1}, n_{\boldsymbol{k}_2}, n_{\boldsymbol{k}_3})\, T_{k123}^2\, \delta(\boldsymbol{k}_1 + \boldsymbol{k}_2 - \boldsymbol{k}_3 - \boldsymbol{k})\, \delta(k_1^2 + k_2^2 - k_3^2 - k^2)\, d\boldsymbol{k}_1\, d\boldsymbol{k}_2\, d\boldsymbol{k}_3, \tag{168}$$

where $\mathcal{Q}(n_{\boldsymbol{k}}, n_{\boldsymbol{k}_1}, n_{\boldsymbol{k}_2}, n_{\boldsymbol{k}_3}) = n_{\boldsymbol{k}_1} n_{\boldsymbol{k}_2} n_{\boldsymbol{k}_3} n_{\boldsymbol{k}} (n_{\boldsymbol{k}}^{-1} + n_{\boldsymbol{k}_3}^{-1} - n_{\boldsymbol{k}_2}^{-1} - n_{\boldsymbol{k}_1}^{-1})$, and the tensor may be written in its symmetric form, $T_{k123} = \frac{1}{4}\left(\tilde{U}_{12} + \tilde{U}_{13} + \tilde{U}_{k3} + \tilde{U}_{k2}\right)$, with $\tilde{U}_{ij} = \tilde{U}(\boldsymbol{k}_i - \boldsymbol{k}_j)$. Note that in the limit of a local interaction [$U(\boldsymbol{x}) \to \delta(\boldsymbol{x})$], we have $T_{k123} = 1$ and Eq. (168) recovers the standard local equation (156).

The kinetic equation (168) exhibits properties analogous to those of the corresponding local limit of the WT kinetic equation. Accordingly, it should describe the process of thermalization of the random wave towards the thermodynamic Rayleigh–Jeans equilibrium state (164). However, recent numerical simulations reveal that the process of thermalization of a nonlocal system slows down in a dramatic way as the nonlocal response length $\sigma$ increases. This numerical observation can be interpreted through a qualitative analysis of the kinetic equation (168). Indeed, the functions $\tilde{U}(\boldsymbol{k})$, i.e., the tensor $T_{k123}$, get all the more narrower as the nonlocal range of the response function increases, which thus quenches the efficiency of the four-wave resonances involved in the collision term of Eq. (168). More precisely, in the highly nonlocal limit, we use the same scaling for the nonlocal response as that used to derive the long-range Vlasov equation [see Eq. (20), $U(\boldsymbol{x}) = \varepsilon U^{(0)}(\varepsilon \boldsymbol{x})$].

The Fourier transform of the response function thus reads $\tilde{U}(\boldsymbol{k}) = \tilde{U}^{(0)}(\boldsymbol{k}/\varepsilon)$. Using the change of variables $\boldsymbol{k}_j = \boldsymbol{k} + \varepsilon\boldsymbol{\kappa}_j$ ($j = 1, 2, 3$), we find after integration in $\boldsymbol{\kappa}_3$ that Eq. (168) is equivalent to

$$\partial_z n_{\boldsymbol{k}} = \frac{\gamma^2\kappa_0}{4\alpha}\varepsilon^{2d-2}\iint \mathcal{Q}(n_{\boldsymbol{k}}, n_{\boldsymbol{k}+\varepsilon\boldsymbol{\kappa}_1}, n_{\boldsymbol{k}+\varepsilon\boldsymbol{\kappa}_2}, n_{\boldsymbol{k}+\varepsilon\boldsymbol{\kappa}_1+\varepsilon\boldsymbol{\kappa}_2})\left[\tilde{U}^{(0)}(\boldsymbol{\kappa}_1-\boldsymbol{\kappa}_2)+\tilde{U}^{(0)}(\boldsymbol{\kappa}_1+\boldsymbol{\kappa}_2)+2\tilde{U}^{(0)}(\boldsymbol{\kappa}_2)\right] \times \delta(2\boldsymbol{\kappa}_1\cdot\boldsymbol{\kappa}_2)\, d\boldsymbol{\kappa}_1 d\boldsymbol{\kappa}_2.$$

To interpret this expression, let us define the characteristic length of thermalization of the mode $k$, say $\lambda_k$, as $\partial_z n_k/n_k \sim 1/\lambda_k$. Since the width of the function $\tilde{U}^{(0)}(\boldsymbol{\kappa})$ is of order one, we see in this expression that a highly nonlocal interaction slows down the thermalization process by a factor of order $\varepsilon^{2d-2}$

$$\lambda_k^{nonloc} \sim \lambda_k^{loc}\,(\sigma/\Lambda)^{2d-2}. \tag{169}$$

We remark that these arguments have no physical meaning in one spatial dimension, because the collision term of the Hasselmann equation vanishes identically for $d = 1$, i.e., Eq. (168) is only relevant for $d > 1$. The slowing down of the thermalization process due to a highly nonlocal response is an important phenomenon which will be the subject of future investigations. We remark in this respect that in the focusing regime, the thermalization effect manifests itself by the spontaneous generation of a coherent soliton, a process termed 'soliton turbulence' that will be discussed in the next Section 5.2.1. In the long-range regime this self-organization process breaks down: Instead of leading to the generation of a coherent soliton, the system self-organizes into an incoherent soliton state, as discussed in Section 2.3.5 [27]. In particular, in this long-range regime, the incoherent wave does not exhibit the natural process of thermalization towards energy equipartition, a property discussed in more detail in Ref. [27].

### 5.2. Wave condensation

In this section we discuss the phenomenon of wave condensation in a conservative and reversible (Hamiltonian) system. The section is structured along the lines of Refs. [71,307,73,323]. It is important to note that the phenomenon of wave condensation has been extended in this last decade to optical cavity systems [74–77,324,80,81], which raises interesting questions on the relation between laser operation and the Bose–Einstein condensation of photons [325–327,82]. These aspects will be discussed in more details in Section 7.

#### 5.2.1. Soliton turbulence

The phenomenon of classical condensation discussed here may be regarded as a self-organization process that occurs in a conservative and reversible wave system. Let us recall in this respect that, contrary to dissipative systems, a conservative Hamiltonian system cannot evolve towards a fully ordered state, because such an evolution would imply a loss of statistical information for the system that would violate its formal reversibility. However, in spite of its formal reversibility, a nonintegrable Hamiltonian system is expected to exhibit an irreversible evolution towards an equilibrium state, as a result of an irreversible process of diffusion in phase-space [129]. In this regard, an important achievement was accomplished when Zakharov and collaborators reported in Ref. [113,114] numerical simulations performed in the framework of the focusing nonintegrable NLS equation. This study revealed that the Hamiltonian system would evolve, as a general rule, towards the formation of a large-scale coherent localized structure, i.e., a solitary-wave, immersed in a sea of small-scale turbulent fluctuations. The solitary wave then plays the role of a 'statistical attractor' for the Hamiltonian system, while the small-scale fluctuations contain, in principle, all the information necessary for time reversal. It is important to note that the solitary-wave solution corresponds to the solution that minimizes the energy (Hamiltonian), so that the system tends to relax towards the state of minimum energy, while the small-scale fluctuations compensate for the difference between the conserved energy and the energy of the coherent structure. This phenomenon of self-organization was termed by the authors of Ref. [113,114] 'soliton turbulence'. Note that this phenomenology of energy localization as a result of nonlinear evolution has been also extensively studied in discrete nonlinear systems, see, e.g., [328–331], in particular in relation with the Fermi–Pasta–Ulam problem [130].

As was initially discussed in Ref. [113,114], a rigorous theoretical description of the long term evolution of the process of soliton turbulence should require a thermodynamic approach. It is only recently that statistical equilibrium formulations have been elaborated in the framework of statistical mechanics [57–59,55,56,60–64]. Whenever the Hamiltonian system is constrained by an additional integral of motion (e.g., number of particles), the increase of entropy of small-scale turbulent fluctuations requires the formation of coherent structures [57–63], so that it is thermodynamically advantageous for the system to approach the ground state which minimizes the energy [113,114]. More precisely, it is shown that a statistical equilibrium is reached, in which the energy not contained in the coherent structure is equally distributed among the modes of the small-scale fluctuations, as illustrated in Fig. 27.

In analogy with wave condensation, soliton turbulence can be described as an inverse cascade of particles towards the low-frequency components, as discussed in detail in Ref. [84] in the framework of the weakly nonlocal 1D-NLS equation. The inverse cascade transports particles to small frequency components (nearby $\boldsymbol{k} = 0$), thus leading to an increase of nonlinearity in the system. As particles accumulates at spatial scales larger than MI period, then MI kicks in and solitons form, with particles spreading along the soliton spectrum—note that spectral components of the soliton are coherent,

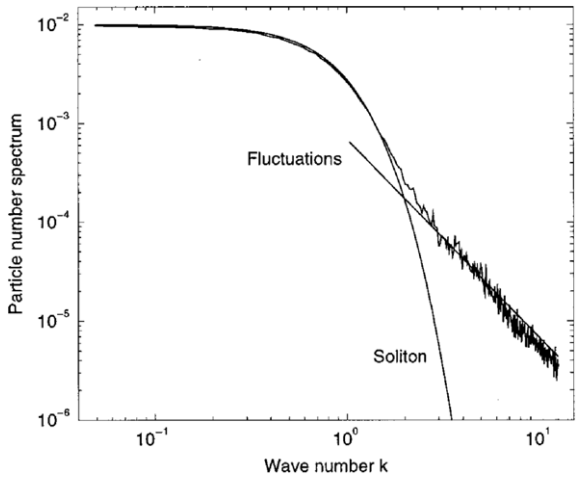


**Fig. 27.** Long-term evolution of soliton turbulence: After a long transient, a (coherent) soliton remains immersed in a sea of small scale fluctuations. Spectrum of the wave $|\tilde{\psi}|^2(k)$ obtained by integrating numerically the following nonintegrable 1D NLS equation $\partial_z\psi + \partial_{xx}\psi + |\psi|\psi = 0$, which was originally considered in [113]. The small-scale fluctuations exhibit a slow thermalization process, characterized by an irreversible evolution towards an equilibrium state of energy equipartition, $|\tilde{\psi}|^2(k) \sim k^{-2}$ (straight line).
*Source:* From Ref. [58].

i.e., fully correlated with each others. The non-integrability of the system allows for the interaction of the solitons with the surrounding small-scale fluctuations, which thus enables an energy exchange. Solitons can collide, occasionally merge or deteriorate via random interactions, and each of these processes leads to emission of energy and particles to the incoherent wave component. This results in a reversal of the particle flux towards high frequency components: The particles re-injected back into the small scale fluctuations fuels the continual process of the inverse cascade. In this way, random waves and coherent structures coexist, interact and get transformed into each other in a WT life cycle [40,84].

From a broader perspective, the phenomenon of soliton turbulence in the presence of forcing and damping at different lengths scales constitutes a difficult fundamental problem, as revealed, e.g., by the following important contributions [47,332,41]. From a more general perspective, soliton turbulence is also relevant to the process of optical filamentation [32], among which we also mention the important issue of inertial confinement fusion (see, e.g., [333–335]). We finally remind that the process of soliton turbulence breaks down in the long-range regime of nonlocal interaction [27], as discussed in Section 5.1.3 in relation with the slowing down of thermalization.

*Simple interpretation of wave condensation*

Let us now refers back to the condensation process. It is important to note that the spontaneous formation of a homogeneous solution corroborates the general rule discussed above [113,114,57–63]: because the homogeneous solution ('condensate') realizes the minimum of the Hamiltonian in the defocusing case, it plays a role of 'statistical attractor' for the Hamiltonian system, in a way akin to the soliton solution for the focusing regime. This analogy between focusing and defocusing regimes reveals that the formation of a condensate may be viewed as a consequence of the natural tendency of the system to increase its disorder (entropy). A simple explanation of this counterintuitive result may be given by recalling that the total energy of the field has a kinetic contribution and a nonlinear contribution. The kinetic energy being proportional to the gradient of the field, it provides a measure of the amount of fluctuations in the system. On the other hand, the nonlinear energy reaches its minimum value for a homogeneous solution. This merely explains why it is advantageous for the field to generate a condensate, because this permits the field to increase its disorder. In other terms, an increase of entropy in the field requires the generation of a homogeneous plane-wave solution. This effect of wave condensation as well as its interpretation are clearly visible in the numerical simulations of the NLS equation, as illustrated in Figs. 28–29. Then according to this physical picture, there is a direct correspondence between the mechanisms underlying the spontaneous generation of a solitary-wave in the focusing regime and the condensation process in the defocusing regime. In both cases, the system tends to reach the most disordered state characterized by the presence of small-scale fluctuations in the field, which requires the generation of a large scale coherent structure.

We remark that despite this interesting analogy, there exist important qualitative differences between wave condensation and soliton condensation. A distinguished feature is that the formation of a plane-wave condensate *requires* a background of thermalized small-scale fluctuations, whereas a soliton is inherently a spatially localized structure that can be generated locally in space—its stability ensuring its long-time persistence. An other important difference relies on the fact that wave condensation exhibits long-range order and coherence [292], in the sense that the correlation function of the field amplitude does not decay at infinity,

$$\lim_{|\boldsymbol{x}-\boldsymbol{x}'|\to\infty} \left\langle \psi(\boldsymbol{x})\, \psi^*(\boldsymbol{x}') \right\rangle \neq 0. \tag{170}$$

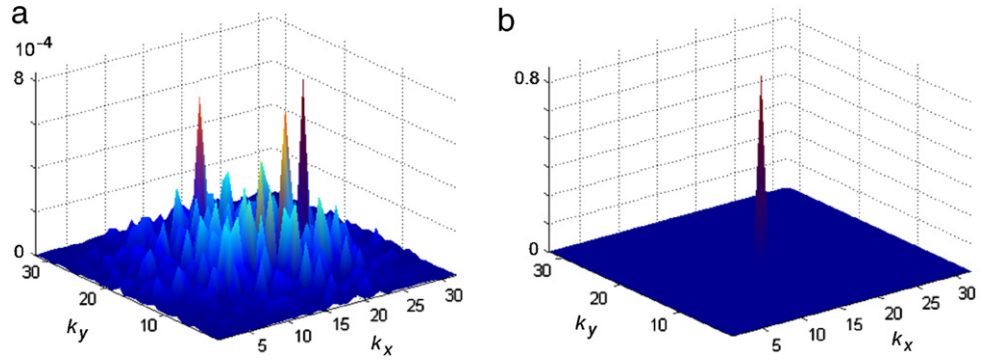


**Fig. 28.** Optical wave condensation: Numerical simulation of the normalized 3D NLS Eq. (159) showing the evolution of a 2D section of the spectrum of the field in normal scale. Initial condition of the spectrum (a), and corresponding equilibrium spectrum at $z = 10^3 L_{nl}$ (b). The concentration of the power of the field in the fundamental mode $\boldsymbol{k} = 0$ solely results from its natural irreversible evolution towards the equilibrium state. The evolution of some relevant quantities of the field corresponding to this numerical simulation are illustrated in Fig. 29. (The spatial discretization of the normalized NLS Eq. (159) is $dx = 1$, with the number of modes $N_* = 64^3$).
*Source:* From Ref. [307].

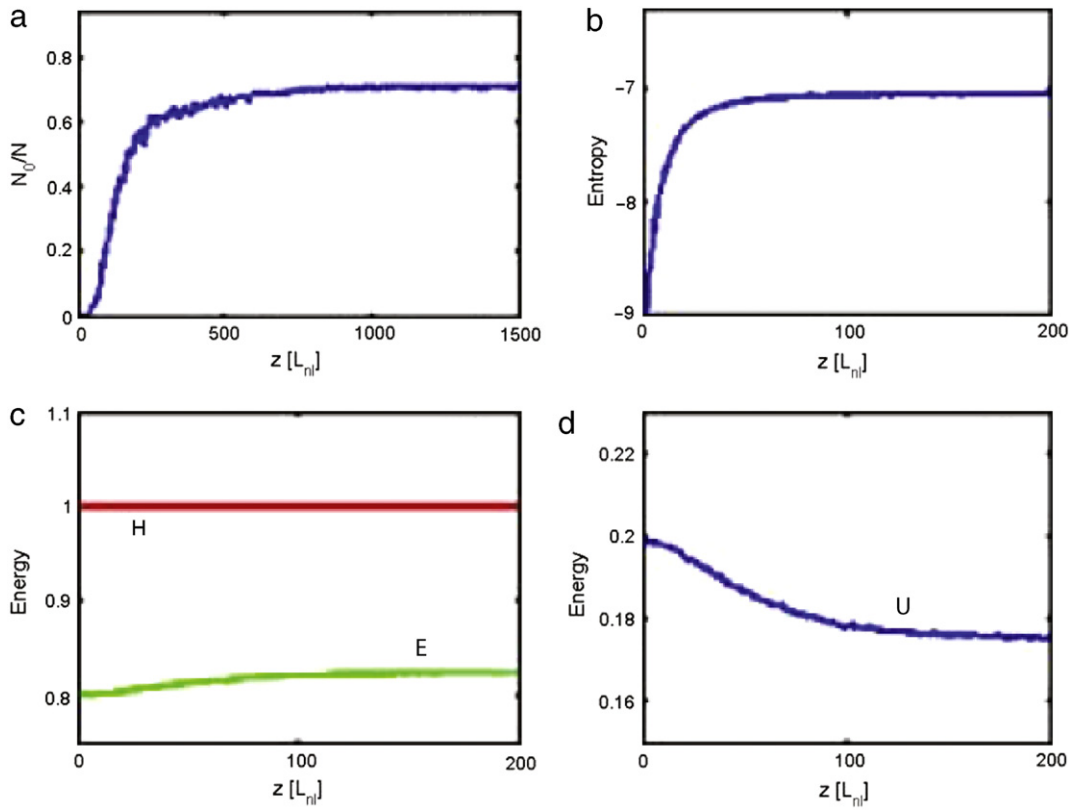


**Fig. 29.** Condensation induced by thermalization of incoherent waves: Evolution of the fraction of condensed power (a), entropy (b), and energy (c,d) corresponding to the numerical simulation illustrated in Fig. 28. The fraction of condensed power irreversibly evolves towards the equilibrium value predicted by the theory ($N_0/N \simeq 71\%$ for a total energy of $H = 1$). The process of entropy growth is saturated once the equilibrium state is reached, as described by the $H$-theorem of entropy growth. Figs. (c) and (d) show that a transfer of energy occurs from the nonlinear contribution $U$ to the linear contribution $E$, while the total energy $H = E + U$ remains constant. This process of energy transfer explains why an increase of entropy in the field requires the generation of a coherent structure (i.e., the plane-wave condensate).
*Source:* From Ref. [307].

This is in contrast with the localized character of a soliton, which naturally limits the range of coherence to the characteristic width of the soliton.

As illustrated in Fig. 28, wave condensation is characterized by a significant narrowing of the spectrum of the incoherent wave. Actually, the field exhibits an irreversible evolution towards equilibrium, as illustrated by the saturation of the process of entropy growth ($d_z S \simeq 0$), as well as the saturation of the fraction of condensed power, i.e., the normalized power

condensed in the fundamental mode $\boldsymbol{k} = 0$ (see Fig. 29). In other terms, the optical field tends to evolve towards a plane-wave. Note however that *the incoherent wave cannot evolve towards a pure plane-wave solution, because such evolution would imply a loss of information for the field, which would violate the formal reversibility of the system*. Actually, the monochromatic plane-wave remains immersed in a sea of small scale fluctuations, which contain, in principle, all the information necessary for a reversible propagation of the field. We underline here that this mechanism of self-organization in inherently associated to the conservative and Hamiltonian nature of the considered wave system. Note however that wave condensation has been also studied in non-conservative systems driven away from equilibrium by the presence of forcing and damping at small and large scales, see e.g., [336–343]. In this respect wave condensation can be viewed as a result of an inverse cascade of particles towards long-wavelengths modes.

*5.2.2. Condensation in 2D and 3D*

In this paragraph we provide analytical expressions of the condensate fraction at equilibrium in both two and three dimensions. We refer the interested reader to, e.g., Refs. [40,73], for more details concerning the nonequilibrium dynamics of condensation.

*3D: Condensation in the thermodynamic limit*

To describe the thermodynamic equilibrium properties of the condensation process in three dimensions it is important to point out some preliminary observations. We remark that the distribution (165) realizes the maximum of the entropy $S[n_{\boldsymbol{k}}]$ and vanishes exactly the collision term, $\mathrm{Coll}[n_k^{eq}] = 0$. However, note that Eq. (165) is only a *formal* solution, because it does not lead to converging expressions for the energy $E$ and the power $N$ in the limits $k \to \infty$, a feature which is usually termed 'ultraviolet catastrophe'. The usual way to regularize such unphysical divergence is to introduce an ultraviolet cut-off $k_c$. Note that a frequency cut-off appears naturally in the numerical simulation through the spatial discretization ($dx$) of the NLS Eq. (159), $k_c = \pi/dx$. As will be discussed in detail in Section 5.2.4, an effective physical frequency cut-off arises naturally in the guided wave configuration of the optical field. A physical frequency cut-off also originates in higher-order dispersion effects in the temporal domain, a feature that will be discussed in Section 6.1.

Following the procedure of Ref. [71], one can combine Eqs. (160)–(162) and (165), which gives the expression for the power of the field at equilibrium

$$\frac{N}{L^3} = 4\pi T k_c \left[1 - \frac{\sqrt{-\mu}}{k_c} \arctan\left(\frac{k_c}{\sqrt{-\mu}}\right)\right], \tag{171}$$

$$\frac{E}{L^3} = \frac{4\pi T k_c^3}{3}\left[1 + 3\frac{\mu}{k_c^2} + 3\left(\frac{-\mu}{k_c^2}\right)^{\frac{3}{2}} \arctan\left(\frac{k_c}{\sqrt{-\mu}}\right)\right]. \tag{172}$$

An inspection of Eq. (171) reveals that $\mu$ tends to $0^-$ for a non-vanishing temperature $T$, keeping a constant power density $N/L^3$. This means that the correlation length $\lambda_c$ diverge to infinity (see Eq. (165)). By analogy with the Bose–Einstein transition in quantum systems, such a divergence of the equilibrium distribution at $\boldsymbol{k} = 0$ reveals the existence of a condensation process.

As in standard Bose–Einstein condensation, the fraction of condensed power $N_0/N$ vs. the temperature $T$ (or the energy $E$), may be calculated by setting $\mu = 0$ in the equilibrium distribution (165). Note that the assumption $\mu = 0$ for $T \leq T_c$ can be justified rigorously in the thermodynamic limit (i.e., $L \to \infty$, $N \to \infty$, keeping $N/L^3$ constant). One readily obtains $(N - N_0)/L^3 = 4\pi T k_c$ and $E/L^3 = 4\pi T k_c^3/3$, which gives

$$N_0/N = 1 - E/E_c, \tag{173}$$

where the critical energy reads $E_c = N k_c^2/3$. Alternatively, the fraction of condensed power may be expressed as a function of the temperature,

$$N_0/N = 1 - T/T_c, \tag{174}$$

where $T_c = 3E_c/(4\pi L^3 k_c^3)$. As in standard Bose–Einstein condensation, $N_0$ vanishes at the critical temperature $T_c$, and $N_0$ becomes the total number of particles as $T$ tends to 0.

*Weakly nonlinear regime: Weak condensate amplitude*

The linear behavior of $n_0$ vs. $E$ in Eq. (173) is consistent with the results of numerical simulations. However note that Eq. (173) is derived for a spherically symmetric continuous distribution of $n_{\boldsymbol{k}}$, while in the numerics the integration is discretized. A discretization of Eq. (173) leads to a better agreement between the theory and the numerical simulations of Eq. (159) [71]. More precisely, making use of wave turbulence theory, one may express the averaged total energy of the field $\langle H \rangle$ in terms of the condensed particles $n_0$, which gives [73]

$$\frac{\langle H \rangle}{L^3} = (n - n_0)\frac{\sum_{\boldsymbol{k}}' 1}{\sum_{\boldsymbol{k}}' \frac{1}{k^2}} + a\left(n^2 - \frac{1}{2}n_0^2\right), \tag{175}$$

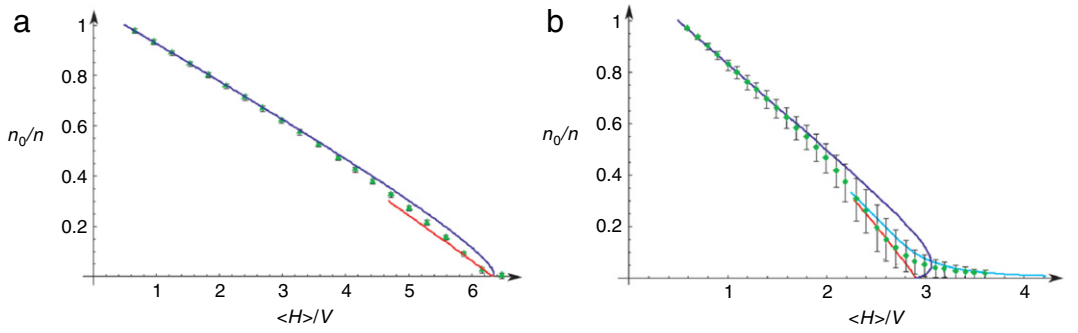


**Fig. 30.** Condensate fraction $n_0/n$ vs. total energy density $\langle H\rangle/L^d$. Points ($\diamond$) refer to numerical simulations of the normalized NLS Eq. (159) for $d = 3, N_* = 32^3$ modes (a), and $d = 2, N_* = 32^2$ modes (b) [$N/L^d = 1, dx = 1$ ($k_c = \pi$)]. Each numerical point corresponds to a time average over 3000 time units once the equilibrium state is reached. The red line corresponds to the condensation curve in the presence of a small condensate amplitude [WT regime, Eq. (175)], while the blue line in the presence of a high-condensate amplitude [Bogoliubov regime, Eq. (176)]. The green line in (b) refers to the condensation curve for a non-vanishing chemical potential, [Eqs. (177) and (178)]. The bars denote the amplitude of the fluctuations of $n_0/n$ at equilibrium. (For interpretation of the references to color in this figure legend, the reader is referred to the web version of this article.)
*Source:* From Ref. [73].

where $\sum'_{\boldsymbol{k}}$ denotes the sum over the whole frequency space which excludes the mode $\boldsymbol{k} = 0$ ($n_0 \equiv N_0/L^d$, $n \equiv N/L^d$). This expression is plotted in Fig. 30 (red line), and it is in good agreement with the numerical simulations in the regime of weak condensation (typically $n_0 < 0.3$).

*Bogoliubov regime: Strong condensate amplitude*

To describe the regime of strong condensation, one has to take into account the "interactions between the quasi-particles". To include the nonlinear (interaction) contribution, the Bogoliubov's expansion procedure of a weakly interacting Bose gas has been adapted to the classical wave problem. The interested reader may find the details of the analysis in Ref. [71,73]. One obtains the following closed relation between the total energy and the fraction of condensed power

$$\frac{\langle H\rangle}{L^3} = (n-n_0)\frac{\sum'_{\boldsymbol{k}} 1}{\sum'_{\boldsymbol{k}} \frac{k^2+an_0}{k^4+2an_0k^2}} + \frac{a}{2}\left[n^2+(n-n_0)^2\right]. \tag{176}$$

In the presence of high-condensate amplitudes, this expression is in quantitative agreement with the numerical simulations of the NLS Eq. (159), without any adjustable parameter (see Fig. 30).

*2D: Condensation beyond the thermodynamic limit*

Let us now consider the condensation process in two dimensions. The analysis exposed above in 3D may readily be applied to 2D, which gives $N/L^2 = \pi T \log(1-k_c^2/\mu)$. It becomes apparent from this expression that, for a fixed power density $N/L^2$, $\mu$ reaches zero for a vanishing temperature $T$. In complete analogy with the Bose–Einstein condensation, this indicates that condensation no longer takes place in 2D. In other terms, the critical temperature $T_c$ tends to zero because of the infrared divergence of the equilibrium distribution $n^{eq}_{\boldsymbol{k}}$. Actually, this result is rigorously correct in the thermodynamic limit (i.e., $L\to\infty, N\to\infty$, keeping $n \equiv N/L^2$ constant). Nevertheless, for situations of physical interest in which $N$ and $L$ are finite, wave condensation is re-established in two dimensions, a property confirmed by the numerical simulations [73]. Indeed, one can calculate the critical temperature for condensation in two dimensions, $T_c = nL^2/\sum'_{\boldsymbol{k}} 1/k^2$ [307]. This expression reveals that the discrete sum in frequency space provides a non-vanishing value of $T_c$, while $T_c$ tends to zero in the thermodynamic limit, because of the (infrared) logarithmic divergence of the continuous integral $\int d\boldsymbol{k}/k^2$.

In complete analogy with quantum Bose–Einstein condensation, for a finite surface of the optical beam, wave condensation occurs for a non-vanishing value of the chemical potential, $\mu \neq 0$. The condensation curve may thus be derived without the implicit assumption $\mu = 0$. The interested reader may find the details in Ref. [73]. One obtains

$$\frac{\langle H\rangle(\mu)}{L^2} = (n-n_0)\frac{\sum'_{\boldsymbol{k}} \frac{k^2}{k^2-\mu}}{\sum'_{\boldsymbol{k}} \frac{1}{k^2-\mu}} + a\left(n^2-\frac{1}{2}n_0^2\right), \tag{177}$$

$$\frac{n_0(\mu)}{n} = \frac{1}{-\mu}\frac{1}{\sum_{\boldsymbol{k}} \frac{1}{k^2-\mu}}. \tag{178}$$

We plotted in Fig. 30(b) the condensate fraction $n_0/n$ [Eq. (178)] vs. the energy density $\langle H\rangle/L^2$ [Eq. (177)], as a parametric function of $\mu$. It reveals that a non-vanishing chemical potential makes the transition to condensation "smoother", with the appearance of a characteristic "tail" in the condensation curve. Such a "tail" progressively disappears as the surface $L^2$ increases, so that the condensation curve $n_0/n$ vs. $\langle H\rangle/L^2$ tends to the expression derived in the thermodynamic limit, i.e., Eq. (177) with $\mu = 0$ recovers Eq. (175). Let us remark that the theory is in quantitative agreement with the numerical simulations of the NLS Eq. (159), as illustrated in Fig. 30.

It results that the critical behavior of the two-dimensional condensation curve looks similar to that of a genuine "phase transition". Note however that, strictly speaking, "phase transitions" only occur in the thermodynamic limit, so that such terminology is not appropriate for the two dimensional problem considered here. Nevertheless, if one considers the macroscopic occupation of the fundamental mode $\boldsymbol{k} = 0$ as the essential characteristic of condensation, one may say that wave condensation do occur in 2D.

Let us note that finite size effects may also play a significant role in 3D for very small box-volumes (typically $L \leq 8$). The corresponding expression of the condensation curve, $n_0/n$ vs $\langle H\rangle/L^3$, is still given by the parametric plot of Eqs. (177) and (178), since these equations hold for any spatial dimension of the system.

### 5.2.3. Condensation beyond the cubic NLS equation: Nonlocal and saturable nonlinearities

The phenomenon of classical wave condensation has been essentially studied in the framework of the NLS equation in the presence of a pure cubic Kerr nonlinearity. In many cases, however, realistic optical experiments are not modeled by a cubic Kerr nonlinearity. In a recent work [323], it has been shown that wave condensation can take place with more complex nonlinearities. The examples of the nonlocal nonlinearity and of the saturable nonlinearity were considered in [323], which refer to natural extensions of the cubic nonlinearity [171]. It was shown that the generalized NLS equation accounting either for a nonlocal or a saturable nonlinearity describes a process of wave condensation completely analogous to that described in the framework of the cubic Kerr nonlinearity. Following the procedure of the previous Section 5.2.2, analytical expressions of the condensate fraction are derived in both the weakly and the strongly nonlinear regimes of propagation [323]. For both the saturable and the nonlocal nonlinearity, a quantitative agreement between the theory and the numerical simulations is obtained, without using adjustable parameters. Moreover, the condensate amplitude is shown to exhibit strong fluctuations near by the transition to condensation, while the fluctuations are suppressed in the highly condensed regime.

### 5.2.4. Condensation in a waveguide

In the previous Section 5.2.2 we have considered wave condensation in the ideal limit in which the incoherent wave is expanded in the plane-wave Fourier basis with periodic boundary conditions. As discussed above, this approach of wave condensation requires the introduction of a frequency cut-off in the theory [71,73], so as to regularize the ultraviolet catastrophe inherent to classical nonlinear waves. From the physical point of view, such a frequency cut-off is not properly justified for classical waves. We will see that an effective frequency cut-off arises naturally in the guided-wave configuration of the optical beam. This frequency cut-off plays a key role in wave condensation (see Section 5.2.2), since it prevents the divergence of the critical energy for condensation [290] [see Eq. (173)]. Moreover, we have also seen that in 2D, wave condensation does not occur in the thermodynamic limit [71,73]. We will see that a parabolic waveguide configuration reestablishes wave condensation in two dimensions, in analogy with quantum Bose–Einstein condensation [292]. Accordingly, wave condensation and thermalization can be studied accurately through the analysis of the two-dimensional spatial evolution of a guided optical beam.

#### *Rayleigh–Jeans distribution in a waveguide*

The starting point is the WT kinetic derived in Section 5.1 into the basis of the eigenfunctions of the potential $V(\boldsymbol{x})$. Here we follow Ref. [290] to describe wave condensation in an optical waveguide. The kinetic equation (151) and (152) conserves the power $N = \beta_0^{-2}\int d\boldsymbol{\kappa} n_{\boldsymbol{\kappa}}$ and the energy $E = \beta_0^{-2}\int d\boldsymbol{\kappa}\beta_{\boldsymbol{\kappa}} n_{\boldsymbol{\kappa}}$, where we recall that $\beta_{\boldsymbol{\kappa}} = \kappa_x + \kappa_y + \beta_0$. Contrarily to the homogeneous WT kinetic equation (156), the kinetic equations (151) and (152) does not conserve the momentum, a feature which is consistent with the fact that the potential $V(\boldsymbol{x})$ prevents momentum conservation in the NLS Eq. (139). The kinetic equation (151) and (152) exhibits a $H$-theorem of entropy growth, $d\mathcal{S}/dz \geq 0$, where the nonequilibrium entropy reads $\mathcal{S}(z) = \beta_0^{-2}\int d\boldsymbol{\kappa}\ \ln(n_{\boldsymbol{\kappa}})$. The Rayleigh–Jeans equilibrium state $n_{\boldsymbol{\kappa}}^{eq}$ realizing the maximum of entropy, subject to the constraints of conservation of $E$ and $N$, is obtained by introducing the corresponding Lagrange's multipliers,

$$n_{\boldsymbol{\kappa}}^{eq} = \frac{T}{\beta_{\boldsymbol{\kappa}} - \mu}. \tag{179}$$

Note that, in a way akin to the usual Rayleigh–Jeans distribution (165), the temperature denotes the amount of energy $\mathcal{E}_{\boldsymbol{\kappa}}$ that is equipartitioned among the modes of the waveguide. Indeed, in the tails of the equilibrium distribution (179), i.e., $\beta_{\boldsymbol{\kappa}} \gg |\mu|$, we have $\mathcal{E}_{\boldsymbol{\kappa}} = \beta_{\boldsymbol{\kappa}} n_{\boldsymbol{\kappa}}^{eq} \sim T$ [see Eq. (147)]. Also note that the equilibrium state (179) cancels both collisions terms of the kinetic equation (151) and (152).

This equilibrium property of energy equipartition has been confirmed by the numerical simulations of the NLS Eq. (139) with a truncated parabolic potential, as illustrated in Fig. 32. To be concrete, in the numerical simulations we considered a realistic graded-index multimode optical fiber, with a radium of 15 $\mu$m and an index difference of $n_1 - n_0 = 10^{-3}$

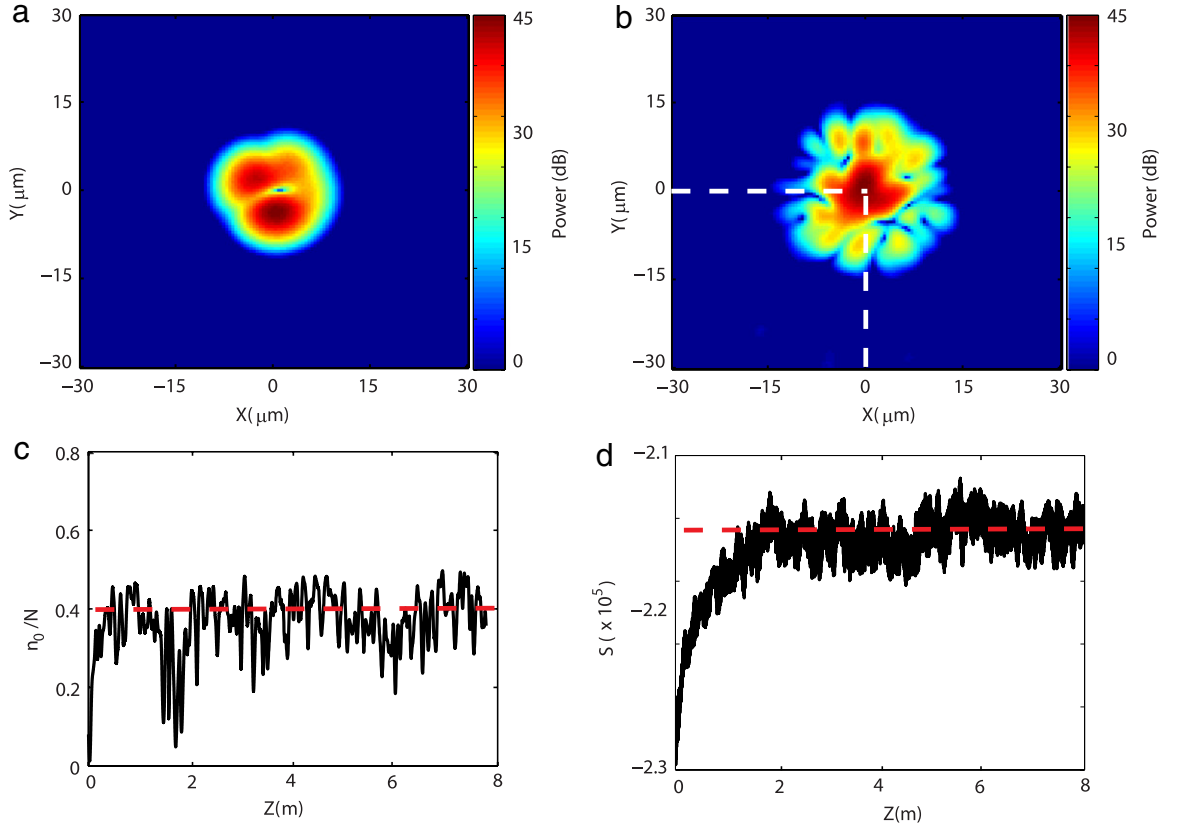


**Fig. 31.** Condensation and thermalization in a trap: Initial field intensity $|\psi|^2(\boldsymbol{x}, z = 0)$ (a), and corresponding intensity distribution at $z = 7$ m (b) obtained by integrating numerically the NLS Eq. (139) with a parabolic potential $V(\boldsymbol{x})$ (in $10\text{Log}_{10}$ scale). (c) Evolution of the fraction of condensed power $n_0/N$ vs. propagation distance $z$. The horizontal dashed red line denotes the value of the condensate amplitude $n_0^{eq}/N$ predicted by the theory [see Eqs. (183) and (184)]. (d) Corresponding evolution of the nonequilibrium entropy $\mathcal{S}$. Parameters of the simulation are given in the text (see Section 5.2.4). *Source:* From Ref. [290].

(see Fig. 26), and a refractive index of reference $n_0 = 1.45$. With these parameters the number of modes is $N_* = 66$. It is important to note that silica fibers exhibit a focusing nonlinearity, $\gamma < 0$ in Eq. (139). The incoherent beam may thus exhibit filamentation effects (i.e., speckle beam fragmentation) during its propagation in the fiber. However, as revealed by the numerical simulations, the beam does not exhibit filamentation effects because we consider the weakly nonlinear regime of propagation, in which the linear energy dominates the nonlinear energy, $U/E \ll 1$. The weakly nonlinear condition can easily be satisfied in the framework of the considered optical fiber system, since the nonlinearity of silica fibers is known to be relatively small as compared to other types of commonly used nonlinear optical media. In the numerical simulations, the following standard value of the nonlinear silica coefficient was considered $n_2 = -2 \times 10^{-8}$ $\mu\text{m}^2/\text{W}$, together with a power of the beam of 94 kW. With these parameters the weakly nonlinear regime is always verified, regardless of the initial degree of coherence of the wave injected into the fiber.

*Frequency cut-off, density of states and thermodynamic limit*

The number of modes involved in the dynamics with a trap $V(\boldsymbol{x})$ is finite because of the truncation of the potential (see Fig. 26, $V_0 < \infty$). In this way the truncated potential introduces an effective frequency cut-off for the classical nonlinear wave, because modes whose eigenvalues exceed the potential depth, $\beta_{\boldsymbol{\kappa}} > V_0$, are not guided during the propagation. A more rigorous justification of this aspect is given in the Appendix of Ref. [290]. Note that this is in contrast with the homogeneous problem [$V(\boldsymbol{x}) = 0$ in Eq. (139)], as discussed in Section 5.2.2. In this case, the frequency cut-off $k_c$ is introduced by the spatial discretization ($dx$) of the NLS equation, i.e., $k_c = \pi/dx$, so that in the continuous limit $k_c \to \infty$ (see, e.g., [71]).

Let us discuss the importance of the truncation of the potential ($V_0 < \infty$) through the example of a parabolic potential considered in the numerical simulations (see Figs. 31–33). Considering the constraint, $\beta_0 \le \beta(\boldsymbol{\kappa}) \le V_0$, as well as the assumption $\beta_0 \ll V_0$ (i.e., large number of modes $N_* \gg 1$), the power of the field at equilibrium reads $N = (T/\beta_0^2)\int_0^{V_0} d\kappa_x \int_0^{V_0-\kappa_x} (\kappa_x + \kappa_y + \beta_0 - \mu)^{-1}\, d\kappa_y$, which gives

$$N = \frac{T}{\beta_0^2}\left[V_0 - \tilde{\mu}\,\ln\left(\frac{-\tilde{\mu}}{V_0 - \tilde{\mu}}\right)\right], \tag{180}$$

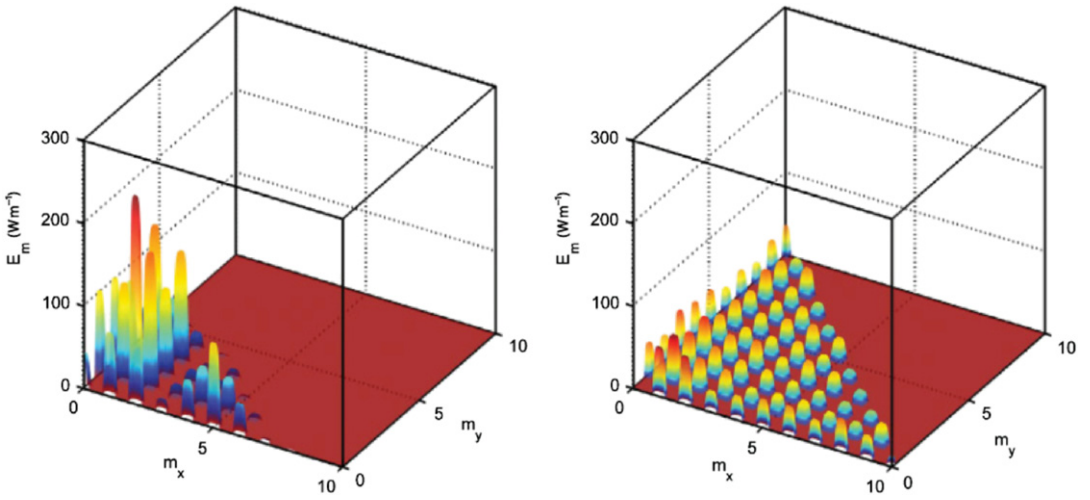


**Fig. 32.** Condensation and thermalization in a trap: Numerical simulation of the NLS Eq. (139) with a parabolic potential $V(\boldsymbol{x})$, showing the establishment of energy equipartition among the modes of the waveguide: Energy per mode, $\mathcal{E}_m = \beta_m n_m$ [see Eq. (147)] vs. the mode $m = (m_x, m_y)$, in the initial condition (a), and averaged over the propagation once the equilibrium state is reached, i.e., $\partial_z \mathcal{S} \simeq 0$ (b). The amount of power $n_m$ in the mode $m = (m_x, m_y)$ is calculated by projecting the field amplitude into the corresponding eigenmode [see Eq. (146)]. Energy almost reaches an equipartition among all modes, except the fundamental condensed mode $m_x = m_y = 0$ which is macroscopically populated [not shown in (a–b)]. Parameters are the same as in Fig. 31 (see the text in Section 5.2.4). In particular, we considered a truncated parabolic potential (Fig. 26), so that $\beta_{m_x,m_y} \simeq \beta_0(m_x + m_y + 1)$ and only modes whose eigenvalue verifies $\beta_{m_x,m_y} \leq V_0$ are guided.
*Source:* From Ref. [290].

where we defined $\tilde{\mu} = \mu - \beta_0$. In order to comment expression (180), we recall that in the homogeneous problem [$V(\boldsymbol{x}) = 0$ in Eq. (139)] wave condensation was shown to only occur in 3D, while in 2D the chemical potential was shown to reach zero for a vanishing temperature [71,307,73]. In analogy with Bose–Einstein condensation in quantum gases, this means that wave condensation does not occur in the thermodynamic limit in 2D. Conversely, Eq. (180) reveals that $\tilde{\mu} \to 0$ for a non-vanishing critical temperature, $T_c = 4\alpha N q / V_0$, which indicates that the presence of a parabolic potential $V(\boldsymbol{x})$ reestablishes wave condensation in the thermodynamic limit in 2D. Indeed, the thermodynamic limit for a parabolic potential corresponds to taking $N \to \infty$ and $q \to 0$, keeping constant the product $Nq$ [292]. This result is in complete analogy with the well-known fact that a parabolic potential reestablishes Bose–Einstein condensation in 2D [292]. There is however a difference with quantum condensation. Bose–Einstein condensation is known to be reestablished in a parabolic potential of infinite depth, $V_0 \to \infty$, while here $T_c$ tends to zero in the limit $V_0 \to \infty$. Contrary to the quantum case, one also needs to introduce a finite depth of the potential, $V_0 < \infty$, to get wave condensation in 2D. This condition is obviously satisfied for any optical waveguide configuration.

Note that the same conclusion is reached through the analysis of the density of states, $\rho(\beta) = \frac{1}{\beta_0^2} \iint_{\mathcal{D}} d^2\boldsymbol{\kappa}\, \delta(\beta - \kappa_x - \kappa_x - \beta_0)$, where the domain of integration $\mathcal{D}$ denotes $\iint_{\mathcal{D}} d^2\boldsymbol{\kappa} = \int_0^{V_0} d\kappa_x \int_0^{V_0 - \kappa_x} d\kappa_y$. As for quantum Bose gases, the presence of a parabolic potential leads to $\rho(\beta) \propto \beta$. Specifically, in the limit $\beta_0/V_0 \ll 1$, we have $\rho(\beta) = \beta/\beta_0^2$ for $\beta \leq V_0$, and $\rho(\beta) = 0$ for $\beta > V_0$. Note that the number of modes simply reads $N_* \simeq \int_0^{V_0} \rho(\beta)\, d\beta = V_0^2/(2\beta_0^2)$. According to this expression of $\rho(\beta)$ and considering the limit $\tilde{\mu} \to 0$, the infrared convergence of the integral $N = \int_0^{V_0} d\beta\, \rho(\beta)\, n_\beta^{eq} = T \int_0^{V_0} d\beta\, \rho(\beta)/\beta$ is ensured by the linear dependence of the density of states $\rho(\beta) \propto \beta$. However, the ultraviolet convergence of $N$ requires $V_0 < \infty$, while it is ensured by the exponential term of the Bose distribution in the quantum case.

*Condensate fraction in the waveguide*

We now look for a relation between the fraction of condensed power $n_0/N$ and the temperature $T$ or the energy $E$, in a way completely analogous to what has been done for the homogeneous problem ($V(\boldsymbol{x}) = 0$) in Section 5.2.2. As in the usual interpretation of Bose–Einstein condensation in a trap, we set $\mu = \beta_0$ in the equilibrium distribution (179). Note that the assumption $\tilde{\mu} = \mu - \beta_0 = 0$ for $T \leq T_c$ can be justified rigorously in the 2D thermodynamic limit. Isolating the fundamental mode, one has $N - n_0 = (T/\beta_0^2) \iint_{\mathcal{D}} 1/(\kappa_x + \kappa_y)\, d^2\boldsymbol{\kappa}$, where $n_0 = T/[\beta_0^2(\beta_0 - \mu)]$. We thus readily obtain $N - n_0 = TV_0/\beta_0^2$. Proceeding in a similar way for the energy, one obtains $E - n_0\beta_0 = \frac{TV_0^2}{2\beta_0^2}(1 + 2\beta_0/V_0)$. Eliminating the temperature from the expressions for $E$ and $N$ gives the following expression of the condensate fraction

$$\frac{n_0}{N} = 1 - \frac{E - E_0}{NV_0/2}, \tag{181}$$

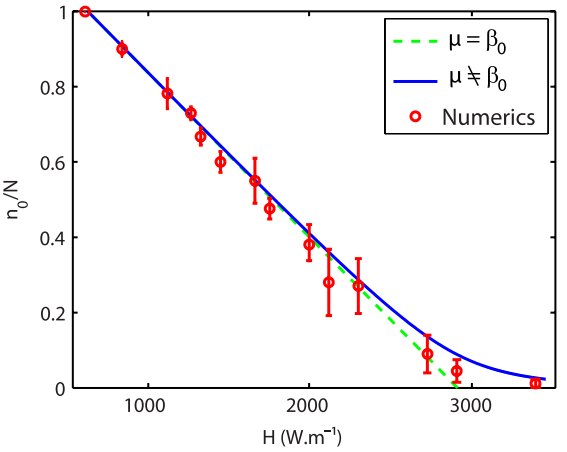


**Fig. 33.** Wave condensation in a trap: Fraction of power condensed in the fundamental mode at equilibrium, $n_0/N$, vs. the energy of the field, $H$, for a truncated parabolic potential (parameters are given in Section 5.2.4). The red points refer to the results of the numerical simulations of the NLS Eq. (139) with a parabolic potential $V(\boldsymbol{x})$. They have been obtained by averaging $n_0/N$ over the propagation distance once the equilibrium state is reached, i.e., $\partial_z \mathcal{S} \simeq 0$. The 'error-bars' denote the amount of fluctuations (standard deviation) of $n_0/N$ once equilibrium is reached. The continuous blue line refers to the theoretical condensation curve given in Eqs. (183)–(185), while the dashed green line refers to the corresponding thermodynamic limit [$\tilde{\mu} \to 0$ in Eqs. (183)–(185)]. In these plots the eigenvalues $\beta_m$ and eigenmodes $u_m(\boldsymbol{x})$ in Eqs. (183)–(185) account for the truncation of the potential ($V_0 < \infty$).
*Source:* From Ref. [290].

where $E_0 = N\beta_0$ refers to the minimum energy, i.e. the energy of the field when all the power is condensed, $n_0/N = 1$. The condensate amplitude $n_0/N$ increases as the energy $E$ decreases, and condensation arises below the critical energy

$$E_c = E_0 + NV_0/2 = \frac{NV_0}{2}\left(1 + \frac{2\beta_0}{V_0}\right). \tag{182}$$

This expression deserves to be commented in two respects. First, because of the truncation of the waveguide potential ($V_0 < \infty$), the value of $E_c$ does not diverge to infinity. This is in contrast with the homogeneous problem [$V(\boldsymbol{x}) = 0$ in Eq. (139)], as discussed above in 2D in Section 5.2.2. In this case the critical value of the energy behaves as $E_c \sim Nk_c^2/\ln(k_c)$, where $k_c = \pi/dx$ is the arbitrary frequency cut-off. In the continuous limit in which the spatial discretization of the NLS equation tends to zero, $dx \to 0$, the critical value of the energy $E_c$ diverges to infinity (see, e.g., [71,73]). A second point that could be remarked in Eq. (182) is that wave condensation is reestablished in the thermodynamic limit in 2D. Indeed, writing Eq. (182) in the following form, $E_c/S = Nq(1 + 2\beta_0/V_0)/(2\pi)$, where $S = \pi a^2$ is the waveguide surface, it becomes apparent that the energy density $E_c/S$ does not tend to zero in the thermodynamic limit ($N \to \infty$, $q \to 0$, keeping $Nq$ constant). As discussed in the previous Section 5.2.4, this is again in contrast with the homogeneous problem and the plane-wave expansion of the field, in which $E_c/S$ tends to zero logarithmically in the thermodynamic limit [307,73].

The simple analysis of Eqs. (181) and (182) outlined above provides physical insight into the process of wave condensation. However, a direct quantitative comparison with the numerical simulations requires the derivation of the condensation curve relating the condensate fraction to the Hamiltonian, as discussed above in Section 5.2.2 for the homogeneous problem, $V(\boldsymbol{x}) = 0$. For this purpose, we note that Eq. (181) can be improved along three lines. (i) The continuous integrals by a discrete sum over the modes of the waveguide. One obtains $n_0/N = 1 - (E - E_0)\sum'(m_x + m_y)^{-1}/(E_0(N_* - 1))$, where we recall that $N_*$ is the number of modes of the waveguide, and $\sum'$ denotes the sum over all modes $\{m = (m_x, m_y)\}$ excluding the fundamental mode $m = 0$. In the continuous limit we have $\sum' \frac{1}{m_x + m_y} \to \beta_0^{-1} \iint_{\mathcal{D}} \frac{d^2\boldsymbol{\kappa}}{\kappa_x + \kappa_y} = V_0/\beta_0$ and the number of modes $N_* = \beta_0^{-2} \iint_{\mathcal{D}} d^2\boldsymbol{\kappa} = V_0^2/(2\beta_0^2)$, so that the above equation recovers Eq. (181). (ii) A generalization of the expression of the condensate fraction, $n_0/N$ vs $E$, can be done beyond the thermodynamic limit [307,73], i.e., without the implicit assumption $\tilde{\mu} = 0$ for $T \le T_c$. From the physical point of view, this means that we take into account the finite size of the optical waveguide. (iii) We include the contribution of the nonlinear energy $U$ into the expression of the condensation curve. We split the contribution of the fundamental mode into the modal expansion of the field, $\psi(\boldsymbol{x}, z) = \psi_0(\boldsymbol{x}, z) + \varepsilon(\boldsymbol{x}, z)$, where $\psi_0(\boldsymbol{x}, z) = c_0(z)u_0(\boldsymbol{x})\exp(-i\beta_0 z)$ is the coherent condensate contribution and $\varepsilon(\boldsymbol{x}, z) = \sum_{m\neq 0} c_m(z)u_m(\boldsymbol{x})\exp(-i\beta_m z)$ is the incoherent contribution. This expansion can be substituted into the expression of $U$ in Eq. (141), and making use of the random phase approximation, we obtain $\langle U\rangle = -\gamma\left(\frac{1}{2}n_0^2\rho + 2n_0\sum_{j\neq 0} n_j W_{00jj} + \sum_{j\neq 0, k\neq 0} n_j n_k W_{jjkk}\right)$, where $\rho = \int u_0^4(\boldsymbol{x})d\boldsymbol{x} = \kappa^2/(2\pi)$. At equilibrium, $n_j$ and $n_k$ in the above sum can be substituted by the corresponding equilibrium distributions.

The generalizations (i–ii) and (iii) finally lead to the following expression of the condensation curve beyond the thermodynamic limit, including the nonlinear contribution of the energy

$$\frac{n_0}{N}(\tilde{\mu}) = \frac{1}{-\tilde{\mu}\sum_m \frac{1}{\beta_m - \beta_0 - \tilde{\mu}}} \tag{183}$$

$$\langle H\rangle(\tilde{\mu}) = N\frac{\sum_m \frac{\beta_m}{\beta_m-\beta_0-\tilde{\mu}}}{\sum_m \frac{1}{\beta_m-\beta_0-\tilde{\mu}}} + \langle U\rangle(\tilde{\mu}), \tag{184}$$

where

$$\langle U\rangle(\tilde{\mu}) = -\gamma\left[\frac{\rho}{2}n_0^2 - 2n_0^2\tilde{\mu}\int |u_0|^2(\boldsymbol{x})\sum_m{}' \frac{|u_m(\boldsymbol{x})|^2}{\beta_m-\beta_0-\tilde{\mu}}\,d\boldsymbol{x} + n_0^2\tilde{\mu}^2\int\left(\sum_m{}' \frac{|u_m(\boldsymbol{x})|^2}{\beta_m-\beta_0-\tilde{\mu}}\right)^2 d\boldsymbol{x}\right]. \tag{185}$$

The fraction of condensed power $n_0/N$ is thus coupled to the total energy $\langle H\rangle$ through the non-vanishing chemical potential, $\tilde{\mu} = \mu - \beta_0 \neq 0$. The parametric plot of (183) and (184) with respect to $\tilde{\mu}$ is reported in Fig. 33 (continuous line). As for the homogeneous problem [$V(\boldsymbol{x}) = 0$], the long tail in the condensation curve at high energies $H$ is due to the non-vanishing chemical potential, $\tilde{\mu} \neq 0$. In the thermodynamic limit $\tilde{\mu} \to 0$, the condensation curve (183) and (184) recovers the straight line discussed above through Eqs. (181) and (182) (see the dashed line in Fig. 33). Let us remark the good agreement between the theoretical condensation curve and the simulations, without using adjustable parameters (see [290] for more details).

Notice that the expression of $\langle U\rangle$ in Eq. (185) is rather involved. This is due to the nontrivial modal expansion (144) of the field $\psi$. In the usual homogeneous problem [$V(\boldsymbol{x}) = 0$] and the plane-wave expansion, Eq. (185) recovers the simple expression used in Eq. (175), namely $\langle U\rangle = -\gamma(n^2 - \frac{1}{2}n_0^2)$.

We finally underline that Eqs. (183) and (184) are valid for various different types of waveguide index profiles, provided one makes use of the appropriate eigenvalues $\beta_m$ and eigenmodes $u_m(\boldsymbol{x})$ (see Ref. [290]).

### 5.3. Velocity locking of incoherent waves

We have seen that the natural process of thermalization can be responsible for the phenomenon of condensation of classical waves. Here we illustrate the thermalization effect with another remarkable phenomenon which was termed 'velocity locking of incoherent waves'. More precisely, we analyze the role of convection (i.e., group-velocity difference) on the thermalization of distinct wave-packets [344]. The thermalization process is characterized by an irreversible evolution of the incoherent waves towards an equilibrium state in which they all propagate with an identical group-velocity. This effect of velocity-locking may be interpreted as a consequence of a fundamental property of statistical equilibrium thermodynamics: A velocity locking is required because it prevents 'a macroscopic internal motion in the wave system' [345]. We will see in the next Section 5.4 that the process of velocity locking plays an important role in the thermodynamic interpretation of the process of spectral broadening inherent to supercontinuum generation.

#### 5.3.1. Trapping of incoherent wave-packets

We consider the interaction of several incoherent waves that propagate with different group-velocities and whose dynamics is described by the vector NLS equation [138]

$$i(\partial_z + u_j^{-1}\partial_t)\psi_j + \beta_j\partial_{tt}\psi_j + \gamma_j\left(|\psi_j|^2 + \kappa\sum_{i\neq j}|\psi_i|^2\right)\psi_j = 0. \tag{186}$$

This set of NLS equations generalizes the scalar temporal NLS equation considered in Section 3 for an instantaneous nonlinearity [Eq. (36)]. The parameters $u_j$ represent the group velocity difference among the waves $\psi_j$, while the dispersion relation of $\psi_j$ reads $k_j(\omega) = \beta_j\omega^2$. In the following we will assume for simplicity that the dispersion coefficients have the same sign, e.g. $\beta_j > 0$. The last term of Eqs. (186) describes the cross-interaction between the fields, i.e., a phase modulation of $\psi_j$ induced by the other wave-packets $\psi_{i\neq j}$ [138]. The dimensionless constant $\kappa$ denotes the ratio between the cross- and self-interaction coefficients. Eq. (186) conserve the power $N_j$ of each field $\psi_j$ and the total Hamiltonian $H$ [138]. Because of the presence of convection effects, we will see that the conservation of the total momentum, $P = \sum_i P_i$, with $P_i = \mathrm{Im}\int \psi_i^*\,\partial_t\psi_i\,dt$, plays an essential role in the thermalization process.

A physical insight into velocity-locking may be obtained from the numerical integration of the vector NLS Eq. (186). Fig. 34(a) illustrates a typical evolution of the mean frequencies $\bar{\omega}_j(z) = \int \omega n_j\,d\omega/\int n_j\,d\omega$ of $M = 3$ incoherent wave-packets, $n_j(z,\omega)$ being the corresponding spectra. As initial condition we took three stochastic amplitudes $\psi_j(z=0,t)$ of zero mean, and whose fluctuations are statistically stationary in time. In the linear limit of their evolutions ($\gamma_j = 0$), the components $\psi_j$ would propagate with their three distinct group-velocities $u_j$. In the presence of a weak nonlinearity, Fig. 34(a) shows that the mean frequencies $\bar{\omega}_j$ are rapidly attracted towards some specific values $\bar{\omega}_j^{eq}$. According to the group-velocity dispersion law $v_j^{-1}(\omega) = \partial k_j/\partial\omega = u_j^{-1} + 2\beta_j\omega$, such a frequency shift is naturally accompanied by a shift of the group-velocity, as schematically explained in Fig. 34(e). The remarkable result is that the frequencies $\bar{\omega}_j^{eq}$ are selected in such a way that the three wave-packets propagate with identical group-velocities, $v_j(\bar{\omega}_j^{eq}) = v^{eq}$ for $j = 1, 2, 3$ (see Fig. 34(b)).

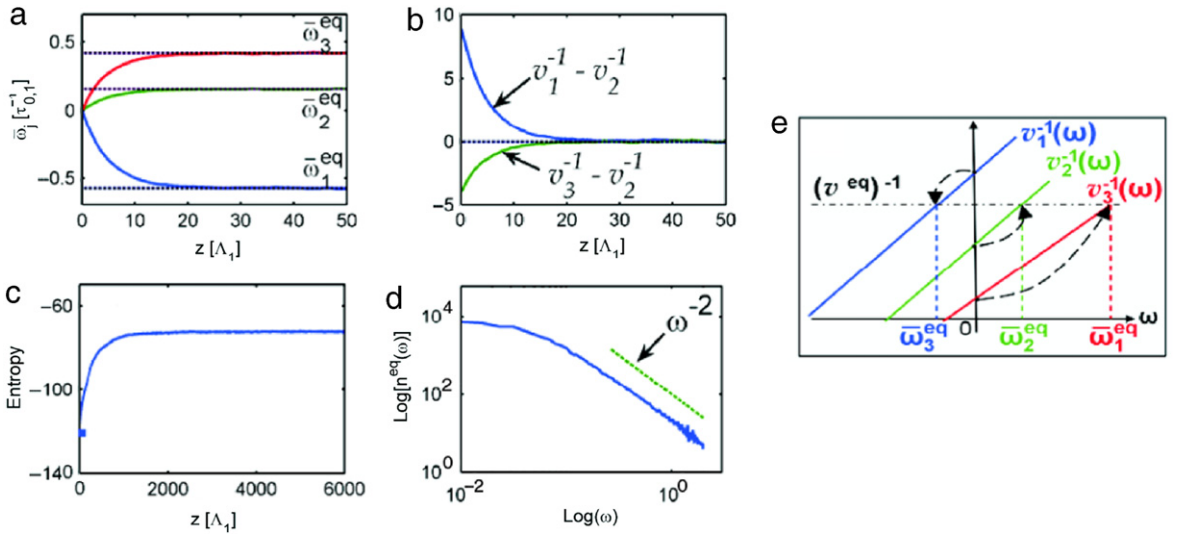


**Fig. 34.** Velocity-locking of incoherent waves: Numerical simulations of Eq. (186) representing the evolution of the mean frequencies $\bar{\omega}_j(z)$ of $M = 3$ incoherent wave packets (a) and corresponding group-velocity differences (b). The dashed lines in (a) refer to the theoretical values $\bar{\omega}_j^{eq}$ calculated from Eq. (188) [$u_1 = 1/14$, $u_2 = 1/5$, $u_3 = 1$ in units of $L_{nl,1}/\tau_{0,1}$, where $L_{nl,j}$ and $\tau_{0,j}$ are respectively the nonlinear length and healing time of $\psi_j$]. Simulations showing thermal wave relaxation to equilibrium at large $z$: The entropy growth saturates to a constant value $d_z \mathcal{S} \simeq 0$ (c), and the spectrum of $\psi_j$ follows a power law $n_j(\omega) \sim \omega^{-2}$ at large $\omega$ (d), in agreement with the Rayleigh–Jeans equilibrium distribution. An average over 200 numerical realizations has been taken ($\kappa = 2, N_1 = N_2 = N_3, \beta_2/\beta_1 = 0.9, \beta_3/\beta_1 = 1.1$, see [344] for details). Schematic illustration of the velocity-locking induced by the frequency-shift of $\psi_j$ (e): The arrows indicate the evolution from $z = 0$ to equilibrium [where $v_j^{-1}(\omega = 0) = u_j^{-1}$ denotes the initial group-velocity of $\psi_j$ at $z = 0$].
*Source:* From Ref. [344].

*Velocity-locking induced by thermalization*

In the following we will see that this effect of velocity-locking is a consequence of the natural thermalization of the waves to thermodynamic equilibrium. The derivation of the vector kinetic equation from the vector NLS Eq. (186) can be performed by following the same procedure as for the scalar case [47]. The resulting vector set of WT kinetic equation conserve the power of each wave-packet, $N_j = T_0 \int n_j(z, \omega) d\omega$, the total kinetic energy $E = \sum_i E_i(z)$, $E_i(z) = T_0 \int k_i(\omega) n_i(z, \omega) d\omega$, and the total momentum $P = \sum_i P_i(z)$, $P_i(z) = T_0 \int \omega n_i(z, \omega) d\omega$, where $T_0$ denotes the numerical temporal window [see Eqs. (160)–(162)]. The equilibrium spectrum is still given by the principle of maximum entropy, as discussed for the scalar case in Section 5.1.2. The main difference with respect to the scalar case is that, because of the frequency-shifts of the spectra, one has to introduce the Lagrange's multiplier associated to the conservation of the total momentum, say $\lambda/T$. One thus obtains,

$$n_j^{eq}(\omega) = \frac{T}{\beta_j \omega^2 + (\lambda + u_j^{-1})\omega - \mu_j}. \tag{187}$$

The distribution (187) is a Lorentzian in which the $M + 2$ constants $T, \lambda$ and $\mu_j$ can be determined from the $M + 2$ conserved quantities $E, P$ and $N_j$. In particular, from the distribution (187) one readily finds $P_j^{eq} = -(\lambda + u_j^{-1}) N_j / 2\beta_j$, so that $\lambda = -\left(2P + \sum_i N_i/u_i\alpha_i\right) / \sum_i N_i/\alpha_i$.

We remark that the multiplier $\lambda$ leads to a frequency shift of the equilibrium spectrum (187), so that the selected equilibrium frequency reads

$$\bar{\omega}_j^{eq} = P_j^{eq}/N_j = -(\lambda + u_j^{-1})/2\beta_j, \tag{188}$$

where the expression of $\lambda$ was given above. According to the group-velocity dispersion law $v_j^{-1}(\omega) = u_j^{-1} + 2\beta_j\omega$, one readily obtains, $v_j(\omega = \bar{\omega}_j^{eq}) = -1/\lambda$, which turns out to be the equilibrium velocity $v^{eq}$ of the fields. This reveals that, regardless of their initial group-velocities $u_j$, each wave-packet $\psi_j$ irreversibly evolves towards an equilibrium state, in which it propagates with the common group-velocity

$$\left\langle 1/v^{eq} \right\rangle = -\lambda = \frac{2P + \sum_i N_i/(u_i\alpha_i)}{\sum_i N_i/\alpha_i}, \tag{189}$$

where the conserved momentum is fixed from the initial condition $P = P(z = 0)$. The theoretical predictions of $\bar{\omega}_j^{eq}$ and $v^{eq}$ [Eqs. (188) and (189)] have been found in quantitative agreement with the numerical simulations of the vector NLS equation, as shown in Fig. 34(a)–(b).

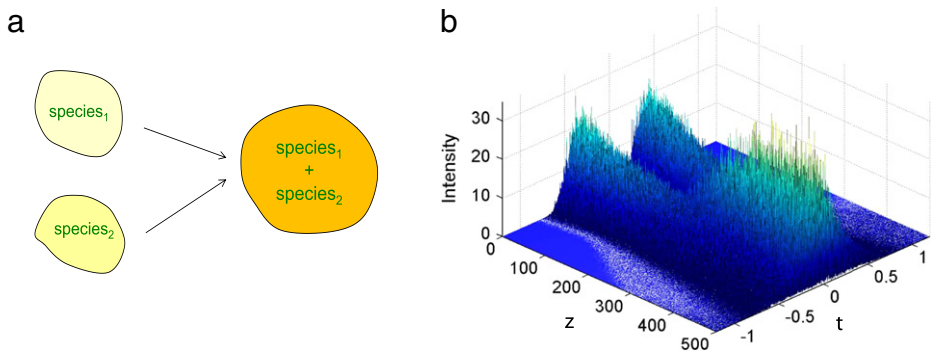


**Fig. 35.** Schematic illustration of the thermodynamic interpretation of velocity-locking: (a) Schematic representation of the collision between two drops of gases (or liquids): After collision and once thermal equilibrium is established, the two species propagate with the same average velocity. This prevents a relative internal motion between the two species: An isolated system at equilibrium can only exhibit a uniform motion of translation as a whole, while any macroscopic internal motion is not possible at equilibrium [346]. (b) The phenomenon of incoherent trapping and velocity-locking of two different wave-packets can be interpreted as a consequence of this general property of equilibrium thermodynamics.

### *5.3.2. Thermodynamic interpretation*

One may wonder whether this effect of velocity locking of incoherent waves can have a simple thermodynamic interpretation. To discuss this point, let us recall an important property established in equilibrium statistical thermodynamics. Consider a macroscopic (e.g., gas or liquid) system which is divided into a set of small, but still macroscopic, sub-systems. The postulate of maximum entropy then leads to the important conclusion that, at thermodynamic equilibrium, all sub-systems necessarily propagate with a constant linear velocity (and a constant angular velocity). In other terms, *an isolated system can only exhibit a uniform motion of translation (and rotation) as a whole, while any macroscopic internal motion is not possible at thermodynamic equilibrium* [346].

It is instructive to illustrate this property by considering the concrete example of a collision of two drops of gases (or liquids) that we assume to be distinguishable. The two drops initially propagate in two different directions, as schematically illustrated in Fig. 35. Once collision has occurred and equilibrium is established, the *average* velocities of the two species must be identical, so as to prevent a relative internal motion between the two species. According to this analogy with standard thermodynamics, the process of velocity-locking identified in a wave system becomes rather natural and intuitive. In the example of supercontinuum generation that will be discussed in Section 5.4.3, velocity-locking occurs by means of a spectral fission of a single initial spectrum. The optical field may thus be regarded as consisting of two 'macroscopic' sub-systems, which eventually relax to equilibrium by propagating with the same velocity.

## *5.4. Wave turbulence approach to supercontinuum generation*

The phenomenon of supercontinuum (SC) generation is characterized by a dramatic spectral broadening of the optical field during its propagation. This process has been extensively studied and different regimes have been identified, which essentially depend on whether the highly nonlinear photonic crystal fiber (PCF) is pumped in the normal or anomalous dispersion regimes, or with short (subpicosecond) or long (picosecond, nanosecond, and quasi-CW) pump pulses. We refer the reader to the reviews [139,31] for a detailed discussion of these aspects.

As a rather general rule, the process of spectral broadening inherent to SC generation is interpreted through the analysis of the following main nonlinear effects: The four-wave mixing effect, the soliton fission, the Raman self-frequency shift and the generation of dispersive waves [139,347,348]. Due to such a multitude of nonlinear effects involved in the process, a complete and satisfactory theoretical description of SC generation is still lacking. However, there is a growing interest in developing new theoretical tools aimed at describing SC generation in more details. Besides the theories describing the interaction between individual soliton pulses and dispersive waves [348], we may quote the effective three-wave mixing theory and the underlying first-Born approximation successfully applied to describe femtosecond SC generation in different configurations [349,350]. We also mention recent works aimed at providing a complete characterization of the coherence properties of SC light by using second-order coherence theory of nonstationary light [351–354].

### *Incoherent turbulent regime of SC generation*

The general physical picture of SC generation in PCFs can be summarized as follows. When the PCF is pumped with long pulses in the anomalous dispersion regime, MI is known to lead to the generation of a train of soliton-like pulses, which in turn lead to the emission of Cherenkov radiation in the form of spectrally shifted dispersive waves. These optical solitons are known to exhibit a self-frequency shift towards longer wavelengths as a result of the Raman effect. One encounters the same picture if the PCF is characterized by two zero dispersion wavelengths. In this case the Raman frequency shift of the solitons is eventually arrested in the vicinity of the second zero dispersion wavelengths. The SC spectrum then results to

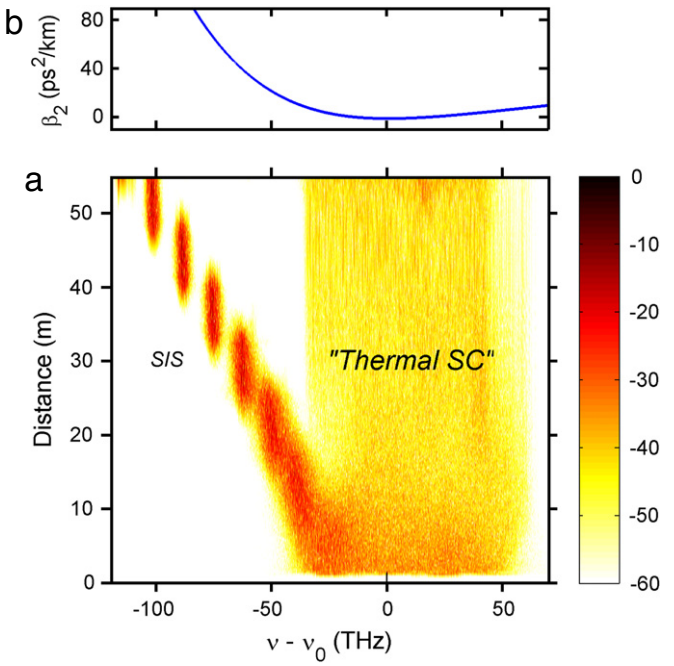


**Fig. 36.** Incoherent turbulent regime of SC generation: (a) Numerical simulations of the generalized NLS Eq. (190) using a logarithmic intensity scale (dB) to illustrate the spectral evolution as a function of propagation distance in a 50 m long PCF, for an input CW power equal to 200W ($\gamma = 0.05\ \mathrm{W}^{-1}\ \mathrm{m}^{-1}$). The corresponding dispersion curve of the PCF used in the simulations is illustrated in (b). The optical spectrum is characterized by two main features: (i) A broad central part governed by the four-wave mixing process that exhibits a process reminiscent of thermalization. (ii) A narrower low-frequency branch governed by the Raman effect that self-organizes into a continuous spectral incoherent soliton and subsequently a discrete spectral incoherent soliton. Both phenomena of optical wave thermalization and spectral incoherent solitons can be described by a nonequilibrium thermodynamic formulation of the optical field based on the WT theory.

be essentially bounded by the corresponding dispersive waves [348,355–357,31]. The important aspect to underline here is that in all these regimes *the existence of coherent soliton structures plays a fundamental role into the process of SC generation.*

This physical picture of SC generation changes in a significant way when one considers the regime in which long and intense pump pulses are injected into the PCF. Indeed, in this highly nonlinear regime, the spectral broadening process is essentially dominated by the combined effects of the Kerr nonlinearity and higher-order dispersion, i.e., by four-wave mixing processes [358]. In this regime the optical field exhibits rapid and random temporal fluctuations, which prevent the formation of robust and persistent coherent soliton structures. It turns out that in this regime the optical field exhibits an incoherent turbulent dynamics, in which coherent soliton structures do not play any significant role. In the following we shall term this regime the 'incoherent regime of SC generation' [359].

*Wave turbulence approach to SC generation*

In these last years a nonequilibrium thermodynamic interpretation of this incoherent regime of SC generation has been formulated [359,184,345,119,30] on the basis of the WT theory. This WT description can be introduced through the analysis of the numerical simulation reported in Fig. 36(a). It reports a typical evolution of the spectrum of the optical field in the incoherent regime of SC generation. It is obtained by integrating numerically the generalized nonlinear Schrödinger (NLS) equation [see Eq. (190)], with the dispersion curve reported in Fig. 36(b). The initial condition is a high-power (200 W) continuous wave whose carrier frequency $\nu_0 = 283$ THz ($\lambda_0 = 1060$ nm) lies in the anomalous dispersion regime and thus leads to the development of the modulational instability process.

We remark in Fig. 36(a) that the spectrum of the field essentially splits into two components during the propagation: (i) On the one hand, one notices a broad central part whose evolution is essentially governed by the dispersion effects and the Kerr nonlinearity. These effects are inherently conservative effects and lead to a process of wave thermalization through SC generation, a feature that has been discussed in Refs. [359,184,345] using the WT theory. Accordingly, the saturation of SC spectral broadening can be ascribed to the natural tendency of the optical field to reach an equilibrium state. Note however that, as will be discussed below, the phenomenon of wave thermalization through SC generation is not achieved in a complete fashion, in the sense that the tails of the numerical spectra exhibit some discrepancy with the corresponding expected tails of the Rayleigh–Jeans distribution. While this discrepancy can be simply ascribed to a limited propagation length in the PCF, an other possible physical origin of such discrepancy will be discussed in the next Section 6. This WT approach also reveals the existence of an unexpected phase-matching process whose origin can be interpreted in a thermodynamic sense.

(ii) On the other hand, one notices in Fig. 36(a) that a low-frequency spectral branch moves away from the central part of the spectrum. This low-frequency branch is essentially governed by the dissipative Raman effect, whose noninstantaneous nonlinear nature is responsible for the generation of the spectral incoherent solitons discussed above in Section 3.2.1. We will see that both continuous and discrete spectral incoherent solitons are spontaneously generated through the process of SC generation, irrespective of the nature of their spectral seeds, which may be either the modulational instability spectral peak, or a spectral peak associated to the Rayleigh–Jeans equilibrium distribution.

In the following we discuss separately the two phenomena of (i) optical wave thermalization through SC generation (Section 5.4.2), and (ii) the spontaneous generation of spectral incoherent solitons (Section 5.4.5) from the SC spectrum.

### 5.4.1. Generalized NLS equation

The generalized NLS equation is known to provide an accurate description of the propagation of an optical field in a PCF [139,138],

$$i\frac{\partial\psi(z,t)}{\partial z}+\sum_{j\geq 2}^{m}\frac{i^j\beta_j}{j!}\frac{\partial^j\psi(z,t)}{\partial t^j}+\gamma\left(1+i\tau_s\frac{\partial}{\partial t}\right)\psi(z,t)\int_{-\infty}^{+\infty}R(t')\,|\psi(z,t-t')|^2\,dt'=0, \tag{190}$$

where we remind that $\gamma$ refers to the nonlinear coefficient and $R(t)=(1-f_R)\delta(t)+f_R h_R(t)$ to the usual nonlinear response function of silica fibers, which accounts for both the instantaneous Kerr effect and the non-instantaneous Raman response function $h_R(t)$ [$\tilde{\psi}(\omega,z)=(2\pi)^{-1/2}\int\psi(t,z)\,\exp(i\omega t)\,dt$] [138]. The inclusion of higher-order dispersion effects is essential for the description of broadband optical wave propagation. More specifically, the higher-order time derivatives originate in a Taylor's expansion series of the dispersion curve of the PCF around the carrier angular-frequency $\omega_0$ [139]. The corresponding linear dispersion relation of Eq. (190) then reads

$$k(\omega)=\sum_{j\geq 2}^{m}\frac{\beta_j\omega^j}{j!}. \tag{191}$$

Eq. (190) also describes the self-steepening effect through the so-called optical shock term, i.e., the term proportional to $\tau_s\partial/\partial t$. This time derivative term accounts for the dispersion of the nonlinearity [138,360]. We refer the reader to Ref. [139,138] for a detailed discussion of the different terms that appear in Eq. (190).

As discussed above through Fig. 36(a), wave thermalization is driven by the combined effects of dispersion and Kerr nonlinearity, which are inherently conservative effects. On the other hand, the Raman effect [$f_R\neq 0$ in Eq. (190)] is a dissipative effect and prevents the establishment of a thermodynamic equilibrium state (see Section 3.1). Note that this is consistent with the fact that the Raman effect breaks the Hamiltonian structure of Eq. (190). In this Section we will thus neglect the dissipative Raman effect.

We report in Fig. 37(a) exactly the same numerical simulation as that reported in Fig. 36(a), except that we removed the Raman effect, $f_R=0$ in Eq. (190). We also removed in this simulation the influence of the shock term ($\tau_s=0$), whose influence will be considered later in Section 5.4.4. The comparison of Figs 36(a) and 37(a) clearly shows that the essential role of the Raman effect is to lead to the generation of a spectral incoherent soliton in the low-frequency branch in the SC spectrum. Besides spectral incoherent solitons, a peculiar feature revealed by Fig. 37(a) is that the spectral broadening inherent to SC generation saturates during the propagation. We shall see below that such saturation effect is related to the natural thermalization of the optical field.

### 5.4.2. Wave thermalization through supercontinuum generation

Neglecting the Raman effect and the shock term, the generalized NLS Eq. (190) reduces to

$$i\frac{\partial\psi}{\partial z}+\sum_{j\geq 2}^{m}\frac{i^j\beta_j}{j!}\frac{\partial^j\psi}{\partial t^j}+\gamma|\psi|^2\psi=0. \tag{192}$$

We recall that, if only the second-order dispersion effect is retained ($m=2$), Eq. (192) recovers the completely integrable 1D-NLS equation. The corresponding infinite number of conserved quantities prevent the thermalization of the wave towards thermodynamic equilibrium, though the system still exhibits a relaxation towards an equilibrium state of a different nature [361,142]. This aspect will be discussed in Section 6.3.

If one includes the influence of third-order dispersion ($m=3$), the system exhibits a process of anomalous thermalization [140,141], which is characterized by an irreversible evolution towards an equilibrium state of a fundamental different nature than the thermodynamic equilibrium state. The wave spectrum is shown to exhibit a highly asymmetric deformation characterized by a lateral spectral shoulder and the subsequent formation of an unexpected constant spectral pedestal [141]. This previous work [141] can be important to study the evolution of an incoherent wave in a PCF characterized by a single zero dispersion wavelength, and will be discussed below in Section 6.2. We also note that third-order dispersion has been shown to notably influence the generation of rogue waves in the evolution of the optical field [362], a feature which is in relation with soliton turbulence and wave condensation [363,364], as commented in Section 7.5.3.

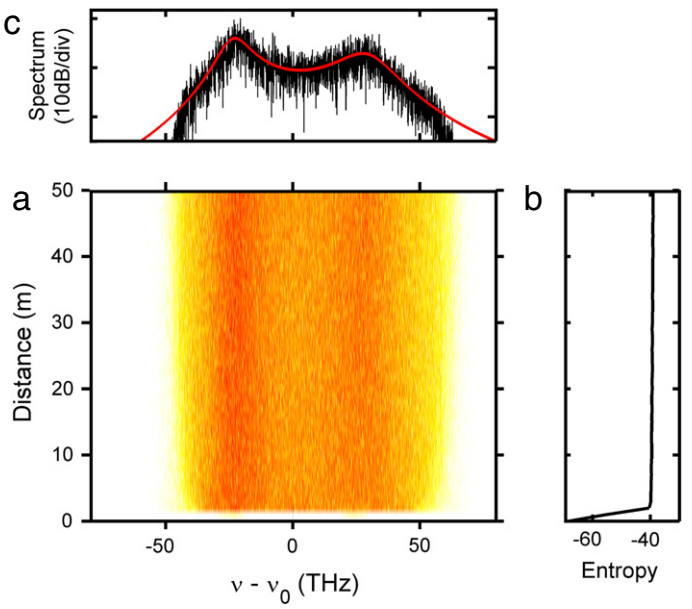


**Fig. 37.** Optical wave thermalization through SC generation. (a) Same as in Fig. 36(a), except that the Raman effect and the shock term have been neglected, $f_R = \tau_s = 0$: This simulations thus refers to the numerical integration of the instantaneous NLS Eq. (192). (b) Optical wave thermalization is characterized by a process of entropy production, which saturates to a constant level once the equilibrium state is reached, as described by the $H-$theorem of entropy growth. (c) Comparison of the thermodynamic Rayleigh–Jeans equilibrium spectrum $n^{eq}(\omega)$ [Eq. (195)] (red line), and the numerical spectrum corresponding to an averaging over the last 20 m of propagation. The good agreement has been obtained without using adjustable parameters. Note however a discrepancy between the simulations and the Rayleigh–Jeans distribution in the tails of the spectrum (see the text for discussion).

If one includes dispersion effects up to the fourth-order ($m = 4$), the simulations reveal the existence of a phenomenon of 'truncated thermalization': The incoherent wave exhibits an irreversible evolution towards the Rayleigh–Jeans thermodynamic equilibrium state characterized by a compactly supported spectral shape. This aspect will be discussed in Section 6.1.

*Thermodynamic equilibrium spectrum*

In the following we consider realistic dispersion curves of PCFs characterized by two zero dispersion wavelengths, whose accurate description requires a high-order Taylor expansion of the dispersion relation ($m > 4$). Starting from the high-order dispersion NLS Eq. (192) and following the standard procedure discussed above in this section in the spatial case, one obtains the irreversible WT kinetic equation governing the evolution of the averaged spectrum of the field $n(z, \omega)$ $[\langle\tilde{\psi}(z, \omega_1)\tilde{\psi}^*(z, \omega_2)\rangle = n(z, \omega_1)\,\delta(\omega_1 - \omega_2)]$:

$$\partial_z n(z, \omega_1) = Coll[n], \tag{193}$$

with the collision term

$$Coll[n] = \int n(\omega_1)n(\omega_2)n(\omega_3)n(\omega_4)\,[n^{-1}(\omega_1) + n^{-1}(\omega_2) - n^{-1}(\omega_3) - n^{-1}(\omega_4)]\,W\,d\omega_2\,d\omega_3\,d\omega_4, \tag{194}$$

where '$n(\omega)$' stands for '$n(z, \omega)$' in Eq. (194). As usual in the WT kinetic equation, the phase-matching conditions of energy and momentum conservation are expressed by the presence of Dirac $\delta$-functions in $W = \frac{\gamma^2}{\pi}\,\delta(\omega_1 + \omega_2 - \omega_3 - \omega_4)\,\delta[k(\omega_1) + k(\omega_2) - k(\omega_3) - k(\omega_4)]$, where $k(\omega)$ refers to the linear dispersion relation (191). Eq. (193) conserves the power density $N/T_0 = \int n(z, \omega)\,d\omega$, the density of kinetic energy $E/T_0 = \int k(\omega)\,n(z, \omega)\,d\omega$ and the density of momentum $P/T_0 = \int \omega\,n(z, \omega)\,d\omega$, where $T_0$ refers to the considered numerical time window. It also exhibits a $H$-theorem of entropy growth, $\partial_z \mathcal{S} \geqslant 0$, where the nonequilibrium entropy reads $\mathcal{S}(z) = \int \log[n(z, \omega)]\,d\omega$. The corresponding Rayleigh–Jeans equilibrium distribution (165) then reads in the temporal domain

$$n^{eq}(\omega) = \frac{T}{k(\omega) + \lambda\omega - \mu}. \tag{195}$$

As discussed above in Section 5.2.2 through the analysis of wave condensation, the three parameters $(T, \mu, \lambda)$ are calculated from the conserved quantities $(E, N, P)$ by substituting the equilibrium spectrum (195) into the definitions of $E$, $N$ and $P$. One thus obtains an algebraic system of three equations for three unknown parameters, which can be solved numerically.

We always obtained a unique triplet solution $(T, \mu, \lambda)$ for a given set $(E, N, P)$, a feature which is consistent with the fact that a 'closed' (conservative and Hamiltonian) system should exhibit a unique thermodynamic equilibrium state [296].

The meaning of the parameter $\lambda$ was already discussed in the framework of the generalized Rayleigh–Jeans distribution (164). Here, its significance becomes apparent through the analysis of the group-velocity $v_g$ of the optical field $[k'(\omega) \equiv \partial k/\partial\omega = 1/v_g(\omega)]$. Indeed, recalling the definition of an average in kinetic theory, $\langle \mathcal{A} \rangle_{eq} = \int \mathcal{A}\, n^{eq}(\omega)\, d\omega / \int n^{eq}(\omega)\, d\omega$ [296] and making use of the equilibrium spectrum (195), one readily obtains

$$\left\langle k'(\omega) \right\rangle_{eq} = -\lambda. \tag{196}$$

According to relation (196), the parameter $\lambda$ has a simple physical meaning, it denotes the average of the inverse of the group-velocity of the optical field at equilibrium.

The three parameters $(T, \mu, \lambda)$ can thus be calculated from the three conserved quantities $(E, N, P)$, which unambiguously determine the thermodynamic equilibrium spectrum (195). We report in Fig. 37(c) the comparison of the theoretical prediction (195) with the results of the numerical simulations of the high-order NLS Eq. (192). A quantitative agreement is obtained between the simulations and the theory (195), without using any adjustable parameter. The Rayleigh–Jeans spectrum is characterized by a double-peaked structure, which results from the presence of two zero dispersion wavelengths in the dispersion curve of the PCF. The relaxation towards thermal equilibrium is also corroborated by the saturation of the process of entropy production illustrated in Fig. 37(b). Note however that a notable discrepancy is visible in the tails of the spectrum in Fig. 37(c), as if the thermalization process were not achieved in a complete fashion. Actually, the simulations reveal that the tails of the spectrum exhibits a very slow process of spectral broadening, which apparently tends to evolve towards the expected Rayleigh–Jeans tails—though the required propagation length is extremely large. This aspect will be discussed in more detail in Section 6.1 in the particular case where the dispersion relation is truncated to the fourth-order [$m = 4$ in Eq. (191)].

The good agreement between the theory and the simulations has been obtained in a variety of configurations, as discussed in detail in Refs. [184,345]. For instance, we considered here the example of a cw source, which is inherently a coherent wave. In this case the transition from the initial coherent pump towards the incoherent SC regime takes place through the process of MI. However, a good agreement with the theory has been also obtained by considering an initial incoherent pump wave, a feature discussed in detail in Ref. [345].

### 5.4.3. Thermodynamic phase-matching

The thermodynamic equilibrium spectrum given in Eq. (195) is characterized by a double peak structure, which originates from the two zero dispersion wavelengths that characterize the PCF dispersion curve. This is illustrated schematically in Fig. 38. It is important to underline, however, that the frequencies $(\omega_1, \omega_2)$ of the two peaks of $n^{eq}(\omega)$ do not simply correspond to the minima of the dispersion relation, i.e. $k'(\omega_{1,2}) \neq 0$, as illustrated in Fig. 38(b). To further analyze this aspect, let us write the thermodynamic equilibrium spectrum in the form $n^{eq}(\omega) = T/\mathcal{F}(\omega)$, with $\mathcal{F}(\omega) = k(\omega) + \lambda\omega - \mu$. Then the two frequencies $(\omega_1, \omega_2)$ which maximize the equilibrium spectrum (195) satisfy $\mathcal{F}'(\omega_1) = \mathcal{F}'(\omega_2) = 0$, i.e., $k'(\omega_1) = k'(\omega_2) = -\lambda$. In other terms, $\omega_1$ and $\omega_2$ correspond to those frequencies for which the straight line $-\lambda\omega + \mu$ is parallel to $k(\omega)$. This simple observation reveals that *the two frequencies $(\omega_1, \omega_2)$ of the double peaked equilibrium spectrum (195) are selected in such a way that the corresponding group-velocities coincide with the average group-velocity of the optical wave*,

$$v_g(\omega_1) = v_g(\omega_2) = 1/\left\langle k'(\omega) \right\rangle_{eq} = -1/\lambda. \tag{197}$$

As illustrated through Fig. 38 there exists, in principle, a unique pair of frequencies $(\omega_1, \omega_2)$ satisfying the conditions given by Eq. (197). In other terms, for a given thermodynamic equilibrium spectrum (195), there exists a *unique* pair of frequencies $(\omega_1, \omega_2)$ that leads to a matched group-velocity of the double peaked spectrum [345]. In this sense, Eq. (197) can be regarded as a thermodynamic phase-matching condition.

We also note that, as revealed by Fig. 38(b), there exists a third frequency $\omega_3$, located between $\omega_1$ and $\omega_2$, which satisfies $v_g(\omega_3) = v_g(\omega_{1,2})$. However, contrary to the frequencies $\omega_1$ and $\omega_2$ that correspond to stable equilibrium points of the potential function $\mathcal{F}(\omega) = k(\omega) + \lambda\omega - \mu$, the frequency $\omega_3$ is associated to an unstable point, $\mathcal{F}''(\omega_3) < 0$. According to the kinetic interpretation of the potential function $\mathcal{F}(\omega)$, this means that quasi-particles tend to flee away from the frequency $\omega_3$, so as to migrate towards the bottom of the potential wells $\mathcal{F}(\omega_1)$ and $\mathcal{F}(\omega_2)$. In this way the frequency $\omega_3$ corresponds to a local minimum of the equilibrium spectrum $n^{eq}(\omega)$, while $\omega_1$ and $\omega_2$ correspond to the maxima of $n^{eq}(\omega)$.

The thermodynamic phase-matching given by Eq. (197) then imposes a matching of the group-velocities of the two spectral peaks of the SC spectrum. The fact that different wave-packets naturally tend to propagate with the same group-velocity has been discussed above in Section 5.3.2. It was shown that a velocity locking is required, in the sense that it prevents "a macroscopic internal motion in the wave system". In this case, a set of distinct interacting wave-packets were considered *a priori*, respectively in the framework of the vector NLS equation, or the resonant three-wave interaction in Ref. [306]. Here, the process of SC generation provides a non-trivial extension of the velocity-locking effect, since velocity-locking occurs within a single wave-packet by means of a fission of its initial spectrum.

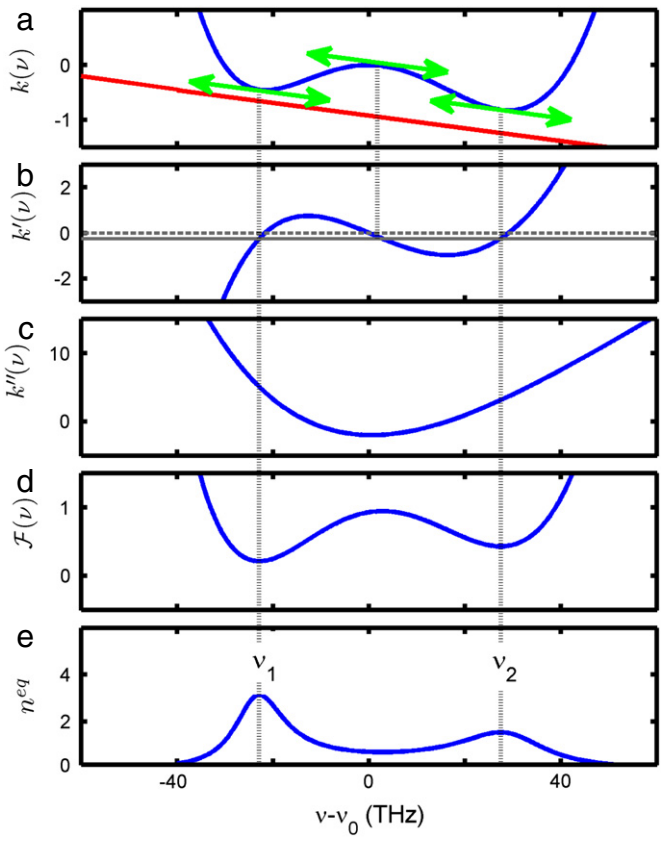


**Fig. 38.** Velocity-locking through SC generation: Dispersion relation $k(\omega)$ (a), corresponding inverse of group-velocity dispersion $k'(\omega) = 1/v_g(\omega)$ (b), and corresponding dispersion curve $k''(\omega)$ that exhibits two zero dispersion wavelengths, $\nu_{ZDW1} = -12.7$ THz, $\nu_{ZDW2} = +16.4$ THz (c). The straight red-line in (a) represents $-\lambda\omega + \mu$: The equilibrium frequencies $\omega_{1,2} = 2\pi\nu_{1,2}$ correspond to those frequencies for which the red-line is parallel to $k(\omega)$. Effective potential $\mathcal{F}(\omega) = k(\omega) + \lambda\omega - \mu$ (d), and corresponding equilibrium spectrum $n^{eq}(\omega) = T/\mathcal{F}(\omega)$ of the kinetic theory [Eq. (195)] (e). The dashed line in (b) represents $k'(\omega_{1,2}) = -\lambda$: The frequencies $\omega_1$ and $\omega_2$ are selected in such a way that $v_g(\omega_1) = v_g(\omega_2) = -1/\lambda$ ($\nu_1 = \omega_1/(2\pi) = -22.9$ THz, $\nu_2 = \omega_2/(2\pi) = +27.5$ THz). Note that the values of these equilibrium frequencies ($\nu_1$, $\nu_2$) also differ from the MI frequencies, $\nu_{\rm MI} = \pm 23.5$ THz.
*Source:* From Ref. [365].

### 5.4.4. *Influence of self-steepening on thermalization*

In this section we consider the WT theory of the NLS equation in the presence of self-steepening

$$i\frac{\partial\psi}{\partial z} + \sum_{j\geq 2}^{m} \frac{i^j\beta_j}{j!}\frac{\partial^j\psi}{\partial t^j} + \gamma|\psi|^2\psi + i\gamma\tau_s\frac{\partial\left(|\psi|^2\psi\right)}{\partial t} = 0. \tag{198}$$

Here we follow Ref. [345] to present some technical details on the derivation of the WT equation because we believe that they can be of pedagogical value. Indeed, the shock term is essentially a dispersive nonlinear term whose WT description is in principle not immediate. However, by means of a simple transformation, we shall see that the NLS Eq. (198) recovers an explicit Hamiltonian structure, a feature that may be exploited to derive the kinetic equation in a straightforward manner [345]. The kinetic theory also sheds new light on the role of the self-steepening effect. In particular, it reveals that the shock term merely introduces a spectral factor $(1 + \tau_s\omega)$ in the equilibrium spectrum of the optical field.

*Hamiltonian structure with self-steepening*

It is instructive to write the NLS Eq. (198) in Fourier space,

$$i\partial_z\tilde{\psi}(\omega, z) + k(\omega)\tilde{\psi}(\omega, z) + \frac{\gamma(1+\tau_s\omega)}{2\pi}\int \tilde{\psi}_{\omega_1}\tilde{\psi}^*_{\omega_2}\tilde{\psi}_{\omega_3}\,\delta_{\omega-\omega_1+\omega_2-\omega_3}\,d\omega_1\,d\omega_2\,d\omega_3 = 0, \tag{199}$$

where '$\tilde{\psi}_\omega$' stands for the Fourier transform of the field amplitude $\left[\tilde{\psi}(\omega, z) = (2\pi)^{-1/2}\int\psi(z, t)\exp(i\omega t)\,dt\right]$. Note that the shock term simply appears *via* the factor $\tau_s\omega$ in front of the nonlinear term. This equation conserves the intensity of the field $N = \int|\tilde{\psi}(\omega, z)|^2\,d\omega$. However, *the shock term prevents the conservation of momentum* $P = \int\omega\,|\tilde{\psi}(\omega, z)|^2\,d\omega \neq$

*const*, an important feature whose consequences will be discussed later. Let us observe, however, that the following transformation

$$\tilde{\varphi}(\omega, z) = \frac{\tilde{\psi}(\omega, z)}{\sqrt{1+\tau_s\omega}}, \tag{200}$$

allows us to write Eq. (199) in an appropriate symmetric form

$$i\partial_z\tilde{\varphi}(\omega, z) + k(\omega)\tilde{\varphi}(\omega, z) + \frac{\gamma}{2\pi}\int L_{\omega\omega_1\omega_2\omega_3}\,\tilde{\varphi}_{\omega_1}\tilde{\varphi}^*_{\omega_2}\tilde{\varphi}_{\omega_3}\,\delta_{\omega-\omega_1+\omega_2-\omega_3}\,d\omega_1\,d\omega_2\,d\omega_3 = 0, \tag{201}$$

where the interaction coefficient $L_{\omega_1\omega_2\omega_3\omega_4} = L(\omega_1, \omega_2, \omega_3, \omega_4)$ denotes the fourth-order tensor

$$L_{\omega_1\omega_2\omega_3\omega_4} = (1+\tau_s\omega_1)^{1/2}(1+\tau_s\omega_2)^{1/2}(1+\tau_s\omega_3)^{1/2}(1+\tau_s\omega_4)^{1/2}. \tag{202}$$

Note that the transformation (200) is relevant provided that the condition $1+\tau_s\omega > 0$ is satisfied. However, the typical time scale of the shock coefficient is $\tau_s \sim 1/\omega_0$, $\omega_0$ being the carrier angular-frequency of the optical field. In this way, the condition $\omega > -1/\tau_s \sim -\omega_0$ is usually verified within the slowly-varying envelope approximation. Let us also remark that, although in Fourier space the variable change (200) appears as rather simple, in the temporal domain the transformation (200) reads $\varphi(t, z) = (1+i\tau_s\partial_t)^{-\frac{1}{2}}\,\psi(t, z)$. In this transformation, the square-root operator should be interpreted as a Taylor's expansion series, $(1+i\tau_s\partial_t)^{-\frac{1}{2}} = \sum_{j=0}^{\infty} C_j^{-\frac{1}{2}}\,(i\tau_s)^j\,\partial_t^j$, where $C_j^{-\frac{1}{2}}$ refers to the corresponding binomial coefficient. This reveals that the equation governing the propagation of the optical field in the variable $\varphi$ no longer refers to a standard 'nonlinear Schrödinger equation'.

The advantage of the variable $\varphi$ relies on the fact that Eq. (201) exhibits an explicit Hamiltonian structure

$$H_\varphi = \int k(\omega)|\tilde{\varphi}_\omega|^2 d\omega + \frac{\gamma}{4\pi}\int L_{\omega_1\omega_2\omega_3\omega_4}\,\tilde{\varphi}_{\omega_1}\tilde{\varphi}^*_{\omega_2}\tilde{\varphi}_{\omega_3}\tilde{\varphi}^*_{\omega_4}\delta_{\omega_1-\omega_2+\omega_3-\omega_4}\,d\omega_1\,d\omega_2\,d\omega_3\,d\omega_4, \tag{203}$$

with the complex canonical variables $\partial_z\tilde{\varphi} = i\delta H_\varphi/\delta\tilde{\varphi}^*$, $\partial_z\tilde{\varphi}^* = -i\delta H_\varphi/\delta\tilde{\varphi}$. Furthermore, Eq. (201) conserves two additional quantities, $N_\varphi = \int|\tilde{\varphi}(\omega, z)|^2\,d\omega$ and $P_\varphi = \int\omega\,|\tilde{\varphi}(\omega, z)|^2\,d\omega$, which respectively represent the power and momentum densities of the field in the new variable $\varphi$.

Let us remark that the conserved quantities $N_\varphi$, $P_\varphi$ and $H_\varphi$ indicate the existence of three additional invariants for the NLS Eq. (198) [or Eq. (199)] in the original variable $\psi$. Indeed, one can easily verify that Eq. (199) conserves $N_\psi = \int|\tilde{\psi}(\omega, z)|^2/(1+\tau_s\omega)\,d\omega$, $P_\psi = \int|\tilde{\psi}(\omega, z)|^2\omega/(1+\tau_s\omega)\,d\omega$ and

$$H_\psi = \int|\tilde{\psi}(\omega, z)|^2\,\frac{k(\omega)}{1+\tau_s\omega}d\omega + \frac{\gamma}{4\pi}\int\tilde{\psi}_{\omega_1}\tilde{\psi}^*_{\omega_2}\tilde{\psi}_{\omega_3}\tilde{\psi}^*_{\omega_4}\delta_{\omega_1-\omega_2+\omega_3-\omega_4}\,d\omega_1\,d\omega_2\,d\omega_3\,d\omega_4. \tag{204}$$

We remark that $H_\psi$ does not refer to a Hamiltonian, in the sense that Eq. (199) does not verify $\partial_z\tilde{\psi} = i\delta H_\psi/\delta\tilde{\psi}^*$. Also note that a simple relation links the above invariants of Eq. (199), $P_\psi = \frac{1}{\tau_s}(N - N_\psi)$, where we recall that $N = \int|\tilde{\psi}(\omega, z)|^2\,d\omega$. As regard the invariants of Eq. (199), let us remark that the so-called 'modified' NLS equation, $\partial_z A + i\partial_{tt}A + \partial_t(|A|^2A) = 0$ (or $\partial_z A + i\partial_{tt}A + i|A|^2A + \partial_t(|A|^2A) = 0$) belongs to the family of completely integrable partial differential equations [366–369]. In a way akin to the standard NLS equation discussed above, the integrability of the modified NLS equation is broken by the presence of higher-order dispersion effects. Let us now discuss the thermalization process that results from the non-integrable character of this equation.

*Wave turbulence equation and equilibrium spectrum*

The Hamiltonian structure of Eq. (201) allows us to derive the corresponding kinetic equation in a straightforward manner. Following the random phase approximation approach, one obtains the following equation governing the evolution of the spectrum $n_\varphi(z, \omega)$ of the field $\varphi$ [$\langle\tilde{\varphi}(z, \omega_1)\tilde{\varphi}^*(z, \omega_2)\rangle = n_\varphi(z, \omega_1)\delta(\omega_1 - \omega_2)$]:

$$\partial_z n_\varphi(z, \omega_1) = Coll[n_\varphi], \tag{205}$$

with the collision term

$$Coll[n_\varphi] = \int L^2_{\omega_1\omega_2\omega_3\omega_4}\,n_\varphi(\omega_1)n_\varphi(\omega_2)n_\varphi(\omega_3)n_\varphi(\omega_4)\,[n_\varphi^{-1}(\omega_1) + n_\varphi^{-1}(\omega_2) - n_\varphi^{-1}(\omega_3) - n_\varphi^{-1}(\omega_4)] \times W\,d\omega_2\,d\omega_3\,d\omega_4. \tag{206}$$

where the function $W = \frac{\gamma^2}{\pi}\,\delta(\omega_1 + \omega_2 - \omega_3 - \omega_4)\,\delta[k(\omega_1) + k(\omega_2) - k(\omega_3) - k(\omega_4)]$ still accounts for the resonant phase-matching conditions of energy and momentum conservation. The kinetic equation (205) has the same structure as the kinetic Eq. (193). Note however an important difference due to the presence of the interaction coefficient $L_{\omega_1\omega_2\omega_3\omega_4}$ in the collision term of Eq. (205). This reveals that the kinetic theory still models the self-steepening effect as a collisional gas

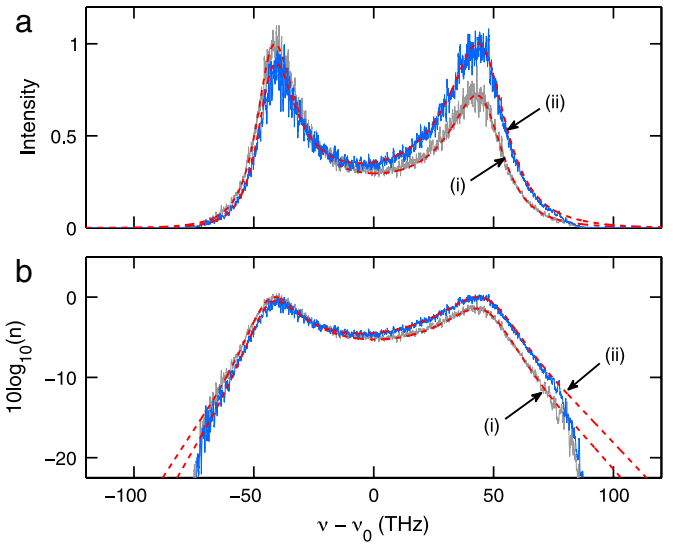


**Fig. 39.** Optical wave thermalization in the presence of self-steepening: Averaged numerical spectrum obtained by solving numerically the NLS Eq. (198) with $\tau_s = 0$ (dark) and $\tau_s = 2/\omega_0$ (blue), in normal (a) and logarithmic (b) scales, $\omega_0 = 2\pi\,\nu_0$. The dashed red lines refer to the corresponding equilibrium spectra $n^{eq}(\omega)$ predicted by the kinetic theory [see Eq. (208)]. An average over 140 spectra has been taken once thermal equilibrium was reached, $\partial_z\,\mathcal{S}_\varphi \simeq 0$. We refer the reader to Ref. [345] for more details regarding the values of the parameters used in the numerical simulation.

of quasi-particles satisfying the resonant conditions of energy and momentum conservation at each collision. However, the novel feature is that the quasi-particles interact with a non-trivial scattering cross-section $L^2_{\omega_1\omega_2\omega_3\omega_4}$ at each elementary collision.

The kinetic equation (205) conserves the intensity (density of power) $N_\varphi/T_0 = \int n_\varphi(z,\omega)\,d\omega$, the density of kinetic energy $E_\varphi/T_0 = \int k(\omega)\,n_\varphi(z,\omega)\,d\omega$, the density of momentum $P_\varphi/T_0 = \int \omega\,n_\varphi(z,\omega)\,d\omega$, and it exhibits a $H$-theorem of entropy growth, $\partial_z S_\varphi \geq 0$, where the nonequilibrium entropy reads $S_\varphi = \int \log[n_\varphi(z,\omega)]\,d\omega$. The thermodynamic equilibrium state that realizes the maximum of nonequilibrium entropy thus takes the same form as in Eq. (195),

$$n^{eq}_\varphi(\omega) = \frac{T}{k(\omega) + \lambda\omega - \mu}. \tag{207}$$

As expected, the scattering cross-section $L^2_{\omega_1\omega_2\omega_3\omega_4}$ only affects the nonequilibrium dynamics of the incoherent field, but not the Rayleigh–Jeans equilibrium distribution (207). We remark that one encounters the same physical picture in kinetic gas theory: The Boltzmann's equation that governs the nonequilibrium evolution of a classical gas depends on the scattering cross-section, but not the corresponding Maxwell's equilibrium distribution [296].

In order to analyze the role of the self-steepening on wave thermalization, let us write the equilibrium distribution (207) in term of the original variable $\psi$. According to the transformation (200), the equilibrium spectrum $n^{eq}(\omega)$ of the field $\psi$ in the presence of self-steepening takes the form

$$n^{eq}(\omega) = \frac{T\ (1+\tau_s\omega)}{k(\omega) + \lambda\omega - \mu}. \tag{208}$$

Note that, contrary to Eq. (207), the equilibrium distribution (208) does not refer, strictly speaking, to a Rayleigh–Jeans distribution. The shock term thus merely introduces a linear gradient into the equilibrium spectrum (208) of the optical field. This remarkable conclusion has been found in quantitative agreement with the numerical simulations of Eq. (198), without adjustable parameters. This is illustrated in Fig. 39, in which the numerical and theoretical equilibrium spectra in the presence and in the absence of self-steepening have been reported. We refer the reader to Ref. [345] for more details. Also note that, as discussed above through Fig. 37, an appreciable discrepancy between the theory and the simulations has been obtained in the tails of the spectrum (Fig. 39), a feature that will be discussed in more detail in Section 6.1.

To summarize, a PCF characterized by a dispersion curve with two zero dispersion wavelengths can lead to a thermalization process characterized by a double peaked Rayleigh–Jeans equilibrium distribution. The frequencies of the double peak spectrum are selected in such a way that the corresponding wave packets propagate with the same group velocity, which also matches the average group velocity of the optical field. This velocity-locking effect has a thermodynamic origin, as discussed in Section 5.3. We finally note that some experimental evidence of this thermalization process driven by SC generation has been discussed in Ref. [184].

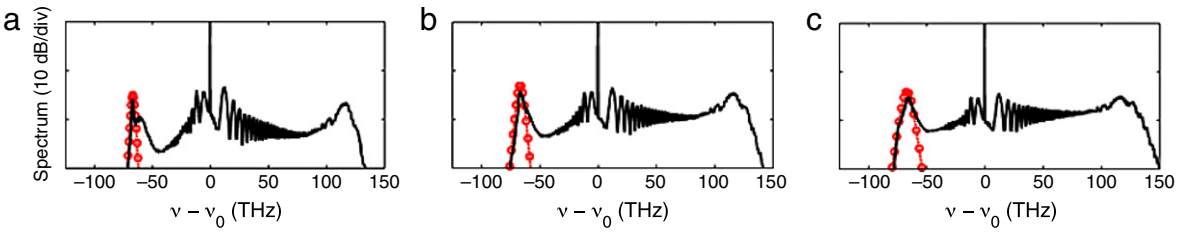


**Fig. 40.** Emergence of spectral incoherent solitons from MI in SC generation: (Black solid line) Experimental spectra recorded after 75 cm of propagation for three distinct values of input peak power: (a) 1.32 kW, (b) 2.22 kW, and (c) 4.52 kW. The red dashed lines with circles are the secant-hyperbolic fits of the low-frequency MI band, which plays the role of a seed for the generation of spectral incoherent solitons. The spectral widths and powers of the corresponding fitted functions are, respectively, (a) 3 THz, 150 W, (b) 6 THz, 250 W, and (c) 9 THz, 350 W.
*Source:* From Ref. [30].

### *5.4.5. Emergence of spectral incoherent solitons through supercontinuum generation*

As discussed above through Fig. 36, an incoherent structure analogous to the spectral incoherent soliton is spontaneously generated in the low-frequency edge of the SC spectrum. In this section we briefly comment this aspect through the analysis of the SC spectrum at the early stage of propagation and refer the reader to Ref. [184,30] for more details.

A first important point to note is that the low-frequency MI spectral peak plays the role of a seed for the generation of spectral incoherent solitons. This is illustrated in Fig. 40, which reports the experimental spectra recorded after 75 cm of propagation in a PCF for three different powers of the laser. Note that the experiment is conceptually simple. In substance a quasi-continuous ($\sim$ns) and intense laser pulse ($\lambda_0 = 1064$ nm) is injected in a PCF characterized by two zero-dispersion wavelengths (at 910 and 1152 nm). We refer the reader to Refs. [184,30] for details concerning the experimental configuration.

*Transition from discrete to continuous spectral incoherent solitons*

We remark in Fig. 40 that 75 cm of propagation are sufficient for a complete development of the MI bands. As in the standard MI process, the spectral bandwidth of MI gain increases as the pump power is increased, a feature which is clearly visible in Fig. 40. Accordingly, the spectral seed of the spectral incoherent soliton becomes larger as the injected power increases. This spectral broadening is responsible for a transition from the discrete to the continuous spectral incoherent soliton.

To analyze this transition in more detail, the low-frequency MI band recorded experimentally has been fitted by a secant hyperbolic function for each of the three input powers. The corresponding fits are shown in red in Fig. 40 and their characteristics (spectral width and peak power) are given in the figure caption. We considered these sech-fitting functions as the initial condition, and performed numerical simulations with both the WT Langmuir kinetic equation (44) and the reduced NLS Eq. (36) accounting solely for second-order dispersion and the delayed Raman nonlinearity. To be consistent, an average value of the second-order dispersion coefficient (160 $ps^2/km$) was considered in the NLS Eq. (36). This value represents a good approximation of the dispersion value of the PCF in the frequency range swept by the spectral incoherent soliton in the experiment. Note that, in all cases considered, we have verified that the optical field evolves in the weakly nonlinear regime.

The numerical simulations of the NLS equation and WT Langmuir equation have been compared with the experimental spectrum for the three input powers considered in Fig. 40, and the corresponding results are reported in Fig. 41. We observe a qualitative agreement between the experimental evolution of the spectral incoherent soliton and the corresponding simulations of the NLS and kinetic equations. In particular, at small power (Fig. 41(a)–(c)), the evolution of the three spectral bands of the discrete soliton is in agreement with the experimental results [note that, because of the limited spectral window of the analyzer (600–1750 nm), the comparison with the experimental evolution has been done over a limited spectral range]. Also, at high power (Fig. 41(g)–(i)), we may note that soliton propagation in frequency space is almost rectilinear for $z > 6$ m, as it should be for a genuine spectral incoherent soliton.

We remark that a transition occurs from the discrete spectral incoherent soliton to the continuous counterpart as the input power is increased. This transition can be intuitively interpreted as a consequence of the broadening of the initial MI spectral seed. Following the reasoning of Section 3.2.1, for a spectral width of 3 THz (Fig. 41(a)–(c)), the optical field exhibits a discrete Raman shift simply because the low-frequency tail of the spectrum exhibits a higher gain as compared to the mean gain of the whole front of the spectrum. Conversely, the Raman shift becomes continuous for the broad spectral width (9 THz) considered in Fig. 41(g)–(i).

We finally note that, besides the low-frequency MI band, there can be different mechanisms which lead to the generation of spectral incoherent solitons. Indeed, in certain cases, the low-frequency peak of the Rayleigh–Jeans distribution can also play the role of a seed for the generation of a spectral incoherent soliton, a feature discussed in Ref. [365]. From a more general perspective, we should note that research on the formation of spectral incoherent solitons through supercontinuum generation is still at his infancy stage [138].

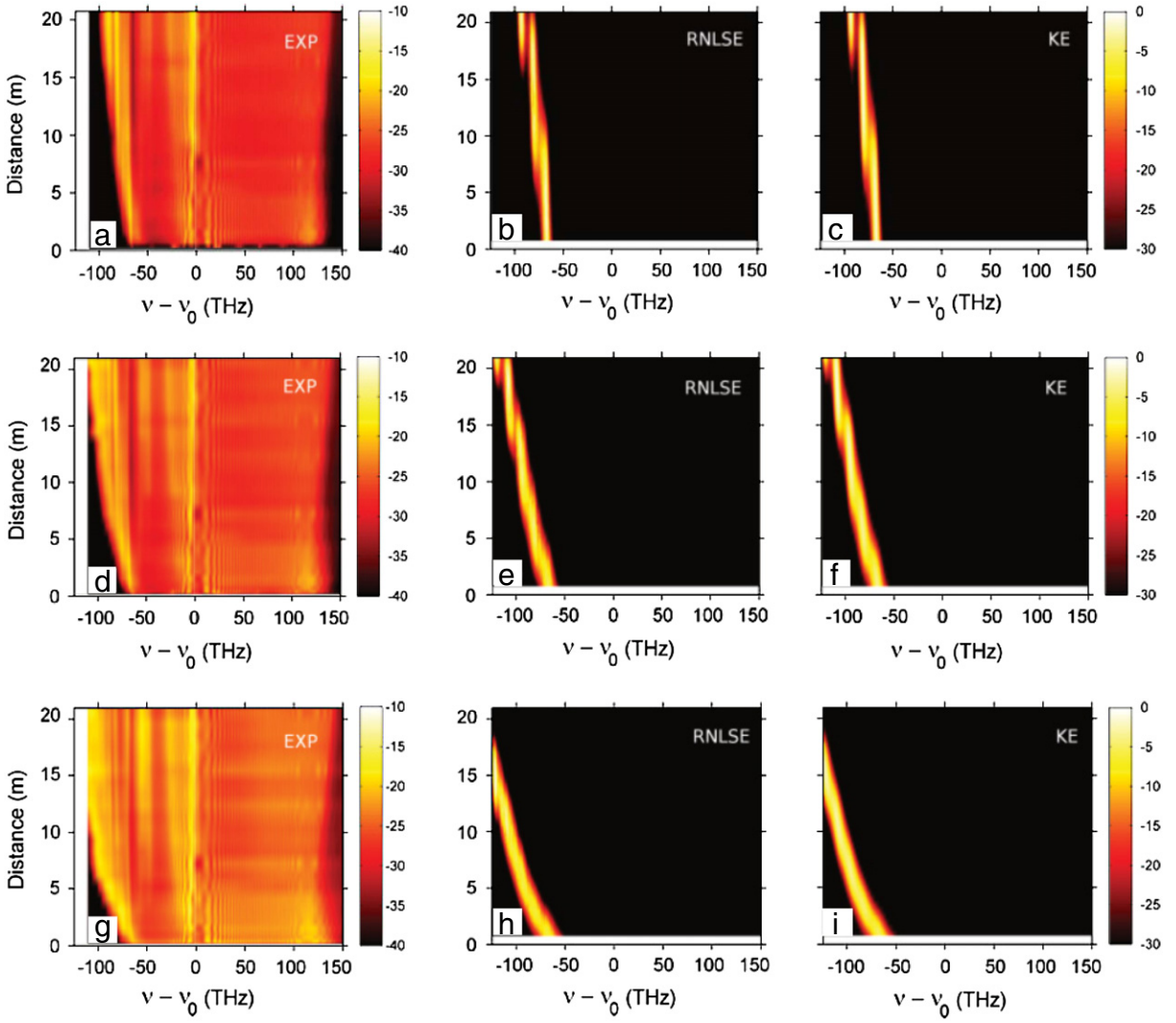


**Fig. 41.** Emergence of spectral incoherent solitons through SC generation. First column: Experimental results illustrating the spectral evolution (in dB scale) as a function of propagation distance in a 21 m long PCF, for an input peak power of 1.32 kW (a), 2.22 kW (d), 4.52 kW (g). Second column: Numerical simulations of the reduced NLS Eq. (36) starting with the secant-hyperbolic fit reported in Fig. 40(a) for (b); in Fig. 40(b) for (e); in Fig. 40(c) for (h). Third column: Corresponding evolutions of the averaged spectra of the optical field, $n(\omega, z)$, obtained by integrating numerically the WT Langmuir kinetic equation (44), with the same initial condition as in the NLS simulations (second column).
*Source:* From Ref. [30].

### 5.5. Experiments

#### 5.5.1. Generalities

There exist a large number of nonlinear optical experiments which involve the propagation of partially incoherent waves. Here we will only briefly comment those experiments which have been specifically designed to the study of optical WT. Let us first note that long-range turbulent behaviors discussed above in Section 2–3 through the long-range Vlasov equation and the singular integro-differential kinetic equations, have not yet been the subject of a specific experimental study. As commented in the end of Section 3, hollow-cores fibers filled with liquids or gases displaying highly noninstantaneous nonlinearities [217–219,222,224] would constitute ideal test beds for the experimental study of long-range turbulence in the temporal domain. On the other hand, some experimental signatures of Raman-induced weak Langmuir turbulence-like phenomena in photonic crystal fibers have been obtained through the formation of spectral incoherent solitons through SC generation [184,30], as discussed above in Section 5.4.5. In this section, we focus the presentation on optical experiments evidencing some features that are, or might be, related to a turbulent behavior described by the WT kinetic equation. In Section 6, we will present different experiments in relation with a breakdown of thermalization described by the WT kinetic

equation. Note that we will not provide here an exhaustive review of all the works made in this field but we will rather present existing attempts, challenges and open questions.

As discussed throughout this review, the field of optics offers a large variety of systems with a great variety of nonlinear interactions and dispersive properties. Many range of parameters (strength of the nonlinearity, sign and shape of the dispersion curve) and many experimental configurations (single pass in a nonlinear media, passive or active optical cavity, waveguides, . . .) can be used to investigate nonlinear propagation of incoherent waves. As an example, it has been shown in Section 5.2.4 that two-dimensional wave condensation can occur in the thermodynamic limit in optical waveguides, such as multimode fibers supporting a finite number of transverse modes [290]. In various nonlinear optical media (silica fibers, photorefractive crystals, liquid crystals), the treatment of the light–matter interaction at lowest order turns out to be relevant [370,171]. In centro-symmetric media like optical fibers, third-order nonlinearity is the dominant process and wave propagation can be accurately described by NLS-like equations with a cubic nonlinearity.

Besides optical cavity systems such as, e.g., Raman fiber lasers that will be discussed in Section 7, so far, experimental setups have been mainly designed to study a single-pass propagation of the incoherent wave through the nonlinear material. As discussed below, such experiments are aimed at studying different regimes of optical wave turbulence. However, because of the single pass experimental configuration, such regimes refer, strictly speaking, to transient regimes, since they cannot lead to the establishment of a genuine statistically stationary state of the turbulent wave.

Following the presentation given in Section 2–3, two different types of optical experiments can be distinguished, which respectively study the temporal or the spatial coherence properties of the optical field as it propagates in the nonlinear medium. In 'temporal experiments', the initial incoherent wave is a function of the physical time which plays the role of a 1D-'space', as described by the temporal version of the NLS Eq. (36) in Section 3. In spatial experiments, the wave propagates either in one or two-transverse dimensions, as described by the spatial version of the NLS Eq. (36) in Section 2. In both cases the variable $z - v_g t$ corresponds to a 'time' evolution in which $z$ is the coordinate along the propagation direction and $v_g$ is the group velocity at the carrier wave frequency. The impact of nonlinear effects in an optical experiment is usually measured by the nonlinear length, $L_{nl}$, while linear dispersion effects (in the time domain) or diffraction effects (in the spatial domain) are measured by the linear length, $L_d$, as they have been defined in Section 2–3.

The experimental observation of WT phenomena, such as wave thermalization to the Rayleigh–Jeans distribution, is a challenging problem because of the unavoidable presence of linear and nonlinear losses in any optical media. As discussed throughout this review, the WT theory is valid in the limit where the linear length $L_d$ is much shorter than the nonlinear length $L_{nl}$, so that dispersive linear effects dominate nonlinear effects (note however the particular case of the long-range Vlasov equation, whose validity goes beyond the weakly nonlinear regime, see Section 2.3.2). This condition can be fulfilled in optical experiments simply by decreasing the optical power of the beam launched as the initial condition into the nonlinear medium. However in this case large propagation distances $L$ are required to observe phenomena such as wave thermalization and wave condensation. As a result, linear losses of the optical medium become non negligible and thus prevent the optical wave system from reaching a Rayleigh–Jeans equilibrium state.

Optical fibers are known to exhibit weak linear losses (between 0.2 and 1 dB/km), so that they appear as appropriate candidates to overcome this obstacle. Unfortunately, stimulated Raman scattering constitutes a major obstacle to the observation of wave thermalization or condensation. As discussed in detail in Section 3, the Raman effect is a non-instantaneous nonlinear effect which breaks the Hamiltonian structure of the NLS equation. In optical fibers, the Raman effect refers to a nonlinear coupling between light and the vibrational modes of silica molecules at a frequency $\nu_R \simeq 14$ THz. If the spectrum of the initial wave (having a carrier optical frequency $\nu_0$) is much narrower than $\nu_R$, spontaneous Raman scattering is amplified, which leads to the emergence of a new optical wave (Stokes wave) at a frequency $\nu_0 - \nu_R$. Therefore stimulated Raman scattering acts as a nonlinear dissipative effect for the incoherent wave propagating in the fiber. In a standard single-mode optical fiber, the Stokes power (and thus the contribution of stimulated Raman scattering) can be neglected as long as $L < 15 L_{nl}$ [138].

We illustrate the impact of the Raman effect with SC experiments reported in [184], in which the Raman effect prevents the establishment of a thermodynamic equilibrium state for the incoherent wave. A comparison between the expected Rayleigh–Jeans spectral distribution (see Section 5.4), the numerical integration of the NLS equation with (and without) the Raman effect, and the experimental results is reported in Fig. 42.

### 5.5.2. Specific experiments

In 2006 Pitois et al. have performed experiments in optical fibers in order to observe the phenomenon of velocity locking of incoherent waves predicted by the WT theory, as discussed in Section 5.3 [344]. An initial incoherent wave was obtained from the amplified spontaneous emission of a dye amplifier and was equally launched along the two polarization axes of a polarization maintaining fiber. These experiments are described by a system of two coupled 1D NLS equations, as discussed in Section 5.3. The velocity mismatch between the two waves is calculated from the measured mean frequencies of the two polarization components and from the values of the birefringence and group-velocity dispersion. Fig. 43 shows the group-velocity mismatch as a function of the optical power of the waves. The interaction between the two incoherent waves leads to a matching of their group-velocities *via* a change of their mean frequencies. This behavior is similar to the velocity locking predicted by WT theory (see Section 5.3). Note however that in the experiments the group velocity dispersions on the two axis are almost identical ($\beta_1 \simeq \beta_2$), so that the transient regime towards the Rayleigh–Jeans distribution may be extremely

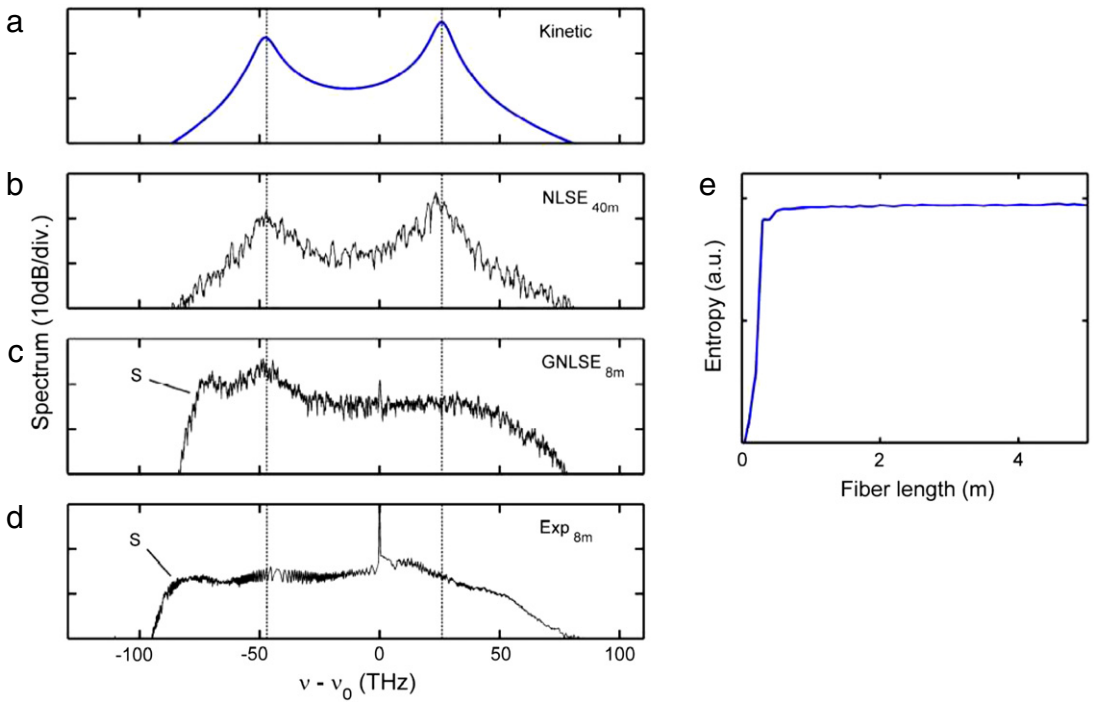


**Fig. 42.** Supercontinuum and wave thermalization through SC generation in a photonic crystal fiber with two zero-dispersion wavelength: Comparison of the theoretical, numerical and experimental spectra plotted in logarithmic scale. (a) Plot of the equilibrium Rayleigh–Jeans spectrum $n_{eq}(\omega)$ given in Eq. (195) without adjustable parameters. (b) Spectrum obtained by solving numerically the generalized NLS Eq. (190) without Raman, loss and shock terms. (c) Spectrum obtained by solving numerically the generalized NLS Eq. (190). (d) Spectrum recorded in experiment. 'S' indicates the position of the spectral incoherent soliton (see Section 5.4.5). Note the good agreement of the frequencies of the spectral peaks. (e) Evolution of the nonequilibrium entropy during the propagation of the optical field corresponding to the simulation of the NLS equation in (b): The process of entropy production saturates as the equilibrium state is approached.
*Source:* From Ref. [184].

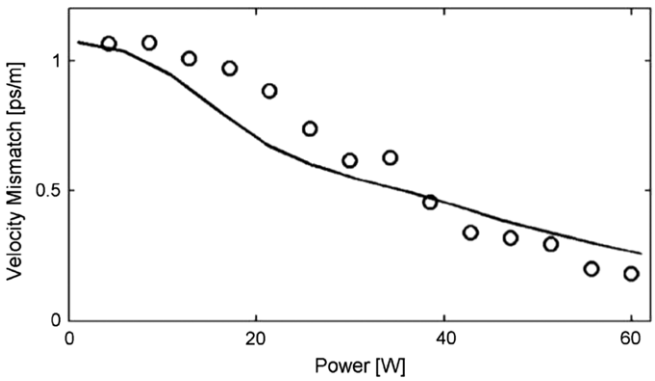


**Fig. 43.** Velocity locking experiments in a high-birefringence optical fiber. Evolution of the group-velocity mismatch as a function of the optical power of each wave packet. Circles: Experimental measurements; solid line: Numerical simulations ($P = 20$ W corresponds to $L = 5L_{nl}$).
*Source:* From Ref. [344].

long and steady states or metastable states corresponding to the process of anomalous thermalization can be expected, as will be discussed in Section 6.2.

Spatial experiments concerning wave condensation in a photorefractive crystal have been performed by Sun et al. [371]. An initial 2D incoherent wave is 'written' on a coherent laser beam by using spatial light modulators. This incoherent spatial field then propagates through the nonlinear crystal. The third order nonlinearity is defocusing and it is controlled by a high voltage. The far field Fourier spectra of the waves ($n(k_x, k_y) = \tilde{\psi}(k_x, k_y)$) is observed in the focal plane of a lens and the authors consider in particular the changes in the cross section $n(k_x, k_y = 0)$ (see Fig. 3d of [371]) of the power spectrum. By increasing the strength of the nonlinearity, the authors record a spectrum that exhibits a narrowing. Moreover the tails of

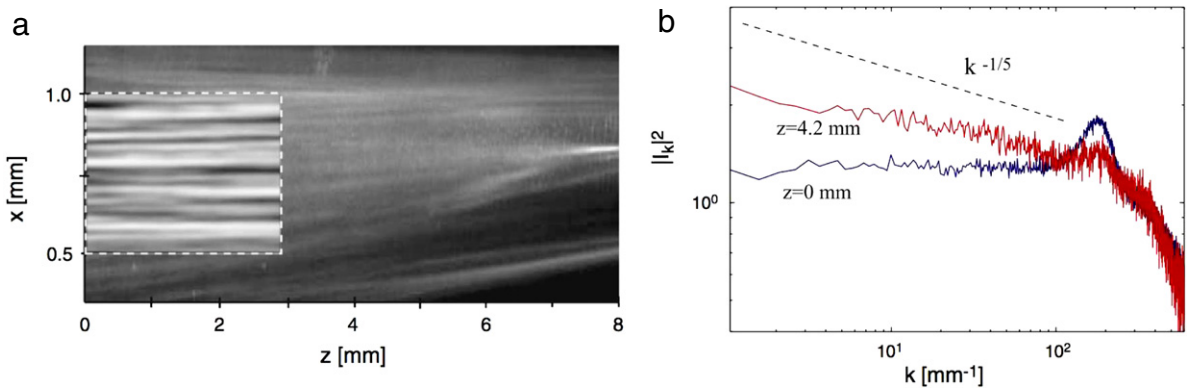


**Fig. 44.** Liquid crystal experiment reporting the observation an inverse WT cascade. (a) Experimental intensity distribution $I(x, z)$. The area marked by the dashed line is shown at a higher resolution. (b) Experimental spectrum of the light intensity, $N_k = |I_k|^2$ at two different propagation lengths $z$, where $I_k$ denotes the spatial Fourier transform of the intensity $I(x)$.
*Source:* From Ref. [84].

the power spectrum decay according to a power law $n(k_x, k_y = 0) \propto k_x^{-2}$. In [371] the former observation is interpreted as wave condensation and the latter observation is associated to the Rayleigh–Jeans distribution.

However these signatures of wave condensation and wave thermalization can arise from simple experimental artifacts. First of all, diffraction through limited-size optical components also leads to a power-law decay $\sim 1/k_x^2$ in the tails of the spectrum. Indeed, the Fourier transform of a slit characterized by a size $2a$ is simply $|\widetilde{\psi}(k_x)|^2 \propto |\sin(k_x a)/(k_x a)|^2$ which indeed decays according to $1/k_x^2$ [372,373]. We also note that the wings of the initial and output spectra exhibit roughly the same power law (see Fig. 3d of [371]).

The nonlinearity-dependent narrowing of the spectrum may also be observed with simple nonlinear Kerr-lens effect combined with a slight mispositioning of the detector [373]. Fig. 5b in [373] is numerically computed from the consideration of this simple effect coupled with the diffraction by the crystal finite square aperture. Surprisingly this gives a spectrum quantitatively very similar to the experimental one plotted on Fig. 3d of Ref. [371].

As a conclusion, the spatial experiments by Sun et al. open many challenging questions about the observation of wave condensation and Rayleigh–Jeans spectra in nonlinear optics. Experiments may be conceived with or without waveguide. Optical experiments with bulk media (such as photorefractive or liquid crystals) can provide very high third-order nonlinearity without any waveguide effect. On the other hand, multimode optical fibers are good candidates to observe wave condensation with a finite number of modes (see Section 5.2.4). However, as discussed here above, the Raman effect limits current experiments to short propagation distances in standard silica fibers.

Bortolozzo et al. have performed 1D spatial WT experiments in liquid crystals [83,84]. An incoherent 1D wave is initially prepared with a spatial light modulator and it is launched inside a nematic liquid crystal layer. One of the originalities of the setup is the direct observation of the evolution of the transverse intensity profile $|\psi(z, t)|^2$ from the use of a microscope objective. This permits the observation of the change in the dynamics of the incoherent wave all along the propagation distance, thus providing nice $(x, t)$ diagrams. Note that in this setup the Fourier Transform (FT) of $|\psi(x)|^2$ can be computed, while $|\widetilde{\psi}(k_x)|^2 = |FT(\psi(x))|^2$ is not directly available.

The authors observe an inverse cascade with an initial spectrum centered on a non-zero wavenumber. This inverse cascade leads to a power law $FT(|\psi(x)|^2) \propto k_x^{-1/5}$. At long propagation distances, soliton formation emerging from the waves interaction is also observed. Moreover, probability distribution functions of the optical intensity decaying slower than exponential laws (corresponding to Gaussian statistics) is observed [83,84].

The authors make use the general framework of the WT theory in order to describe the experimental results. As discussed in Section 4.6.1, a liquid crystal exhibits a nonlocal Kerr nonlinearity. The weakly nonlocal regime was considered in the experiment, so that the nonlocal interaction can be treated in a perturbative way, as discussed in after Eq. (158). The theoretical study reveals that the wave interaction refers to a six-waves process [84]. This allows the authors to derive kinetic equations with a collision term involving six-waves resonances. In this way, stationary nonequilibrium solutions of the Kolmogorov–Zakharov type are obtained (see Ref. [84] for details). In this way, an inverse WT cascade has been predicted theoretically and found in good agreement with the experimental results [83,84] (see Fig. 44).

To the best of our knowledge, these experiments in liquid crystals provide the unique observation of a WT (inverse) cascade in optics. Note in Refs. [83,84] that the optical system is forced at the input of the nonlinear medium ($z = 0$), and the formation of the nonstationary spectrum is observed in the transient propagation of the optical wave. From a phenomenological point of view, this experimental configuration can be compared with 'decaying turbulence' in hyrdodynamics [374]. As discussed above, the propagation length $z$ plays the role of time in optics, so that the observation of a permanent nonequilibrium stationary state would require a forcing and a damping at any $z$, a situation which is rather artificial in optics.

Raman fiber lasers are active 1D optical systems that can exhibit a turbulent-like behavior. In this system described by a generalized 1D NLS equation, one should not expect Zakharov–Kolmogorov-like cascades, though many interesting behaviors such as a laminar to turbulent transition have been observed [81]. An overview of these experiments will be given in Section 7.

We finally note that Section 6 reports other WT experiments realized in optical fibers, in relation with breakdown of thermalization. Indeed, when the wave system is accurately modeled by an equation which is almost integrable, it can exhibit a process of anomalous thermalization through degenerate resonances (see Section 6.2 for the theory and Section 6.2.3 for the experiments) or a process of irreversible relaxation through non-resonant interactions (see Section 6.3 for theoretical developments based on the integrable NLS equation, and Section 6.3.3 for experiments).

## 6. Breakdown of thermalization in 1D-NLS equation

As commented in the introduction (Section 1.2.4) through the Fermi–Pasta–Ulam problem [130], the natural phenomenon of thermalization towards the Rayleigh–Jeans distribution discussed in the previous section does not necessarily occur in a nonlinear system. In this section we discuss this possible breakdown of thermalization in the light of the WT kinetic equation (see Section 5). We consider the 1D NLS equation accounting for higher-order dispersion effects, which is known to describe light propagation in photonic crystal fibers (see Section 5.4.1). We present three different processes which inhibit the phenomenon of optical wave thermalization towards the Rayleigh–Jeans spectrum. Indeed, depending on whether the dispersion relation is truncated up to the second, third, or fourth-order, the wave system exhibits different types of relaxation processes. We will see that the WT theory provides an accurate description of the three mechanisms underlying this breakdown of thermalization. We remark that, besides the WT approach [375], the long term evolution of the dynamics of incoherent optical waves has been also explored in different circumstances. For instance, many studies of thermalization in nonlinear discrete systems have concentrated on the discrete NLS equation in one [60,61,63,55,56,376,64] or two [377] dimensions.

### 6.1. Influence of fourth-order dispersion: Truncated thermalization

We consider here the 1D NLS equation in which the dispersion relation is truncated to the fourth-order. In this case, the WT theory reveals the existence of an irreversible evolution towards a Rayleigh–Jeans equilibrium state characterized by a compactly supported spectral shape [143]. This phenomenon of truncated thermalization may explain the physical origin of the abrupt SC spectral edges discussed above in Section 5.4.2. More generally, it can shed new light on the mechanisms underlying the formation of bounded spectra in SC generation [357,378,355,356,184]. Besides its relevance in the context of SC generation, this phenomenon is also important from a fundamental point of view. Indeed, *it unveils the existence of a genuine frequency cut-off that arises in a system of classical waves described by the generalized NLS equation*, a feature of importance considering the well-known ultraviolet catastrophe of ensemble of classical waves (see Section 5.2.2).

*NLS model*

The starting point is the NLS equation (192) accounting for third- and fourth-orders dispersion effects. For convenience, we present the results in dimensionless units, for which the NLS equation takes the form

$$i\partial_z\psi = -s\partial_t^2\psi - i\tilde{\alpha}\partial_t^3\psi + \tilde{\beta}\partial_t^4\psi + |\psi|^2\psi, \tag{209}$$

where the spatial and temporal variables have been normalized with respect to the nonlinear length $L_{nl} = 1/(\gamma\rho)$ and the 'healing time' $\tau_0 = (|\beta_2|L_{nl}/2)^{1/2}$. As discussed in Section 3, $\gamma(>0)$ is the nonlinear coefficient, $\rho$ the average intensity, $\beta_2$ the second-order dispersion coefficient with $s = \text{sign}(\beta_2)$. In these units, the normalized dispersion parameters read $\tilde{\alpha} = L_{nl}\beta_3/(6\tau_0^3)$, and $\tilde{\beta} = L_{nl}\beta_4/(24\tau_0^4)$, $\beta_3$ and $\beta_4$ being the third- and fourth-order dispersion coefficients. We recall that the NLS Eq. (209) conserves three important quantities, the normalized power $N = \int|\psi(t)|^2dt$, the momentum $M = \int\omega|\tilde{\psi}(\omega)|^2d\omega$ and the total 'energy' (Hamiltonian) $H = E + U$, which has a linear (dispersive) kinetic contribution $E(z) = \int k(\omega)|\tilde{\psi}(\omega)|^2d\omega$ and a nonlinear contribution $U(z) = \frac{1}{2}\int|\psi(t)|^4dt$, where

$$k(\omega) = s\omega^2 + \tilde{\alpha}\omega^3 + \tilde{\beta}\omega^4 \tag{210}$$

is the dispersion relation [we recall that $\tilde{\psi}(z,\omega) = \frac{1}{\sqrt{2\pi}}\int\psi(z,t)\ \exp(i\omega t)\,dt$].

#### 6.1.1. Refined wave turbulence analysis

The WT kinetic equation associated to the NLS Eq. (209) has been reported above in Eqs. (193) and (194). As discussed in Section 5.4.2, it describes an irreversible evolution towards the Rayleigh–Jeans thermodynamic spectrum (195). Here we show that this process of thermalization to the Rayleigh–Jeans spectrum is not achieved in a complete way, but turns out to be truncated within a specific frequency interval. We show that this effect can be described by a refined analysis of the kinetic equations (193) and (194) with the dispersion relation (210).

As in the usual configuration of SC generation, we assume that the pump wave frequency lies in the anomalous dispersion regime ($s = -1$). Then we integrate the collision term of the kinetic equations (193) and (194) over one of the frequencies, so that the kinetic equation can be written in the form

$$\partial_z n(z,\omega) = \frac{1}{2\pi}\int \frac{\widetilde{\mathcal{N}}_{\omega_2\omega_3}(\mathbf{n})}{|\omega_2-\omega|\,|\omega_3-\omega|}\,\delta[\varphi_\omega(\omega_2,\omega_3)]\,d\omega_{2,3} \tag{211}$$

where $\widetilde{\mathcal{N}}_{\omega_2\omega_3}(\mathbf{n})$ is the functional $\widetilde{\mathcal{N}}_{\omega_1\omega_2\omega_3}(\mathbf{n})$ in which $n_{\omega_1}(z)$ has been changed with $n_{\omega_2+\omega_3-\omega}(z)$, and

$$\varphi_\omega(\omega_2,\omega_3) = \frac{3}{2}\tilde{\alpha}(\omega_2+\omega_3) + \tilde{\beta}[2(\omega_2^2+\omega_3^2) + 3\omega_2\omega_3 - \omega(\omega_2+\omega_3) + \omega^2] - 1. \tag{212}$$

This function is a quadric in the two dimensional space $(\omega_2, \omega_3)$. It can be recast into its canonical form with the following change of variables: $\left(\Omega_2 = (\omega_2+\omega_3)/\sqrt{2},\ \Omega_3 = (\omega_2-\omega_3)/\sqrt{2}\right)$, and then $\left(\tilde{\Omega}_2 = \Omega_2 + q/(7\tilde{\beta}),\ \tilde{\Omega}_3 = \Omega_3\right)$, with $q = 3\tilde{\alpha}/\sqrt{2} - \sqrt{2}\tilde{\beta}\omega$. The kinetic equation (211) then takes the form

$$\partial_z n(z,\omega) = \frac{1}{\pi}\int \frac{\widetilde{\mathcal{N}}_{\tilde{\Omega}_2\,\tilde{\Omega}_3}(\mathbf{n})\,\delta\left[(\tilde{\Omega}_2/a_2)^2 + (\tilde{\Omega}_3/a_3)^2 - \rho\right]}{|\tilde{\Omega}_2+\tilde{\Omega}_3-r_\omega|\,|\tilde{\Omega}_2-\tilde{\Omega}_3-r_\omega|}\,d\tilde{\Omega}_{2,3} \tag{213}$$

where $a_2 = \sqrt{2/(7\tilde{\beta})}$, $a_3 = \sqrt{2/\tilde{\beta}}$ and $r_\omega = 6\sqrt{2}\omega/7 + 3\sqrt{2}\tilde{\alpha}/(14\tilde{\beta})$. It becomes apparent that the condition

$$\rho = 1 - \frac{3}{28}\left(8\tilde{\beta}\omega^2 + 4\tilde{\alpha}\omega - \frac{3\tilde{\alpha}^2}{\tilde{\beta}}\right) \geq 0 \tag{214}$$

must be satisfied in Eq. (213). This reveals that the resonant four-wave interaction underlying the Kerr effect can only take place within a specific frequency interval defined by the bounds, $\omega \in [\omega_-, \omega_+]$, with

$$\omega_\pm = -\frac{\tilde{\alpha}}{4\tilde{\beta}} \pm \frac{\sqrt{21}}{12\tilde{\beta}}\sqrt{3\tilde{\alpha}^2 + 8\tilde{\beta}}. \tag{215}$$

Finally remark that, by introducing the following parametrization of the ellipse, $\left(\tilde{\Omega}_2 = \tilde{a}_2\cos(\theta),\ \tilde{\Omega}_3 = \tilde{a}_3\sin(\theta)\right)$, with $\tilde{a}_{2,3} = a_{2,3}\sqrt{\rho}$, the kinetic equation (213) can be recast in the following compact form

$$\partial_z n(z,\omega) = \frac{\tilde{a}_2\tilde{a}_3}{2\pi|\rho|}\int_0^{2\pi} \frac{\widetilde{\mathcal{N}}_{\cos(\theta)\ \sin(\theta)}(\mathbf{n})}{\mathcal{F}_\omega(\theta)}\,d\theta, \tag{216}$$

where $\mathcal{F}_\omega(\theta) = |\tilde{a}_2\cos(\theta) + \tilde{a}_3\sin(\theta) - r_\omega| \times |\tilde{a}_2\cos(\theta) - \tilde{a}_3\sin(\theta) - r_\omega|$.

### 6.1.2. Numerical simulations

The confirmation of this process of truncated thermalization by the numerical simulations is not obvious. This is due to the fact that in the usual configurations of SC generation discussed in Section 5.4, the cascade of MI side-bands generated by the cw pump in the early stage of propagation spreads beyond the frequency interval predicted by the theory. As already discussed, the MI process is inherently a coherent nonlinear phase-matching effect which is not described by the WT kinetic equation [Eqs. (193) and (194)]. This explains why the numerical simulations reported in Section 5.4 (see Refs. [184,345]) did not evidence a precise signature of this phenomenon of truncated thermalization.

In order to analyze the theoretical predictions in more detail, we need to decrease the injected pump power so as to maintain the (cascaded) MI side-bands within the frequency interval (215). Intensive numerical simulations of the NLS Eq. (209) in this regime of reduced pump power have been performed in Ref. [143]. This study reveals that the nonlinear dynamics slows down in a dramatic way, so that the expected process of thermalization requires huge nonlinear propagation lengths and huge CPU time computations. This results from the fact that the normalized parameters $\tilde{\alpha}$ and $\tilde{\beta}$ decrease as the pump power decreases, so that Eq. (209) approaches the integrable limit of the NLS equation, which does not exhibit thermalization [142] (see Section 6.3). We report in Fig. 45 the wave spectra at different propagation lengths obtained by solving the NLS Eq. (209) with $\tilde{\alpha} = 0.1$ and $\tilde{\beta} = 0.02$. In the early stage of propagation, $z \sim 200$, the spectrum remains confined within the frequency interval $[\omega_-, \omega_+]$ predicted by the theory [Eq. (215)], although the spectrum exhibits a completely different spectral profile than the expected Rayleigh–Jeans distribution. As a matter of fact, the process of thermalization requires enormous propagation lengths, as illustrated in Fig. 45(d), which shows that the wave spectrum eventually relaxes towards a truncated Rayleigh–Jeans distribution. Here, the Lagrangian multipliers $(\mu, \lambda, T)$ have been calculated from the conserved quantities $(N, M, E)$ (once the system has reached a weakly nonlinear regime), without using adjustable parameters.

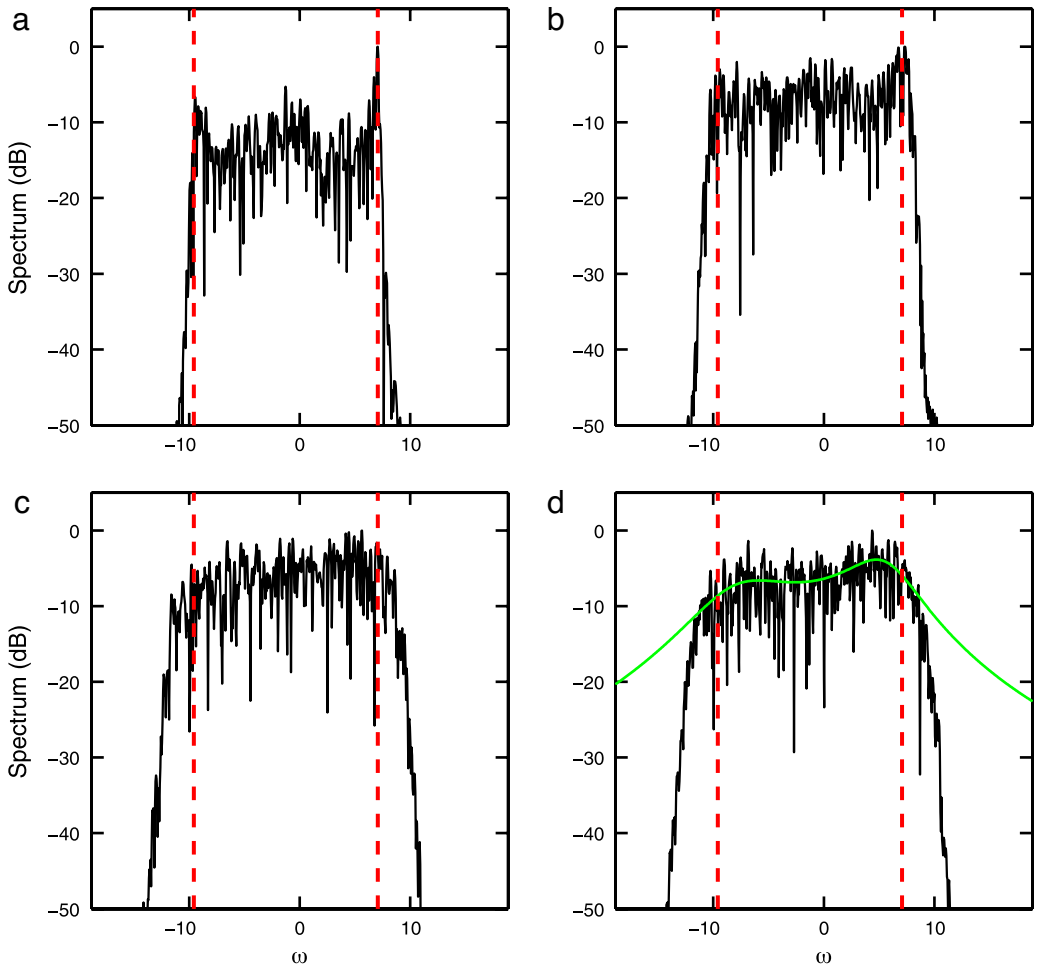


**Fig. 45.** Truncated thermalization of incoherent waves: Spectra $|\tilde{\psi}|^2(\omega, z)$ obtained by solving the NLS Eq. (209) for $s = -1$, $\tilde{\alpha} = 0.1$, $\tilde{\beta} = 0.02$: (a) $z = 200$, (b) $z = 10^4$, (c) $z = 5 \times 10^5$, (d) $z = 10^6$. After a long transient, the wave relaxes towards a truncated Rayleigh–Jeans distribution [Eq. (195), green line] (d). The dashed red lines denote the frequencies $\omega_\pm$ in Eq. (215).
*Source:* From Ref. [143].

*Role of the nonlinearity*

Note however in Fig. 45(d) that, despite the good agreement, the whole spectrum spans a frequency band which exceeds the frequency interval $[\omega_-, \omega_+]$ predicted by the kinetic theory in Eq. (215). Indeed, in the first stage of evolution (see Fig. 45(a)–(c) for $200 < z < 5 \times 10^5$), the SC spectrum exhibits a slow process of spectral broadening, so that the corresponding SC edges spread beyond the frequency bound $[\omega_-, \omega_+]$. Such a discrepancy decreases in a significant way as the system becomes weakly nonlinear, as discussed below through Fig. 47. Accordingly, this discrepancy can be ascribed to a deviation from Gaussian statistics of the incoherent wave. Indeed, we report in Fig. 46 the PDF of the wave intensity calculated at different propagation lengths. A deviation from Gaussian statistics is visible for $z < 10^4$, which can merely explain the slow process of spectral broadening beyond the frequency interval (215) predicted by the theory. This conclusion is corroborated by the analysis of the kurtosis of the intensity distribution, $K(z) = \langle I^2 \rangle(z)/(2\langle I \rangle^2) - 1$ (data not shown). The value of $K(z)$ and the variance of its fluctuations are shown to slowly decay during the propagation to zero. Then as the system evolves, it eventually reaches a kinetic regime of Gaussian statistics, which is subsequently preserved in the further evolution. It is interesting to underline that, once the state of Gaussian statistics is reached, the incoherent wave does not exhibit any significant spectral broadening (for $z > 5 \times 10^5$), while its spectral profile slowly relaxes towards the truncated Rayleigh–Jeans distribution, as described by the kinetic theory.

This conclusion as regard the role of the nonlinearity in the process of truncated thermalization is corroborated by the analysis of the impact of the parameter $\tilde{\beta}$. As $\tilde{\beta}$ increases, the typical bandwidth of MI decreases, so that the system evolves towards the nonlinear regime of interaction. Note however that in the process of spectral broadening, the increase of the second order contribution in the kinetic energy $\left(E_2 = s \int \omega^2 |\tilde{\psi}|^2(\omega)\, d\omega\right)$ is compensated by the reduction of the fourth-order contribution $\left(E_4 = \tilde{\beta} \int \omega^4 |\tilde{\psi}|^2(\omega)\, d\omega\right)$, while the third-order contribution plays a negligible role here. Then

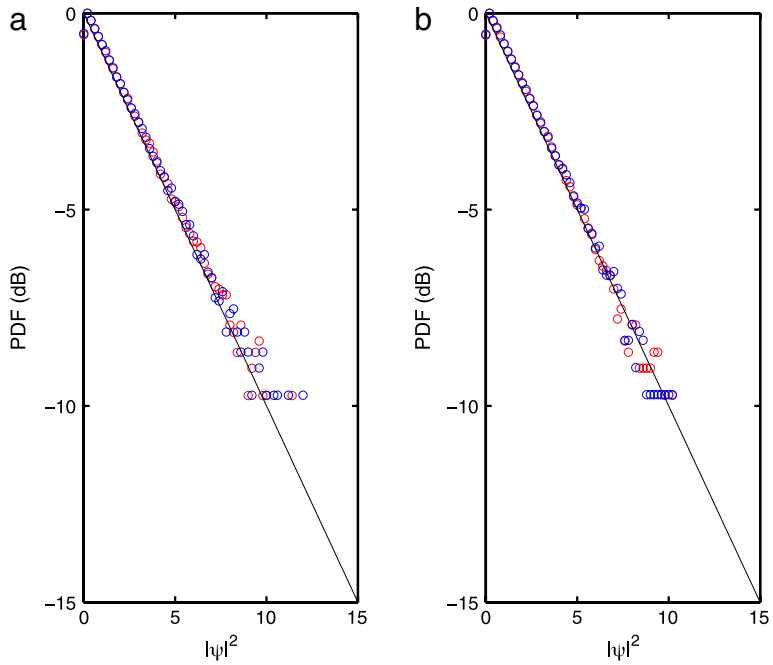


**Fig. 46.** Probability density function of the wave intensity, $I = |\psi|^2$, corresponding to the simulation of Fig. 45 at $z = 200$ (blue), $z = 10^4$ (red) (a); $z = 5 \times 10^5$ (blue), $z = 10^6$ (red) (b): The random wave eventually enters the kinetic regime of Gaussian statistics. (For interpretation of the references to color in this figure legend, the reader is referred to the web version of this article.)
*Source:* From Ref. [143].

to quantify the role of the nonlinearity, one needs to compare $E_2(\sim -E_4)$ with $U$. Fig. 47 reports the evolution of the spectra obtained by solving the NLS Eq. (209) in the same conditions as in Fig. 45, but for different values of $\tilde{\beta}$. In Fig. 47(a)–(d) we set $\tilde{\beta} = 0.05$ and $\tilde{\beta} = 0.1$, which respectively correspond to $|U/E_2| \sim 0.09$ and $|U/E_2| \sim 0.2$, while in Fig. 45 $|U/E_2| \sim 0.03$ for $\tilde{\beta} = 0.02$. The comparison of the three different cases confirms that, as the system approaches a weakly nonlinear regime, the generated spectrum tends to remain confined within the frequency interval [Eq. (215)] predicted by the WT theory.

*The case* $\tilde{\alpha} = 0$

We finally note that the same numerical study has been performed for $\tilde{\alpha} = 0$, for which the frequency bounds (215) reduce to

$$\omega_{\pm} = \pm\sqrt{7/(6\tilde{\beta})}.$$

A study analogous to that discussed above for $\tilde{\alpha} \neq 0$ confirms the process of relaxation towards a spectrally truncated Rayleigh–Jeans distribution for the incoherent wave.

### 6.2. Influence of third-order dispersion: Anomalous thermalization

In this section we present another mechanism that inhibits the natural process of thermalization. We consider the 1D NLS equation by truncating the dispersion relation up to the third order. We will see that the incoherent wave exhibits an irreversible evolution towards an equilibrium state of a different nature than the conventional Rayleigh–Jeans equilibrium state. The WT kinetic equation reveals that this effect of anomalous thermalization is due to the existence of a local invariant in frequency space $J_\omega$, which originates in degenerate resonances of the system [140,141]. In contrast to conventional integral invariants that lead to a generalized Rayleigh–Jeans distribution, here, it is the local nature of the invariant $J_\omega$ that makes the new equilibrium states different than the usual Rayleigh–Jeans equilibrium states. We remark that local invariants and the associated process of anomalous thermalization have been also identified in the 1D vector NLS equation, a feature that will be discussed in Section 6.2.3 in relation with experimental results (for details, see Ref. [140]).

#### 6.2.1. Local invariants and local equilibrium states

The dimensionless 1D NLS Eq. (209) accounting for third-order dispersion reads

$$i\partial_z\psi = -s\partial_t^2\psi - i\tilde{\alpha}\partial_t^3\psi + |\psi|^2\psi, \tag{217}$$

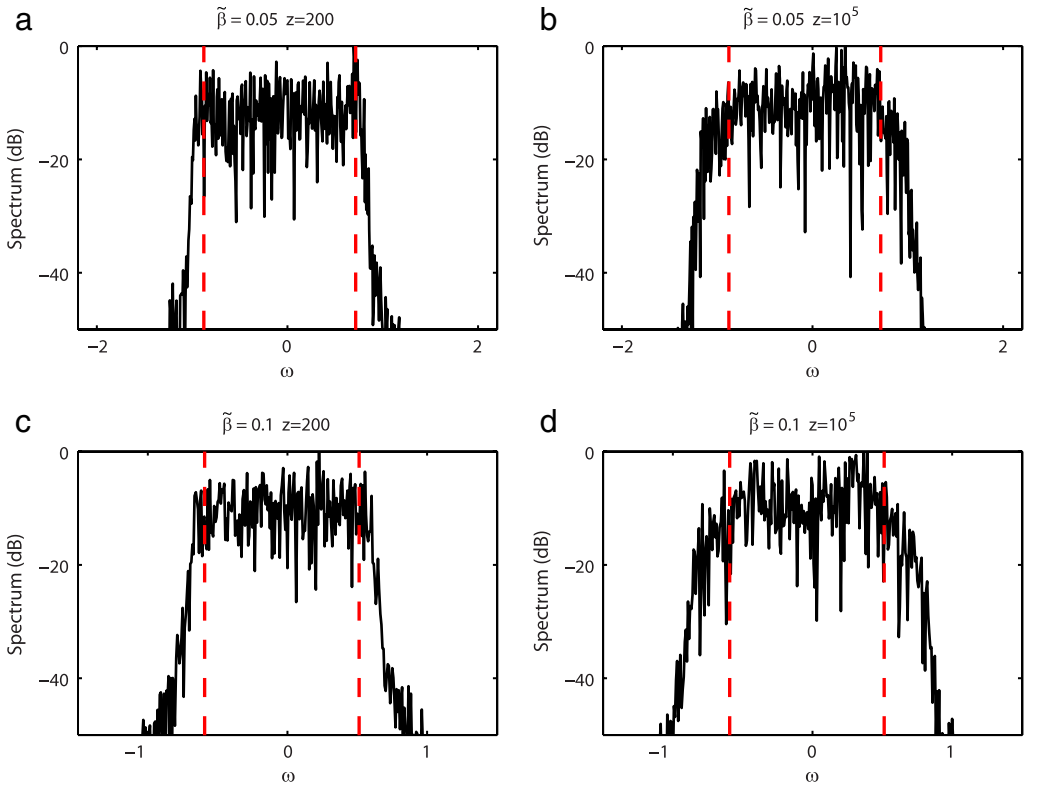


**Fig. 47.** Influence of the nonlinearity on the process of truncated thermalization: Spectra $|\tilde{\psi}|^2(\omega, z)$ obtained by solving the NLS Eq. (209) for $s = -1$, $\tilde{\alpha} = 0.1$, $\tilde{\beta} = 0.5$, so that $|U/E_2| \sim 0.09$: (a) $z = 200$, (b) $z = 10^5$. (c–d) same as (a–b), except that $\tilde{\beta} = 0.1$, so that $|U/E_2| \sim 0.2$. The dashed red lines denote the frequencies $\omega_\pm$ in Eq. (215). As the system approaches the weakly nonlinear regime, the generated spectrum tends to remain confined within the frequency interval predicted by the WT theory, Eq. (215).

with the dispersion relation

$$k(\omega) = s\omega^2 + \tilde{\alpha}\omega^3. \tag{218}$$

$k(\omega)$ exhibits an inflection point at the frequency $\omega_* = -s/(3\tilde{\alpha})$. This frequency plays an important role in the theory and refers to the zero-dispersion frequency. We note in particular that the frequency components of the wave exhibit different dispersion properties: Assuming $\tilde{\alpha} > 0$, the wave evolves in the normal dispersion regime $[\partial^2 k(\omega)/\partial\omega^2 > 0]$ for those frequencies verifying $\omega > \omega_*$, whereas for $\omega < \omega_*$ the wave evolves in the anomalous dispersion regime $[\partial^2 k(\omega)/\partial\omega^2 < 0]$. Without loss of generality, we shall assume in the following that $\tilde{\alpha} > 0$. We note that the NLS model (217) has been considered to study optical rogue waves phenomena [362,379], as discussed in Section 7.5.3.

*Wave turbulence analysis*

The WT kinetic equation associated to Eq. (217) is given by Eqs. (193) and (194), with the dispersion relation (218). Two integrals in the kinetic equation may be computed exactly owing to the Dirac $\delta$-functions, which gives

$$\partial_z n(\omega, z) = \frac{1}{3\pi|\tilde{\alpha}|}\int \frac{n_\omega n_{q-\omega} n_{\omega_1} n_{q-\omega_1}}{|\omega-\omega_1|\,|\omega+\omega_1-q|}\left(\frac{1}{n_\omega}+\frac{1}{n_{q-\omega}}-\frac{1}{n_{\omega_1}}-\frac{1}{n_{q-\omega_1}}\right) d\omega_1 \tag{219}$$

where $q = -2s/3\tilde{\alpha} = 2\omega_*$. The integrand of this equation exhibits a remarkable property: It is invariant under the substitution $\omega \to \bar{\omega} = q - \omega$. This peculiar property implies $\partial_z n(\omega, z) = \partial_z n(\bar{\omega}, z)$, which thus reveals the existence of the following 'local' invariant

$$J(\omega) = n(\omega, z) - n(q-\omega, z). \tag{220}$$

This invariant is 'local' in the sense that it is verified for each frequency $\omega$ individually, $\partial_z J(\omega) = 0$. It means that the subtraction of the spectrum by the reverse of itself translated by $q = 2\omega_*$, remains invariant during the whole evolution of the wave. The invariant (220) finds its origin in the following degenerate resonance of the phase-matching conditions: A pair of frequencies $(\omega, q-\omega)$ may resonate with any pair of frequencies $(\omega', q-\omega')$, because $k(\omega) + k(q-\omega) = sq^2/3$

does not depend on $\omega$. The invariant $J_\omega$ may thus be used to derive the following kinetic equation governing the evolution of the averaged spectrum $n(\omega, z)$

$$\partial_z n(\omega,z) = \frac{1}{3\pi|\tilde{\alpha}|}\int \frac{n_\omega(n_\omega - J_\omega)n_{\omega_1}(n_{\omega_1}-J_{\omega_1})}{|\omega-\omega_1|\,|\omega+\omega_1-q|}\left(\frac{1}{n_\omega}+\frac{1}{n_\omega - J_\omega}-\frac{1}{n_{\omega_1}}-\frac{1}{n_{\omega_1}-J_{\omega_1}}\right)d\omega_1. \tag{221}$$

The kinetic equation (221) is characterized by a $H$-theorem of entropy growth, $\partial_z S \geq 0$, where the nonequilibrium entropy reads $S(z)/T_0 = \int \log[n_\omega(z)]\,d\omega$. One may also verify that the kinetic equation (221) conserves the power $N$, the energy $E$ and the momentum $P$. As outlined above in Section 5, the equilibrium spectrum is obtained by looking at the extremum of $S[n_\omega]$ given the constraints of conservation of $E$, $P$ and $N$. Introducing the corresponding Lagrange multipliers $\lambda_j$ ($j = E, P, N$) and making use of the variable change $\omega \to q-\omega$, the extremum condition reads $1/n_\omega^{loc} + 1/(n_\omega^{loc} - J_\omega) = \lambda$, where $\lambda = \lambda_E q^2/3 + \lambda_P q + 2\lambda_N$. The important point to underline is that, because of the existence of the local invariant $J_\omega$, the condition of extremum entropy does not involve the frequency, i.e. $\lambda$ does not depend on $\omega$. This simply means that the conservations of the energy $E$ and of the momentum $P$ are implicitly verified as a consequence of the invariant $J_\omega$. The corresponding local equilibrium spectrum thus reads

$$n^{loc}(\omega) = \frac{J_\omega}{2} + \frac{1}{\lambda}\left(1+\sqrt{1+\left(\frac{\lambda J_\omega}{2}\right)^2}\right), \tag{222}$$

where we chose the positive sign indetermination in front of the square-root because of the condition of positivity of the spectrum, $n_\omega^{loc}(z) \geq 0$. The parameter $\lambda$ is determined from the initial condition through the conservation of the power, $N/T_0 = \int n^{loc}(\omega)\,d\omega = \int n(\omega, z=0)\,d\omega$. Note that the equilibrium spectrum $n^{loc}(\omega)$ verifies the conservations of the energy $E$ and of the momentum $M$. We remark that the equilibrium distribution (222) vanishes exactly the collision term of the kinetic equation, i.e., it is a stationary solution of Eq. (221).

The equilibrium distribution is characterized by a remarkable property: it exhibits a constant spectral pedestal, $n^{loc}(\omega) \to 2/\lambda$ for $|\omega| \gg |\omega_*|$. This property is confirmed by the numerical simulations of both the NLS Eq. (217) and the kinetic equation (221), a feature that will be discussed below. We remark in this respect that in the tails of the spectrum ($|\omega| \gg |\omega_*|$), the invariant $J_\omega$ vanishes, so that a constant spectrum ($n_\omega = const$) turns out to be a stationary solution of the kinetic equation (221).

*Local vs. integral invariants*

The equilibrium distribution (222) is of a fundamental different nature than the conventional Rayleigh–Jeans distribution. In particular, as discussed just above, $n^{loc}(\omega)$ is characterized by a constant spectral pedestal in the tails of the spectrum. The kinetic theory reveals that the difference between $n^{loc}(\omega)$ and $n^{eq}(\omega)$ is due to the existence of the local invariant $J_\omega$. Let us briefly discuss the 'local' nature of the invariant $J_\omega$ in regard to the *integral* invariants investigated in Refs. [380–383] in line with the problem of integrability. First of all, one may note that the possible existence of a set of additional *integral* invariants, $Q_j = \int \varphi_j(\omega)\, n_\omega(z)\, d\omega$, would still lead to a (generalized) Rayleigh–Jeans distribution,

$$n^{eq}(\omega) = \frac{T}{k(\omega) + \sum_j \lambda_j \varphi_j(\omega) - \mu}, \tag{223}$$

where $\lambda_j$ refer to the Lagrangian multipliers associated to the conservation of $Q_j$ [383]. The *local* invariant $J_\omega$ thus leads to an equilibrium spectrum $n^{loc}(\omega)$ of a different nature than the generalized Rayleigh–Jeans spectrum (223).

One may wonder whether the local invariant $J_\omega$ may generate the existence of integral invariants of the kinetic equation (221). We can easily verify that $Q = \int \varphi_\omega\, n_\omega(z)\, d\omega$ is a conserved quantity of (221) whenever $\varphi_\omega$ satisfies the following relation

$$\varphi_{\omega_1} + \varphi_{q-\omega_1} = \varphi_{\omega_2} + \varphi_{q-\omega_2}, \tag{224}$$

for any couple of frequencies $(\omega_1, \omega_2)$. In other terms, it is sufficient that $\varphi_\omega + \varphi_{q-\omega}$ does not depend on $\omega$ for $Q$ to be a conserved quantity of (221). A simple way to satisfy this condition is to construct $\varphi_\omega$ as follows, $\varphi_\omega = \varphi_\omega - \varphi_{q-\omega}$. In this way, regardless of the particular choice of the function $\varphi_\omega$,

$$Q = \int \left(\varphi_\omega - \varphi_{q-\omega}\right)\, n_\omega(z)\, d\omega, \tag{225}$$

is a conserved quantity of the kinetic equation (221). These considerations show that the existence of a local invariant ($J_\omega$) may generate an infinite set of integral invariants $Q$.

*6.2.2. Numerical simulations*

We analyze the anomalous thermalization process by performing numerical simulations of both the NLS Eq. (217) and of the corresponding wave turbulence kinetic equation (221). The evolution of the spectrum of the field is essentially characterized by two stages. In the following we analyze the two stages separately.

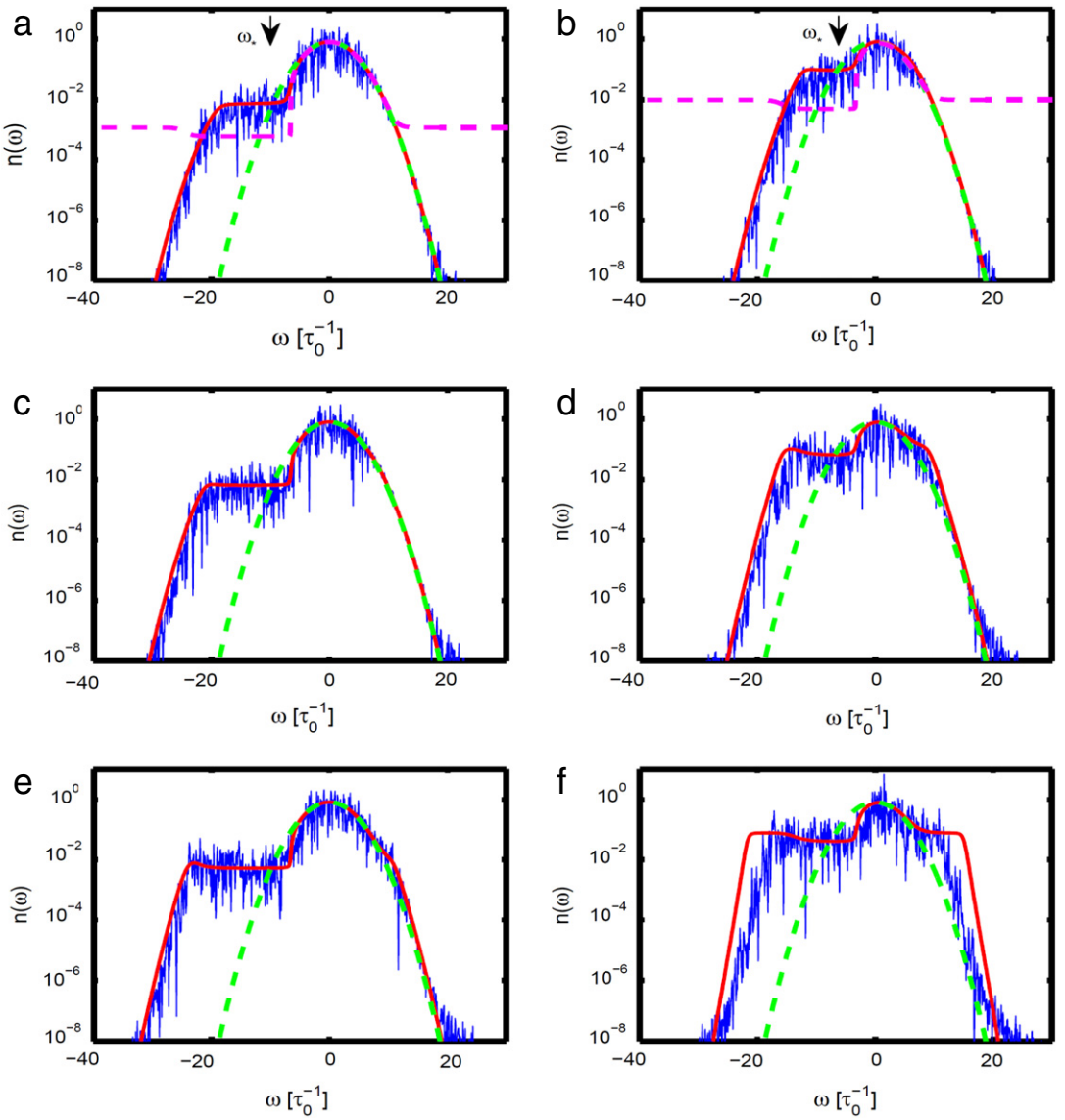


**Fig. 48.** Anomalous thermalization of incoherent waves: First stage of the spectral evolution obtained by integrating numerically the NLSE Eq. (217) (blue) and the kinetic equation (221) (red). First column: $\tilde{\alpha} = 0.05$, second column $\tilde{\alpha} = 0.1$, for $z = 30$ (first row), $z = 200$ (second row), $z = 2000$ (third row). The green dashed line represents the initial condition ($z = 0$). We set here $s = 1$. (For interpretation of the references to color in this figure legend, the reader is referred to the web version of this article.)
*Source:* From Ref. [384].

*First stage: Formation of the spectral shoulder*

Typical evolutions of the spectrum of the field are reported in Fig. 48 for two different values of the parameter $\tilde{\alpha}$. We remark in Fig. 48 that for small propagation lengths (typically $z < 200$) the high-frequency tail of the spectrum does not exhibit any significant spectral broadening, whereas in the low-frequency part a broad spectral shoulder emerges [379], which is then preserved for long propagation lengths (Fig. 48 left column). Note that this asymmetric spectral evolution preserves the momentum (barycenter) $P$ of the spectrum. For small values of the parameter $\tilde{\alpha}$ (left column of Fig. 48), a quantitative agreement is obtained between the numerical simulations of the NLS Eq. (217) and the WT kinetic equation (221). We underline that such a quantitative agreement is obtained without any adjustable parameter. This good agreement is corroborated by the fact that the NLS Eq. (217) conserves, in average, the invariant $J_\omega$, as illustrated in Fig. 49(a), in which an average over 50 NLS spectra (from $z = 2500$ to $z = 2550$) has been realized. Besides such a quantitative agreement, we note in the second column of Fig. 48 that an appreciable discrepancy between the NLS evolution and the kinetic evolution arises as the parameter $\tilde{\alpha}$ increases. The origin of such discrepancy has been studied in Ref. [384] through the analysis of an improved criterion of applicability of the WT theory [51,385,73]. In substance, as the parameter $\tilde{\alpha}$ increases, a significant amount of power of the wave evolves in the neighborhood of the zero dispersion frequency, $\omega \sim \omega_*$. In this region, nonlinear effects

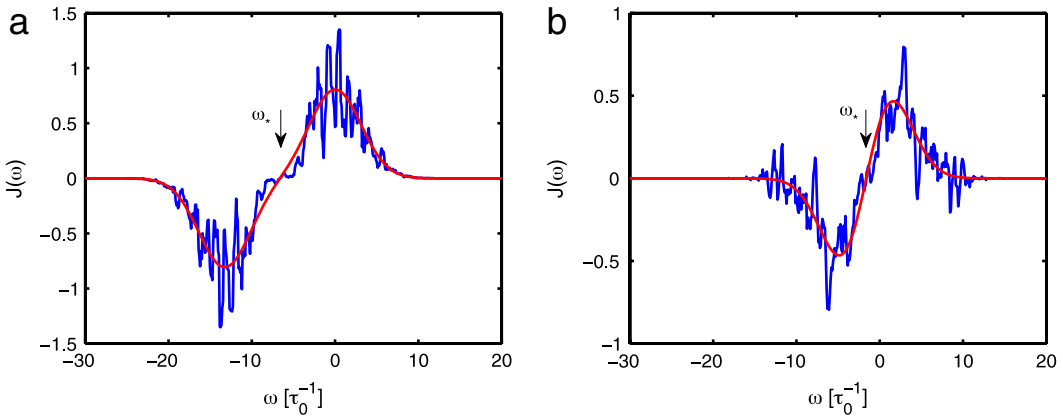


**Fig. 49.** Local invariants underlying the process of anomalous thermalization: Invariants $J(\omega)$ corresponding to the two values, (a) $\tilde{\alpha} = 0.05$, (b) $\tilde{\alpha} = 0.2$. The dashed red line shows $J_\omega$ as determined from the initial condition, while the blue line corresponds to the numerical integration of the NLSE Eq. (217) at $z = 2500$ ($s = 1$). (For interpretation of the references to color in this figure legend, the reader is referred to the web version of this article.)
*Source:* From Ref. [384].

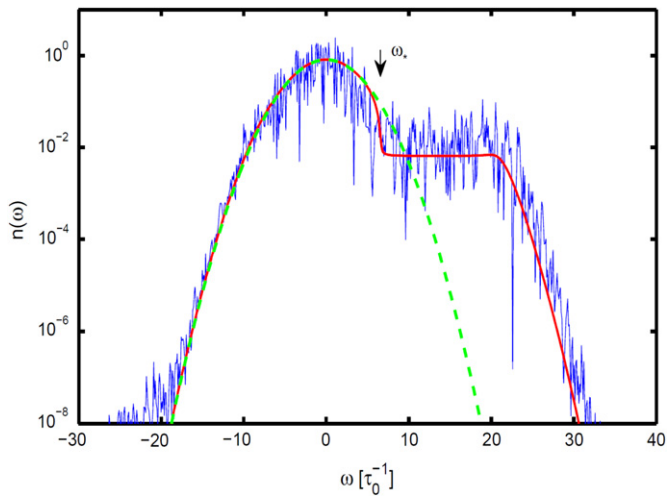


**Fig. 50.** Anomalous thermalization of incoherent waves: Spectrum of the wave obtained by solving numerically the NLS Eq. (217) (blue) and the kinetic equation (221) (red), for the same conditions as in Fig. 48 (left column) but in the anomalous dispersion regime, $s = -1$ ($z = 200$, $\tilde{\alpha} = 0.05$). The green dashed line represents the initial condition ($z = 0$). (For interpretation of the references to color in this figure legend, the reader is referred to the web version of this article.)
*Source:* From Ref. [384].

dominate dispersive effects, which invalidates the kinetic approach. Note that, despite such discrepancy, the invariant $J_\omega$ is still preserved by the NLS evolution, as illustrated in Fig. 49.

Let us note that a spectral evolution similar to that discussed in Fig. 48 is obtained by setting the carrier frequency of the wave in the anomalous dispersion regime. This is illustrated in Fig. 50, which reports the spectrum of the field obtained by integrating numerically the NLS Eq. (217) in the same conditions as in Fig. 48 (left column, $\tilde{\alpha} = 0.05$), except that $s = -1$. As expected, in this case the deformation of the spectrum is reversed, so that the spectral shoulder emerges in the normal dispersion regime (i.e. for $\omega > \omega_*$). The fact that the system is not sensitive to the sign of the dispersion coefficient ($s$) is consistent with the kinetic equation (221), which globally does not depend on the sign of the dispersion coefficient $s$. We note in Fig. 50 that a good agreement is obtained between the NLS wave evolution and the kinetic evolution. We also verified that, as discussed in the framework of SC generation in Section 5.4, the weakly nonlinear regime considered here prevents the formation of robust coherent structures, such as 'quasi-soliton' solutions of the NLS Eq. (217) [47].

Let us now show that the invariant $J_\omega$ provides a simple qualitative interpretation of the asymmetric deformation of the spectrum discussed in Fig. 48. For this purpose, one should consider that, in general, the natural tendency of a nonlinear wave is to generate new frequency components in the tails of its spectrum, which thus leads to a lowering of the central part of the spectrum. In the particular case considered here, the lowering of the spectrum is constrained by the existence of the invariant $J_\omega$, because $n_\omega = J_\omega + n_{q-\omega} \geq J_\omega$. It turns out that the spectrum tends to approach the spectral profile of $J_\omega$ for those frequencies verifying $J_\omega \geq 0$ i.e., $n_\omega \simeq J_\omega$ for $\omega \geq q/2$. Making use of the substitution $\omega \to q - \omega$, the above expression reads

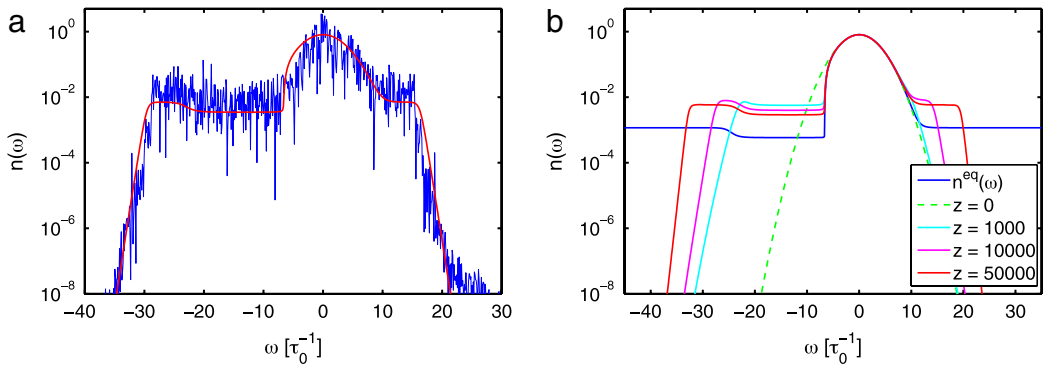


**Fig. 51.** Anomalous thermalization of incoherent waves: (a) Second stage of the spectral evolution obtained by integrating numerically the NLSE Eq. (217) (blue) and the kinetic Eq. (221) (red) at $z = 20\,000$ for $\tilde{\alpha} = 0.05$ ($s = +1$) (a). (b) Numerical simulations of the kinetic equation (221) showing the spectral profile $n(z, \omega)$ at different propagation lengths $z$: A constant spectral pedestal emerges in the tails of the spectrum ($\tilde{\alpha} = 0.05$). The spectrum slowly relaxes towards the equilibrium state $n^{loc}(\omega)$ given by Eq. (222) (blue). (For interpretation of the references to color in this figure legend, the reader is referred to the web version of this article.)
*Source:* From Ref. [384].

$n_{q-\omega} \simeq -J_\omega$, because $J_{q-\omega} = -J_\omega$. For the frequencies $\omega \leq q/2$, we thus obtain $n_\omega = J_\omega + n_{q-\omega} \simeq 0$, i.e. the field essentially exhibits a small amplitude constant spectrum. In summary, in the normal dispersion regime ($\omega \geq \omega_*$), the spectrum evolves towards $J_\omega$, while in the anomalous dispersion regime ($\omega \leq \omega_*$) the spectral amplitude is small and almost constant. This provides a simple interpretation of the emergence of the spectral shoulder discussed in Fig. 48, which characterizes the *first stage* of the spectral evolution.

*Second stage of the numerical evolution: Formation of a constant spectral pedestal*

The second stage of the spectral evolution of the wave is characterized by the emergence of a constant spectral pedestal in the far tails of the spectrum. This is illustrated in Fig. 51, which reports the numerical simulations of the NLS Eq. (217) and of the kinetic Eq. (221) for long propagations. Let us note the remarkable agreement between the NLS wave equation and the kinetic equation for a very long propagation ($z = 20\,000$), and down to $\sim 10^{-8}$ in the tails of the spectrum. We see that a constant spectral pedestal progressively emerges as a result of two fronts that propagate in opposite directions in frequency space, and symmetrically with respect to the zero dispersion frequency, $\omega_* = q/2$. Such a symmetric propagation of the two fronts may be interpreted as a consequence of the degenerate resonance discussed above through the invariant $J_\omega$ [see Eq. (220)], simply because the pairs of frequencies $(\omega_j, q - \omega_j)$ involved in the conversion $(\omega_1, q - \omega_1) \rightarrow (\omega_2, q - \omega_2)$ are always symmetric with respect to $\omega_*$. It turns out that the two fronts propagate *with the same velocity in frequency space*, although they are asymmetric with respect to the carrier frequency of the wave, i.e. $\omega = 0$.

*Constant spectral pedestal of the local equilibrium state*

As discussed above in the framework of the local equilibrium distribution (222), a peculiar property of $n^{loc}(\omega)$ is precisely the fact that it exhibits a constant spectral pedestal, $n^{loc}(\omega) \rightarrow 2/\lambda$ for $|\omega| \gg |\omega_*|$. The numerical simulations of both the NLS Eq. (217) and the kinetic equation (221) thus confirm that the wave slowly relaxes towards the local equilibrium spectrum given by Eq. (222). Note that a complete relaxation of the simulations towards the exact analytical expression (222) cannot be demonstrated in practice, simply because the numerical schemes used to solve the NLS equation and the kinetic equation break down as the two symmetric fronts approach the frequency cut-off $\omega_c$ associated to the numerical discretization of the equations. In this way, the analytical expression of the equilibrium distribution should be regarded as the *asymptotic* evolution to which the wave spectrum tends to evolve.

The local equilibrium spectrum (222) also provides physical insight into the long term evolution of the field. Indeed, we may notice in Fig. 52 that $n^{loc}(\omega)$ exhibits a lateral dip for $\omega < \omega_*$, i.e. into the anomalous dispersion regime. Such a spectral dip is in fact reminiscent of the spectral shoulder generated in the first stage of the evolution discussed in Fig. 48. The central frequency of the spectral dip precisely corresponds to the frequency in which the invariant $J(\omega)$ reaches its minimum value, a feature that is illustrated by various different examples in Fig. 52. Note also that, for very small values of $\tilde{\alpha}$, we observed a discrepancy between the kinetic [Eq. (221)] and the NLS [Eq. (217)] evolutions. We observed in this case a negligible contribution of $E_3$ with respect to $E_2$. This means that third-order dispersion becomes negligible and the NLS Eq. (217) tends to recover the integrable scalar NLS equation, whose dynamics will be discussed in Section 6.3.

*6.2.3. Anomalous thermalization in the vector NLS equation*

To conclude this discussion, we remark that local invariants as well as the associated process of anomalous thermalization can be found in different types of nonintegrable model equations. In particular, they have been identified in the vector NLS equation in the particular case where the dispersion coefficients coincide [140]. Indeed, when the dispersion coefficients

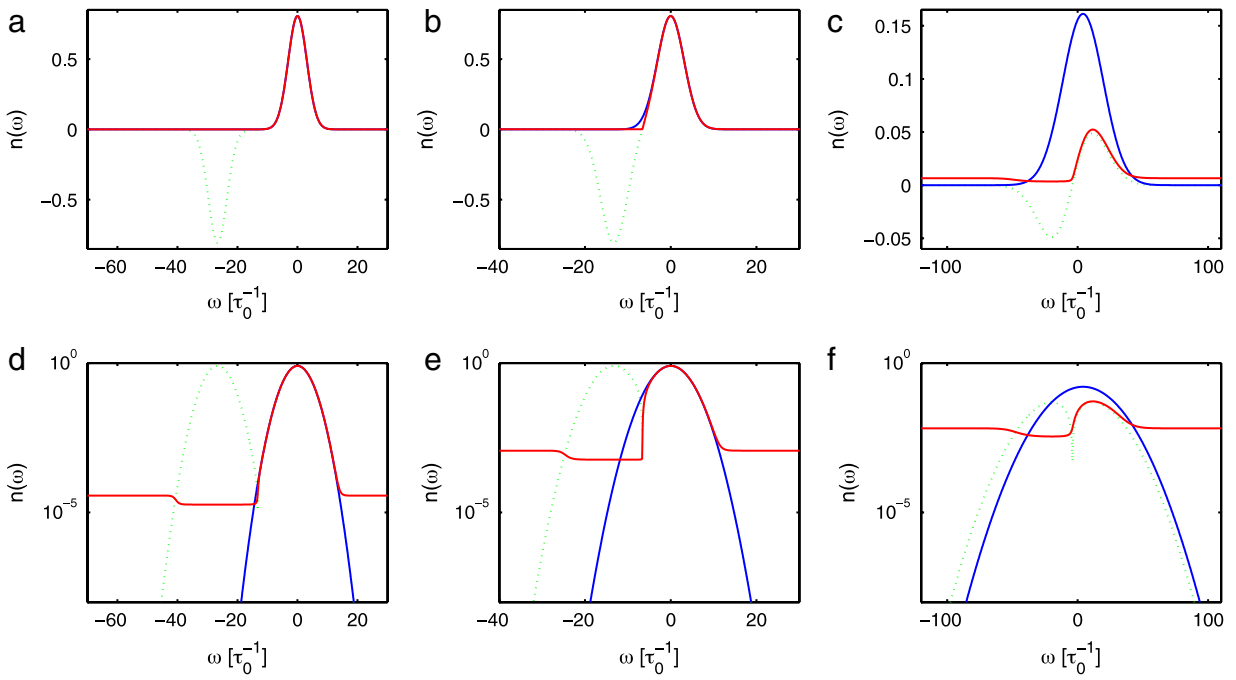


**Fig. 52.** Local equilibrium spectrum $n^{loc}(\omega)$ [Eq. (222)] (red), initial condition (blue) and corresponding invariant $J_\omega$ (dashed green), for $\tilde{\alpha} = 0.02$ (a), $\tilde{\alpha} = 0.05$ (b), and $\tilde{\alpha} = 0.08$ (c). The second row (d–f) shows the same plots in logarithmic scale [because of the sign change of the invariant, we plotted $|J_\omega|$ in (d–f)]. (For interpretation of the references to color in this figure legend, the reader is referred to the web version of this article.)
*Source:* From Ref. [384].

of the vector NLS equation coincide, the WT kinetic equations reveal the existence of a local invariant which is simply the sum of the two spectra of the two waves involved in the vector NLS equation, $J(\omega) = n_1(\omega, z) + n_2(\omega, z)$. In complete analogy with the scalar NLS equation with third-order dispersion, the existence of this local invariant finds its origin in degenerate resonances: In the particular case where the dispersion coefficients of the vector NLS equation coincide, the resonant conditions of energy and momentum turn out to be trivially satisfied. The existence of the local invariant predicts an irreversible evolution of the coupled random waves towards local equilibrium states, whose structure is analogous to the local equilibrium state discussed above for the scalar NLS equation. The numerical simulations of the vector NLS equation with random waves confirm the existence of the irreversible relaxation process towards the local equilibrium states. A quantitative agreement between the NLS simulations and the analytical expression of the local equilibrium states has been obtained, without using adjustable parameters [140].

*Experimental results*

We briefly comment here some experimental results in optical fibers aimed at providing some signatures of this process of anomalous thermalization (for more details see [140]). Two different incoherent waves with left- and right-handed circular polarization are launched in an isotropic fiber of length $L = 1.6$ m. In this experiment, light propagation is described by a set of two coupled NLS Eq. (186) with identical group velocities, $u_1 = u_2$, and group-velocity dispersion coefficients, $\beta_1 = \beta_2$. The experiment is aimed at observing the mutual interaction of two incoherent waves whose initial spectra have very different width (see Fig. 53(a)).

In the particular limit in which the two waves have the same power, $N_1 = N_2$, the process of anomalous thermalization predicts an irreversible evolution towards a local equilibrium state characterized by two identical spectra for the two waves, $n_1^{eq}(\omega) = n_2^{eq}(\omega) = \big(n_1(\omega, z = 0) + n_2(\omega, z = 0)\big)/2$ [140]. The black line of Fig. 53(b) represents the output spectrum $n_1(\omega, z = L)$ when $n_2(\omega) = 0$. When the wave with a broad spectrum ($n_2(\omega)$ blue curve in Fig. 53(a)) is launched inside the fiber, the output spectrum $n_1(\omega)$ broadens (red curve Fig. 53(b)). This constitutes a signature of the existence of a mutual interaction between the two incoherent waves. However, the experiment involves several difficulties.

As discussed above in Section 5.5, stimulated Raman scattering is unavoidable in optical fibers and prevents the system from reaching the local equilibrium state predicted by the WT theory. It should be noted that numerical simulations of the vector NLS equation neglecting the Raman effect confirm the process of anomalous thermalization towards the local equilibrium state, $n_1^{eq}(\omega) = n_2^{eq}(\omega)$ [140]. However, considering the range of experimentally available parameters, the system does not relax towards the expected local equilibrium spectra of the WT theory, i.e., $n_1^{eq}(\omega) = n_2^{eq}(\omega) \neq \big(n_1(\omega, z = 0) + n_2(\omega, z = 0)\big)/2$. Indeed, in order to keep the isotropy of the fiber, one needs to use a short fiber length and thus a high pump power, so that the experiments were performed far from the weakly nonlinear regime of propagation. We note in this

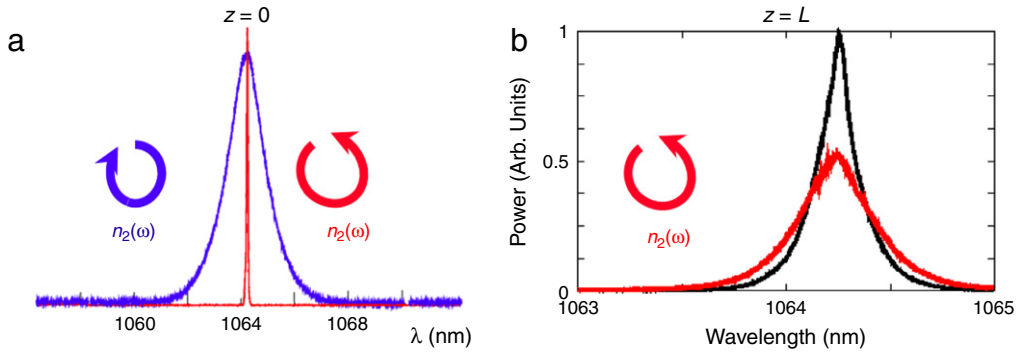


**Fig. 53.** Anomalous thermalization: Experiments. (a) Initial spectra $n_1(\lambda)$ in red and $n_2(\lambda)$ in blue of wave $\psi_1$ and $\psi_2$ at $z = 0$. (b) Spectrum $n_1(\lambda)$ at the output of the fiber. $n_1(z = L)$ when $\psi_1$ propagates alone in the fiber is represented in black. $n_1(z = L)$ when $\psi_1$ and $\psi_2$ interact along the propagation is represented in red. (note that $\omega = 2\pi\lambda/c$ with $c$ the speed of light in vacuum). (For interpretation of the references to color in this figure legend, the reader is referred to the web version of this article.)
*Source:* From Ref. [140].

respect that propagation of a single wave in the fiber is well described by the (integrable) 1D NLS equation and the optical spectrum undergoes a significant broadening in the nonlinear regime of propagation [386]. Comparing the initial spectrum (red in Fig. 53(a)) and the output spectrum (black in Fig. 53(b)), such spectral broadening induced by self-phase modulation is clearly visible. Note that a generalized WT approach for the 1D scalar NLS equation will be discussed in Section 6.3 to describe the evolution of the incoherent wave in the weakly nonlinear regime. It turns out that the experimental observation of the process of anomalous thermalization still constitutes an open challenging problem. We refer the reader to Ref. [140] for details concerning this process of anomalous thermalization for the vector NLS equation and a detailed presentation of the corresponding experimental setup.

### 6.3. *Influence of second-order dispersion: Integrable limit*

In this section we consider the case where the dispersion relation of the NLS equation is truncated to the second-order, so that the equation recovers the completely integrable NLS equation. This integrable equation is known to have a class of special solutions called bright and dark solitons, which are sustained in the anomalous (focusing) and normal (defocusing) dispersion regimes respectively. During the past fifty years, the question of the interaction among solitons has been extensively studied by using the method of the inverse scattering transform (see, e.g., [387]). From a different perspective, the formation and the dynamics of shock-waves in the defocusing regime have been studied in different experimental circumstances (see, e.g., [102,103,200]). The evolution of a dense gas of uncorrelated NLS solitons has been also examined in Ref. [388], in which a general method to derive kinetic equations describing the evolution of the spectral distribution function of solitons has been proposed.

As discussed in the introduction section (Section 1.2.4), the non-integrability of the model equation is usually considered as a prerequisite for the applicability of WT theory, because it implies a process of irreversible diffusion in phase space that is consistent with the formal irreversibility of the kinetic equation. On the other hand, the dynamics of integrable systems is expected to be essentially periodic in time, reflecting the underlying regular phase-space of nested-tori [389]. This is consistent with the fact that when one applies the conventional WT procedure to the integrable NLS equation, one obtains that all collision terms in the kinetic equation vanish identically at any order [390]. Accordingly, the conventional WT procedure predicts that the spectrum of a weakly nonlinear wave does not evolve during the propagation. We note in this respect that accurate experiments were performed in optical fibers since 2006 [386], which revealed that a significant evolution of the spectrum of the wave occurs beyond the weakly nonlinear regime of propagation. This issue was subsequently addressed in Refs. [361,142], in which a generalized WT kinetic equation was proposed by considering that the fourth-order moment of the field is not necessarily a stationary quantity. It is important to note that similar generalizations of the WT kinetic equation were originally developed in the context of hydrodynamic waves (see [391] for a review), and are still important when one considers the early stage of the evolution of the turbulent system, see, e.g., [392]. Contrary to the conventional WT kinetic equation, the collision term of such generalized WT equation does not vanish, but relaxes rapidly to zero. In spite of such a fast relaxation, the spectrum of the field can exhibit significant changes depending on the initial conditions. Considering Gaussian-shaped initial conditions, the evolution of the spectrum is characterized by a rapid growth of the spectral tails, which subsequently exhibit damped oscillations, until the whole spectrum ultimately reaches a statistically stationary state. The generalized WT kinetic equation provides an analytical expression of the damped oscillations, which is found in agreement with the numerical simulations of both the NLS and kinetic equations [142].

We remind that the applicability of the generalized WT kinetic equation to the description of the dynamics of the integrable NLS equation is constrained by the usual assumption of weakly nonlinear interaction. A rigorous mathematical treatment of the evolution of the incoherent wave beyond this weakly nonlinear regime would require the application of

the inverse scattering machinery (see, e.g., [393–395]), a feature which is also of interest considering the recent Hanbury Brown and Twiss experiment [396,397].

*6.3.1. Generalized wave turbulence kinetic equation*

We consider the 1D integrable NLS equation

$$i\partial_z\psi = -s\partial_t^2\psi + |\psi|^2\psi, \tag{226}$$

where $s = \mathrm{sign}(\beta_2)$. For convenience, we adopt here a different normalization with respect to that used above. The time variable $t$ has been normalized to $\tau_0 = 1/\Delta\omega$, where $\Delta\omega$ denotes the initial spectral width of the incoherent wave [for a Gaussian spectrum, $n_\omega = n_0\exp(-\omega^2/\Delta\omega^2)$, $\Delta\omega$ denotes the half-width at $1/e$ of the spectrum]. The space variable $z$ has been normalized with respect to the linear dispersion length $L_d = 2/(\beta_2\Delta\omega^2)$, while the field amplitude $\psi(z,t)$ is expressed in units of $1/\sqrt{\gamma L_d}$, where we recall that $\gamma$ denotes the nonlinear Kerr coefficient. The variables can be recovered in real units through the transformations $z \to zL_d$, $t \to t\tau_0$ and $\psi \to \psi/\sqrt{\gamma L_d}$.

In order to derive the generalized WT kinetic equation, we consider the evolution of the second-order moment, $\langle\tilde\psi(z,\omega_1)\psi^*(z,\omega_2)\rangle = n_{\omega_1}(z)\,\delta(\omega_1-\omega_2)$, and of the fourth-order moment

$$\langle\tilde\psi(z,\omega_1)\tilde\psi(z,\omega_2)\tilde\psi^*(z,\omega_3)\tilde\psi^*(z,\omega_4)\rangle = J_{1,2}^{3,4}(z)\,\delta(\omega_1+\omega_2-\omega_3-\omega_4), \tag{227}$$

where we recall that $\tilde\psi(z,\omega) = \frac{1}{\sqrt{2\pi}}\int\psi(z,t)\,\exp(i\omega t)\,dt$. Following the standard procedure to derive the WT kinetic equation (see Appendix A.7 in the appendix), one obtains the following coupled equations for the evolutions of the second and fourth-order moments

$$\partial_z n_{\omega_1}(z) = -\frac{1}{\pi}\iiint \mathrm{Im}[J_{1,2}^{3,4}]\,\delta(\omega_1+\omega_2-\omega_3-\omega_4)\,d\omega_2 d\omega_3 d\omega_4 \tag{228}$$

$$\partial_z J_{1,2}^{3,4}(z) + i\Delta k J_{1,2}^{3,4} = -\frac{i}{\pi}\,\mathcal{Q}[n] \tag{229}$$

where

$$\mathcal{Q}[n] = n_{\omega_1}(z)n_{\omega_3}(z)n_{\omega_4}(z) + n_{\omega_2}(z)n_{\omega_3}(z)n_{\omega_4}(z) - n_{\omega_1}(z)n_{\omega_2}(z)n_{\omega_3}(z) - n_{\omega_1}(z)n_{\omega_2}(z)n_{\omega_4}(z), \tag{230}$$

and $\Delta k = k(\omega_1)+k(\omega_2)-k(\omega_3)-k(\omega_4)$, $k(\omega) = s\omega^2$. The solution to Eq. (229) reads

$$J_{1,2}^{3,4}(z) = J_{1,2}^{3,4}(z=0)\exp(-i\Delta k z) - \frac{i}{\pi}\int_0^z \mathcal{Q}[n(z')]\,\exp[-i\Delta k(z-z')]\,dz'. \tag{231}$$

As discussed in Appendix A.7, the usual way to proceed at this point is to consider that the dominant contribution to $J_{1,2}^{3,4}(z)$ arises from the phase-matched terms, $\Delta k = 0$. For $\Delta k \neq 0$, the contribution of the fast oscillating function $\exp(-i\Delta k z)$ is considered as being unessential for propagation distances larger than $1/\Delta k$. With these assumptions, one obtains the usual WT kinetic equation (193) and (194). Now, it is easy to verify that, because of the 1D geometry and the quadratic dispersion relation $k(\omega) = s\omega^2$, the Dirac $\delta$-functions involved in the usual WT equation lead to a vanishing collision term. Indeed, the 1D integrable NLS equation only permits trivial interactions among frequency components i.e., the phase-matching is degenerate $\omega_{3,4} = \omega_{1,2}$. This discussion reveals that a natural way to describe an evolution of the spectrum, $\partial_z n_\omega(z) \neq 0$, is to take into account non phase-matched interactions, i.e., $\Delta k \neq 0$. Hence, the corresponding generalized WT kinetic equation is obtained by the substitution of (231) into Eq. (228)

$$\partial_z n_{\omega_1}(z) = \frac{1}{\pi^2}\int_0^z dz' \iiint \mathcal{Q}[n(z')]\,\cos[\Delta k(z'-z)]\,\delta(\omega_1+\omega_2-\omega_3-\omega_4)\,d\omega_2 d\omega_3 d\omega_4. \tag{232}$$

We note the important point that, because of the presence of the cosine function, the collision term of this kinetic equation no longer vanishes, despite the degenerate phase-matching interaction.

*6.3.2. Irreversible relaxation to stationary state*

We present here numerical simulations of the NLS Eq. (226) and of the kinetic equations. The NLS equation has been integrated numerically with periodic boundary conditions and a standard pseudo-spectral step-adaptive numerical scheme. As usual, the initial condition is characterized by a Gaussian spectrum with random phases uniformly distributed between 0 and $2\pi$. The spectra are computed by performing an averaging over an ensemble of 100 numerical integrations of the NLS Eq. (226).

The numerical simulations of the NLS Eq. (226) reveal that the spectrum of the incoherent wave reaches a statistically stationary state after a transient stage, whose duration and amplitude critically depend on the shape of the spectrum considered in the initial condition. The most significant evolutions are observed when the tails of the initial spectrum decay faster than exponentially (i.e., $n_\omega^0 = n_0\exp(-|\omega/\Delta\omega|^\alpha)$ with $\alpha > 1$). This is illustrated in Fig. 54 that shows the spectra

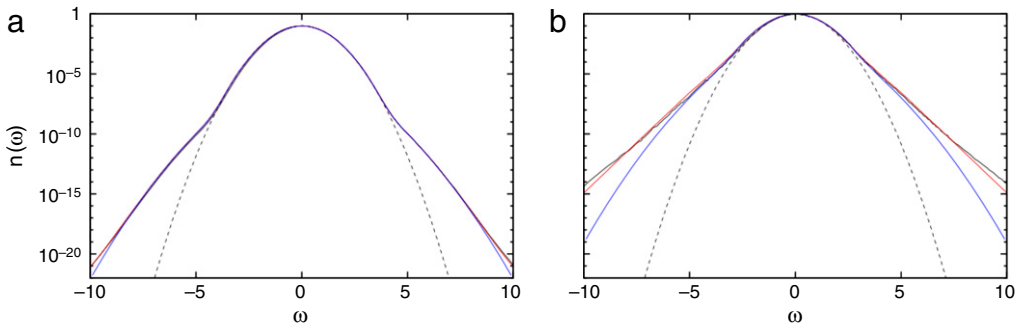


**Fig. 54.** Irreversible relaxation to stationary state in the integrable NLS equation: The averaged spectrum $n_\omega(z=1)$ plotted in black line has been obtained by integrating numerically the integrable NLS Eq. (226) (an average over 100 realizations of the initial noise has been taken). The spectrum $n_\omega(z=1)$ plotted in red line is obtained from the numerical integration of the coupled equations (228) and (229). The spectrum $n_\omega(z=1)$ plotted in blue line is obtained from the numerical integration of the coupled equations (235). The initial Gaussian spectrum $n_\omega(z=0)$ is plotted in dashed black line. Simulations plotted in (a) correspond to the weakly nonlinear regime, $|U/E| \simeq 0.05$ ($n_0 = 0.1$, $s = +1$). Simulations plotted in (b) correspond to a slightly nonlinear regime, $|U/E| \simeq 0.5$ ($n_0 = 1$, $s = +1$). (For interpretation of the references to color in this figure legend, the reader is referred to the web version of this article.) *Source:* From Ref. [142].

(black lines) computed with the following initial Gaussian spectrum (dashed black lines) $n^0_\omega = n_0 \exp(-\omega^2)$. We recall that with the adopted normalization, the half-width $\Delta\omega$ at $1/e$ is unity, while the variable $n_0$ is an important parameter which measures the amount of nonlinearity in the system, $n_0 = 2\sqrt{\pi} L_d/L_{nl}$.

As illustrated in Fig. 54, the simulations reveal the existence of an irreversible evolution of the spectrum towards a statistically stationary state. It is important to note that this relaxation process is very short and occurs over a propagation distance in the range of $0.1 L_{nl}$. It is also worth-noting that the central part of the spectrum does not exhibit significant changes, in contrast with the tails of the spectrum, which tend to approach an exponential decay. Let us emphasize that the power carried by the frequency components lying in the wings of the spectrum increases by several orders of magnitude.

We also report numerical simulations of the coupled kinetic Eqs. (228) and (229). We note in Fig. 54 that Eqs. (228) and (229) describe the evolution of the spectrum in a quantitative way for various different values of the parameter $n_0$ (see the spectra plotted in red lines in Fig. 54). As previously mentioned, $n_0$ reflects the amount of nonlinearity in the system, so that changes in $n_0$ are associated with changes in the ratio between the nonlinear and linear contributions to the Hamiltonian [we remind that $H = E + U$, $E$ ($U$) being the linear (nonlinear) contribution]. Considering the weakly nonlinear regime $|U/E| \simeq 0.05$, Fig. 54(a) shows that the simulations of Eqs. (228) and (229) are in quantitative agreement with those of the NLS equation over more than 20 decades. As shown in Fig. 54(b), this quantitative agreement is preserved over ∼15 decades even beyond the weakly nonlinear regime, $|U/E| \simeq 0.5$. Whatever the interaction regime explored in the simulations (i.e., from $|U/E| \sim 0.01$ to $|U/E| \sim 1$), the central part of the spectrum that carries the essential of the power of the incoherent wave is not significantly modified during the propagation.

In the following, we make use of this numerical observation that the spectrum of the incoherent wave only slightly evolves and then we assume that the term $Q[n(z)]$ in Eq. (232) can be approximated by its initial value at $z = 0$. The generalized WT kinetic equation then reduces to the simpler form

$$\partial_z n_{\omega_1}(z) = \frac{1}{\pi^2} \iiint \mathcal{Q}[n(z=0)] \frac{\sin(\Delta k z)}{\Delta k} \delta(\omega_1 + \omega_2 - \omega_3 - \omega_4)\, d\omega_2 d\omega_3 d\omega_4. \tag{233}$$

If $z \gg 1/\Delta k$, the function $\sin(\Delta k z)/\Delta k$ tends to the Dirac $\delta$-function, $\pi\delta(\Delta k)$, so that the collision term vanishes, as discussed above. However, as long as $z \sim 1/\Delta k$, non-phase-matched interactions among spectral components cannot be neglected. The collision term in Eq. (233) does not vanish and thus describes an evolution of the spectrum. Eq. (233) can be further simplified by performing the integration over $\omega_2$

$$\partial_z n_{\omega_1}(z) = \frac{1}{\pi^2} \iint \mathcal{M}[n(z=0)] \frac{\sin(\Delta k z)}{\Delta k} d\omega_3 d\omega_4, \tag{234}$$

with $\Delta k = k(\omega_1) + k(\omega_3 + \omega_4 - \omega_1) - k(\omega_3) - k(\omega_4) = 2s(\omega_1 - \omega_3)(\omega_1 - \omega_4)$, while $\mathcal{M}[n(z=0)] = n^0_{\omega_1} n^0_{\omega_3} n^0_{\omega_4} + n^0_{\omega_3} n^0_{\omega_4} n^0_{\omega_3+\omega_4-\omega_1} - n^0_{\omega_1} n^0_{\omega_3} n^0_{\omega_3+\omega_4-\omega_1} - n^0_{\omega_1} n^0_{\omega_4} n^0_{\omega_3+\omega_4-\omega_1}$, with $n^0_{\omega_j} = n_{\omega_j}(z=0)$. Observing that two terms among these four terms cancel each others, we obtain

$$\partial_z n_{\omega_1}(z) = \frac{1}{\pi^2} \iint n^0_{\omega_3} n^0_{\omega_4} n^0_{\omega_3+\omega_4-\omega_1} \frac{\sin(\Delta k z)}{\Delta k} d\omega_3 d\omega_4 - \frac{n^0_{\omega_1}}{\pi^2} \iint n^0_{\omega_3} n^0_{\omega_4} \frac{\sin(\Delta k z)}{\Delta k} d\omega_3 d\omega_4. \tag{235}$$

This equation has been integrated numerically and the corresponding spectra are plotted in blue lines in Fig. 54. Fig. 54(a) shows that our approximation is accurate in the weakly nonlinear regime ($n_0 = 0.1$, $|U/E| \simeq 0.05$). Beyond the weakly

nonlinear regime (Fig. 54(b) for $n_0 = 0.5$), the approximation becomes less effective, though a quantitative agreement with the simulation of Eq. (226) is preserved over ∼8 decades.

The simulations of Eq. (235) reveal that the first term in its right-hand side mainly contributes to changes occurring in the wings of the spectrum, whereas the second term essentially contributes to small changes occurring nearby the center of the spectrum, $\omega_1 \sim 0$. In the following, we restrict the analysis to the study of the evolution of the spectral wings, $\omega_1 \gg \Delta\omega$, and thus consider solely the contribution of the first term in Eq. (235). If the power spectrum is initially Gaussian [$n^0_\omega = n_0 \exp(-\omega^2)$], the dominant contributions from $n^0_{\omega_3} n^0_{\omega_4} n^0_{\omega_3+\omega_4-\omega_1}$ in the first term of Eq. (235) are obtained for $\omega_3 \simeq \omega_4 \simeq \omega_1/3$, $\omega_2 \simeq -\omega_1/3$. This can be easily seen by introducing the variables $x = \omega_3 - \omega_1/3$ and $y = \omega_4 - \omega_1/3$, so that $n^0_{\omega_3} n^0_{\omega_4} n^0_{\omega_3+\omega_4-\omega_1} = n_0^3 \exp[2(x^2 + y^2 + xy)] \exp(-\omega_1^2/3)$, which corresponds to a peaked function localized around $x = y = 0$. With an initial Gaussian spectrum, the power growth rate carried by a spectral component at a frequency $\omega_1$ falling in the tails of the spectrum is determined by the interaction among spectral components at frequencies $\pm\omega_1/3$ falling in the center of the Gaussian spectrum. This result is not intuitive: The evolution of the component at a frequency $\omega_1$ is not driven by degenerate four-wave mixing among the pairs of frequencies $(0, 0)$ and $(-\omega_1, +\omega_1)$. Indeed, the dominant contribution corresponds to degenerate four-wave mixing among the pairs of frequencies $(+\omega_1/3, +\omega_1/3)$ and $(-\omega_1/3, +\omega_1)$. Note that this result is valid for any initial spectrum with an hyper-Gaussian shape, i.e., $n^0_\omega = n_0 \exp(-\omega^{2p})$, where $p > 0$ is an integer.

Making use of a common approximation for integral involving oscillating functions, we consider that the term $\Delta k$ in the denominator of the first term of Eq. (235) can be assumed constant ($\Delta k = 8s\omega_1^2/9$), which gives

$$\partial_z n_{\omega_1}(z) \simeq \frac{9}{8\pi^2\omega_1^2} \iint n^0_{\omega_3} n^0_{\omega_4} n^0_{\omega_3+\omega_4-\omega_1} \sin[2(\omega_1 - \omega_3)(\omega_1 - \omega_4)z]\, d\omega_3 d\omega_4. \tag{236}$$

Keeping in mind that $n^0_\omega = n_0 \exp(-\omega^2)$, this integral can be computed analytically. However the corresponding expression is complicated. It can be further simplified by approximating the expression of $\Delta k$ in the sine function by $\Delta k \simeq 4s\omega_1(\omega_4 - \omega_3)/3$, which gives

$$\partial_z n_{\omega_1}(z) \simeq \frac{n_0^3}{\sqrt{3}\pi} \frac{9}{8\omega_1^2} \exp\left[-\frac{\omega_1^2}{3}\left(1 + \frac{8z^2}{9}\right)\right] \sin\left(\frac{8\omega_1^2 z}{9}\right). \tag{237}$$

Eq. (237) describes the growth of frequency components found in the tails of the spectrum ($\omega \gg \Delta\omega$) with propagation distance $z$. For the sake of clarity, we rephrase its expression in physical units

$$\partial_z n_{\omega_1}(z) \simeq \frac{\gamma^2 n_0^3 \Delta\omega^2}{\sqrt{3}\pi} \frac{9}{8\beta\omega_1^2} \exp\left[-\frac{\omega_1^2}{3\Delta\omega^2}\left(1 + \frac{8\beta^2\Delta\omega^4 z^2}{9}\right)\right] \sin\left(\frac{8\beta\omega_1^2 z}{9}\right) \tag{238}$$

with $\beta = \beta_2/2$.

This equation shows that a spectral component in the wings of the Gaussian spectrum grows with the propagation distance $z$. More precisely, Eq. (238) shows that $n_{\omega_1}$ will reach a steady value after a transient characterized by damped oscillations. This phenomenon is illustrated in Fig. 55, that shows the decay of the oscillations of two different spectral components. As illustrated in Fig. 55, there is a good quantitative agreement between the results obtained from the numerical integrations of the NLS Eq. (226) and the plot of Eq. (237). We remind that the NLS simulations refer to an averaging over 100 realizations and that the curves plotted with black lines in Fig. 55 represent an averaged result. Note also that the decay of the oscillations plotted in Fig. 55 correspond to the simulation reported in Fig. 54(a).

As revealed by Eq. (237), the spatial period $\Lambda \simeq 9\pi/(4\omega_1^2)$ of the decaying oscillations is inversely proportional to $\omega_1^2$. In dimensional units, the expression of the period reads $\Lambda \simeq (9\pi/4)(\Delta\omega/\omega_1)^2 L_d$. We remind that these oscillations find their origin in transient and non-phase-matched interactions among frequency components of the incoherent wave. The period of the oscillations is determined by the fact that the spectral component at $\omega_1$ essentially interact with the frequency components $\omega_3 \simeq \omega_4 \simeq \omega_1/3$ and $\omega_2 \simeq -\omega_1/3$. In these conditions, the dominant spatial frequency $\Delta k$ is around $\Delta k = 8s\omega_1^2/9$. The amount of damping in the oscillations is given by the Gaussian function in Eqs. (237) and (238). This estimate reveals that the damping length measuring the propagation distance needed for the wave system to reach its steady state scales as $1/(\beta\omega_1\Delta\omega)$.

*Influence of the sign of the nonlinearity*

Let us finally briefly comment on the influence of the sign of the nonlinearity on the dynamics of the spectrum. As discussed above, the WT kinetic equation is inherently unable to distinguish the normal or anomalous dispersion regime. In the weakly nonlinear regime ($|U/E| \ll 1$), coherent structures such as solitons do not emerge from the propagation of the incoherent wave. Moreover, in this regime, the typical MI frequencies are usually much smaller than the initial spectral width of the incoherent wave, so that MI results to be suppressed by wave incoherence. We have checked this from the simulations of the NLS Eq. (226) and verified that the averaged spectra reported in Fig. 54(a) do not depend on the sign of $s$ in the weakly nonlinear regime ($|U/E| \simeq 0.05$).

On the other hand, beyond this weakly nonlinear regime ($|U/E| \simeq 0.5$, see Fig. 54(b)), the averaged spectra at $z = 1$ do depend on the sign of $s$. Simulations performed in the anomalous dispersion regime ($s = -1$) show that $n_\omega(z = 1)$ is

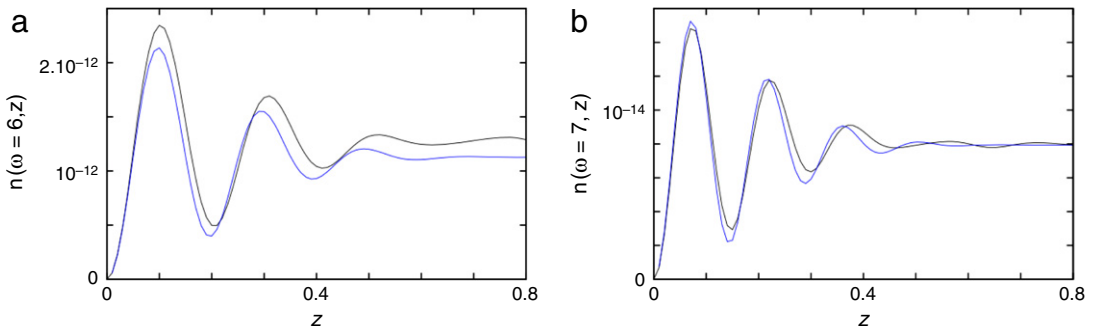


**Fig. 55.** Irreversible relaxation to stationary state in the integrable NLS equation: Numerical simulations of the integrable NLS Eq. (226) (black line) and of Eq. (237) (blue line) showing the decaying of the oscillations of two spectral components taken in the wings of the spectrum plotted in Fig. 54(a). The initial condition is the Gaussian spectrum plotted in Fig. 54(a) ($n_0 = 0.1$, $s = +1$). In (a), the spatial period $\Lambda \simeq 9\pi/(4\omega^2)$ of the decaying oscillations is close to $1.96 \times 10^{-2}$ for a spectral component at the frequency $\omega = 6$. In (b), the period decreases to $\Lambda \simeq 1.44 \times 10^{-2}$ for a spectral component at the frequency $\omega = 7$. (For interpretation of the references to color in this figure legend, the reader is referred to the web version of this article.)
*Source:* From Ref. [142].

broader than that plotted in black line in Fig. 54(b) for the normal dispersion regime ($s = +1$). This feature can be interpreted from the fact that soliton-like structures and incoherent MI can start to play a role in the anomalous dispersion regime for $|U/E| \simeq 0.5$. We have checked that the analytical results obtained from the kinetic theory are still in good agreement with the simulations of NLS Eq. (226) at $|U/E| \simeq 0.5$ (see Fig. 54(b)). In other words, the range of values of the small parameter $|U/E|$ over which WT theory provides results that are quantitatively correct is wider in the normal dispersion regime than in the anomalous dispersion regime.

We finally note that it would be interesting to study this nonequilibrium relaxation process of the integrable NLS equation through the analysis of nonvanishing fluxes of conserved quantities, in relation with Kolmogorov–Zakharov nonequilibrium stationary solutions discussed in Section 5.1.2. We remark in this respect that, because of the absence of the Dirac $\delta$-function associated to energy conservation in the generalized WT kinetic equation (232), one cannot directly apply the Zakharov transformation to find nonequilibrium stationary spectra. This interesting issue will be the subject of future investigations.

### 6.3.3. Experiments

We report in this section experimental results concerning the relaxation process of the integrable NLS equation discussed here above. The optical fiber setup is reported schematically in Fig. 56. The partially-coherent light source used in the experiment is a solid-state Nd:YVO4 continuous-wave laser. The laser is linearly-polarized and its central emission wavelength of ∼1064 nm is far from the zero-dispersion wavelength $\lambda_0$ of the optical fiber ($\lambda_0 \sim 1400$ nm), so that third-order dispersion effects can be neglected. The laser optical power spectrum has a full-width at half maximum (FWHM) of ∼0.15 nm (i.e. ∼36 GHz). We have analyzed the time evolution of the laser power with a photodiode whose bandwidth is much greater than the free spectral range $\Delta\nu_{FSR}$ of the laser cavity ($\Delta\nu_{FSR} \simeq 150$ MHz), and no significant changes in the laser power on time scales of the order of $1/\Delta\nu_{FSR}$ have been observed. Therefore the laser emits a radiation composed of approximately 200 longitudinal modes whose phases can be considered as uncorrelated.

The power of the laser light is controlled by adjusting a half-wave plate (HWP1) placed between the Nd:YVO4 laser and a Faraday isolator. The laser light is launched inside a 1.5 km-long single-mode polarization-maintaining fiber. The polarization direction of the input light is adjusted along one of the birefringence axes of the fiber by using another half-wave plate (HWP2). In the experiments, the light wave remains linearly polarized all along the fiber and the extinction ratio between the two axes is greater than 20 dB. The nonlinear Kerr coefficient of the polarization maintaining fiber is $\gamma = 6\ \mathrm{W^{-1}\ km^{-1}}$ and its second-order dispersion coefficient is $\beta_2 = 20\ \mathrm{ps^2\ km^{-1}}$ at 1064 nm.

The experiment is aimed at investigating the weakly nonlinear regime discussed in Section 6.3, in which only the wings of the spectrum are modified during the propagation ($|U/E| \ll 1$). So far, only the nonlinear interaction regime has been explored in experiments ($|U/E| \gg 1$) [386]. In the nonlinear regime, the spectrum of the incoherent wave exhibits deep changes which affect both the wings and the central part of the spectrum (see Fig. 2 of Ref. [386]). For incoherent light waves with wavelength around 1 μm and with a typical spectral width of ∼1 nm, the nonlinear interaction regime in a standard single mode fiber typically refers to optical powers of ∼1 W [386]. The weakly nonlinear regime explored in Ref. [142] corresponds to an optical power typically lower than ∼1 mW. As illustrated in Fig. 56, the changes occurring in the wings of the spectrum in the linear interaction regime involve spectral components carrying an optical power that is typically $10^{10}$ times (equivalently 100 dB) lower than the power of spectral components lying in the center of the spectrum. The possibility of exploring the linear interaction regime therefore critically depends on the sensitivity and the dynamic range of the optical spectrum analyzer used in the measurement.

In the experiment, the output end of the polarization maintaining fiber has been directly connected to the optical spectrum analyzer (Ando AQ6317B). With this experimental setup and using the highest degree of sensibility of the spectrum analyzer, we have observed changes in the optical spectrum that can be undoubtedly associated to the effects predicted

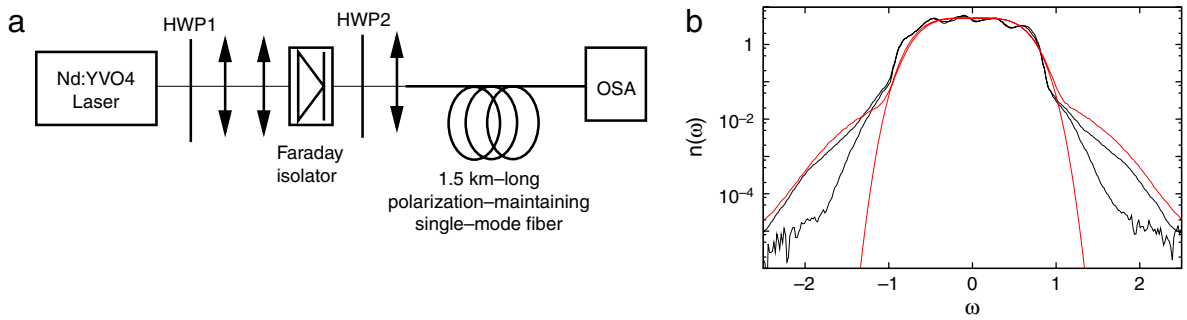


**Fig. 56.** Irreversible relaxation process of the integrable NLS equation: Experiments. (a) Schematic representation of the experimental setup. HWP: Half-wave plate. OSA: Optical spectrum analyzer. (b) Power spectra recorded in experiments (black lines) and obtained from numerical simulations (red lines) of Eq. (226). Note that numerical simulations of Eq. (235) give identical results (not represented here, see [142]). The narrow spectrum plotted in black line is the spectrum of the Nd:YVO4 laser launched inside the polarization maintaining fiber. The wide spectrum plotted in black line is the spectrum recorded at the output of the polarization maintaining fiber. In numerical simulations of the normalized NLS Eq. (226), the initial incoherent wave has a power spectrum approximated by $n^0_\omega = n_\omega(z=0) = n_0 \exp(-\omega^4/\Delta^4)$ ($\Delta = 0.73$, $n_0 = 4.72$, $\sigma = +1$). (For interpretation of the references to color in this figure legend, the reader is referred to the web version of this article.)
*Source:* From Ref. [142].

by the generalized WT theory discussed in the previous section. The optical power measured at the output of the fiber is of ∼12 mW. At this poser level, our experiment corresponds to a nonlinear regime in which $|U/E| \simeq 1$. To explore the weakly nonlinear regime, the optical power should be decreased by at least one order of magnitude, but the detection of the minor changes occurring in the wings of the spectrum would become impossible with the spectrum analyzer used in the experiment of [142].

As predicted by the generalized WT theory, Fig. 56 shows that the power of spectral components falling in the wings of the spectrum has increased with propagation distance, whereas the central part of the spectrum does not exhibit changes, as expected from the simulations. We note that the experiment only permits to explore the first stage of the transient regime corresponding to a monotonic growth of the power carried by spectral components in the tails of the spectrum. In particular, the damped oscillations of the power of these frequency components have not been observed by using the setup presented in Fig. 56.

The question of the changes of the statistical properties of an integrable system described by the 1D-NLSE have been also considered in the context of nonlinear interferometry [396]. Taking a geometry in which an incoherent light wave propagates along one direction and is free to diffract along another, experiments performed in the strongly nonlinear focusing and defocusing regimes have evidenced strong changes in the statistics of the incoherent field. Considering an initial incoherent wave with Gaussian statistics, the probability to record high intensity values is enhanced in the focusing regime while it is reduced in the defocusing regime [396]. These experimental results have stimulated a theoretical work in which tools of the inverse scattering theory have been used to describe the changes in the field statistics [397]. Note finally that statistics of light intensity has been also experimentally and theoretically studied in 1D discrete lattice described by a tight-binding model [376]. This work revealed the existence of a spontaneous emergence of a correlation between neighboring sites, while the field correlation takes a universal shape independent of the parameters [376].

## 7. Recent advances and perspectives

In the first part of this Section we review some recent advances and perspectives of optical WT, in particular with its study in optical cavities, in relation with condensation-like phenomena and lasers. We remind in this respect that nonlinear optical systems with feedback and associated phenomenologies, such as pattern formation [398] and cavity solitons [265, 266], have been continuously drawing attention from both the fundamental [399] and applicative [265,266] points of views.

In the second part of this Section we briefly discuss the role of vortices in the thermalization and condensation processes in relation with the Berezinskii–Kosterlitz–Thouless (BKT) theory, as well as the possible role of coherent phase effects in the dynamics of incoherent nonlinear waves. Finally, we comment some additional open problems and possible interesting perspectives for future developments of optical WT.

### *7.1. Condensation phenomena and lasers*

A laser system is known to be characterized by the property of delivering a narrow spectral radiation. However, one expects the mechanism underlying the generation of such a coherent radiation of a different nature than the thermalization process underlying wave condensation, as discussed in the conservative (Hamiltonian) limit in Section 5. The essential difference relies on the fact that a laser system is usually described as a dissipative system driven far from equilibrium by an external source, while wave condensation discussed above relies on the natural relaxation of a conservative ('closed')

system to thermal equilibrium. Accordingly, wave condensation is characterized by the formation of the Rayleigh–Jeans equilibrium distribution reflecting the property of energy equipartition among the modes, while laser radiation is usually expected to exhibit different (Poisson) statistics [2]. In other terms, the nonequilibrium nature of the laser device introduces crucial differences with respect to the standard equilibrium Bose–Einstein condensation: The steady state of the laser is not determined by a thermal equilibrium condition, but rather follows from a dynamical balance between the pumping and losses [399].

*Bose–Einstein condensation in optical microcavities*

From the experimental point of view, a relation between Bose–Einstein condensation and spontaneous coherence effects in optical systems has been recently recognized with the so-called Bose–Einstein condensation of exciton polaritons in semiconductor micro-cavities [400–403,82]. These studies are in contrast with the strongly nonequilibrium regimes of laser operation observed in a vertical cavity surface emitting laser device [404]. Hence, questions related to common and different properties of laser operation and photon–polariton Bose–Einstein condensation have attracted strong interest, with particular attention to the issue of thermalization, see [82] for a review.

It is important to note that the thermalization and the Bose–Einstein condensation of a photon gas have been recently reported in an optical micro-cavity [405,77,406]. In spite of its bosonic nature, the photon gas involved in blackbody radiation does not exhibit a Bose–Einstein transition because the number of photons is not conserved due to the interactions of the photon gas with the cavity walls. In the experiments [405,77] the authors achieve a number conserving thermalization process by considering a dye-filled optical micro-resonator, which plays the role of a 'white-wall box' for the two dimensional photon gas. In this way the authors report an equilibrium Bose–Einstein phase transition that results from the thermalization of the photon gas. It should be remarked that the thermalization process is achieved thanks to an external thermostat—the photons exhibit repeated absorption and reemission processes in the dye molecules, which thus act as a thermal heat bath reservoir that equilibrates the photon gas to the temperature of the dye molecules. Conversely, in the passive cavity configuration considered below in Section 7.3, the process of thermalization solely results from the four-wave interaction mediated by the intracavity Kerr medium [78].

As a matter of fact, the relation between lasing and Bose–Einstein condensation is still the subject of vivid debate—we refer the reader to Refs. [325–327,82] for some recent discussions on this important problem. In the following we briefly comment some other experiments, which have pointed out interesting analogies with optical wave condensation.

*Condensation-like phenomena*

An important analogy with condensation has been discussed in the dynamics of active mode-locked laser systems in the presence of additive noise source [76,407,327]. On the basis of their previous works [408,409], the authors show that the formation of coherent pulses in actively mode-locked lasers exhibits in certain conditions a transition of the laser mode system to a light pulse state that is similar to Bose–Einstein condensation, in the sense that it is characterized by a macroscopic occupation of the fundamental mode as the laser power is increased. The analysis is based on statistical light-mode dynamics with a mapping between the distribution of the laser eigenmodes to the equilibrium statistical physics of noninteracting bosons in an external potential.

Another analogy with condensation has been pointed out to interpret the radiation emitted by a random laser system in [74]. Random lasers are a rapidly growing field of research, with implications in soft-matter physics, light localization, and photonic devices. In Ref. [74] the analogy with condensation is supported by the fact that the random laser linewidth is ruled by a nonlinear differential equation, which is the equivalent of the Schwalow–Townes law in standard lasers, and is formally identical to the NLS (Gross–Pitaevskii) equation with a trapping potential. In this way, the random laser emission has been related to a condensation process of several wave resonances in the presence of disorder, the distribution of their decay times playing the role of a temporal trapping potential. An analogy has thus been pointed out between the simultaneous spectral and temporal narrowing with the number photons in the random laser and the spectral and spatial narrowing that typically characterizes condensation.

### *7.2. Wave turbulence in Raman fiber lasers*

The dynamics of Raman fiber lasers has been also shown to exhibit some interesting analogies with condensation-like phenomena [75,80,81]. In this section we discuss in more detail these systems in light of the WT theory that has been developed to describe their dynamics. We remark in this respect that Raman fiber lasers are the only example of laser systems whose dynamics has been described by the WT kinetic equation. We refer the interested reader to Ref. [79] for an overview on the WT description of Raman fiber lasers.

#### *7.2.1. Spectral and statistical properties of Raman fiber lasers*

Raman fiber lasers are reliable and efficient light sources that have attracted a great interest in recent years because of the wide range of their potential applications and also because they constitute an important example of nonlinear photonic

device that can be used for the investigation of some new concepts in nonlinear science [410,81]. Raman fiber lasers exploit the well-known nonlinear process of stimulated Raman scattering in silica fibers [138]. Pumping a conventional single mode fiber with a germanium doped silica core, the Raman process provides gain around a Stokes wavelength that is shifted by ∼14 THz from the pump wavelength [411]. Oscillation of the Raman fiber laser is achieved by placing the Raman active fiber inside a cavity that is typically formed by a set of two fiber Bragg grating mirrors located at each end of the fiber. As the Raman gain curve is rather broad, the fiber laser has the ability to operate at some discrete wavelengths that can be selected over wide wavelength ranges, including the telecommunication window around 1.5 μm. Moreover several frequency conversion cascades can also be exploited in nested cavities so as to reach longer Stokes wavelengths [412,413].

Although ultrashort distributed-feedback [414] cavities or ultralong (∼100 km) [415,416] cavities have been demonstrated, standard Raman fiber lasers have a typical configuration in which a single mode fiber having a length of several hundreds meters is inserted between the two fiber Bragg grating mirrors. The free spectral range of the cavity is typically of the order of 100 kHz, which is much smaller than the typical laser linewidth (∼100 GHz) measured well above threshold. In other words, Raman fiber lasers are strongly multimode light sources whose output is determined by the nonlinear interaction among approximately one million longitudinal cavity modes.

Understanding the spectral properties of Raman fiber lasers is a question that has been initially considered of importance for the optimization of the laser output power [417,418]. By increasing the pump power, the laser optical power spectrum significantly broadens. Well above threshold, it can become even broader that the reflectivity spectrum of the cavity mirrors. This spectral broadening phenomenon has first been treated in a phenomenological way by introducing an effective reflectivity for the cavity output mirror. Using simple single-mode models with only one frequency component for the pump wave and one frequency component for the Stokes wave, some empirical modifications of the reflectivity coefficient of the cavity output mirror have proven to provide laser power characteristics close to those experimentally recorded [417]. However this kind of procedure ignores the fundamental multimode nature of the laser operation [418]. Subsequently, the four-wave mixing process underlying the optical Kerr effect has been identified as being responsible for the phenomenon of spectral broadening. In this way, several phenomenological treatments of the four-wave mixing process have been proposed to describe the properties of Random fiber lasers [419,420].

*Wave turbulence description of Raman fiber lasers*

From a fundamental different point of view, Babin et al. proposed to describe the dynamics of Raman fiber lasers by making use of the WT theory [410]. In Ref. [410], the Raman fiber laser is modeled as a turbulent system whose optical power spectrum results from a weakly nonlinear interaction among the multiple modes of the cavity. Performing a mean field approach in which they assume that the Raman Stokes field does not evolve significantly over one cavity round trip, the authors of Ref. [410] first establish a differential equation for the evolution of the complex amplitude $E_n$ of the $n$th longitudinal mode

$$\tau_{rt}\frac{dE_n}{dt} - \frac{1}{2}(g-\delta_n)E_n(t) = -\frac{i}{2}\gamma L\sum_{l\neq 0}E_{n-l}(t)\sum_{m\neq 0}E_{n-m}(t)E^*_{n-m-l}(t)\exp(2i\beta\, ml\Delta^2\, c\, t). \tag{239}$$

In their approach, the time evolution of $E_n$ is determined by the Raman gain $g$, the dispersion of the fiber, the losses $\delta_n$ of the fiber and of the cavity mirrors, and the four-wave mixing process. $\gamma$ is the Kerr coupling coefficient and $\beta$ represents the second-order dispersion coefficient of the cavity fiber. $\Delta = 1/\tau_{rt} = c/2L$ is the free spectral range of the Fabry–Perot cavity that has a length $L$. Gain, losses and dispersive effects occurring inside the whole laser cavity are supposed to influence the formation of the optical power spectrum through their dependence in frequency-space. In particular fiber Bragg grating mirrors are considered as spectral filters introducing parabolic losses in frequency space ($\delta_n = \delta_0 + \delta_2(n\Delta)^2$). Dispersive effects occurring inside the laser cavity are supposed to be dominantly governed by the second-order dispersion $\beta$ of the cavity fiber. It must be emphasized that Eq. (239) refers to the discretized version of the one-dimensional NLS equation, in which gain and losses terms have been added [421]. In other words, the approach developed by the authors of Ref. [410] amounts to apply a WT treatment to a one-dimensional NLS equation, whose integrability is broken by the presence of gain and loss terms.

Assuming an exponential decay for the correlation function among the modes, $\langle E_n(t)E^*_n(t')\rangle = I_n\exp(-|t-t'|/\tau)$, Babin et al. derive the following WT kinetic equation that governs the temporal evolution of the intracavity optical power spectrum [410]

$$\tau_{rt}\frac{dI(\Omega)}{dt} = (g-\delta(\Omega))I(\Omega) + S_{FWM}(\Omega), \tag{240}$$

where $I(\Omega) = \langle E_nE^*_n\rangle/\Delta$. The mathematical expression of the collision term $S_{FWM}(\Omega)$ can be separated into two parts

$$S_{FWM}(\Omega) = -\delta_{NL}I(\Omega) + (\gamma L)^2\int\frac{I(\Omega-\Omega_1)I(\Omega-\Omega_2)I(\Omega-\Omega_1-\Omega_2)}{(3\tau_{rt}/\tau)[1+(4\tau L\beta/3\tau_{rt})^2\Omega_1^2\Omega_2^2]}\,d\Omega_2, \tag{241}$$

and the nonlinear term responsible for four-wave-mixing-induced losses $\delta_{NL}$ reads

$$\delta_{NL} = (\gamma L)^2\int\frac{[I(\Omega-\Omega_1)+I(\Omega-\Omega_2)]I(\Omega-\Omega_1-\Omega_2) - I(\Omega-\Omega_1)I(\Omega-\Omega_1)}{(3\tau_{rt}/\tau)[1+(4\tau L\beta/3\tau_{rt})^2\Omega_1^2\Omega_2^2]}\,d\Omega_2. \tag{242}$$

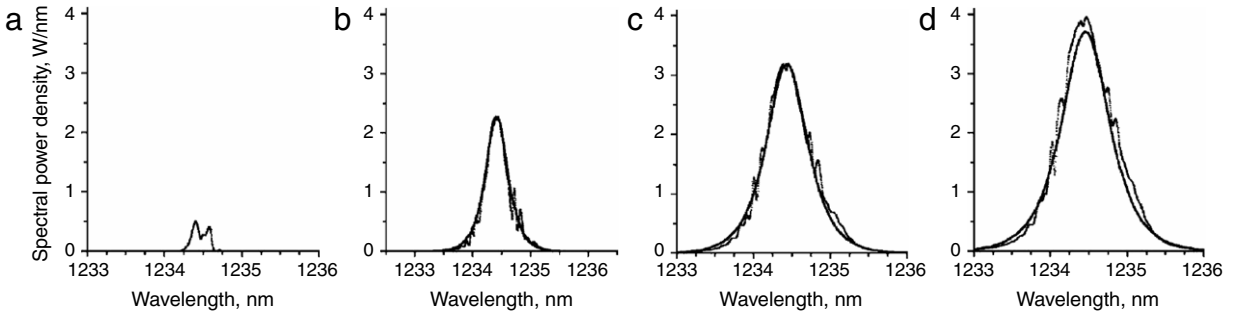


**Fig. 57.** Wave turbulence in Raman fiber lasers: Measured (dots) and calculated (solid curve) intracavity Stokes power spectrum for increasing values of the pump power $P_0$. The solid line refers to a plot of the stationary solution (243) of the WT kinetic equation (240)–(242). (a) $P_0 = 0.4$ W, (b) $P_0 = 1$ W, (c) $P_0 = 2$ W, (d) $P_0 = 3$ W.
*Source:* From Ref. [410].

With respect to standard mathematical developments commonly used in the framework of WT theory, the originality of the treatment made by Babin et al. mainly relies on the introduction of the finite correlation time $\tau$. The idea of the introduction of this parameter stems from radio-frequency measurements of the inter-mode beating spectrum of the Stokes intensity [422]. These measurements have evidenced that the peaks associated to the beating phenomenon are separated by the cavity free spectral range and that their widths increase with the intracavity Stokes power. This indicates that there exist an interesting relation between this phenomenon observable at the level of a few individual modes and the global phenomenon of spectral broadening that involves a very large number of cavity modes.

A stationary solution of the WT kinetic Eq. (240) has been obtained by Babin et al. in Ref. [410], which exhibits the following hyperbolic-secant structure

$$I(\Omega) = \frac{2I}{\pi\,\Gamma\cosh(2\Omega/\Gamma)} \tag{243}$$

where $\Gamma$ is the width of the intracavity laser power spectrum. As shown in Fig. 57, the hyperbolic secant shape found from the WT treatment performed by Babin et al. is in very good agreement with spectra recorded in experiments in which the fiber laser operates well above threshold. This particular shape of the solution has been observed in a very robust fashion in several experiments, even in regimes in which the mean field approximation should no longer hold [423].

Although the WT approach developed in Ref. [410] has undoubtedly provided a new insight into the physics of Raman fiber lasers, some other numerical and experimental works have raised some interesting questions concerning the applicability of the WT approach to the description of the spectral broadening phenomenon. In particular, numerical simulations of the mean field equations introduced in Ref. [410] revealed that the shape of the laser optical power spectrum dramatically depends on the sign of the second-order dispersion coefficient [75]. This feature of importance cannot be captured by the WT theory, which is inherently insensitive to the sign of the second-order dispersion parameter [75]. As pointed out in Refs. [424,421], the formation of the Stokes spectrum is also deeply influenced both by dispersive effects and by the spectral shape of the fiber Bragg grating mirrors used to close the laser cavity. In particular, dispersive effects occurring at light reflection on the fiber Bragg grating mirrors can be so important that the cavity zero-dispersion wavelength might be shifted inside the reflectivity bandwidth of the mirrors. This induces an asymmetry in the spectrum which is observed when the laser operates close above threshold [421].

*Statistics of the radiation*

The question of the statistics of the Stokes radiation delivered by Raman fiber lasers has also been examined both experimentally and numerically [75,425,423]. When the Raman fiber laser operates well above threshold, numerical simulations have shown that the statistics of the Stokes radiation significantly deviates from Gaussianity [425]. It has also been shown that the statistics of the Stokes radiation varies all along the fiber cavity. In particular, the Stokes wave has Gaussian statistics just after reflection onto a cavity mirror, but the statistics becomes non-Gaussian as the Stokes wave propagates inside the cavity fiber [423]. These results about statistical deviations from Gaussianity obviously raise some questions concerning the applicability of the WT theory to the description of the dynamics of Raman fiber lasers. However it should be emphasized that numerical simulations presented in Refs. [425,423] rely on a model in which generalized NLS equations are integrated in an iterative way, in both forward and backward propagation directions. Although this kind of model provides a quantitative description of the spectral broadening phenomenon, it is not obvious that it describes their statistical properties in a correct way. The experimental verification of the statistical predictions of iterative models is not an easy task because the fluctuations of the Stokes field are so fast that it is not possible to record them, even by using fast detection techniques. This has been circumvented by the introduction of spectral filtering techniques [426,427]. Slicing the intracavity broadened Stokes spectrum by using highly selective optical filters, high contrast fast fluctuations of Stokes field are observed by using fast oscilloscope and photodiode. The study of the statistical properties of the radiation recorded

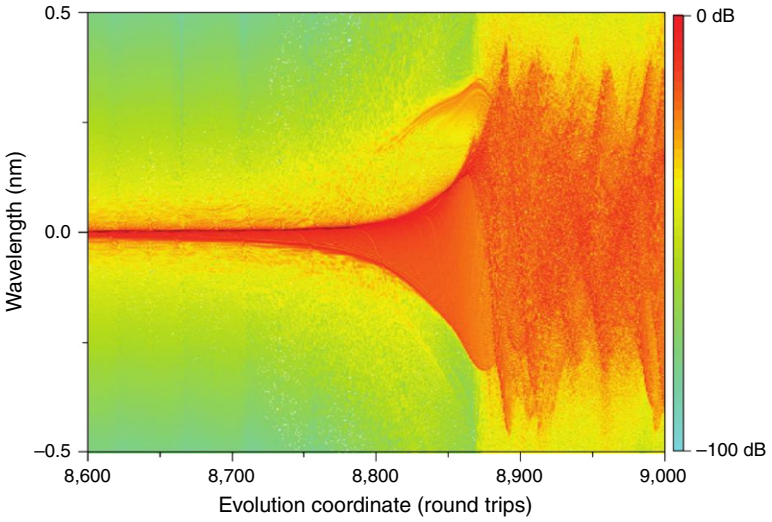


**Fig. 58.** Numerical simulations evidencing the laminar–turbulent transition in a Raman fiber laser. The evolution of the laser optical power spectrum is plotted as a function of number of round trips inside the laser cavity.
*Source:* From Ref. [81].

experimentally revealed that the Stokes field filtered from the central part of the spectrum has Gaussian statistics. However, this is not the case when the filtering procedure is applied in the wings of the spectrum. In this part of the spectrum, the statistics deviates from Gaussianity, with a probability of emergence of rare and intense events significantly higher than the one defined by the Gaussian distribution [426,427].

### *7.2.2. Laminar–turbulent transition in Raman fiber lasers*

Fast detection techniques have also recently proven to be useful for the observation of a laminar–turbulent transition in a Raman fiber lasers [81]. The fiber laser designed and used in the new experiments reported in Ref. [81] has been specifically designed. It is made with dispersion-free ultra-wideband super-Gaussian fiber grating mirrors. Slightly changing the pump power, an abrupt transition with a sharp increase in the width of laser spectrum has been observed, together with an abrupt change of the statistical properties of the Stokes radiation. The laminar state observed before the transition is associated to a multimode Stokes emission with a relatively narrow linewidth and relatively weak fluctuations of the Stokes power. The turbulent state corresponds to a high multimode operation with a wider spectrum and stronger fluctuations of the Stokes power. The laminar–turbulent transition has been also studied by means of intensive numerical simulations (see Fig. 58) [80, 75,81]. The theoretical analysis made by the authors of Ref. [81] reveals that, by increasing the pump power, the mechanism underlying the laminar–turbulent transition relies on the generation of an increasing number of dark (or gray) solitons. This experimental work opens new fields of investigations, in particular for what concerns the developments of WT formulations of one-dimensional optical fiber systems.

## *7.3. Condensation and thermalization in a passive optical cavity*

The thermalization and the condensation of a classical optical wave have been discussed in Section 5 in different regimes in the framework of the WT theory. In this section we show that a phenomenon completely analogous to the conservative condensation process discussed in Section 5 can occur in an incoherently pumped passive optical cavity, despite the fact that this system is inherently dissipative. This section is structured along the lines of Ref. [78].

In this section we consider a *passive optical cavity* pumped by an incoherent optical wave, whose time correlation, $t_c$, is much smaller than the round trip time, $t_c \ll \tau_{rt}$. In this way, the optical beam from different cycles are mutually incoherent with one another, which makes the optical cavity *non-resonant*. As already discussed above in Section 4.6.4, because of this non-resonant property, the cavity does not exhibit the widely studied dynamics of pattern formation [266,398]. Instead, the dynamics of the cavity exhibits a turbulent behavior that can be characterized by an irreversible process of thermalization towards energy equipartition. A mean-field WT equation is derived, which accounts for the incoherent pumping, the nonlinear interaction and both the cavity losses and propagation losses [78]. In spite of the dissipative nature of the cavity dynamics, the intracavity field undergoes a condensation process below a critical value of the incoherence (kinetic energy) of the pump, which thus plays the role of the control parameter of the transition to wave condensation. The condensate fraction in the dissipative optical cavity is found in agreement with the theory inherited from the conservative Hamiltonian NLS equation, without using adjustable parameters [78].

We note an important difference that distinguishes the thermalization and condensation processes discussed here with those reported in the quantum context in Refs. [405,77]. As discussed above, in these works the thermalization process is

achieved thanks to the dye molecules, which thus play the role of an external thermostat. Conversely, in the passive cavity configuration considered here, the process of thermalization solely results from the four-wave interaction mediated by the intracavity Kerr medium, while the 'temperature' is controlled by varying the kinetic energy (degree of coherence) of the injected pump.

*Model of the incoherently pumped passive cavity*

We are interested in the transverse spatial evolution of an optical beam that circulates in a passive optical cavity containing a nonlinear Kerr medium, whose nonlinear response is assumed to be local and instantaneous for simplicity. We thus consider the usual spatial NLS equation

$$i\partial_z\psi = -\alpha\nabla^2\psi - \gamma|\psi|^2\psi - i\delta\psi, \tag{244}$$

which also accounts for the propagation losses through the parameter $\delta$. As usual $z$ ($0 \le z \le L_0$) denotes the longitudinal spatial coordinate, $L_0$ being the length of the Kerr medium and $\nabla^2$ denotes the 2D Laplacian in the transverse plane $\boldsymbol{x} = (x, y)$. As usual in wave condensation (Section 5), we assume that the Kerr nonlinearity is defocusing ($\gamma < 0$), so as to guarantee the modulational stability of the plane wave solution.

The cavity is pumped by an incoherent optical beam of constant intensity $J_0 = A^{-1}\int|\varphi_m(\boldsymbol{x})|^2 d\boldsymbol{x}$, where $\varphi_m(\boldsymbol{x})$ is the amplitude of the pump field injected at the time $t = m\tau_{rt}$, with $m$ the number of round trips, while $A$ denotes the area of integration (i.e., the typical transverse surface section of the beam). As discussed above, the time correlation of the incoherent pump is much smaller than the round trip time, $t_c \ll \tau_{rt}$, i.e., the longitudinal coherence length of the light is much smaller than the cavity length. This means that, in a loose sense, the passive cavity does not behave as a resonant 'phase-sensitive interferometer' [428,266], so that the temporal modes of the cavity do not play any role in the dynamics. In this way, the beam circulating in the cavity and the pump beam are mutually incoherent with each other, and the boundary conditions are not sensitive to the random relative phase among them

$$\psi_{m+1}(z = 0, \boldsymbol{x}) = \sqrt{\rho}\,\psi_m(z = L_0, \boldsymbol{x}) + \sqrt{\theta}\,\varphi_m(\boldsymbol{x}), \tag{245}$$

where $\psi_m(z, \boldsymbol{x})$ denotes the intracavity optical field after $m$ round trips, with $0 \le z \le L_0$, while $\rho$ and $\theta$ respectively refer to the reflection and transmission coefficients of the field intensity, $\rho + \theta = 1$. Note that, for simplicity, we wrote the boundary conditions (245) with the assumption that the length of the cavity $L_0$ coincides with the length of the nonlinear Kerr medium. Because the time correlation ($t_c$) of the pump is much smaller than $\tau_{rt}$, the pump beam $\varphi_m(\boldsymbol{x})$ is uncorrelated with itself at each round trip, $\langle\varphi_m(\boldsymbol{x})\,\varphi_p^*(\boldsymbol{x})\rangle = \delta^K_{m,p}J_0$, where $J_0$ is the average intensity of the pump field and $\delta^K_{m,p}$ denotes the Kronecker symbol. Note that, for the same reason, there is no correlation between the pump and the intracavity field, $\langle\psi_m(z = L_0, \boldsymbol{x})\,\varphi_m^*(\boldsymbol{x})\rangle \simeq 0$. We also assume that the fluctuations of the incoherent pump are statistically homogeneous in space, i.e., its spatial spectrum is characterized by uncorrelated random spectral phases and the average pump intensity $J_0$ does not depend on $\boldsymbol{x}$. Besides the time correlation $t_c$, the incoherent pump is characterized by a spatial correlation length in its transverse surface section, say $\lambda_c$. This correlation length determines the amount of kinetic energy $E_J$ in the pump field, a parameter that will be shown to play a key role in wave condensation.

In order to neglect the temporal dynamics of the cavity, we assume the time correlation of the pump field to be large enough to neglect dispersion effects through the propagation in the Kerr medium. Note that this condition is compatible with the non-resonant cavity condition discussed above, $t_c \ll \tau_{rt}$. For instance, considering a cavity length $L_0$ in the range of a meter, we typically have $\tau_{rt}$ in the range $\sim$10 ns. A time correlation $t_c$ typically less than 1 ns would thus make the cavity non-resonant, while chromatic (or modal) dispersion effects in the Kerr material are usually negligible with such large time correlations [6]. Along the same line, we also assume that the Kerr medium exhibits an anomalous dispersion at the pump frequency, which guarantees the modulational stability of the 3D monochromatic plane wave.

We note that pattern formation in a cavity longer than the coherence length of the light has been considered in Section 4.6.4 (see [262,261]). However, in these previous works the nonlinear medium was characterized by an inertial (photorefractive) nonlinearity, whose response time $\tau_R$ is much longer than the time correlation of the optical field, $t_c$. As discussed in Section 4, such inertial nonlinearity prevents the thermalization of the incoherent optical wave. To summarize, the process of cavity condensation investigated here requires the following hierarchy of the relevant time scales, $\tau_R \ll t_c \ll \tau_{rt}$.

*7.3.1. Mean-field WT kinetic equation*

We combine here the WT kinetic equation that describes the propagation of the field through the Kerr medium ($0 \le z \le L_0$) together with the cavity boundary conditions (245) to derive a mean-field WT kinetic equation. We consider the WT kinetic equation (156) which governs the averaged evolution of the spectrum of the wave at the round-trip $m$, $n_m(z, \boldsymbol{k}_1)\delta(\boldsymbol{k}_1 - \boldsymbol{k}_2) = \langle\tilde{\psi}_m(z, \boldsymbol{k}_1)\tilde{\psi}_m^*(z, \boldsymbol{k}_2)\rangle$. Ignoring for the moment the cavity boundary conditions, the WT equation reads

$$\partial_z n_m(z, \boldsymbol{k}) = -2\delta n_m(z, \boldsymbol{k}) + \mathrm{Coll}[n_m(z, \boldsymbol{k})], \tag{246}$$

where $\mathrm{Coll}[n_m(z, \boldsymbol{k})]$ denotes the collision term [see Eq. (156)]. As discussed in many circumstances, this collision term describes an irreversible evolution towards the Rayleigh–Jeans equilibrium distribution (see Section 5.1.2).

Let us now consider the boundary conditions of the passive cavity. Taking the Fourier transform of Eq. (245) and neglecting the correlations between the intracavity field and the pump field, we have

$$n_{m+1}(z=0,\boldsymbol{k}) = \rho\, n_m(z=L_0,\boldsymbol{k}) + \theta J(\boldsymbol{k}), \tag{247}$$

where the averaged spectrum of the pump field, $J(\boldsymbol{k}_1)\delta(\boldsymbol{k}_1-\boldsymbol{k}_2) = \langle \varphi_m(\boldsymbol{k}_1)\,\varphi_m^*(\boldsymbol{k}_2)\rangle$, is independent of the round trip $m$. The absence of correlation between the intracavity field and the pump field, $\langle \tilde{\psi}_m(z=L_0,\boldsymbol{k})\,\tilde{\varphi}_m^*(\boldsymbol{k})\rangle \simeq 0$, is justified by the assumption $t_c \ll \tau_{rt}$, which makes the pump field uncorrelated with itself at each round trip, $\langle \tilde{\varphi}_m(\boldsymbol{k})\,\tilde{\varphi}_p^*(\boldsymbol{k})\rangle = 0$ if $m \neq p$.

In order to derive a mean-field kinetic equation, we assume that the *averaged* spectrum of the field, $n_m(z,\boldsymbol{k})$, exhibits a slow variation within a single round trip. We note that, contrary to the usual mean-field approach [429,430], we do not assume that the field amplitude $\psi_m(z,\boldsymbol{x})$ exhibits a slow variation within a round trip—the individual speckles of $\psi_m(z,\boldsymbol{x})$ can exhibit rapid variations resulting from the incoherent nature of the beam. Actually, the assumption that the averaged spectrum exhibits slow variations is a rather weak assumption, which implies, in particular, $\theta \ll 1$, $\delta L \ll 1$, and a weak nonlinearity ($U/E \ll 1$). Under this assumption, the evolution of the kinetic equation (246) can be averaged over a round trip. Introducing the slow time derivative of the averaged spectrum, $\partial_t \tilde{n}(t,\boldsymbol{k}) = [n_{m+1}(z=0,\boldsymbol{k}) - n_m(z=0,\boldsymbol{k})]/\tau_{rt}$, where $t = m\tau_{rt} = mL/v_g$, $v_g$ being the group-velocity of the optical field in the Kerr material, we obtain a mean-field kinetic equation

$$\tau_{rt}\,\partial_t \tilde{n}(t,\boldsymbol{k}) = L\,\mathrm{Coll}[\tilde{n}(t,\boldsymbol{k})] + \theta J(\boldsymbol{k}) - \Gamma\,\tilde{n}(t,\boldsymbol{k}), \tag{248}$$

where $\Gamma = \theta + 2\delta L_0$. Note that the parameter $\Gamma$ is related to the finesse of the cavity, which is usually defined as $\mathcal{F} = 2\pi/\Gamma$. This kinetic equation simply provides an averaged description of the evolution of the wave spectrum under the influence of the various different effects, namely the nonlinear interaction, the incoherent pump, and both the cavity losses and the propagation losses. Note that the kinetic equation (248) does not exhibit a $H$-theorem for the nonequilibrium entropy $S[\tilde{n}]$ because of the presence of the losses $\theta$ and $\Gamma$.

As discussed above through the usual kinetic equation (246), the collision term in (248) conserves the intensity $N$ and the density of kinetic energy $E$ of the wave. Then integrating (248) over $\boldsymbol{k}$, the collision term vanishes, which readily gives the expression of the temporal evolution of the intensity of the intracavity optical field

$$N(t) = N(0)\exp(-\Gamma t/\tau_{rt}) + \frac{\theta}{\Gamma} J_0\,[1-\exp(-\Gamma t/\tau_{rt})]\,, \tag{249}$$

where $J_0 = \int J(\boldsymbol{k})d\boldsymbol{k}$ is the pump intensity. According to (249) the time required to fill the cavity, i.e., the injection time, $\tau_{inj} = \tau_{rt}/\Gamma$, plays an important role and it can also be viewed as the 'average life-time that a photon spends in the cavity' ($1/\Gamma$ being the corresponding average number of round trips). Note that Eq. (249) can be obtained directly from the boundary conditions (245) and the NLS Eq. (244) without making use of the high finesse assumption underlying the derivation of the mean field Eq. (248). Eq. (249) reveals that, regardless of its initial value, the intracavity intensity relaxes exponentially towards a stationary value, $N^{st}$, determined by the pump intensity and the cavity-propagation losses

$$N^{st} = \frac{\theta}{\Gamma} J_0. \tag{250}$$

Note that when the propagation losses can be neglected ($\delta = 0$), then the intracavity field intensity coincides with the pump intensity, $N^{st} = J_0$. Proceeding in a similar way, the evolution of the kinetic energy reads,

$$E(t) = E(0)\exp(-\Gamma t/\tau_{rt}) + \frac{\theta}{\Gamma} E_J\,[1-\exp(-\Gamma t/\tau_{rt})]\,, \tag{251}$$

where $E_J = \int \omega(k) J(\boldsymbol{k})d\boldsymbol{k}$ is the kinetic energy of the pump. Accordingly, the energy $E(t)$ relaxes towards the stationary value

$$E^{st} = \frac{\theta}{\Gamma}\, E_J. \tag{252}$$

It is important to note that the energy per particle, $E_J/J_0$, provides a natural measure of the amount of incoherence in the pump field [431]. Then for a fixed value of the pump intensity, $J_0$, the energy $E_J$ will appear as the control parameter of the condensation process in the cavity.

The kinetic equation (248) explicitly shows that the evolution of the spectrum of the intracavity field is ruled by two antagonist effects. On the one hand, the *linear effects* due to the incoherent pumping and to the cavity-propagation losses enforces the spectrum to relax towards the pump spectrum: Neglecting the collision term, the analytical solution of (248) gives $\tilde{n}(t,\boldsymbol{k}) \to \frac{\theta}{\Gamma} J(\boldsymbol{k})$ for $t \gg \tau_{inj} = \tau_{rt}/\Gamma$. On the other hand, as discussed above through the conventional WT equation (246), the *nonlinear Kerr effect* described by the collision term in (248) enforces the field to relax towards the Rayleigh–Jeans distribution (165). We shall see in the next section that in its high-finesse regime ($\Gamma \ll 1$), the dynamics of the cavity is dominated by the collision term in (248), so that the optical field experiences both the processes of thermalization and condensation.

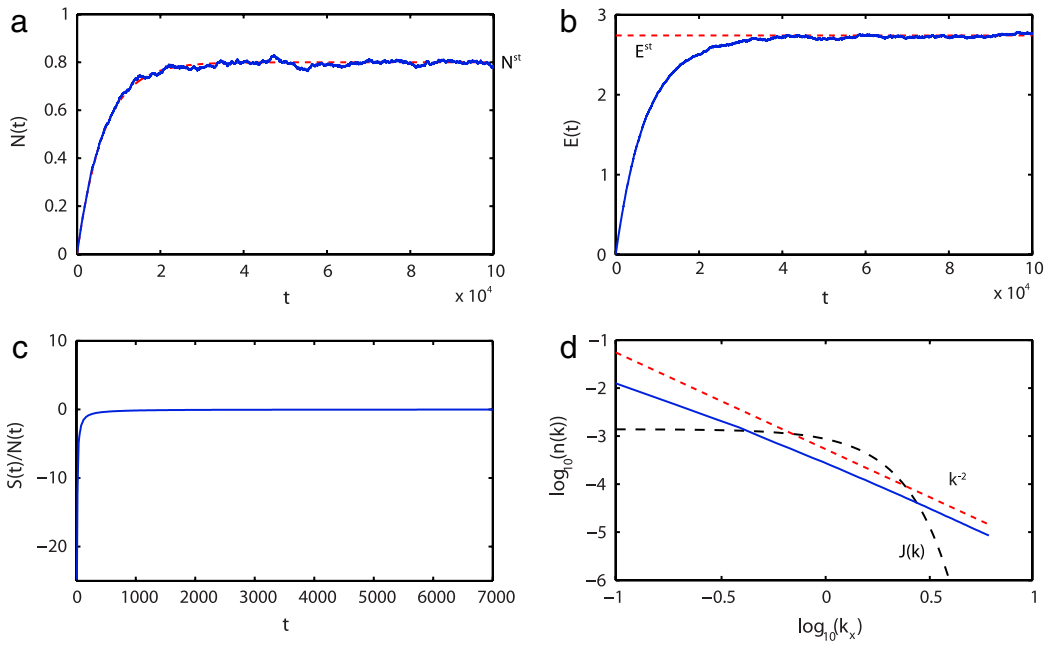


**Fig. 59.** Thermalization in an incoherently pumped passive optical cavity: (a) Evolution of the intracavity field intensity $N$ (in units of the pump power $J_0$) vs. time $t$ (in units of $mL/L_0$), and corresponding temporal evolution of the kinetic energy $E$ (b) and of the 'entropy per particle' $\mathcal{S}/N$ (c). The red dashed line in (a) reports the theoretical prediction of the evolution of the intensity given by (249), the red dashed line in (b) the theoretical stationary value (252), $E^{st}$. (d) Averaged spectrum of the field once the cavity dynamics has reached the stationary state (continuous blue line): The tails of the spectrum exhibits an equipartition of energy among the modes, as described by the Rayleigh–Jeans equilibrium distribution (165), i.e., the power-law $n^{st}(k) \sim k^{-2}$ (red dashed line). The dark dashed line reports the spectrum of the incoherent pump, $J(\boldsymbol{k})$ (characterized by random spectral phases). The parameters are discussed in the text: $A = 64^2\Lambda^2$, $128^2$ modes, $L = 8L_0$, $\theta = 0.001$, and $\alpha = 1.5625 \times 10^{-5}L_0^{-1}$ so that $N^{st} = 0.8J_0$. (For interpretation of the references to color in this figure legend, the reader is referred to the web version of this article.)
*Source:* From Ref. [78].

### *7.3.2. Numerical simulations*

The simulations of the incoherently pumped passive cavity have been performed by integrating numerically the NLS Eq. (244) for the field $\psi_m(z, \boldsymbol{x})$ from $z = 0$ to $z = L_0$. Then we calculate the field $\psi_{m+1}(z = 0, \boldsymbol{x})$ by applying the boundary conditions given by the cavity map (245) at each round trip. For convenience, we normalized the problem with respect to the pump intensity $J_0$, the longitudinal nonlinear length $L_{nl} = 1/(\gamma J_0)$, the healing length $\Lambda = \sqrt{\alpha L_{nl}}$ and the time $\tau_0 = L_0/v_g$. The dimensionless variables are obtained through the transformations $z/L_{nl} \to z$; $\boldsymbol{x}/\Lambda \to \boldsymbol{x}$; $\psi/\sqrt{J_0} \to \psi$; $\varphi/\sqrt{J_0} \to \varphi$; $\delta L_{nl} \to \delta$; $L_0/L_{nl} \to L_0$ and $t/\tau_0 \to t = mL_0$.

*Cavity thermalization*

We report in Fig. 59 a typical behavior of the dynamics of the incoherently pumped passive cavity. We considered here the natural configuration in which an initial empty cavity, $\psi_{m=0}(z, \boldsymbol{x}) = 0$ for $0 \le z \le L_0$, is progressively filled by the incoherent pump. The injected pump wave is characterized by a Gaussian-shaped spectrum with random spectral phases—the realizations of the random spectral phases are generated independently of each others, so as to make the incoherent pumps $\varphi_m(\boldsymbol{x})$ uncorrelated at each round trip $m$. In this example we considered a transverse area of $A = 64^2\Lambda^2$ with $128^2$ modes, a cavity length of $L_0 = 8L_{nl}$ and a reflection coefficient of $\theta = 0.001$. The value of the loss parameter $\delta = 1.5625 \times 10^{-5}L_{nl}^{-1}$ has been chosen in such a way that $N^{st} = 0.8J_0$. Note that the small value of the transmission coefficient considered here can be increased by considering a longer cavity [78]. As expected, the cavity exhibits a turbulent behavior, in which the random field amplitude $\psi_m(z, \boldsymbol{x})$ is characterized by statistically homogeneous spatial fluctuations. Because of the high finesse the pump wave slowly enters into the cavity. As predicted by expression (249), the intracavity intensity $N(t)$ relaxes exponentially to the stationary value $N^{st}$ (see Fig. 59(a)). The kinetic energy $E$ of the field in the cavity follows a similar behavior, as illustrated in Fig. 59(b), which indicates that the optical field reaches a statistical stationary state in the cavity. This is corroborated by the evolution of the entropy 'per particle', $S/N$, which has been normalized to the intensity $N(t)$, so as to compensate for the growth of the 'number of particles' in the cavity. Despite the fact that the kinetic equation (248) does not exhibit a $H$-theorem, the temporal evolution of $S/N$ is reminiscent of the usual process of entropy production and saturation encountered in a conservative wave system (see e.g., [431,307,73]). This is due to the fact the collision term in the kinetic equation (248) dominates the dissipative terms related to the cavity and the propagation losses. In particular, the saturation of the process of entropy growth reported in Fig. 59(c) corroborates the fact that the turbulent

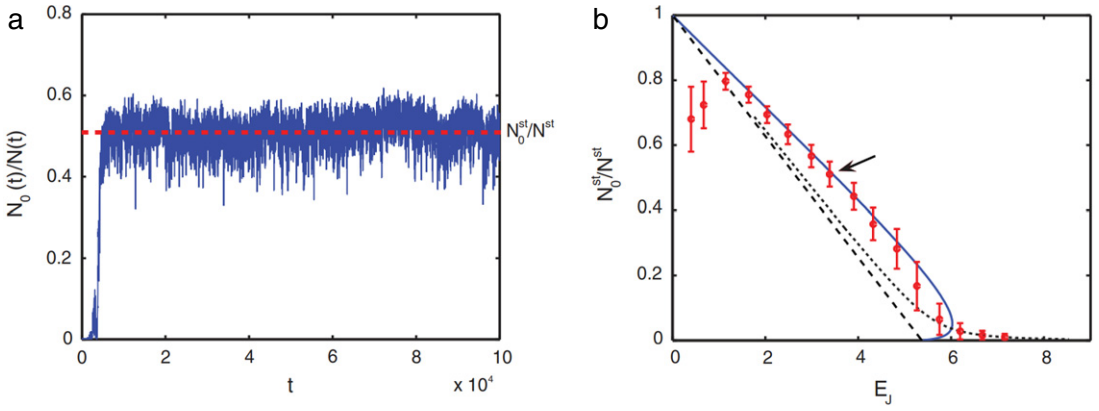


**Fig. 60.** Wave condensation in an incoherently pumped passive optical cavity: (a) Evolution of the fraction of condensed power $N_0(t)/N(t)$ vs. time $t$ (in units of $mL/L_0$) corresponding to the simulation reported in Fig. 59. The condensate growth saturates to a constant value $N_0^{st}/N^{st}$, which is in agreement with the theory given by Eq. (255) (red dashed line). (b) Condensation curve: fraction of condensed power in the stationary equilibrium state $N_0^{st}/N^{st}$ vs. the kinetic energy of the pump $E_J$. The condensation curve is computed for a constant value of the pump intensity $J_0$, while $E_J$ is varied by modifying the degree of coherence of the pump (i.e., its spectral width). The blue solid line is a plot of Eq. (255) and refers to the Bogoliubov's regime. The black dotted line is a plot of Eqs. (253) and (254) and refers to the WT regime beyond the thermodynamic limit ($\mu \neq 0$), while the dashed black line refers to the thermodynamic limit [$\mu \to 0$ in Eqs. (253) and (254)]. The red points correspond to the numerical simulations of the NLS Eq. (244) with the cavity boundary conditions (245). The bars denote the amount of fluctuations in $N_0^{st}/N^{st}$ once the equilibrium state is reached. The arrow in (b) denotes the point corresponding to the simulation reported in (a), $N_0^{st}/N^{st} \simeq 0.51$. Parameters are the same as in Fig. 59.
*Source:* From Ref. [78].

dynamics of the cavity tends to relax towards a statistical stationary state. We recall in this respect that the entropy, by its definition, is very sensitive to small variations of the tails of the spectrum of the field.

We have analyzed with care the evolution of the spectrum of the field, which has been averaged over the time once the stationary state has been reached, i.e., for $t \gg \tau_{inj} = \tau_{rt}/\Gamma$. More specifically, we compared an averaging of 1000 spectra recorded in different time intervals spaced by 10 000 $\tau_0$, and we did not identify any evolution of the averaged spectrum. We underline that, in the presence of a high finesse, the spectrum of the field relaxes towards a steady state whose tails verify the property of *energy equipartition* among the modes (see Section 7.3.1). This is illustrated in Fig. 59(d), which shows that the tails of the averaged spectrum exhibit the power-law distribution, $n^{st}(k) \sim k^{-2}$, inherent to the thermodynamic equilibrium distribution (165).

*Cavity condensation*

In the previous paragraph we have shown that, in the presence of a high finesse, the intracavity field exhibits a relaxation towards an equilibrium state that verifies the property of energy equipartition. As a consequence of this thermalization effect, we shall see that the optical field exhibits a condensation process that can be described quantitatively by adapting the theory developed for the purely conservative and Hamiltonian NLS equation [71,73].

We report in Fig. 60(a) the fraction of power, $N_0/N$, condensed into the fundamental Fourier mode, $\boldsymbol{k} = 0$, as a function of time. This evolution of the condensate amplitude corresponds to the simulation of the cavity discussed in the previous paragraph through Fig. 59. Fig. 60(a) shows that the growth of the condensate fraction $N_0/N$ saturates to a constant value during the temporal evolution of the cavity. It is interesting to note that the condensate fraction reaches its asymptotic stationary value ($t \sim 5000$ in Fig. 60(a)) *well before* that the cavity reaches its stationary regime ($t \sim 40\,000$ in Fig. 59(a)). We shall see below in Section 7.3.2 that this is due to the fact that, thanks to the large finesse considered here, the condensate amplitude $N_0(t)$ follows adiabatically the corresponding equilibrium value determined by the instantaneous intensity $N(t)$ of the intracavity field. Let us analyze here the asymptotic condensate amplitude that the field reaches in the stationary regime of the cavity, $N_0^{st}$. Since the passive cavity behaves essentially as a conservative system, we may expect that the stationary value of the condensate amplitude $N_0^{st}/N^{st}$ may be predicted from the theory developed for the conservative (Hamiltonian) problem. We shall now adapt the Hamiltonian condensation theory to the dissipative cavity problem considered here. We anticipate that, as illustrated in Fig. 60(b), a good agreement is obtained between the theory and the cavity simulations without using adjustable parameters.

We have discussed in Section 5.2 the condensate fraction as a function of the Hamiltonian ('condensation curve') in the weak and strong nonlinear regimes of interaction. In the cavity problem discussed here, the essential difference with respect to the conservative (Hamiltonian) problem is that the intensity ('particle density') $N(t)$ and the energy $H(t)$ are not conserved quantities (see Fig. 59). However, as discussed above, in the high finesse regime the cavity behaves as a conservative system, so that the condensation theory of [73] can be considered into the stationary regime. There is another important aspect to note. *Contrary to the conservative NLS equation where the conserved Hamiltonian plays the role of the control parameter in the condensation curve, in the cavity configuration considered here the natural control parameter is the energy of*

*the pump field.* Below we shall thus express the condensate fraction as a function of the kinetic energy of the pump, $E_J$, and the cavity-propagation losses $(\delta, \theta)$. The condensate amplitude at equilibrium is calculated by following two different approaches.

*Weak condensation: Wave turbulence regime*

In the presence of a pump characterized by a poor coherence (i.e., a high kinetic energy $E_J$), the condensate fraction $N_0^{st}/N^{st}$ is weak, and the dynamics is well described by the WT theory, $U/E \ll 1$. In this case the theory of wave condensation can be applied straightforwardly by simply replacing the values of the intensity and condensate amplitude by the corresponding values in the stationary regime of the cavity, $N \to N^{st}$ and $N_0 \to N_0^{st}$ [see Eqs. (177) and (178)]. Introducing the kinetic energy of the pump from (252), one obtains

$$E_J(\mu) = \left(J_0 - \frac{\Gamma N_0^{st}}{\theta}\right) \frac{\sum_{\boldsymbol{k}}{}' \frac{\alpha k^2}{\alpha k^2 - \mu}}{\sum_{\boldsymbol{k}}{}' \frac{1}{\alpha k^2 - \mu}}, \tag{253}$$

$$\frac{N_0^{st}(\mu)}{N^{st}} = \frac{1}{-\mu} \frac{1}{\sum_{\boldsymbol{k}} \frac{1}{\alpha k^2 - \mu}}. \tag{254}$$

We recall here that finite size effects of the system are taken into account through the non-vanishing chemical potential, $-\mu > 0$ (see Section 5.2.2). The fraction of condensed particles $N_0/N$ vs. the energy of the pump $E_J$ is reported in Fig. 60(a) (dotted line). In particular, in the thermodynamic limit ($\mu \to 0$), the condensation curve reduces to a straight line (dashed line in Fig. 60(a)), $E_J = (J_0 - \Gamma N_0^{st}/\theta)/Q$, where $Q = \sum' \alpha^{-1} k^{-2}/(M-1)$ and $M$ is the number of modes. The thermodynamic limit thus allows us to define a critical value of the pump energy below which the cavity system undergoes wave condensation, $E_J^c = J_0/Q$.

*Strong condensation: Bogoliubov's regime*

As the coherence of the pump field is increased (i.e., the kinetic energy $E_J$ decreases), the condensate amplitude becomes strong, so that the dynamics enters into the nonlinear Bogoliubov regime, as discussed in detail in Section 5.2.2. In this regime one can still derive a closed relation between the condensate amplitude and the energy into the Bogoliubov basis [71,73]. However, caution should be exercised when applying the procedure of Refs. [71,73] to the cavity configuration considered here. We refer the reader to Ref. [78] for a discussion of this point. It turns out that, instead of expressing the condensate fraction as a function of the total energy $H$, the condensate fraction can be expressed in terms of the kinetic energy of the pump $E_J$ and of the losses $(\theta, \delta)$ in the following form

$$E_J = -\gamma N_0^{st} \left(J_0 - \frac{\Gamma N_0^{st}}{\theta}\right) + \left(J_0 - \frac{\Gamma N_0^{st}}{\theta}\right) \frac{M-1}{\sum_{\boldsymbol{k}}{}' \frac{\alpha k^2 + \gamma N_0^{st}}{\alpha^2 k^4 + 2\alpha\gamma N_0^{st} k^2}}. \tag{255}$$

The condensation curve (255) is plotted in Fig. 60(b) (blue line). We recall here that the hysteresis predicted at the transition to condensation $E_J \sim E_J^c$ is not physical [73], since the transition is continuous, as described by the WT theory [see Eqs. (253) and (254)].

*Adiabatic condensation*

In Fig. 60(b) we compare the theoretical condensation curves in the weak [Eqs. (253) and (254)] and strong [Eq. (255)] condensation regimes with the numerical simulations of the passive cavity. The 'error bars' denote the amount of fluctuations (variances) of the condensate fraction $N_0^{st}(t)/N^{st}(t)$ once the stationary state is reached in the cavity. We note that in the very high condensation regime ($E_J < 1$) there exists some significant discrepancy between the theory and the simulations, a feature that will be discussed in the next paragraph. Besides such high condensation regime, we note that the theory is in quantitative agreement with the simulations of the cavity, without using any adjustable parameter. This good agreement stems from the fact that we considered a cavity characterized by a large finesse, $\mathcal{F} > 10^3$. As mentioned above in Section 7.3.2, thanks to such a large finesse, the intracavity field reaches thermal equilibrium before that the cavity reaches its stationary regime, i.e., the time required to achieve thermalization, say $\tau_{th}$, is smaller than the injection time, $\tau_{inj} = \tau_{rt}/\Gamma$ [see Eq. (249)]. In this way, the variations of the intensity $N(t)$ and of the energy $E(t)$ in the cavity are very slow as compared to the thermalization process, so that the equilibrium state of the intracavity field follows adiabatically the slow growths of $N(t)$ and $E(t)$.

It is interesting to note in Fig. 60(a) that the condensate fraction rapidly reaches its asymptotic equilibrium value $N_0^{st}/N^{st}$, and subsequently keeps such a constant value in spite of the slow growths of $N(t)$ and of $E(t)$. This is a consequence of the fact that the intracavity field is permanently at equilibrium during the adiabatic condensation process. This aspect becomes apparent through the analysis of the WT condensation curve (254) and (253). Indeed, in the thermodynamic limit ($\mu \to 0$),

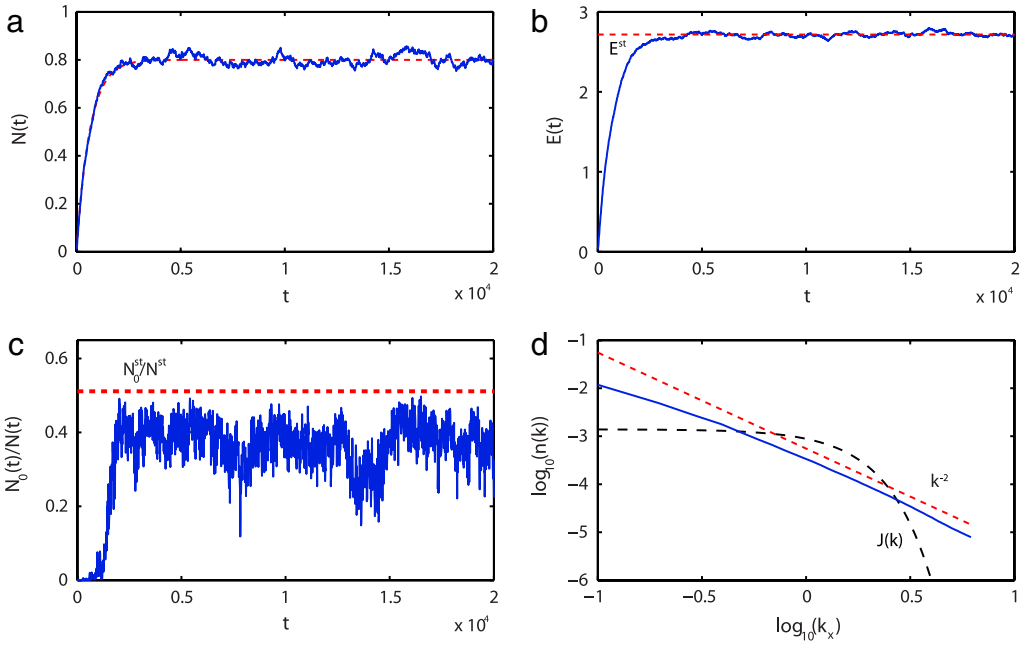


**Fig. 61.** Partial condensation and thermalization in an incoherently pumped passive optical cavity: Simulation of the same configuration of the cavity considered in Figs. 59–60, except that the transmission coefficient is $\theta = 0.01$. (a) Evolution of the intracavity field intensity $N$ vs. time $t$ (in units of $mL/L_0$), and corresponding temporal evolution of the kinetic energy $E$ (b). The red dashed line in (a) reports the theoretical prediction of the evolution of the intensity given by (249), the red dashed line in (b) the theoretical stationary value (252). (c) Temporal evolution of the condensate fraction $N_0(t)/N(t)$ (solid blue line), and corresponding theoretical value predicted by Eq. (255) (red dashed line). (d) Averaged spectrum of the field once the cavity dynamics has reached the stationary state (solid blue line). The red dashed line reports the Rayleigh–Jeans (165) power-law $n^{st}(k) \sim k^{-2}$. The dark dashed line reports the spectrum of the incoherent pump, $J(\boldsymbol{k})$ (characterized by random spectral phases). (For interpretation of the references to color in this figure legend, the reader is referred to the web version of this article.)
*Source:* From Ref. [78].

the fraction of condensed power takes the following simple expression, $N_0/N = 1 - QE(t)/N(t)$. Recalling that the intensity and the energy evolve according to $N(t) = N^{st}[1 - \exp(-\Gamma t/\tau_{rt})]$ and $E(t) = E^{st}[1 - \exp(-\Gamma t/\tau_{rt})]$ (see Section 7.3.1), then it becomes apparent that the condensate fraction does not depend on time, $N_0/N = const$, simply because the ratio $E(t)/N(t) = E^{st}/N^{st}$ remains constant. The same conclusion is obtained from an inspection of the condensation curve in the Bogoliubov's regime. The analysis of Eq. (255) reveals that, except for small values of $N$ for which the Bogoliubov approach is not justified, the condensate fraction $N_0/N$ does not depend on the variations of the intensity [i.e., $N(t)$] if the ratio $E(t)/N(t)$ is kept constant. This result may be interpreted intuitively by recalling that the 'energy per particle' $E/N$ provides a natural measure of the amount of incoherence in a random wave [431]. In this way, an increase of the number of particles with a constant value of $E/N$ does not lead to a change of the fraction of condensed particles. To summarize, as the cavity gets filled by the incoherent pump, the intracavity optical field rapidly relaxes towards a thermal equilibrium state, which thus follows adiabatically the slow growths of the intensity and of the energy in the cavity.

*Influence of the finesse: Partial condensation and thermalization*

Up to now we have restricted our study to the analysis of the cavity in its high-finesse regime. However, as one may expect, the cavity no longer behave as a conservative system as the finesse decreases. This is illustrated in Fig. 61, which reports the simulation of the same configuration of the cavity considered in Fig. 59, except that the transmission coefficient has been increased to $\theta = 0.01$. We see in Fig. 61 that, while the intensity $N(t)$ and the energy $E(t)$ follow the expected exponential relaxation towards the stationary regime, the condensate fraction $N_0^{st}/N^{st}$ no longer reach the expected theoretical value of $N_0^{st}/N^{st} = 0.51$ [from Eq. (255)], and the tails of the equilibrium spectrum exhibit some appreciable deviations from the $k^{-2}$ Rayleigh–Jeans power law. In other therms, the cavity and propagation losses $(\delta, \theta)$ are no longer negligible with respect to the collision term in the mean-field kinetic Eq. (248). Nevertheless, the dynamics of the cavity still relaxes towards a stationary regime, which is characterized by a non-vanishing value of the condensate amplitude, i.e., the cavity dynamics exhibits a process of partial condensation and partial thermalization.

The analysis of the numerical simulations reveal that the transition from the complete to the partial thermalization typically occurs when the thermalization time inherent to the conservative (Hamiltonian) NLS equation, $\tau_{th}$, becomes of the same order as the average life time of a photon in the cavity, $\tau_{inj} = \tau_{rt}/\Gamma$. In the regime of adiabatic thermalization discussed here above we had $\tau_{th} \ll \tau_{inj}$. Conversely, when $\tau_{inj} \sim \tau_{th}$ the optical field does not spend sufficient time in the

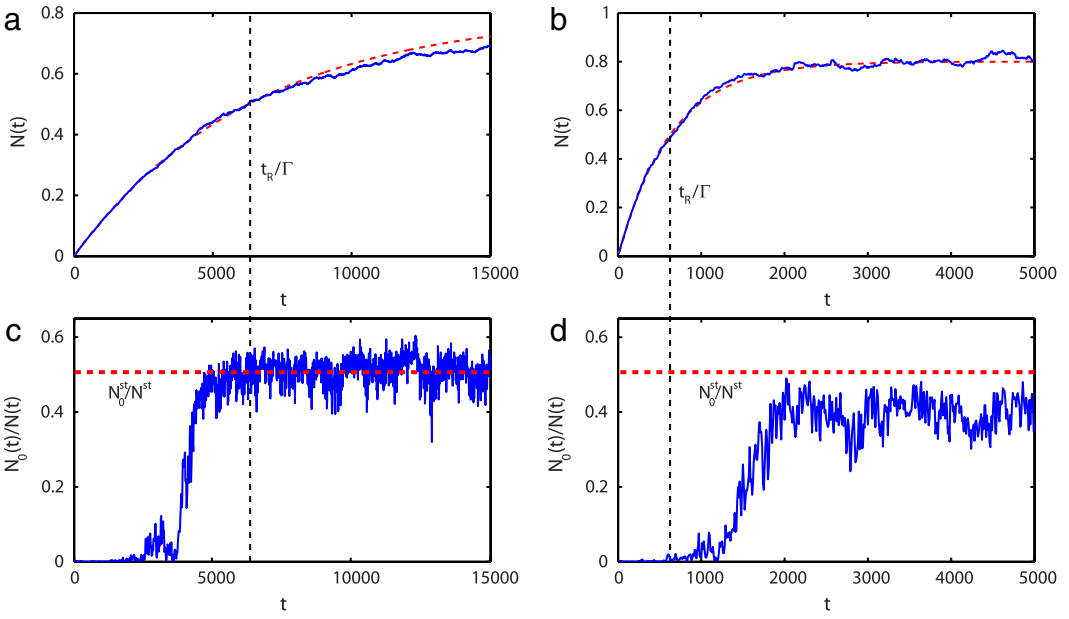


**Fig. 62.** Comparison of the condensate growth time, $N_0(t)/N(t)$, with the injection time $\tau_{inj}$ in a passive optical cavity. (a) and (c) respectively report a zoom of Figs. 59(a) and 60(a) ($\theta = 0.001$). (b) and (d) respectively report a zoom of Fig. 61(a) and (c) ($\theta = 0.01$). For a high finesse [(a) and (c)], the condensate fraction adiabatically reaches its thermal equilibrium value over a time smaller than $\tau_{inj} = \tau_{rt}/\Gamma$. As the finesse decreases [(b) and (d)], a partial condensation takes place and the growth of the condensate occurs over a time larger than $\tau_{inj}$.
*Source:* From Ref. [78].

cavity to achieve a complete thermalization process. This interpretation of the cavity dynamics also explains the discrepancy between the theory and the simulations observed in Fig. 60(b) in the high condensation regime, i.e., for $E_J < 1$. Indeed, the thermalization time $\tau_{th}$ of the conservative (Hamiltonian) problem, is known to increase in a significant way in the highly condensed regime. For instance, the numerical simulations reveal that $\tau_{th}$ typically increases by a factor $\sim$10 when the equilibrium condensate fraction increases from 50% to 95%. This can be explained by the fact that in the highly condensed regime the energy $H$ is very small, so that the correlation length of the initial field exceeds the system size, $\lambda_c > \sqrt{A}$. The time required to reach thermal equilibrium starting from such a highly coherent state is very large: The generation of the new frequency components necessary to reach the Bogoliubov's equilibrium state (i.e., energy equipartition $\langle |b_k|^2 \rangle = T/\omega_B(k)$, see Section 7.3.2) requires a very long transient as compared to the corresponding transient of a highly energetic initial condition verifying $\lambda_c \ll \sqrt{A}$, a feature which is clearly apparent in the simulations. Accordingly, in the high condensation regime of the cavity (small values of $E_J$), the transient time $\tau_{th}$ becomes larger than the injection time $\tau_{inj}$, which merely explains the significant discrepancy between the theory and the numerics observed for $E_J < 1$ in Fig. 60(b).

It is interesting to note in Fig. 61 that, although the intracavity field does not reach thermal equilibrium, the growth of the condensate fraction may take place over a time larger than $\tau_{inj}$. This is illustrated in Fig. 62, which compares the injection time $\tau_{inj}$ with the growth-time of the condensate for the two cases analyzed previously through Figs. 60–61. Contrary to the adiabatic regime in which the condensate fraction reaches its asymptotic equilibrium value before $\tau_{inj}$ (Fig. 62(a), (c)), in the presence of a lower finesse the growth-time of the condensate becomes larger than $\tau_{inj}$ (Fig. 62(b), (d)). This indicates that, beyond the simple reasoning that compares $\tau_{inj}$ and $\tau_{th}$, the cavity system has a kind of cumulative memory effect, which allows the intracavity optical field to build the coherent dynamics necessary for the emergence of the condensate.

Finally, we refer the reader to Ref. [78] for a study of cavity condensation for different values of the transmission coefficient, $\theta$. The study reveals that the condensation process is degraded as the parameter $\theta$ increases. More precisely, the equilibrium condensate fraction $N_0^{st}/N^{st}$ still grows as the pump energy $E_J$ is decreased. However, at small energies $E_J$, the condensate fraction saturates for the same reason as that discussed above in Fig. 60(b).

The influence of the cavity length $L$ on the dynamics of condensation was also considered in Ref. [78]. The idea was to qualitatively assess the influence of the perturbation induced by the pump at each round trip on the coherent state of the condensed optical field. The analysis of the numerical results do not reveal any qualitative difference in the dynamics of the cavity or in the stationary value of the condensate fraction $N_0/N$. This indicates that the there exists a large flexibility in the choice of the parameters that define a particular experimental configuration of the passive optical cavity. For instance, the small value of the transmission coefficient considered in Figs. 59–60 (i.e., $\theta = 0.001$), may be increased in a substantial way by considering a longer cavity.

We finally note that experiments are in progress in different configurations in order to study these effects of thermalization and condensation in incoherently pumped passive optical cavities.

### 7.4. Importance of coherent structures and coherent phase effects

#### 7.4.1. Role of coherent structures (wave collapse and quasi-solitons)

The dynamics of large scale coherent structures in a turbulent environment is a long standing problem that is still the subject of current investigations in different area of nonlinear physics. Indeed, together with the weak turbulence component, the system can include coherent structures which are characterized by a strong spectral phase correlation, and thus violate the assumption of phase randomness. Note that, from a general perspective, the dynamic breakdown of the weak turbulence approximation associated with nonlinear coherent structures was addressed in Refs. [385,51]. In this review we have already discussed two important classes of large scale coherent structures. On the one hand, the homogeneous plane-wave solution was discussed in Section 5.2.2 in the defocusing regime of the NLS equation in the framework of 2D or 3D condensation. In this case, owing to the Bogoliubov transformation, the WT theory provides an accurate description of the interaction between the coherent plane-wave component and the incoherent fluctuations about the condensate [40,73]. On the other hand, in Section 5.2.1 we discussed the role of soliton-like coherent structures in the framework of soliton turbulence through the analysis of non-integrable focusing NLS equations. In the following we briefly comment two other important examples of large scale coherent structures evolving in a turbulent environment, namely, collapse filaments and quasi-solitons.

Let us first comment wave collapse in the framework of the focusing regime of the multi-dimensional NLS equation [46]. In this case, the inverse cascade of particles (i.e., power) towards the fundamental mode $\boldsymbol{k} = 0$ does not lead to condensation, because the homogeneous plane wave solution is modulationally unstable. In the focusing regime collapsing filaments are known to form, and their main role is to reverse the flux of particles, i.e., they induce a *secondary cascade* which carries particles towards high frequency components. While the primary cascades of energy and particles can be accurately described by the WT theory through Kolmogorov–Zakharov nonequilibrium stationary solutions [37,40] (see Section 5.1.2), the situation is different for the secondary cascade of particles induced by wave collapse. In this case, the flow in frequency space simply results from the collapsing filament in real physical space, in which the wave intensity is squeezed from large scales to small scales in a highly organized and coherent fashion. In this case, statistical considerations can be introduced by considering the intermittent nature of such collapse events, especially as regard their uncertainty of occurrence in time and space. Because the events involve large amplitude fluctuations, their impact on the probability density function of the field is to cause an elevation in the tails of the distribution. It was argued in Ref. [46] that collapse filaments can be at the origin of intermittent-like behaviors in WT—though a rigorous theoretical description of this idea still needs to be elaborated, in relation with the existence of WT cycles discussed in Ref. [40].

Quasi-soliton turbulence is another important example in which large scale coherent structures deeply affect the turbulent behavior of the system [47]. Quasi-solitons refer to soliton with a finite life-time: The soliton solution slowly loses its power through a process analogous to Cherenkov radiation. The presence of quasi-solitons in a system of random waves then leads to a breakdown of the WT predictions. In particular, numerical simulations of the so-called Majda, McLaughlin, Tabak equation [432–434] in the presence of forcing and damping at different scales revealed the formation of nonequilibrium stationary spectra of turbulence which can significantly differ from the Kolmogorov–Zakharov predictions. This problem was recently addressed in Ref. [332]. In this work the authors proposed a new mechanism of turbulent transfer that is radically different from that described by the weakly nonlinear WT approach. In Ref. [332] the authors recognized the fundamental role that play quasi-solitons in the formation of the nonequilibrium stationary state discussed in [432–434]. They showed that the direct energy cascade is carried by gradually deforming the quasi-soliton pulse heads, while the inverse cascade is carried by radiation to the corresponding tails. Furthermore, by remarking that quasi-solitons exhibit a weak interaction among each others, they have been able to predict a nonequilibrium stationary spectrum by computing an adiabatic change of the wave packet. A remarkable good agreement between this theoretical prediction and the numerical simulations has been obtained in Ref. [332].

#### 7.4.2. Role of vortices and the BKT transition

As discussed in Section 5, the WT theory provides an accurate prediction of the condensate fraction vs. the energy of the wave. We underline that a quantitative agreement between the theory and the simulations has been obtained, without using adjustable parameters. It is important to remark that the WT theory ignores the role of vortices, since they are inherently coherent topological structures that cannot be described by the kinetic approach. However, vortices are robust topological phase defects that have been the subject of lot of studies in relation with wave condensation in different configurations of forcing and damping at small and large scales (see e.g., [337–341]). For some reviews on this vast literature we refer the reader to [435,82].

In the weakly nonlinear regime near by the transition to condensation, $H \sim H_{\rm tr}$, the random wave exhibits a large number of zeros. These are not nonlinear (Pitaevskii) vortices, because the nonlinearity is small so that their shapes are rapidly evolving during the temporal evolution. For this reason such zeros of the field are called 'ghost vortices'. As the energy is decreased, the mean inter-vortex distance becomes larger than the healing length, then the system becomes nonlinear and most of the zeros of the field can be identified as nonlinear vortices. In particular, true nonlinear vortices can exist in the highly nonlinear regime in the presence of a strong condensate. In this regime, vortices of opposite circulation can annihilate by pairs in 2D. But they may also exhibit complex motions analogous to those known in 2D-Euler systems. In particular, two

close like-signed vortices can rotate one around each other, while vortices of opposite signs (vortex dipole) can move along a straight line perpendicular to the line connecting the vortex pair. As a rather general rule, the number of vortices decay in time following a logarithmically law in 2D [338], a property that has not been explained theoretically so far. In 3D the vortex centers are located on 1D curves and the annihilation takes the form of a shrinking of vortex loops that suddenly disappear. Vortex loops can also be interlocked one with each other, a noteworthy property of superfluid turbulence [435].

To summarize, the general idea is that vortices affect the nonequilibrium transient process leading to the formation of the condensate, while in the final stage, when all vortices have annihilated, the system comprises a coherent uniform component immersed in a sea of turbulent fluctuations ('phonons'). The regime in which vortices may play a relevant role in the process of wave condensation is in the transition regime, in which the system is just between the weak and the strong nonlinear regimes. In particular, as compared to 3D, in 2D the numerical simulations reveal the existence of significant large fluctuations in the condensate fraction, as illustrated in Fig. 30 in Section 5. Indeed, large jumps in the condensate fraction have been observed in the long term evolution of the wave system [73]. A different perspective to study these properties is provided by the BKT theory.

*BKT transition*

The BKT transition has been experimentally observed in liquid helium films, 2D superconductors, superconducting Josephson-junction arrays, and more recently in ultracold Bose gases [436]. In this latter case, the BKT theory provides the general framework to study 2D superfluidity. We refer the reader to [437] for a recent pedagogical review on this subject. In two dimensions the random wave does not exhibit true long-range coherence, but rather 'quasi-long-range coherence'. Indeed, the logarithmic divergence of the correlation function indicates that the destruction of long-range order is only marginal in two dimension. Making use of the Bogoliubov approach, one can show that a quantum Bose gas at low temperature exhibits a strong suppression of density fluctuations, so that its fluctuations are in substance only *phase fluctuations*. This allows one to point out interesting analogies with different systems, such as, e.g., spins on a lattice, since in the limit of purely phase fluctuations, the low energy Hamiltonian can be approximated by the continuous version of the Hamiltonian of the XY spin model. It turns out that, at low temperature, an interacting 2D Bose gas is characterized by a correlation function which decays algebraically at large distances. Such a slow decay reflects the property of quasi long-range-order.

From the microscopic point of view, the key conceptual ingredient of the BKT theory is that, in addition to phonons described by the Bogoliubov approach, vortices constitute a natural source of phase fluctuations. Below the BKT critical temperature, $T_{\mathrm{BKT}}$, vortices can exist only in the form of bound dipole pairs with opposite circulation. These pairs have a short-range effect and weakly affect the long-range behavior of the correlation function. On the other hand, above $T_{\mathrm{BKT}}$, unbinding of vortex pairs and proliferation of free vortices becomes energetically favorable, which leads to a scrambling of the phase dynamics and thus to a destruction of quasi long-range-order. The BKT transition may thus be viewed as a 2D phase transition characterized by the apparition of a topological 'quasi-long-range' order.

Although these aspects have been the subject of many theoretical and experimental efforts in different physical contexts, they have not yet been studied in detail in purely classical wave systems, although semi-classical approaches have been developed to describe the BKT transition observed in Bose gases [438,439]. Note in this respect that nonlinear optics opens the experimental access to study the BKT transition using standard optical setups [377]. In this way, we can envisage the experimental observation of the BKT transition with optical waves in a near future.

### 7.4.3. Role of coherent phase effects

The WT theory has been shown to provide a reliable statistical description of the evolution of weakly nonlinear incoherent waves in different circumstances. In its basic form, the theory does not account for the existence of phase correlations between distinct incoherent waves. However, there exists particular conditions in which phase correlations emerge spontaneously in a system of incoherent waves. We note in this respect that the Bogoliubov transformation can be viewed as a reformulation of the problem in a different basis so as to avoid such correlations. In this way, anomalous correlations have been recently studied in the process of wave condensation, so as to provide a description of a periodic evolution of the condensate fraction with time (propagation distance) [343].

The spontaneous emergence of correlations between distinct incoherent wave components has been also clearly identified in the important problem of the resonant three-wave interaction. It has been shown that, when the group-velocity of the high-frequency component (pump wave) coincides with the group-velocity of one of the daughter waves (i.e., idler wave), then this latter idler component absorbs the incoherence of the pump wave, then allowing the other daughter wave (signal) to evolve towards a fully coherent state [21,440–443]. Note that this phenomenon has been shown to also occur in optical parametric oscillators [444]. As a matter of fact, this effect of coherent signal generation from an incoherent pump wave is the essential mechanism underlying the existence of mixed coherent–incoherent solitons (i.e., solitons composed of both coherent and incoherent waves) in instantaneous response nonlinear media [21,22]. This is illustrated in Fig. 63, which represents the one-dimensional evolution of three resonantly interacting waves. The initial condition (a) refers to an incoherent pump ($A_3$) in the presence of a small random noise of the signal ($A_1$) and idler ($A_2$) waves. When the group-velocities of the pump and idler waves are matched ($v_3 = v_1$), the incoherence of the pump is transferred to the idler field, which permits the signal to reach a highly coherent soliton-like structure (Fig. 63(c)). We note in particular that the

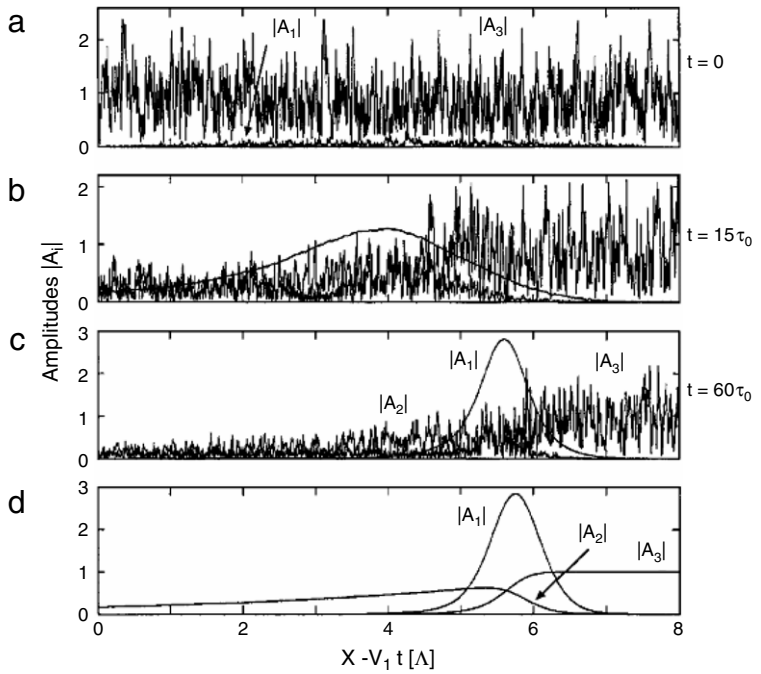


**Fig. 63.** Three-wave solitons composed of both coherent and incoherent waves: (a–c) Generation of the coherent soliton component (signal wave, $A_1$) from the incoherent component (pump wave, $A_3$) in the 1D three-wave interaction. The evolution of the three waves is represented in the reference frame travelling at the group-velocity of the signal wave ($v_1$). The incoherence of the pump is transferred to the idler wave ($A_2$), which allows the signal component to evolve towards a highly coherent state. The existence of this mixed coherent–incoherent soliton relies on the spontaneous emergence of a phase correlation (mutual coherence) between the incoherent pump and idler fields ($\langle A_3 A_2^* \rangle \neq 0$). Panel (d) shows the corresponding coherent three-wave interaction soliton that is generated from a fully coherent pump wave.
*Source:* From Ref. [21].

generated coherent signal pulse exhibits the same soliton-shape as the corresponding soliton generated by a fully coherent pump [445–447], as revealed by the comparison of Fig. 63(c) and (d). The spontaneous emergence of correlations between incoherent waves can also lead to a condensation-like process that occurs far from thermal equilibrium [448,441]. From a more general perspective, the evolution of the spatio-temporal coherence properties of three resonantly coupled partially incoherent waves has been widely studied in the past [449–452] and is still the subject of current investigations [448,444, 453–457,443,458,459]. It would be interesting to construct a generalized WT formulation of random nonlinear waves that would account for a possible mutual correlation between distinct incoherent wave components.

### *7.5. Some additional open problems*

#### *7.5.1. Spontaneous repolarization*

The statistical description of partially polarized optical waves in the framework of the WT theory has not been specifically discussed in this review. In principle, nonlinear polarization effects require a vector description of the optical field which can be formulated on the basis of a vector NLS equation, as discussed in many different cases [171,138,6]. From this point of view, the WT theory considered in the framework the scalar NLS equation should be extended to the vector NLS equation. Note that this aspect has already been discussed in different contexts in the literature [97,460,344,431,461,462,140,463].

From a different perspective, the study of nonlinear polarization effects revealed a remarkable phenomenon of repolarization of an optical wave without loss of energy. Contrarily to conventional polarizers which are known to waste 50% of unpolarized light, Heebner et al. proposed in 2000 a "universal polarizer" performing repolarization of unpolarized light with 100% efficiency [464]. By using the photorefractive two-beam coupling, it was shown in [464] that unpolarized light can be converted to a state of linear polarization with essentially a unit efficiency. This phenomenon can be termed "polarization attraction", in the sense that all input polarization configurations are transformed into a well-defined polarization state. The existence of a phenomenon of polarization attraction has been also demonstrated in the framework of a *counter-propagating configuration of the four-wave interaction* in optical fiber systems [465]. This effect contrasts with the commonly accepted idea that an optical field should undergo a depolarization process in the presence of Kerr nonlinearity, as discussed in several pioneering works [466–471]—although repolarization effects with different originating mechanisms have been discussed in nonlinear media [461], or even linear disordered media [472,473]. Subsequently, this phenomenon of polarization attraction due to the counter-propagating interaction has been the subject of a growing interest, from both the theoretical [474–482]

and experimental [465,483–487] points of view. Specifically, polarization attraction has been shown to exhibit different properties depending on the experimental configuration [488,487], and on the type of the optical fiber used, e.g., isotropic fibers [465,475,476,483], highly birefringent spun fibers [489,479], as well as randomly birefringent fibers used in optical telecommunications [478,479,484]. The theoretical description of this effect of polarization attraction has been developed through the analysis of the stationary states of the system on the basis of mathematical techniques recently developed for the study of Hamiltonian singularities [474,476,479,490,491]. This geometrical approach revealed the essential role that play the peculiar topological properties of singular tori in the process of polarization attraction. The analysis has been also extended to study the stability properties of soliton states in a medium of finite extension [489,78]. However, so far, no statistical description of partially polarized beams has been developed to describe this phenomenon of polarization attraction. This problem raises important difficulties, since the phenomenon of repolarization is inherently associated to the existence of a mutual correlation between orthogonal polarization components. From a broader perspective, the statistical description of a counter-propagating interaction raises interesting difficulties, which are of interest in their own and deserve to be considered in future developments of the WT theory.

#### *7.5.2. Thermalization and condensation in disordered systems*

It is well-known that even a weak structural disorder of the medium of propagation can change in a dramatic way the properties of the physical system thus giving rise to a plethora of unexpected behaviors, among which the celebrated phenomenon of Anderson localization. This phenomenon is characterized by two equivalent properties, (i) the suppression of transport in disordered media, (ii) the exponential decay of the eigenmode of the (e.g., Schrödinger) wave equation with a random potential $V(\boldsymbol{x})$. We remind that these properties differ from those of a wave that evolves in a periodic potential, in which the eigenmodes are spatially extended throughout the system, as described by the Bloch theorem. Anderson localization finds its origin in the destructive interference of waves multiply diffused by the modulations of the random potential. Because of the universality of this underlying mechanism, this phenomenon is encountered in a large variety of physical systems, e.g., light, acoustic, elastic or matter waves [492–496].

The problem of understanding the influence of a weak nonlinearity on the wave evolution of a wave that evolves in a disordered systems is the subject of several current intense investigations, in particular, in the context of Bose–Einstein condensates [497–500]. The WT theory can shed new light into this vast problematic. In particular, the thermalization of a nonlinear wave in a random potential $V(\boldsymbol{x})$ is expected to be strongly affected by the spatially localized nature of Anderson modes, a feature that may be described by the collision term of the kinetic Eq. (151)–(152). A natural important question to be addressed is to see whether a weak disorder can prevent the thermalization process to take place. In other words one may wonder whether the thermalization process can take place on the basis of the localized Anderson modes solutions of the linearized NLS equation. If such thermalization process can occur, then one may expect a process of classical wave condensation on a localized Anderson mode. From a more general perspective, this issue can be extended to forced and damped systems driven far from equilibrium by an external source. In the optical context, the analysis of stationary nonequilibrium Zakharov–Kolmogorov spectra in a disordered environment would find a direct application in random laser systems [33].

#### *7.5.3. Emergence of rogue waves from wave turbulence*

The evolution of turbulent waves can be characterized by the spontaneous emergence of short lived high amplitude waves. These rogue waves events that "appear from nowhere and disappear without a trace" [501] are among the most studied phenomena in nature in these last years. Besides the hydrodynamic context [502–506], rogue waves have been recently identified in various different fields, including optical waves [507–511,427,512] capillary waves [513], superfluid helium [514], atmosphere [515] or microwaves [516].

The common feature characterizing rogue wave phenomena in the different systems is the observation of deviations from the Gaussian statistics of the wave amplitude, with long tails of the probability density function accounting for the rather frequent emission of such giant waves. We refer the reader to the following recent reviews for a detailed discussion of this vast area of research [34–36].

Recent optical and hydrodynamics studies suggest that rogue wave events can be interpreted in the light of exact analytical solutions of 1D integrable nonlinear wave equations, i.e., breathers solutions [517,518,501,519,502], or more specifically their limiting cases of infinite spatial and temporal periods, the rational soliton solutions [520,521]. Because of this key property of localization in both the spatial and temporal domains, rational solutions may be viewed as a kind of 'rogue wave prototype'. The hierarchy of rational solitons has been found, in particular, in the framework of the integrable 1D NLS equation [521]. A remarkable property of rational solitons is that they are characterized by an increasing value of the central amplitude of the wave field, a feature that can be used to interpret the emergence of rogue wave events of higher amplitudes from a chaotic field. The Peregrine soliton solution refers to the first order rational solution [522–526].

Rational solitons are exact analytical solutions of integrable wave equations, and for this reason they can be regarded as a coherent and deterministic approach to the understanding of rogue wave phenomena. However, rogue waves events are known to spontaneously emerge from an incoherent turbulent state of the system. It is thus important to understand whether rational solitons can emerge from a turbulent environment [503,527–529,519,530,531]. This actually constitutes

a difficult problem, since the description of the turbulent wave system necessarily requires a statistical approach, whereas rational solitons are inherently coherent deterministic structures.

An interesting problem is to consider the emergence of rogue waves and rational solitons in a genuine turbulent wave system, such as a system that can be described by the WT theory. In other words, one may wonder whether the coherent description of rogue waves provided by rational solitons is consistent with the WT description of the random wave. This problem was addressed in particular in Ref. [364] by considering the NLS equation with third-order dispersion (see Section 6.2). In its focusing regime, this model exhibits a quasi-soliton turbulence scenario [47] that can be interpreted in analogy with wave condensation: As the Hamiltonian increases, a transition occurs from the purely coherent and deterministic quasi-soliton regime towards the fully incoherent turbulent regime [363]. As discussed in detail in Section 6.2, this latter turbulent regime is described in detail by the WT theory, which thus brings the question of the existence of rogue wave events in the framework of the WT regime of the incoherent wave.

We note in this respect that caution should be exercised when drawing conclusions as regard the applicability of the WT theory. It is indeed well-known that the existence of a permanent large scale coherent structure (such as a stable soliton or a condensate) leads to a breakdown of the WT theory [47,73], as discussed above through the Bogoliubov regime of condensation in Section 5.2.2. However, contrary to solitons, rogue waves are, by nature, very short and very rare events. In this way, although the WT theory is inherently unable to describe rogue waves, their occurrence should not invalidate the applicability of the WT theory. It was shown in [364] that rogue waves can emerge in the genuine turbulent state of the random field and that their coherent deterministic description provided by rational solitons is compatible with the accurate WT description of the random waves. In particular, the nearly Gaussian statistics for the field amplitudes inherent to the WT theory was compatible with the asymmetric long tail observed in the pdf of the maxima of the field intensity [363]. However, it is important to note that the comparisons between rational soliton solutions and the WT theory have been realized near by the transition to condensation (i.e., for values of the Hamiltonian in the vicinity of the threshold value $H_c$ for quasi-soliton condensation), and thus far from the highly nonlinear regime where the WT theory is known to break down. Rational solutions have been identified in this weakly nonlinear regime, while in the strong nonlinear regime robust quasi-soliton states are generated and thus characterized by large deviations from the Gaussian statistics of the wave amplitude [363].

The problem of occurrence of rogue waves in a turbulent environment has been addressed in the context of hydrodynamics, see, e.g., [503,527–529] (also see the recent review [36]). In this context, the amount of nonlinearity in the turbulent system is measured by the Benjamin–Feir index. By increasing this index, the random wave spontaneously generates breather-like modes. The interesting aspect is that, by further increasing the Benjamin–Feir index, such breathers are no longer generated sporadically, but in some ordered fashion. In this respect, numerical simulations of the NLS equation revealed that, as a result of the incoherent modulational instability, 'oscillating coherent structures' may be excited from initial random spectra [116]. Then, by increasing further the Benjamin–Feir index, the system generates robust quasi-coherent solitons, which lead to a significant deviation from Gaussian statistics. We remark that this phenomenology exhibits some interesting analogies with the three turbulent regimes discussed in Ref. [363], in which different types of rogue waves events have been identified by increasing the Hamiltonian in the condensation curve, i.e., the quasi-soliton regime, the intermittent regime, and the sporadic regime.

From a more general point of view, there is still no satisfactory understanding of several important questions concerning the mechanism underlying the generation of extreme events from a turbulent environment. We refer the reader to [36] for a recent review on this topic.

#### 7.5.4. Thermodynamics of a pure wave system?

Let us finally remark that the process of thermal wave relaxation to equilibrium paves the way for the study of the thermodynamics of a pure optical wave system. To illustrate this aspect, let us underline that the equilibrium distribution (164) allows one to derive the $T\,dS$ equation of thermodynamics (see Ref. [307]):

$$T\,dS = dE - \mu dN, \tag{256}$$

where $E$ refers to the kinetic energy of the optical wave. This corresponds to the familiar $T\,dS$ equation for a fixed volume of interaction [296]. Furthermore, an analogous of the thermodynamic pressure for a pure wave system may be defined from the conservation of the momentum of the field.

Along this line, one can imagine a way to analyze the second principle of thermodynamics in a pure wave system. Consider for instance an optical wave that propagates in a multimode waveguide characterized by a large transverse surface section $A$. We assume that the optical wave has reached, owing to a Kerr-like nonlinearity, an equilibrium state characterized by some entropy $S_1$. Then suppose that the waveguide is realized in such a way that its transverse area $A(z)$ increases suddenly at some propagation distance $z_0$. For $z \geq z_0$, the optical wave then irreversibly relaxes towards a novel state of equilibrium, with a different value of entropy $S_2$. In analogy with thermodynamics, this experiment may be considered as the analogous of the expansion of a gas enclosed in a box, in which a piston is removed at some time $t_0$—the propagation distance $z$ playing the role of time $t$. According to the second principle of thermodynamics, the lift of the constraint on the system 'volume' implies that the entropy $S_2$ must be greater than the entropy $S_1$. As illustrated by this additional example, the WT theory seems to open a variety of novel fascinating opportunities for the study of nonlinear optics with partially incoherent waves.

## Acknowledgments

The authors are grateful to many collaborators for fruitful discussions: D. Anderson, P. Aschieri, S.A. Babin, J. Barré, B. Barviau, P. Béjot, F. Biancalana, G. Brodin, A. Campa, D. Churkin, S. Coen, C. Conti, M. Conforti, J. Coste, S. Derevyanko, F. Dias, P. Di Trapani, V. Doya, D. Faccio, E. Falcon, J. Fatome, B. Fischer, M. Guasoni, R. Kaiser, B. Kibler, M. Haelterman, K. Hammani, H.R. Jauslin, C. Josserand, S. Lagrange, M. Lisak, M. Marklund, C. Michel, C. Montes, N. Mordant, S. Nazarenko, A.C. Newell, M. Onorato, U. Österberg, S. Pitois, E.V. Podivilov, B. Rumpf, M. Segev, V.E. Semenov, S. Trillo, S. Turitsyn, S. Wabnitz, G. Xu, V.E. Zakharov. A.P. is especially grateful to S. Rica for several illuminating discussions on the wave turbulence theory and the phenomenon of wave condensation, he also thanks T. Dauxois and S. Ruffo for their introduction into the physics of long-range interactions.

A.P., P.S., S.R. and G.M. acknowledge support from the French National Research Agency (ANR-12-BS04-0011 OPTIROC), as well as from the Labex ACTION (ANR-11-LABX-01-01) and the Labex CEMPI (ANR-11-LABX-0007-01) programs. A.P. also acknowledges support from the European Research Council under the European Community's Seventh Framework Programme (FP7/20072013 Grant Agreement No. 306633, PETAL project). The work of D.N.C. was partially supported by the Office of Naval Research (MURI Grant No. N000141310649).

## Appendix

### *A.1. Derivation of the short-range spatial Vlasov equation*

We use the multiscale expansion, $B(\boldsymbol{x}, \boldsymbol{\xi}, z) = B^{(0)}\left(\varepsilon\boldsymbol{x}, \boldsymbol{\xi}, \varepsilon z\right)$, where $n_{\boldsymbol{k}}^{(0)}(\boldsymbol{X}, Z) = \int B^{(0)}(\boldsymbol{X}, \boldsymbol{\xi}, Z)\exp(-i\boldsymbol{k}.\boldsymbol{\xi})\,d\boldsymbol{\xi}$, with $\boldsymbol{X} = \varepsilon x$ and $Z = \varepsilon z$. In this way, the second term in the equation for the autocorrelation function (5), $\int P(\boldsymbol{x}, \boldsymbol{\xi}, z)\exp(-i\boldsymbol{k}.\boldsymbol{\xi})d\boldsymbol{\xi} = \int P(\boldsymbol{X}/\varepsilon, \boldsymbol{\xi}, Z/\varepsilon)\exp(-i\boldsymbol{k}.\boldsymbol{\xi})d\boldsymbol{\xi}$, can be calculated explicitly, which gives

$$\int P(\boldsymbol{x}, \boldsymbol{\xi}, z)\exp(-i\boldsymbol{k}.\boldsymbol{\xi})d\boldsymbol{\xi} = \frac{1}{(2\pi)^{2d}}\int U(\boldsymbol{y})\left[n_{\boldsymbol{k}_2}^{(0)}(\boldsymbol{X} - \varepsilon\boldsymbol{y} + \varepsilon\boldsymbol{\xi}/2, Z) - n_{\boldsymbol{k}_2}^{(0)}(\boldsymbol{X} - \varepsilon\boldsymbol{y} - \varepsilon\boldsymbol{\xi}/2, Z)\right] \times n_{\boldsymbol{k}_1}^{(0)}(\boldsymbol{X}, Z)\exp[i(\boldsymbol{k}_1 - \boldsymbol{k}).\boldsymbol{\xi}]\,d\boldsymbol{k}_1\,d\boldsymbol{k}_2\,d\boldsymbol{\xi}\,d\boldsymbol{y}. \tag{257}$$

Expanding the integrand to first-order in $\varepsilon$ and integrating by parts with respect to $\boldsymbol{k}_1$ gives

$$\int P(\boldsymbol{x}, \boldsymbol{\xi}, z)\exp(-i\boldsymbol{k}.\boldsymbol{\xi})d\boldsymbol{\xi} = i\varepsilon\partial_{\boldsymbol{k}}n_{\boldsymbol{k}}^{(0)}(\boldsymbol{X}, Z).\partial_{\boldsymbol{X}}\left(\frac{1}{(2\pi)^d}\int n_{\boldsymbol{k}'}^{(0)}(\boldsymbol{X}, Z)d\boldsymbol{k}'\right). \tag{258}$$

The third term in the equation for the autocorrelation function (39) can be calculated in a similar way. Expanding in powers of $\varepsilon$, one obtains $\int Q(\boldsymbol{x}, \boldsymbol{\xi}, z)\exp(-i\boldsymbol{k}.\boldsymbol{\xi})d\boldsymbol{\xi} = \tilde{Q}_0 + \varepsilon\tilde{Q}_1$, where

$$\tilde{Q}_0 = \frac{1}{(2\pi)^d}\int U(\boldsymbol{y})\,n_{\boldsymbol{k}_1}^{(0)}(\boldsymbol{X}, Z)\,n_{\boldsymbol{k}}^{(0)}(\boldsymbol{X}, Z)\left[\exp[i(\boldsymbol{k}_1 - \boldsymbol{k}).\boldsymbol{y}] - \exp[-i(\boldsymbol{k}_1 - \boldsymbol{k}).\boldsymbol{y}]\right]d\boldsymbol{k}_1\,d\boldsymbol{y}. \tag{259}$$

Defining the Fourier transform of the response function, $\tilde{U}_{\boldsymbol{k}} = \int U(\boldsymbol{x})\ \exp(-i\boldsymbol{k}.\boldsymbol{x})\,d\boldsymbol{x}$, one readily obtains

$$\tilde{Q}_0 = \frac{2i}{(2\pi)^d}n_{\boldsymbol{k}}^{(0)}(\boldsymbol{X}, Z)\int \mathrm{Im}(\tilde{U}_{\boldsymbol{k}-\boldsymbol{k}'})\,n_{\boldsymbol{k}'}^{(0)}(\boldsymbol{X}, Z)\,d\boldsymbol{k}', \tag{260}$$

where $\mathrm{Im}(\tilde{U}_{\boldsymbol{k}})$ denotes the imaginary part of $\tilde{U}_{\boldsymbol{k}}$. The contribution $\tilde{Q}_0$ vanishes because the response function $U(\boldsymbol{x})$ is real-valued and even, which thus leads to $\mathrm{Im}(\tilde{U}_{\boldsymbol{k}}) = 0$. Note that this will not be the case in the temporal domain, because of the causality condition of the response function, as discussed here below. The contribution of order $\varepsilon$ can be written

$$\tilde{Q}_1 = \frac{1}{(2\pi)^{2d}}\int U(\boldsymbol{y})\left[(u_+ + v)\exp[-i(\boldsymbol{k}_1 - \boldsymbol{k}_2).\boldsymbol{y}] + (u_- - v)\exp[i(\boldsymbol{k}_1 - \boldsymbol{k}_2).\boldsymbol{y}]\right] \times \exp[-i(\boldsymbol{k} - \boldsymbol{k}_2).\boldsymbol{\xi}]\,d\boldsymbol{k}_1\,d\boldsymbol{k}_2 d\boldsymbol{y}\,d\boldsymbol{\xi}, \tag{261}$$

where $u_\pm = \frac{1}{2}n_{\boldsymbol{k}_2}^{(0)}(\boldsymbol{X}, Z)\,(\boldsymbol{\xi} \pm \boldsymbol{y}).\partial_{\boldsymbol{X}}n_{\boldsymbol{k}_1}^{(0)}(\boldsymbol{X}, Z)$, $v = \frac{1}{2}n_{\boldsymbol{k}_1}^{(0)}(\boldsymbol{X}, Z)\,\boldsymbol{Y}.\partial_{\boldsymbol{X}}n_{\boldsymbol{k}_2}^{(0)}(\boldsymbol{X}, Z)$. By means of some algebraic manipulations, this expression reads

$$\tilde{Q}_1 = -\frac{i}{2(2\pi)^d}\partial_{\boldsymbol{X}}\int U(\boldsymbol{y})\partial_{\boldsymbol{k}_1}\left(n_{\boldsymbol{k}_1}^{(0)}(\boldsymbol{X}, Z)\right)n_{\boldsymbol{k}}^{(0)}(\boldsymbol{X}, Z)\left[\exp[i(\boldsymbol{k}_1 - \boldsymbol{k}).\boldsymbol{y}] + \exp[-i(\boldsymbol{k}_1 - \boldsymbol{k}).\boldsymbol{y}]\right]d\boldsymbol{k}_1\,d\boldsymbol{y} + \frac{i}{2(2\pi)^d}\partial_{\boldsymbol{k}}\int U(\boldsymbol{y})n_{\boldsymbol{k}}^{(0)}(\boldsymbol{X}, Z)\,\partial_{\boldsymbol{X}}\left(n_{\boldsymbol{k}_1}^{(0)}(\boldsymbol{X}, Z)\right)\left[\exp[i(\boldsymbol{k}_1 - \boldsymbol{k}).\boldsymbol{y}] + \exp[-i(\boldsymbol{k}_1 - \boldsymbol{k}).\boldsymbol{y}]\right]d\boldsymbol{k}_1\,d\boldsymbol{y} \tag{262}$$

and can finally be written in the following compact form

$$\tilde{Q}_1 = \frac{i}{(2\pi)^d}\partial_{\boldsymbol{X}}\left(\int \tilde{U}_{\boldsymbol{k}-\boldsymbol{k}_1} n^{(0)}_{\boldsymbol{k}_1}(\boldsymbol{X},Z)\,d\boldsymbol{k}_1\right).\partial_{\boldsymbol{k}} n^{(0)}_{\boldsymbol{k}}(\boldsymbol{X},Z) - \frac{i}{(2\pi)^d}\partial_{\boldsymbol{k}}\left(\int \tilde{U}_{\boldsymbol{k}-\boldsymbol{k}_1} n^{(0)}_{\boldsymbol{k}_1}(\boldsymbol{X},Z)\,d\boldsymbol{k}_1\right).\partial_{\boldsymbol{X}} n^{(0)}_{\boldsymbol{k}}(\boldsymbol{X},Z). \tag{263}$$

Then collecting all terms in Eqs. (263) and (258), and coming back to the original variables, $z = Z/\varepsilon$ and $\boldsymbol{x} = \boldsymbol{X}/\varepsilon$, one obtains the short-range Vlasov-like kinetic equation (11), with the effective potential given in Eq. (13).

### A.2. Derivation of the long-range spatial Vlasov equation

We proceed as in Appendix A.1, but we use the following scaling for the highly nonlocal potential $U(\boldsymbol{x}) = \varepsilon U^{(0)}(\varepsilon\boldsymbol{x})$. We thus have

$$\begin{aligned}\int P(\boldsymbol{x},\boldsymbol{\xi},z)\exp(-i\boldsymbol{k}.\boldsymbol{\xi})d\boldsymbol{\xi} = \frac{1}{(2\pi)^d}\int U^{(0)}(\boldsymbol{Y})\left[n^{(0)}_{\boldsymbol{k}_2}(\boldsymbol{X}-\boldsymbol{Y}+\varepsilon\boldsymbol{\xi}/2,Z) - n^{(0)}_{\boldsymbol{k}_2}(\boldsymbol{X}-\boldsymbol{Y}-\varepsilon\boldsymbol{\xi}/2,Z)\right]\\ \times n^{(0)}_{\boldsymbol{k}_1}(\boldsymbol{X},Z)\exp[i(\boldsymbol{k}_1-\boldsymbol{k}).\boldsymbol{\xi}]\,d\boldsymbol{k}_1\,d\boldsymbol{k}_2\,d\boldsymbol{\xi}\,d\boldsymbol{Y}.\end{aligned} \tag{264}$$

Expanding the difference in the brackets to the first order in $\varepsilon$, one obtains

$$\int P(\boldsymbol{x},\boldsymbol{\xi},z)\exp(-i\boldsymbol{k}.\boldsymbol{\xi})d\boldsymbol{\xi} = i\varepsilon\partial_{\boldsymbol{k}} n^{(0)}_{\boldsymbol{k}}(\boldsymbol{X},Z).\partial_{\boldsymbol{X}}\int U^{(0)}(\boldsymbol{X}-\boldsymbol{X}')\left(\frac{1}{(2\pi)^d}\int n^{(0)}_{\boldsymbol{k}'}(\boldsymbol{X}',Z)d\boldsymbol{k}'\right)d\boldsymbol{X}'. \tag{265}$$

The same procedure applied to the term $Q$ in the equation for the autocorrelation function reveals that the expansion in the first order in $\varepsilon$ vanishes—the first nonvanishing term is of second order, $\varepsilon^2$. Coming back to the original variables, one thus obtains the Vlasov equation (11) with the effective potential (22).

### A.3. Derivation of the weak Langmuir turbulence equation

The method for the derivation of the WT Langmuir equation follows the procedure reported in Appendix A.1 for the derivation of the short-range Vlasov equation in the spatial domain. The main difference is that the calculation is carried out in the temporal domain, i.e., the variables are transformed as follows $\boldsymbol{x} \to t$, $\boldsymbol{\xi} \to \tau$, while the nonlocal response function is substituted by the noninstantaneous response. Accordingly, the multiscale expansion reads, $B(t,\tau,z) = B^{(0)}(\varepsilon t,\tau,\varepsilon z) + O(\varepsilon)$, where $n^{(0)}_{\omega}(T,Z) = \int B^{(0)}(T,\tau,Z)\,\exp(i\omega\tau)\,d\tau$, with $T = \varepsilon t$ and $Z = \varepsilon z$. Expanding the term $P$ in first-order in $\varepsilon$ gives

$$\int_{-\infty}^{+\infty} P(t,\tau,z)\exp(-i\omega\tau)d\tau = i\varepsilon\partial_{\omega} n^{(0)}_{\omega}(T,Z)\partial_T\left(\frac{1}{2\pi}\int_{-\infty}^{+\infty} n^{(0)}_{\omega}(T,Z)d\omega'\right). \tag{266}$$

The term $Q$ can be expanded in the same way, $\int Q(t,\tau,z)\exp(i\omega\tau)d\tau = \tilde{Q}_0 + \varepsilon\tilde{Q}_1$, where

$$\tilde{Q}_0 = \frac{-1}{\pi} n^{(0)}_{\omega}(T,Z)\int_{-\infty}^{+\infty}\mathrm{Im}(\tilde{R}_{\omega-\omega'})\,n^{(0)}_{\omega'}(T,Z)\,d\omega', \tag{267}$$

where $\mathrm{Im}(\tilde{R}_{\omega})$ denotes the imaginary part of the Fourier transform of the response function $R(t)$. Contrarily to the spatial case where this function vanishes, in the temporal domain it refers to the gain spectrum of the nonlinearity, $\mathrm{Im}(\tilde{R}_{\omega}) = g(\omega)$, as discussed through Eq. (37). It turns out that, thanks to the causality condition, the zeroth order expansion in $\varepsilon$ no longer vanish in (267). In this way the first term $P$ in Eq. (266) of order $\varepsilon$ is negligible with respect to the term (267). Coming back to the original $z = Z/\varepsilon$ and $t = T/\varepsilon$, one obtains the WT Langmuir kinetic equation (44).

### A.4. Derivation of the Korteweg–de Vries equation

By substituting the form of the spectral gain curve, $g(\omega) = g^{(0)}(\frac{\omega}{\varepsilon})$, and of the spectrum, $n_{\omega}(z) = n_0 + \varepsilon^2\tilde{n}^{(0)}_{\omega}(\varepsilon^2 z) + O(\varepsilon^4)$, into the rhs of Eq. (44), we obtain:

$$\begin{aligned}\frac{\gamma}{\pi}n_{\omega}\int_{-\infty}^{+\infty} g(\omega-\omega')n_{\omega'}d\omega' &= \frac{\gamma\varepsilon}{\pi}\left[n_0+\varepsilon^2\tilde{n}^{(0)}_{\omega}\right]\int_{-\infty}^{+\infty} g^{(0)}(\omega')\left[n_0+\varepsilon^2\tilde{n}^{(0)}_{\omega-\varepsilon\omega'}\right]d\omega'\\ &= \frac{\gamma\varepsilon^4}{\pi}\left[n_0+\varepsilon^2\tilde{n}^{(0)}_{\omega}\right]\int_{-\infty}^{+\infty} g^{(0)}(\omega')\left[-\omega'\partial_{\omega}\tilde{n}^{(0)}_{\omega} - {\omega'}^3\frac{\varepsilon^2}{6}\partial^3_{\omega}\tilde{n}^{(0)}_{\omega}\right]d\omega'\\ &= \frac{\gamma\varepsilon^4 n_0 g^{(0)}_1}{\pi}\partial_{\omega}\tilde{n}^{(0)}_{\omega} + \frac{\gamma\varepsilon^6 g^{(0)}_1}{\pi}\tilde{n}^{(0)}_{\omega}\partial_{\omega}\tilde{n}^{(0)}_{\omega} + \frac{\gamma\varepsilon^6 n_0 g^{(0)}_3}{6\pi}\partial^3_{\omega}\tilde{n}^{(0)}_{\omega},\end{aligned}$$

up to terms of order $\varepsilon^8$, where we have used the fact that $g^{(0)}$ is an odd function and we have defined

$$g_1^{(0)} = -\int_{-\infty}^{+\infty} \omega g^{(0)}(\omega) d\omega, \qquad g_3^{(0)} = -\int_{-\infty}^{+\infty} \omega^3 g^{(0)}(\omega) d\omega.$$

Of course the lhs of Eq. (44) reads:

$$\partial_z n_\omega(z) = \varepsilon^4 \partial_Z \tilde{n}_\omega^\varepsilon(\varepsilon^2 z),$$

with $Z = \varepsilon^2 z$. By dividing Eq. (44) by $\varepsilon^4$ and by collecting the terms of order up to $O(\varepsilon^2)$, we find:

$$\partial_Z \tilde{n}_\omega^{(0)}(Z) - \frac{\gamma n_0 g_1^{(0)}}{\pi} \partial_\omega \tilde{n}_\omega^{(0)}(Z) = \frac{\gamma \varepsilon^2 g_1^{(0)}}{\pi} \tilde{n}_\omega^{(0)}(Z) \partial_\omega \tilde{n}_\omega^{(0)}(Z) + \frac{\gamma \varepsilon^2 n_0 g_3^{(0)}}{6\pi} \partial_\omega^3 \tilde{n}_\omega^{(0)}(Z).$$

By coming back to the original variables we obtain the Korteweg–de Vries equation (52).

### *A.5. Derivation of the singular integro-differential kinetic equations*

We report the mathematical procedure underlying the derivation of the singular integro-differential kinetic equations starting from the WT Langmuir equation. We first the derivation for general response function and show that the leading-order terms of the singular integro-differential equations are related to the properties of the response function close to zero. Then we apply the general results to the damped harmonic oscillator response and the purely exponential response.

#### *A.5.1. General response function*

The starting point is to carefully address the singularities involved in the convolution operator of the WT Langmuir Eq. (44). The response function can be written in the following general form

$$R(t) = \frac{1}{\tau_R} \bar{R}\left(-\frac{t}{\tau_R}\right) H(-t),$$

where $\bar{R}$ is a smooth function (that is at least five times differentiable with integrable derivatives over $[0, \infty)$). By using integration by parts one finds that the imaginary part of the Fourier transform of the response function

$$g(\omega) = \mathrm{Im}\left(\int_{-\infty}^{\infty} R(t) e^{i\omega t} dt\right) = -\mathrm{Im}\left(\int_0^{\infty} \bar{R}(t)\ \exp(i\omega t)\, dt\right)$$

has the form

$$g(\omega) = g^0(\omega\tau_R), \qquad g^0(\omega) = -\frac{1}{\omega}\bar{R}(0) + \frac{1}{\omega^3}\bar{R}^{(2)}(0) - \frac{1}{\omega^5}\bar{R}^{(4)}(0) - \frac{1}{\omega^5}\mathrm{Re}\left(\int_0^{\infty} \bar{R}^{(5)}(t) e^{i\omega t} dt\right),$$

where $\bar{R}^{(j)}(t)$ denotes the $j$th derivative of $\bar{R}(t)$. This allows us to identify the two 'singularities' (the terms in $1/\omega$ and $1/\omega^3$) that are important when addressing the convolution operator of the WT Langmuir Eq. (44).

For a smooth function $n_\omega$ we want to find the expression of

$$N_\omega = \int_{-\infty}^{\infty} g(\omega - u) n_u du, \tag{268}$$

in particular in the regime $\tau_R/\tau_0 \gg 1$. In the following we will denote $g_\omega = g(\omega)$.

*Summary of the general results:*

(1) For any $\tau_R > 0$, the convolution operator can be written in the following form without approximations

$$N_\omega = -\frac{\pi \bar{R}(0)}{\tau_R} \mathcal{H} n_\omega + \frac{\pi \bar{R}^{(1)}(0)}{\tau_R^2} \partial_\omega n_\omega + \frac{\pi \bar{R}^{(2)}(0)}{2\tau_R^3} \mathcal{H} \partial_\omega^2 n_\omega + \frac{1}{\tau_R^4} \int_0^{\infty} \left[\partial_\omega^3 n_{\omega + \frac{u}{\tau_R}} + \partial_\omega^3 n_{\omega - \frac{u}{\tau_R}}\right] G^0(u) du, \tag{269}$$

where we have defined for $u > 0$:

$$G^0(u) = -\frac{1}{2} \int_u^{\infty} \left(g_v^0 + \frac{\bar{R}(0)}{v} - \frac{\bar{R}^{(2)}(0)}{v^3}\right)(v - u)^2 dv, \tag{270}$$

and $\mathcal{H}$ is the Hilbert transform.

(2) When $\tau_R/\tau_0 \gg 1$,

$$N_\omega = -\frac{\pi \bar{R}(0)}{\tau_R} \mathcal{H} n_\omega + \frac{\pi \bar{R}^{(1)}(0)}{\tau_R^2} \partial_\omega n_\omega + \frac{\pi \bar{R}^{(2)}(0)}{2\tau_R^3} \mathcal{H} \partial_\omega^2 n_\omega - \frac{\pi \bar{R}^{(3)}(0)}{6\tau_R^4} \partial_\omega^3 n_\omega + o\left(\frac{1}{\tau_R^4}\right). \tag{271}$$

These results show that the leading-order term in the expansion (271) is determined by the behavior of the response function at 0. We will address in the two following sections two examples for which $\bar{R}(0) = 0$ and $\bar{R}(0) \neq 0$, respectively.

**Proof.** We can write $N_\omega$ in the form

$$\begin{aligned} N_\omega &= -\frac{\bar{R}(0)}{\tau_R}\mathcal{P}\int_{-\infty}^{\infty} n_{\omega-u}\frac{1}{u}du + \frac{1}{\tau_R}\mathcal{P}\int_{-\infty}^{\infty}\Big(g_u^0 + \frac{\bar{R}(0)}{u}\Big)n_{\omega-\frac{u}{\tau_R}}du \\ &= -\frac{\pi\bar{R}(0)}{\tau_R}\mathcal{H}n_\omega - \frac{1}{\tau_R}\int_0^{\infty}\Big(g_u^0 + \frac{\bar{R}(0)}{u}\Big)\Big[n_{\omega+\frac{u}{\tau_R}} - n_{\omega-\frac{u}{\tau_R}}\Big]du \\ &= -\frac{\pi\bar{R}(0)}{\tau_R}\mathcal{H}n_\omega - \frac{1}{\tau_R}\int_0^{\infty}\partial_u f^0(u)\big[n_{\omega+\frac{u}{\tau_R}} - n_{\omega-\frac{u}{\tau_R}}\big]du, \end{aligned}$$

where we have introduced the function $f^0$ defined by (for $u > 0$):

$$f^0(u) = -\int_u^{\infty} g_v^0 + \frac{\bar{R}(0)}{v}dv.$$

Note that $f^0$ can be expanded as $f^0(u) = -\frac{\bar{R}^{(2)}(0)}{2u^2} + O(\frac{1}{u^4})$ as $u \to \infty$ and $f^0(u) = \bar{R}(0)\ln u + O(1)$ as $u \to 0$, so that $\lim_{u\to 0} f^0(u)\big[n_{\omega+\frac{u}{\tau_R}} - n_{\omega-\frac{u}{\tau_R}}\big] = 0$. Therefore we can write after integration by parts

$$\begin{aligned} N_\omega &= -\frac{\pi\bar{R}(0)}{\tau_R}\mathcal{H}n_\omega + \frac{1}{\tau_R^2}\int_0^{\infty} f^0(u)\big[\partial_\omega n_{\omega+\frac{u}{\tau_R}} + \partial_\omega n_{\omega-\frac{u}{\tau_R}}\big]du \\ &= -\frac{\pi\bar{R}(0)}{\tau_R}\mathcal{H}n_\omega + \frac{\bar{f}}{\tau_R^2}\partial_\omega n_\omega + \frac{1}{\tau_R^2}\int_0^{\infty} f^0(u)\big[\partial_\omega n_{\omega+\frac{u}{\tau_R}} + \partial_\omega n_{\omega-\frac{u}{\tau_R}} - 2\partial_\omega n_\omega\big]du, \end{aligned}$$

where

$$\bar{f} = 2\int_0^{\infty} f^0(u)du = -2\int_0^{\infty} u\,g_u^0 + \bar{R}(0)\,du = -\int_{-\infty}^{\infty} ug_u^0 + \bar{R}(0)du.$$

After integration by parts:

$$ug_u^0 + \bar{R}(0) = -\mathrm{Re}\Big(\int_0^{\infty}\bar{R}^{(1)}(t)e^{-iut}dt\Big),$$

and therefore

$$\bar{f} = \pi\bar{R}^{(1)}(0).$$

We can write

$$N_\omega = -\frac{\pi\bar{R}(0)}{\tau_R}\mathcal{H}n_\omega + \frac{\pi\bar{R}^{(1)}(0)}{\tau_R^2}\partial_\omega n_\omega + \frac{1}{\tau_R^2}\int_0^{\infty}\partial_u F^0(u)\big[\partial_\omega n_{\omega+\frac{u}{\tau_R}} + \partial_\omega n_{\omega-\frac{u}{\tau_R}} - 2\partial_\omega n_\omega\big]du,$$

where we have introduced the function $F^0$ defined by (for $u > 0$):

$$F^0(u) = -\int_u^{\infty} f^0(v)dv.$$

Note that $F^0$ can be expanded as $F^0(u) = \frac{\bar{R}^{(2)}(0)}{2u} + O(\frac{1}{u^3})$ as $u \to \infty$ and $F^0(u) = -\pi\bar{R}^{(1)}(0)/2 + o(1)$ as $u \to 0$, so that $\lim_{u\to 0} F^0(u)\big[\partial_\omega n_{\omega+\frac{u}{\tau_R}} + \partial_\omega n_{\omega-\frac{u}{\tau_R}} - 2\partial_\omega n_\omega\big] = 0$. Therefore, after integration by parts we find

$$\begin{aligned} N_\omega &= -\frac{\pi\bar{R}(0)}{\tau_R}\mathcal{H}n_\omega + \frac{\pi\bar{R}^{(1)}(0)}{\tau_R^2}\partial_\omega n_\omega - \frac{1}{\tau_R^3}\int_0^{\infty} F^0(u)\big[\partial_\omega^2 n_{\omega+\frac{u}{\tau_R}} - \partial_\omega^2 n_{\omega-\frac{u}{\tau_R}}\big]du \\ &= -\frac{\pi\bar{R}(0)}{\tau_R}\mathcal{H}n_\omega + \frac{\pi\bar{R}^{(1)}(0)}{\tau_R^2}\partial_\omega n_\omega + \frac{\pi\bar{R}^{(2)}(0)}{2\tau_R^3}\mathcal{H}\partial_\omega^2 n_\omega \\ &\quad - \frac{1}{\tau_R^3}\int_0^{\infty}\Big(F^0(u) - \frac{\bar{R}^{(2)}(0)}{2u}\Big)\big[\partial_\omega^2 n_{\omega+\frac{u}{\tau_R}} - \partial_\omega^2 n_{\omega-\frac{u}{\tau_R}}\big]du \\ &= -\frac{\pi\bar{R}(0)}{\tau_R}\mathcal{H}n_\omega + \frac{\pi\bar{R}^{(1)}(0)}{\tau_R^2}\partial_\omega n_\omega + \frac{\pi\bar{R}^{(2)}(0)}{2\tau_R^3}\mathcal{H}\partial_\omega^2 n_\omega - \frac{1}{\tau_R^3}\int_0^{\infty}\partial_u G^0(u)\big[\partial_\omega^2 n_{\omega+\frac{u}{\tau_R}} - \partial_\omega^2 n_{\omega-\frac{u}{\tau_R}}\big]du, \end{aligned}$$

where we have introduced

$$G^0(u) = -\int_u^\infty F^0(v) - \frac{\bar{R}^{(2)}(0)}{2v} dv.$$

After some calculations, this expression of $G^0(u)$ can be written in the form given in Eq. (270). Note that $G^0(u) = O(\frac{1}{u^2})$ as $u \to \infty$ and $G^0(u) = O(\ln u)$ as $u \to 0$, so that $\lim_{u\to 0} G^0(u)\big[\partial_\omega^2 n_{\omega+\frac{u}{\tau_R}} - \partial_\omega^2 n_{\omega-\frac{u}{\tau_R}}\big] = 0$ and we can integrate by parts the last term

$$N_\omega = -\frac{\pi\bar{R}(0)}{\tau_R}\mathcal{H}n_\omega + \frac{\pi\bar{R}^{(1)}(0)}{\tau_R^2}\partial_\omega n_\omega + \frac{\pi\bar{R}^{(2)}(0)}{2\tau_R^3}\mathcal{H}\partial_\omega^2 n_\omega + \frac{1}{\tau_R^4}\int_0^\infty G^0(u)\big[\partial_\omega^3 n_{\omega+\frac{u}{\tau_R}} + \partial_\omega^3 n_{\omega-\frac{u}{\tau_R}}\big]du,$$

which is the first desired result. This expression of $N_\omega$ is exact, and $G^0$ is an integrable function over $(0, \infty)$. As a result $N_\omega$ has the following expansion as $\tau_R/\tau_0 \gg 1$:

$$N_\omega = -\frac{\pi\bar{R}(0)}{\tau_R}\mathcal{H}n_\omega + \frac{\pi\bar{R}^{(1)}(0)}{\tau_R^2}\partial_\omega n_\omega + \frac{\pi\bar{R}^{(2)}(0)}{2\tau_R^3}\mathcal{H}\partial_\omega^2 n_\omega + \frac{\bar{G}}{\tau_R^4}\partial_\omega^3 n_\omega + o\Big(\frac{1}{\tau_R^4}\Big),$$

with

$$\bar{G} = 2\int_0^\infty G^0(u)du = -\frac{1}{6}\int_{-\infty}^\infty u^3 g_u^0 + u^2\bar{R}(0) - \bar{R}^{(2)}(0)du.$$

After iterated integration by parts:

$$u^3 g_u^0 + u^2\bar{R}(0) - \bar{R}^{(2)}(0) = \mathrm{Re}\Big(\int_0^\infty \bar{R}^{(3)}(t)e^{iut}dt\Big),$$

and therefore

$$\bar{G} = -\frac{\pi}{6}\bar{R}^{(3)}(0),$$

which completes the proof.

*A.5.2. Application to the damped harmonic oscillator response*

We apply the general theory exposed above to the particular example of a damped harmonic oscillator response function. In this way we derive the singular integro-differential kinetic equations (56) and (57). The normalized nonlinear response function is $\bar{R}(t) = \frac{1+\eta^2}{\eta\tau_R}\sin(\eta t/\tau_R)\exp(-t/\tau_R)$, with

$$g_\omega = \frac{1+\eta^2}{2\eta}\left(\frac{1}{1+(\eta+\tau_R\omega)^2} - \frac{1}{1+(\eta-\tau_R\omega)^2}\right). \tag{272}$$

For a smooth function $n_\omega$ we want to find the expression of

$$N_\omega = \int_{-\infty}^\infty g_{\omega-u}n_u du, \tag{273}$$

in particular in the regime $\tau_R/\tau_0 \gg 1$. Applying the general theory reported in the previous section, we find the following results.

(1) For any $\tau_R, \eta > 0$,

$$N_\omega = \frac{\pi(1+\eta^2)}{\tau_R^2}\partial_\omega n_\omega - \frac{\pi(1+\eta^2)}{\tau_R^3}\mathcal{H}\partial_\omega^2 n_\omega + \frac{1}{\tau_R^4}\int_0^\infty \big[\partial_\omega^3 n_{\omega+\frac{u}{\tau_R}} + \partial_\omega^3 n_{\omega-\frac{u}{\tau_R}}\big]G^0(u)du, \tag{274}$$

where we have defined for $u > 0$:

$$G^0(u) = \frac{1+\eta^2}{\eta}\int_u^\infty \frac{\pi\eta}{2} - \frac{1}{2}\Big[w\ \arctan(w) - \frac{1}{2}\log(1+w^2)\Big]_{v-\eta}^{v+\eta} - \frac{\eta}{v}dv, \tag{275}$$

and $\mathcal{H}$ is the Hilbert transform.

(2) When $\tau_R/\tau_0 \gg 1$,

$$N_\omega = \frac{\pi(1+\eta^2)}{\tau_R^2}\partial_\omega n_\omega - \frac{\pi(1+\eta^2)}{\tau_R^3}\mathcal{H}\partial_\omega^2 n_\omega - \frac{\pi(1+\eta^2)(3-\eta^2)}{6\tau_R^4}\partial_\omega^3 n_\omega + o\Big(\frac{1}{\tau_R^4}\Big). \tag{276}$$

*–Derivation of (56) and (57)*

With an initial condition without background:

$$n_\omega(z=0) \overset{\omega\to\pm\infty}{\longrightarrow} 0, \tag{277}$$

in the asymptotic regime $\tau_R/\tau_0 \gg 1$, the spectrum satisfies the singular integrodifferential kinetic equation

$$\tau_R^2 \partial_z n_\omega = \gamma(1+\eta^2)\left(n_\omega \partial_\omega n_\omega - \frac{1}{\tau_R} n_\omega \mathcal{H}\partial_\omega^2 n_\omega\right), \tag{278}$$

in which the small regularization term is dispersive.

With an initial condition with background:

$$n_\omega(z) = n_0 + \tilde{n}_\omega(z), \quad n_0 > 0, \tag{279}$$

introducing the scaling

$$\tilde{n}_\omega(z) = \frac{1}{\tau_R}\tilde{n}_\omega^{(0)}(z/\tau_R^3), \tag{280}$$

the spectrum satisfies in the asymptotic regime $\tau_R/\tau_0 \gg 1$

$$\partial_Z \tilde{n}_\omega^{(0)} = \gamma(1+\eta^2)\left(\tau_R n_0 \partial_\omega \tilde{n}_\omega^{(0)} + \tilde{n}_\omega^{(0)}\partial_\omega \tilde{n}_\omega^{(0)} - n_0 \mathcal{H}\partial_\omega^2 \tilde{n}_\omega^{(0)}\right). \tag{281}$$

where $Z = z/\tau_R^3$. The first term of this equation can be removed by a change of Galilean reference frame, ($\Omega = \omega + \gamma(1+\eta^2)\tau_R n_0 Z, \xi = Z$), so that Eq. (281) recovers the Benjamin–Ono (BO) equation.

*A.5.3. Application to the exponential response*

Here we apply the general theory reported above to the particular example of a purely exponential response function. In this way we derive the singular integro-differential kinetic Eqs. (60) and (62). The nonlinear response function is $\bar{R}(t) = \frac{1}{\tau_R}\exp\left(-\frac{t}{\tau_R}\right)$, with

$$g_\omega = -\frac{\tau_R\omega}{1+(\tau_R\omega)^2}. \tag{282}$$

We want to find the expression of

$$N_\omega = \int_{-\infty}^{\infty} g_{\omega-u} n_u du, \tag{283}$$

in particular in the regime $\tau_R/\tau_0 \gg 1$. Applying the general results derived in the previous section, we find the following results.

(1) For any $\tau_R > 0$,

$$N_\omega = -\frac{\pi}{\tau_R}\mathcal{H}n_\omega - \frac{\pi}{\tau_R^2}\partial_\omega n_\omega + \frac{\pi}{2\tau_R^3}\mathcal{H}\partial_\omega^2 n_\omega + \frac{1}{\tau_R^4}\int_0^\infty \left[\partial_\omega^3 n_{\omega+\frac{u}{\tau_R}} + \partial_\omega^3 n_{\omega-\frac{u}{\tau_R}}\right] G^0(u) du, \tag{284}$$

where we have defined for $u > 0$:

$$G^0(u) = -\frac{3}{4} + \frac{1}{4}(1-u^2)\ln\left(1+\frac{1}{u^2}\right) + u\ \arctan\left(\frac{1}{u}\right). \tag{285}$$

(2) When $\tau_R/\tau_0 \gg 1$,

$$N_\omega = -\frac{\pi}{\tau_R}\mathcal{H}n_\omega - \frac{\pi}{\tau_R^2}\partial_\omega n_\omega + \frac{\pi}{2\tau_R^3}\mathcal{H}\partial_\omega^2 n_\omega + \frac{\pi}{6\tau_R^4}\partial_\omega^3 n_\omega + o\left(\frac{1}{\tau_R^4}\right). \tag{286}$$

*–Derivation of Eqs. (60) and (62)*

With an initial condition without background:

$$n_\omega(z=0) = \tilde{n}_\omega^0, \quad \text{with } \tilde{n}_\omega^0 \overset{\omega\to\pm\infty}{\longrightarrow} 0, \tag{287}$$

in the asymptotic regime $\tau_R/\tau_0 \gg 1$, the spectrum satisfies

$$\frac{\tau_R}{\gamma}\partial_z n_\omega = -n_\omega \mathcal{H}n_\omega - \frac{1}{\tau_R} n_\omega \partial_\omega n_\omega + \frac{1}{2\tau_R^2} n_\omega \mathcal{H}\partial_\omega^2 n_\omega. \tag{288}$$

As discussed in Section 3.2.3, the dynamics is dominated by the leading-order term in the rhs of this equation, which leads to a collapse-like behavior.

With an initial condition with background:

$$n_\omega(z) = n_0 + \tilde{n}_\omega(z), \quad n_0 > 0, \tag{289}$$

introducing the scaling

$$\tilde{n}_\omega(z) = \frac{1}{\tau_R}\tilde{n}^{(0)}_\omega(z/\tau_R), \tag{290}$$

the spectrum satisfies in the asymptotic regime $\tau_R/\tau_0 \gg 1$

$$\frac{1}{\gamma}\partial_Z\tilde{n}^{(0)}_\omega = -n_0\mathcal{H}\tilde{n}^{(0)}_\omega - \frac{1}{\tau_R}\left(\tilde{n}^{(0)}_\omega\mathcal{H}\tilde{n}^{(0)}_\omega + n_0\partial_\omega\tilde{n}^{(0)}_\omega\right) + \frac{1}{\tau_R^2}\left(-\tilde{n}^{(0)}_\omega\partial_\omega\tilde{n}^{(0)}_\omega + \frac{1}{2}n_0\mathcal{H}\partial^2_\omega\tilde{n}^{(0)}_\omega\right) \tag{291}$$

where $Z = z/\tau_R$. The leading-order linear term is

$$\partial_Z\tilde{n}^{(0)}_\omega = -\gamma n_0\mathcal{H}\tilde{n}^{(0)}_\omega. \tag{292}$$

The solution to this linear equation is periodic

$$\tilde{n}^{(0)}_\omega(Z) = \cos\left(\gamma n_0 Z\right)\tilde{n}^{(0)}_{\omega,0} - \sin\left(\gamma n_0 Z\right)\mathcal{H}\tilde{n}^{(0)}_{\omega,0}, \tag{293}$$

where $\tilde{n}^{(0)}_\omega(Z=0) = \tilde{n}^{(0)}_{\omega,0}$.

### A.6. Derivation of the long-range temporal Vlasov equation

The derivation of the long-range Vlasov equation in the temporal domain follows the lines of the corresponding derivation in the spatial domain outlined in Appendix A.2. In particular, the scaling for the long-range response function reads $R(t) = \varepsilon R^{(0)}(\varepsilon t)$. For the term $P$ one thus obtains

$$\int_{-\infty}^{+\infty} P(t,\tau,z)\exp(i\omega\tau)d\tau = i\varepsilon\partial_\omega n^{(0)}_\omega(T,Z)\partial_T\int_{-\infty}^{+\infty} R^{(0)}(T-T')\left(\frac{1}{2\pi}\int_{-\infty}^{+\infty} n^{(0)}_{\omega'}(T',Z)d\omega'\right)dT'. \tag{294}$$

As in the spatial case, the same procedure applied to the term $Q$ in the equation for the autocorrelation function reveals that the first nonvanishing term is of second order, $\varepsilon^2$. Coming back to the original variables, one thus obtains the Vlasov equation (64) with the effective potential (66).

### A.7. Derivation of the WT kinetic equation with a trap $V(\mathbf{r})$

Starting from Eq. (148), one obtains the following equation for the evolution of $\mathbf{n}(z) = (n_m(z))_m$

$$\partial_z n_m(z) = 2\gamma\sum_{p,q,s}\mathrm{Im}\left(W_{mpqs}J_{mpqs}(z)\right) \tag{295}$$

where $J_{mpqs} = \left\langle a^*_m a_p a^*_q a_s\right\rangle$ denotes the fourth-order moment. The equation governing the evolution of $J_{mpqs}$ depends on the corresponding sixth order moment. In this way one obtains an infinite hierarchy of moment equations, in which the $n$th order moment depends on the $n+2$th order moment. The closure of the hierarchy can be achieved following the random phase approximation [37,47]. Assuming that $|U/E| \ll 1$, linear dispersive effects dominate the interaction and bring the field close to Gaussian statistics [37,51]. By virtue of the factorizability property of statistical Gaussian fields, the sixth order moment in the equation for $J_{mpqs}$ can be factorized as a product of second-order moments. We obtain in this way

$$\partial_z J_{mpqs}(z) = i\Delta_{mpqs}J_{mpqs}(z) + 2i\gamma W^*_{mpqs}M_{mpqs}(\mathbf{n}(z)) + 2i\gamma R_{mpqs}(\mathbf{n}(z)) \tag{296}$$

with

$$\Delta_{mpqs} = \beta_m + \beta_q - \beta_p - \beta_s, \tag{297}$$

$$M_{mpqs}(\mathbf{n}) = n_m n_p n_q n_s(n_m^{-1} + n_q^{-1} - n_p^{-1} - n_s^{-1}), \tag{298}$$

$$\begin{aligned} R_{mpqs}(\mathbf{n}) \;=\; & \delta^K_{q,s}U_{pm}(\mathbf{n})(n_p - n_m)n_q + \delta^K_{q,p}U_{sm}(\mathbf{n})(n_s - n_m)n_p \\ & + \delta^K_{m,s}U_{pq}(\mathbf{n})(n_p - n_q)n_s + \delta^K_{m,p}U_{sq}(\mathbf{n})(n_s - n_q)n_m, \end{aligned} \tag{299}$$

$$U_{pq}(\mathbf{n}) = \sum_s W_{pqss}n_s = \int u^*_p(\mathbf{r})u_q(\mathbf{r})\sum_s n_s|u_s(\mathbf{r})|^2 d\mathbf{r} \tag{300}$$

where $\delta^K_{q,s}$ denotes the Kronecker symbol, $\delta^K_{q,s}=1$ if the mode index $\{q\}$ equals $\{s\}$, $\delta^K_{q,s}=0$ otherwise. We recall here that $\{q\}$ labels the two numbers $(q_x, q_y)$ that specify the eigenmode $u_{q_x,q_y}(\boldsymbol{r})$ and its eigenvalue $\beta_{q_x,q_y}$.

We integrate the equation for $J_{mpqs}$:

$$J_{mpqs}(z)=e^{i\Delta_{mpqs}z}J_{mpqs}(0)+2i\gamma\int_0^z e^{i\Delta_{mpqs}(z-\zeta)}\big(W^*_{mpqs}M_{mpqs}(\mathbf{n}(\zeta))+R_{mpqs}(\mathbf{n}(\zeta))\big)d\zeta$$

and substitute into the equation for $\mathbf{n}$:

$$\begin{aligned}\partial_z n_m(z)=\;&2\gamma\sum_{p,q,s}\mathrm{Im}\big(e^{i\Delta_{mpqs}z}W_{mpqs}J_{mpqs}(0)\big)\\&+4\gamma^2\sum_{p,q,s}\int_0^z d\zeta\,\cos(\Delta_{mpqs}(z-\zeta))\Big[\mathrm{Re}\big(W_{mpqs}R_{mpqs}(\mathbf{n}(\zeta))\big)+|W_{mpqs}|^2M_{mpqs}(\mathbf{n}(\zeta))\Big]\\&-4\gamma^2\sum_{p,q,s}\int_0^z d\zeta\,\sin(\Delta_{mpqs}(z-\zeta))\mathrm{Im}\big(W_{mpqs}R_{mpqs}(\mathbf{n}(\zeta))\big).\end{aligned}$$

Under the assumption $V_0/\beta_0\gg 1$, we can take the continuum limit. If we denote $\tilde{n}_{\boldsymbol{k}}(z)=n_{[\boldsymbol{k}/\beta_0]}(z)$, then

$$\begin{aligned}\partial_z\tilde{n}_{\boldsymbol{\kappa}}(z)=\;&\frac{2\gamma}{\beta_0^6}\iiint d\boldsymbol{\kappa}_1d\boldsymbol{\kappa}_2d\boldsymbol{\kappa}_3\mathrm{Im}\big(e^{i\tilde{\Delta}_{\boldsymbol{\kappa}\boldsymbol{\kappa}_1\boldsymbol{\kappa}_2\boldsymbol{\kappa}_3}z}\tilde{W}_{\boldsymbol{\kappa}\boldsymbol{\kappa}_1\boldsymbol{\kappa}_2\boldsymbol{\kappa}_3}\tilde{J}_{\boldsymbol{\kappa}\boldsymbol{\kappa}_1\boldsymbol{\kappa}_2\boldsymbol{\kappa}_3}(0)\big)\\&+\frac{4\gamma^2}{\beta_0^6}\iiint d\boldsymbol{\kappa}_1d\boldsymbol{\kappa}_2d\boldsymbol{\kappa}_3\int_0^z d\zeta\,\cos(\tilde{\Delta}_{\boldsymbol{\kappa}\boldsymbol{\kappa}_1\boldsymbol{\kappa}_2\boldsymbol{\kappa}_3}(z-\zeta))\\&\times\Big[\mathrm{Re}\big(\tilde{W}_{\boldsymbol{\kappa}\boldsymbol{\kappa}_1\boldsymbol{\kappa}_2\boldsymbol{\kappa}_3}\tilde{R}_{\boldsymbol{\kappa}\boldsymbol{\kappa}_1\boldsymbol{\kappa}_2\boldsymbol{\kappa}_3}(\tilde{\mathbf{n}}(\zeta))\big)+|\tilde{W}_{\boldsymbol{\kappa}\boldsymbol{\kappa}_1\boldsymbol{\kappa}_2\boldsymbol{\kappa}_3}|^2\tilde{M}_{\boldsymbol{\kappa}\boldsymbol{\kappa}_1\boldsymbol{\kappa}_2\boldsymbol{\kappa}_3}(\tilde{\mathbf{n}}(\zeta))\Big]\\&-\frac{4\gamma^2}{\beta_0^6}\iiint d\boldsymbol{\kappa}_1d\boldsymbol{\kappa}_2d\boldsymbol{\kappa}_3\int_0^z d\zeta\,\sin(\tilde{\Delta}_{\boldsymbol{\kappa}\boldsymbol{\kappa}_1\boldsymbol{\kappa}_2\boldsymbol{\kappa}_3}(z-\zeta))\mathrm{Im}\big(\tilde{W}_{\boldsymbol{\kappa}\boldsymbol{\kappa}_1\boldsymbol{\kappa}_2\boldsymbol{\kappa}_3}\tilde{R}_{\boldsymbol{\kappa}\boldsymbol{\kappa}_1\boldsymbol{\kappa}_2\boldsymbol{\kappa}_3}(\tilde{\mathbf{n}}(\zeta))\big)\end{aligned}$$

where $\tilde{\beta}_{\boldsymbol{\kappa}}=\beta_{[\boldsymbol{\kappa}/\beta_0]}$, $\tilde{\Delta}_{\boldsymbol{\kappa}\boldsymbol{\kappa}_1\boldsymbol{\kappa}_2\boldsymbol{\kappa}_3}=\Delta_{[\boldsymbol{\kappa}/\beta_0][\boldsymbol{\kappa}_1/\beta_0][\boldsymbol{\kappa}_2/\beta_0][\boldsymbol{\kappa}_3/\beta_0]}$ and so on, $[x]$ being the integer part of $x$. The presence of the rapid phase allows us to use the following results:

$$\begin{aligned}m\int\int_0^z\cos(m\Delta y)dy\varphi(\Delta)d\Delta&=\int\mathrm{sinc}(v)\varphi\left(\frac{v}{mz}\right)dv\overset{m\to\infty}{\longrightarrow}\pi\varphi(0)\\m\int\int_0^z\sin(m\Delta y)dy\varphi(\Delta)d\Delta&=2\int\frac{\sin^2(v)}{v}\varphi\left(\frac{2v}{mz}\right)dv\overset{m\to\infty}{\longrightarrow}0\end{aligned}$$

and we find

$$\partial_z\tilde{n}_{\boldsymbol{\kappa}}(z)=\frac{4\pi\gamma^2}{\beta_0^6}\iiint d\boldsymbol{\kappa}_1d\boldsymbol{\kappa}_2d\boldsymbol{\kappa}_3\delta(\tilde{\Delta}_{\boldsymbol{\kappa}\boldsymbol{\kappa}_1\boldsymbol{\kappa}_2\boldsymbol{\kappa}_3})\Big[\mathrm{Re}\big(\tilde{W}_{\boldsymbol{\kappa}\boldsymbol{\kappa}_1\boldsymbol{\kappa}_2\boldsymbol{\kappa}_3}\tilde{R}_{\boldsymbol{\kappa}\boldsymbol{\kappa}_1\boldsymbol{\kappa}_2\boldsymbol{\kappa}_3}(\tilde{\mathbf{n}}(z))\big)+|\tilde{W}_{\boldsymbol{\kappa}\boldsymbol{\kappa}_1\boldsymbol{\kappa}_2\boldsymbol{\kappa}_3}|^2\tilde{M}_{\boldsymbol{\kappa}\boldsymbol{\kappa}_1\boldsymbol{\kappa}_2\boldsymbol{\kappa}_3}(\tilde{\mathbf{n}}(z))\Big].$$

We remark that the Kronecker symbol involved in $\tilde{R}_{\boldsymbol{\kappa}\boldsymbol{\kappa}_1\boldsymbol{\kappa}_2\boldsymbol{\kappa}_3}(\tilde{\mathbf{n}}(z))$ can be converted to a Dirac $\delta$-function, $\delta^K_{[\boldsymbol{\kappa}_1/\beta_0],[\boldsymbol{\kappa}_2/\beta_0]}\to\beta_0^2\delta(\boldsymbol{\kappa}_1-\boldsymbol{\kappa}_2)$. The contribution of the first term $I_1$ of $\tilde{R}_{\boldsymbol{\kappa}\boldsymbol{\kappa}_1\boldsymbol{\kappa}_2\boldsymbol{\kappa}_3}(\tilde{\mathbf{n}}(z))$ can thus be written as

$$\begin{aligned}I_1&=\iiint d\boldsymbol{\kappa}_1d\boldsymbol{\kappa}_2d\boldsymbol{\kappa}_3\delta(\tilde{\Delta}_{\boldsymbol{\kappa}\boldsymbol{\kappa}_1\boldsymbol{\kappa}_2\boldsymbol{\kappa}_3})\mathrm{Re}\big[\tilde{W}_{\boldsymbol{\kappa}\boldsymbol{\kappa}_1\boldsymbol{\kappa}_2\boldsymbol{\kappa}_3}\delta^K_{[\boldsymbol{\kappa}_2/\beta_0],[\boldsymbol{\kappa}_3/\beta_0]}U_{[\boldsymbol{\kappa}_1/\beta_0][\boldsymbol{\kappa}/\beta_0]}(\mathbf{n})(n_{[\boldsymbol{\kappa}_1/\beta_0]}-n_{[\boldsymbol{\kappa}/\beta_0]})n_{[\boldsymbol{\kappa}_2/\beta_0]}\big]\\&=\beta_0^2\int d\boldsymbol{\kappa}_1\delta(\tilde{\beta}_{\boldsymbol{\kappa}_1}-\tilde{\beta}_{\boldsymbol{\kappa}})\mathrm{Re}\Big[\Big(\int d\boldsymbol{\kappa}_2\tilde{W}_{\boldsymbol{\kappa}\boldsymbol{\kappa}_1\boldsymbol{\kappa}_2\boldsymbol{\kappa}_2}n_{[\boldsymbol{\kappa}_2/\beta_0]}\Big)U_{[\boldsymbol{\kappa}_1/\beta_0][\boldsymbol{\kappa}/\beta_0]}(\mathbf{n})(n_{[\boldsymbol{\kappa}_1/\beta_0]}-n_{[\boldsymbol{\kappa}/\beta_0]})\Big]\\&=\beta_0^4\int d\boldsymbol{\kappa}_1\delta(\tilde{\beta}_{\boldsymbol{\kappa}_1}-\tilde{\beta}_{\boldsymbol{\kappa}})|U_{[\boldsymbol{\kappa}_1/\beta_0][\boldsymbol{\kappa}/\beta_0]}(\mathbf{n})|^2(n_{[\boldsymbol{\kappa}_1/\beta_0]}-n_{[\boldsymbol{\kappa}/\beta_0]}).\end{aligned}$$

We also made use of the fact that $U_{[\boldsymbol{\kappa}_1/\beta_0][\boldsymbol{\kappa}/\beta_0]}(\mathbf{n})=\tilde{U}_{\boldsymbol{\kappa}_1\boldsymbol{\kappa}}(\tilde{\mathbf{n}})=\frac{1}{\beta_0^2}\int d\boldsymbol{\kappa}'\tilde{W}_{\boldsymbol{\kappa}_1\boldsymbol{\kappa}\boldsymbol{\kappa}'\boldsymbol{\kappa}'}\tilde{n}_{\boldsymbol{\kappa}'}$, and $\tilde{U}_{\boldsymbol{\kappa}_1\boldsymbol{\kappa}}(\tilde{\mathbf{n}})=\tilde{U}^*_{\boldsymbol{\kappa}\boldsymbol{\kappa}_1}(\tilde{\mathbf{n}})$. Proceeding similarly for the second term $I_2$ of $\tilde{R}_{\boldsymbol{\kappa}\boldsymbol{\kappa}_1\boldsymbol{\kappa}_2\boldsymbol{\kappa}_3}(\tilde{\mathbf{n}}(z))$, one obtains $I_1=I_2$. The contributions of the third and fourth terms of $\tilde{R}_{\boldsymbol{\kappa}\boldsymbol{\kappa}_1\boldsymbol{\kappa}_2\boldsymbol{\kappa}_3}(\tilde{\mathbf{n}}(z))$ lead to

$$I_3=I_4=\beta_0^4\int d\boldsymbol{\kappa}_1d\boldsymbol{\kappa}_2\delta(\tilde{\beta}_{\boldsymbol{\kappa}_1}-\tilde{\beta}_{\boldsymbol{\kappa}_2})\mathrm{Re}\left[\tilde{W}_{\boldsymbol{\kappa}\boldsymbol{\kappa}\boldsymbol{\kappa}_2\boldsymbol{\kappa}_1}\tilde{U}_{\boldsymbol{\kappa}_1\boldsymbol{\kappa}_2}(\mathbf{n})(\tilde{n}_{\boldsymbol{\kappa}_1}-\tilde{n}_{\boldsymbol{\kappa}_2})\tilde{n}_{\boldsymbol{\kappa}}\right].$$

A permutation of the variables $\boldsymbol{\kappa}_1$ and $\boldsymbol{\kappa}_2$ in this expression readily gives $I_3=I_4=0$. Collecting all terms, we finally obtain the irreversible kinetic equation (151) governing the evolution of $\tilde{n}_{\boldsymbol{\kappa}}(z)$.

## References


[1] J. Ducuing, N. Bloembergen, Statistical fluctuations in nonlinear optical processes, Phys. Rev. 133 (1964) A1493.
[2] L. Mandel, E. Wolf, Optical Coherence and Quantum Optics, Cambridge university press, 1995.
[3] M. Mitchell, Z. Chen, M. Shih, M. Segev, Self-trapping of partially spatially incoherent light, Phys. Rev. Lett. 77 (1996) 490.
[4] M. Mitchell, M. Segev, Self-trapping of incoherent white light, Nature 387 (1997) 880.
[5] M. Segev, D. Christodoulides, Incoherent Solitons, in: S. Trillo, W. Torruellas (Eds.), Spatial Solitons, Springer, Berlin, 2001.
[6] Y. Kivshar, G. Agrawal, Optical Solitons: From Fibers to Photonic Crystals, Academic Press, 2003.
[7] G.A. Pasmanik, Self-interaction of incoherent light beams, Sov. Phys.—JETP 39 (1974) 234.
[8] M. Mitchell, M. Segev, T. Coskun, D. Christodoulides, Theory of self-trapped spatially incoherent light beams, Phys. Rev. Lett. 79 (1997) 4990.
[9] D. Christodoulides, T. Coskun, M. Mitchell, M. Segev, Theory of incoherent self-focusing in biased photorefractive media, Phys. Rev. Lett. 78 (1997) 646.
[10] B. Hall, M. Lisak, D. Anderson, R. Fedele, V.E. Semenov, Statistical theory for incoherent light propagation in nonlinear media, Phys. Rev. E 65 (2002) 035602.
[11] D.N. Christodoulides, E.D. Eugenieva, T.H. Coskun, M. Segev, M. Mitchell, Equivalence of three approaches describing partially incoherent wave propagation in inertial nonlinear media, Phys. Rev. E 63 (2001) 035601.
[12] M. Lisak, L. Helczynski, D. Anderson, Relation between different formalisms describing partially incoherent wave propagation in nonlinear optical media, Opt. Commun. 220 (2003) 321.
[13] D.N. Christodoulides, T.H. Coskun, M. Mitchell, Z. Chen, M. Segev, Theory of incoherent dark solitons, Phys. Rev. Lett. 80 (1998) 5113.
[14] Z. Chen, M. Mitchell, M. Segev, T.H. Coskun, D.N. Christodoulides, Self-trapping of dark incoherent light beams, Science 280 (1998) 889.
[15] M. Soljacic, M. Segev, T. Coskun, D. Christodoulides, A. Vishwanath, Modulation instability of incoherent beams in noninstantaneous nonlinear media, Phys. Rev. Lett. 84 (2000) 467.
[16] D. Kip, M. Soljacic, M. Segev, E. Eugenieva, D. Christodoulides, Modulation instability and pattern formation in spatially incoherent light beams, Science 290 (2000) 495–498.
[17] L. Helczynski, M. Lisak, D. Anderson, Influence of higher-order dispersion on modulational instability and pulse broadening of partially incoherent light, Phys. Rev. E 67 (2003) 026602.
[18] B. Kibler, C. Michel, J. Garnier, A. Picozzi, Temporal dynamics of incoherent waves in noninstantaneous response nonlinear Kerr media, Opt. Lett. 37 (2012) 2472.
[19] H. Buljan, O. Cohen, J. W. Fleischer, T. Schwartz, M. Segev, Z.H. Musslimani, N.K. Efremidis, D.N. Christodoulides, Random-phase solitons in nonlinear periodic lattices, Phys. Rev. Lett. 92 (2004) 223901.
[20] O. Cohen, G. Bartal, H. Buljan, T. Carmon, J. Fleischer, M. Segev, D. Christodoulides, Observation of random phase lattice solitons, Nature 433 (2005) 500.
[21] A. Picozzi, M. Haelterman, Parametric three-wave soliton generated from incoherent light, Phys. Rev. Lett. 86 (2001) 2010–2013.
[22] A. Picozzi, M. Haelterman, S. Pitois, G. Millot, Incoherent solitons in instantaneous response nonlinear media, Phys. Rev. Lett. 92 (2004) 143906.
[23] M. Peccianti, G. Assanto, Incoherent spatial solitary waves in nematic liquid crystals, Opt. Lett. 26 (2001) 1791–1793.
[24] M. Peccianti, G. Assanto, Nematic liquid crystals: a suitable medium for self-confinement of coherent and incoherent light, Phys. Rev. E 65 (2002) 035603–1.
[25] O. Cohen, H. Buljan, T. Schwartz, J.W. Fleischer, M. Segev, Incoherent solitons in instantaneous nonlocal nonlinear media, Phys. Rev. E 73 (2006) 015601.
[26] C. Rotschild, T. Schwartz, O. Cohen, M. Segev, Incoherent spatial solitons in effectively-instantaneous nonlocal nonlinear media, Nature Photonics 2 (2008) 371.
[27] A. Picozzi, J. Garnier, Incoherent soliton turbulence in nonlocal nonlinear media, Phys. Rev. Lett. 107 (2011) 233901.
[28] M. Wu, P. Krivosik, B. Kalinikos, C. Patton, Random generation of coherent solitary waves from incoherent waves, Phys. Rev. Lett. 96 (2006) 227202.
[29] A. Picozzi, S. Pitois, G. Millot, Spectral incoherent solitons: A localized soliton behavior in frequency space, Phys. Rev. Lett. 101 (2008) 093901.
[30] B. Kibler, C. Michel, A. Kudlinski, B. Barviau, G. Millot, A. Picozzi, Emergence of spectral incoherent solitons through supercontinuum generation in a photonic crystal fiber, Phys. Rev. E 84 (2011) 066605.
[31] J.M. Dudley, J.R. Taylor, Supercontinuum Generation in Optical Fibers, Cambridge University Press, Cambridge, 2010.
[32] A. Couairon, A. Mysyrowicz, Femtosecond filamentation in transparent media, Phys. Rep. 441 (2007) 47–189.
[33] D.S. Wiersma, The physics and applications of random lasers, Nat. Phys. 4 (2008) 359–367.
[34] N. Akhmediev, E. Pelinovsky, Editorial–introductory remarks on discussion & debate: Rogue waves–towards a unifying concept, The European Physical Journal Special Topics 185 (2010) 1–4.
[35] V. Ruban, Y. Kodama, M. Ruderman, J. Dudley, R. Grimshaw, P. McClintock, M. Onorato, C. Kharif, E. Pelinovsky, T. Soomere, et al., Rogue waves–towards a unifying concept: Discussions and debates, Eur. Phys. J. Spec. Top. 185 (2010) 5–15.
[36] M. Onorato, S. Residori, U. Bortolozzo, A. Montina, F. Arecchi, Rogue waves and their generating mechanisms in different physical contexts, Phys. Rep. 528 (2013) 47–89.
[37] V.E. Zakharov, V.S. L'vov, G. Falkovich, Kolmogorov Spectra of Turbulence I, Springer, Berlin, 1992.
[38] U. Frisch, Turbulence. The legacy of A. N. Kolmogorov, Cambridge University Press, Cambridge, 1995.
[39] A.C. Newell, R. Rumpf, Wave turbulence, Annu. Rev. Fluid Mech. 43 (2011) 59–78.
[40] S. Nazarenko, Wave Trubulence, in: Lecture Notes in Physics, 825, Springer, 2011.
[41] A.C. Newell, B. Rumpf, V.E. Zakharov, Spontaneous breaking of the spatial homogeneity symmetry in wave turbulence, Phys. Rev. Lett. 108 (2012) 194502.
[42] V.N. Tsytovich, Nonlinear Effects in Plasma, Plenum, New York, 1970.
[43] A. Hasegawa, Plasma Instabilities and Nonlinear Effects, Springer-Verlag, New York, 1975.
[44] K. Hasselmann, On the non-linear energy transfer in a gravity-wave spectrum. part 1. general theory, J. Fluid Mech. 12 (1962) 481–500.
[45] K. Hasselmann, On the non-linear energy transfer in a gravity-wave spectrum. part 2. conservation theorems; wave-particle analogy; irreversibility, J. Fluid Mech. 15 (1963) 273–281.
[46] S. Dyachenko, A.C. Newell, A. Pushkarev, V.E. Zakharov, Optical turbulence: weak turbulence, condensates and collapsing filaments in the nonlinear Schrödinger equation, Physica D 57 (1992) 96.
[47] V. Zakharov, F. Dias, A. Pushkarev, One-dimensional wave turbulence, Phys. Rep. 398 (2004) 1.
[48] D.J. Benney, P.G. Saffman, Nonlinear interactions of random waves in dispersive medium, Proc. R. Soc. Lond. Ser. A 289 (1966) 301.
[49] A. Newell, The closure problem in a system of random gravity waves, Rev. Geophys. 6 (1968) 1.
[50] D.J. Benney, A. Newell, Random wave closure, Stud. Appl. Math. 48 (1969) 29.
[51] A.C. Newell, S. Nazarenko, L. Biven, Wave turbulence and intermittency, Physica D 152–153 (2001) 520–550.
[52] Y.V. Lvov, S. Nazarenko, Noisy spectra, long correlations, and intermittency in wave turbulence, Phys. Rev. E 69 (2004) 066608.
[53] Y. Choi, Y.V. Lvov, S. Nazarenko, Probability densities and preservation of randomness in wave turbulence, Phys. Lett. A 332 (2004) 230.
[54] Y. Choi, Y.V. Lvov, S. Nazarenko, Joint statistics of amplitudes and phases in wave turbulence, Physica D 201 (2005) 121.
[55] K. Rasmussen, T. Cretegny, P.G. Kevrekidis, N. Gronbech-Jensen, Statistical mechanics of a discrete nonlinear system, Phys. Rev. Lett. 84 (2000) 3740.
[56] M. Johansson, K.O. Rasmussen, Statistical mechanics of general discrete nonlinear Schrödinger models: Localization transition and its relevance for Klein–Gordon lattices, Phys. Rev. E 70 (2004) 066610.
[57] R. Jordan, B. Turkington, C.L. Zirbel, A mean-field statistical theory for the nonlinear Schrödinger equation, Physica D 137 (2000) 353.
[58] R. Jordan, C. Josserand, Self-organization in nonlinear wave turbulence, Phys. Rev. E 61 (2000) 1527.

[59] A. Eisner, B. Turkington, Nonequilibrium statistical behavior of nonlinear Schrödinger equations, Physica D 213 (2006) 85.
[60] R. Rumpf, A.C. Newell, Coherent structures and entropy in constrained, modulationally unstable, nonintegrable systems, Phys. Rev. Lett. 87 (2001) 054102.
[61] R. Rumpf, A.C. Newell, Localization and coherence in nonintegrable systems, Physica D 184 (2003) 162.
[62] R. Rumpf, A.C. Newell, Intermittency as a consequence of turbulent transport in nonlinear systems, Phys. Rev. E 69 (2004) 026306.
[63] B. Rumpf, Simple statistical explanation for the localization of energy in nonlinear lattices with two conserved quantities, Phys. Rev. E 69 (2004) 016618.
[64] S.A. Derevyanko, Thermalized polarization dynamics of a discrete optical-waveguide system with four-wave mixing, Phys. Rev. A 88 (2013) 033851.
[65] L. Leuzzi, C. Conti, V. Folli, L. Angelani, G. Ruocco, Phase diagram and complexity of mode-locked lasers: From order to disorder, Phys. Rev. Lett. 102 (2009) 083901.
[66] C. Conti, L. Leuzzi, Complexity of waves in nonlinear disordered media, Phys. Rev. B 83 (2011) 134204.
[67] A. Fratalocchi, C. Conti, G. Ruocco, S. Trillo, Free-energy transition in a gas of noninteracting nonlinear wave particles, Phys. Rev. Lett. 101 (2008) 044101.
[68] A. Fratalocchi, Statistical analysis of complex systems with nonclassical invariant measures, Phys. Rev. E 83 (2011) 021116.
[69] M. Davis, S. Morgan, K. Burnett, Simulations of Bose fields at finite temperature, Phys. Rev. Lett. 87 (2001) 160402.
[70] M. Davis, S. Morgan, K. Burnett, Simulations of thermal Bose fields in the classical limit, Phys. Rev. A 66 (2002) 053618.
[71] C. Connaughton, C. Josserand, A. Picozzi, Y. Pomeau, S. Rica, Condensation of classical nonlinear waves, Phys. Rev. Lett. 95 (2005) 263901.
[72] V. Zakharov, S. Nazarenko, Dynamics of the Bose–Einstein condensation, Physica D 201 (2005) 203.
[73] G. During, A. Picozzi, S. Rica, Breakdown of weak-turbulence and nonlinear wave condensation, Physica D 238 (2009) 1524.
[74] C. Conti, M. Leonetti, A. Fratalocchi, L. Angelani, G. Ruocco, Condensation in disordered lasers: Theory, 3d+1 simulations, and experiments, Phys. Rev. Lett. 101 (2008) 143901.
[75] E. Turitsyna, G. Falkovich, V. Mezentsev, S. Turitsyn, Optical turbulence and spectral condensate in long-fiber lasers, Phys. Rev. A 80 (2009) 031804.
[76] R. Weill, B. Fischer, O. Gat, Light-mode condensation in actively-mode-locked lasers, Phys. Rev. Lett. 104 (2010) 173901.
[77] J. Klaers, J. Schmitt, F. Vewinger, M. Weitz, Bose–Einstein condensation of photons in an optical microcavity, Nature 468 (2010) 545.
[78] C. Michel, M. Haelterman, P. Suret, S. Randoux, R. Kaiser, A. Picozzi, Thermalization and condensation in an incoherently pumped passive optical cavity, Phys. Rev. A 84 (2011) 033848.
[79] S.K. Turitsyn, S.A. Babin, E.G. Turitsyna, G.E. Falkovich, E. Podivilov, D. Churkin, Optical wave turbulence, in: V. Shira, S. Nazarenko (Eds.), in: Wave Turbulence, World Scientific Series on Nonlinear Science Series A, vol. 83, 2013.
[80] E. Turitsyna, G. Falkovich, A. El-Taher, X. Shu, P. Harper, S. Turitsyn, Optical turbulence and spectral condensate in long fibre lasers, Proc. R. Soc. A 468 (2012) 2145.
[81] E. Turitsyna, S. Smirnov, S. Sugavanam, N. Tarasov, X. Shu, S. Babin, E. Podivilov, D. Churkin, G. Falkovich, S. Turitsyn, The laminar-turbulent transition in a fibre laser, Nature Photonics 7 (2013) 783–786.
[82] I. Carusotto, C. Ciuti, Quantum fluids of light, Rev. Modern Phys. 85 (2013) 299–366.
[83] U. Bortolozzo, J. Laurie, S. Nazarenko, S. Residori, Optical wave turbulence and the condensation of light, J. Opt. Soc. Amer. B Opt. Phys. 26 (2009) 2280.
[84] J. Laurie, U. Bortolozzo, S. Nazarenko, S. Residori, One-dimensional optical wave turbulence: Experiment and theory, Phys. Rep. 514 (2012) 121.
[85] I. Bernstein, J. Green, M. Kruskal, Exact nonlinear plasma oscillations, Phys. Rev. 108 (1957) 546.
[86] A. Hasegawa, Dynamics of an ensemble of plane waves in nonlinear dispersive media, Phys. Fluids 18 (1975) 77.
[87] A. Hasegawa, Envelope soliton of random phase waves, Phys. Fluids 20 (1977) 2155.
[88] M. Marklund, P.K. Shukla, Nonlinear collective effects in photon–photon and photon-plasma interactions, Rev. Modern Phys. 78 (2006) 591–640.
[89] L. Silva, J. T. Mendonça, Photon kinetic theory of self-phase modulation, Opt. Commun. 196 (2001) 285.
[90] D. Dylov, J. Fleischer, Observation of all-optical bump-on-tail instability, Phys. Rev. Lett. 100 (2008) 103903.
[91] J. Garnier, J.-P. Ayanides, O. Morice, Propagation of partially coherent light with the maxwell-debye equation, J. Opt. Soc. Amer. B Opt. Phys. 20 (2003) 1409.
[92] J. Garnier, A. Picozzi, Unified kinetic formulation of incoherent waves propagating in nonlinear media with noninstantaneous response, Phys. Rev. A 81 (2010) 033831.
[93] J.T. Mendonça, N.L. Tsintsadze, Analog of the Wigner–Moyal equation for the electromagnetic field, Phys. Rev. E 62 (2000) 4276–4282.
[94] M. Marklund, P.K. Shukla, B. Bingham, J.T. Mendonça, Modulational instability of spatially broadband nonlinear optical pulses in four-state atomic systems, Phys. Rev. E 74 (2006) 067603.
[95] F. Hebenstreit, A. Ilderton, M. Marklund, J. Zamanian, Strong field effects in laser pulses: The Wigner formalism, Phys. Rev. D 83 (2011) 065007.
[96] R. Fedele, D. Anderson, M. Lisak, Landau-type damping in nonlinear wavepacket propagation, Phys. Scr. 2000 (2000) 27.
[97] B. Hall, M. Lisak, D. Anderson, V. Semenov, Effect of partial incoherence on modulation instability of two non-linearly interacting optical waves, Phys. Lett. A 321 (2004) 255–262.
[98] T. Lahaye, C. Menotti, L. Santos, M. Lewenstein, T. Pfau, The physics of dipolar bosonic quantum gases, Rep. Progr. Phys. 72 (2009) 126401.
[99] S. Skupin, M. Saffman, K. Krolikowski, Nonlocal stabilization of nonlinear beams in a self-focusing atomic vapor, Phys. Rev. Lett. 98 (2007) 263902.
[100] C. Conti, M. Peccianti, G. Assanto, Route to nonlocality and observation of accessible solitons, Phys. Rev. Lett. 91 (2003) 073901.
[101] C. Conti, M. Peccianti, G. Assanto, Observation of optical spatial solitons in a highly nonlocal medium, Phys. Rev. Lett. 92 (2004) 113902.
[102] N. Ghofraniha, C. Conti, G. Ruocco, S. Trillo, Shocks in nonlocal media, Phys. Rev. Lett. 99 (2007) 043903.
[103] C. Conti, A. Fratalocchi, M. Peccianti, G. Ruocco, S. Trillo, Observation of a gradient catastrophe generating solitons, Phys. Rev. Lett. 102 (2009) 083902.
[104] M. Segev, B. Crosignani, A. Yariv, B. Fischer, Spatial solitons in photorefractive media, Phys. Rev. Lett. 68 (1992) 923–926.
[105] A. Litvak, A. Sergeev, One dimensional collapse of plasma waves, JETP Lett. 27 (1978) 517.
[106] J. Wyller, W. Krolikowski, O. Bang, J.J. Rasmussen, Generic features of modulational instability in nonlocal Kerr media, Phys. Rev. E 66 (2002) 066615.
[107] S. Turitsyn, Spatial dispersion of nonlinearity and stability of multidimensional solitons, Theoret. and Math. Phys. 64 (1985) 226.
[108] O. Bang, W. Krolikowski, J. Wyller, J.J. Rasmussen, Collapse arrest and soliton stabilization in nonlocal nonlinear media, Phys. Rev. E 66 (2002) 046619.
[109] A. Dreischuh, D.N. Neshev, D.E. Petersen, O. Bang, W. Krolikowski, Observation of attraction between dark solitons, Phys. Rev. Lett. 96 (2006) 043901.
[110] W. Krolikowski, O. Bang, N. Nikolov, D. Neshev, J. Wyller, J. Rasmussen, D. Edmundson, Modulational instability, solitons and beam propagation in spatially nonlocal nonlinear media, J. Opt. B: Quant. Semicl. Opt. 6 (2004) S288.
[111] A. Snyder, D. Mitchell, Accessible solitons, Science 276 (1997) 1538.
[112] O. Cohen, H. Buljan, T. Schwartz, J. Fleischer, M. Segev, Incoherent solitons in instantaneous nonlocal nonlinear media, Phys. Rev. E 73 (2006) 015601.
[113] V. Zakharov, A. Pushkarev, V. Shvets, V. Yan'kov, Soliton turbulence, JETP Lett. 48 (1988) 83.
[114] A.I. D'yachenko, V.E. Zakharov, A.N. Pushkarev, V.F. Shvets, V.V. Yan'kov, Soliton turbulence in nonintegrable wave systems, JETP 69 (1989) 1144.
[115] V.E. Zakharov, S.L. Musher, A.M. Rubenchik, Hamiltonian approach to the description of non-linear plasma phenomena, Phys. Rep. 129 (1985) 285.
[116] M. Onorato, A. Osborne, R. Fedele, M. Serio, Landau damping and coherent structures in narrow-banded $1+1$ deep water gravity waves, Phys. Rev. E 67 (2003) 046305.
[117] A. Campa, T. Dauxois, S. Ruffo, Statistical mechanics and dynamics of solvable models with long-range interactions, Phys. Rep. 480 (2009) 57–159.
[118] S. Musher, A. Rubenchik, V. Zakharov, Weak Langmuir turbulence, Phys. Rep. 252 (1995) 177.
[119] C. Michel, B. Kibler, A. Picozzi, Discrete spectral incoherent solitons in nonlinear media with noninstantaneous response, Phys. Rev. A 83 (2011) 023806.
[120] J. Garnier, G. Xu, S. Trillo, A. Picozzi, Incoherent dispersive shocks in the spectral evolution of random waves, Phys. Rev. Lett. 111 (2013) 113902.
[121] G. Whitham, Linear and Nonlinear Waves, Wiley, New York, 1974.
[122] P. Constantin, P. Lax, A. Majda, A simple one-dimensional model for the three-dimensional vorticity equation, Comm. Pure Appl. Math. 38 (1985) 715–724.

[123] A. Fokas, M. Ablowitz, The inverse scattering transform for the Benjamin–Ono equation—a pivot to multidimensional problems, Stud. Appl. Math. 68 (1983) 1.
[124] R. Coifman, V. Wickerhauser, The scattering transform for the Benjamin–Ono equation, Stud. Appl. Math. 6 (1990) 825.
[125] T. Benjamin, Internal waves of permanent form in fluids of great depth, J. Fluid Mech. 29 (1967) 559.
[126] H. Ono, Algebraic solitary waves in stratified fluids, J. Phys. Soc. Japan 39 (1975) 1082.
[127] E. Bettelheim, A.G. Abanov, P. Wiegmann, Orthogonality catastrophe and shock waves in a nonequilibrium Fermi gas, Phys. Rev. Lett. 97 (2006) 246402.
[128] P. Wiegmann, Nonlinear hydrodynamics and fractionally quantized solitons at the fractional quantum hall edge, Phys. Rev. Lett. 108 (2012) 206810.
[129] R.Z. Sagdeev, D.A. Usikov, G.M. Zaslavsky, Nonlinear Physics, Harwood Academic Publ., Chur; Switzerland, 1988.
[130] G.E. Gallavotti, The Fermi–Pasta–Ulam problem: a status report, in: Lecture Notes in Physics, Springer, 2007.
[131] B. Lake, H. Yuen, H. Rundgaldier, W. Ferguson, Nonlinear deep-water waves: theory and experiment. part 2. evolution of a continuous wave train, J. Fluid Mech. 83 (1977) 49.
[132] M. Wu, C. Patton, Experimental observation of Fermi–Pasta–Ulam recurrence in a nonlinear feedback ring system, Phys. Rev. Lett. 98 (2007) 047202.
[133] G. Simaeys, P. Emplit, M. Haelterman, Experimental demonstration of the Fermi–Pasta–Ulam recurrence in a modulationally unstable optical wave, Phys. Rev. Lett. 87 (2001) 033902.
[134] G. Simaeys, P. Emplit, M. Haelterman, Experimental study of the reversible behavior of modulational instability in optical fibers, J. Opt. Soc. Amer. B Opt. Phys. 19 (2002) 477.
[135] J. Beeckman, X. Hutsebaut, M. Haelterman, K. Neyts, Induced modulation instability and recurrence in nematic liquid crystals, Opt. Express 15 (2007) 11185.
[136] C. Cambournac, H. Maillotte, E. Lantz, J.M. Dudley, M. Chauvet, Spatiotemporal behavior of periodic arrays of spatial solitons in a planar waveguide with relaxing Kerr nonlinearity, J. Opt. Soc. Amer. B Opt. Phys. 19 (2002) 574–585.
[137] K. Hammani, B. Wetzel, B. Kibler, J. Fatome, C. Finot, G. Millot, N. Akhmediev, J.M. Dudley, Spectral dynamics of modulation instability described using Akhmediev breather theory, Opt. Lett. 36 (2011) 2140–2142.
[138] G. Agrawal, Nonlinear Fiber Optics, fifth Ed., Academic Press, New York, 2012.
[139] J.M. Dudley, G. Genty, S. Coen, Supercontinuum generation in photonic crystal fiber, Rev. Modern Phys. 78 (2006) 1135.
[140] P. Suret, S. Randoux, H. Jauslin, A. Picozzi, Anomalous thermalization of nonlinear wave systems, Phys. Rev. Lett. 104 (2010) 054101.
[141] C. Michel, P. Suret, S. Randoux, H. Jauslin, A. Picozzi, Influence of third-order dispersion on the propagation of incoherent light in optical fibers, Opt. Lett. 35 (2010) 2367.
[142] P. Suret, A. Picozzi, S. Randoux, Wave turbulence in integrable systems: nonlinear propagation of incoherent optical waves in single-mode fibers, Opt. Express 19 (2011) 17852.
[143] B. Barviau, J. Garnier, G. Xu, B. Kibler, G. Millot, A. Picozzi, Truncated thermalization of incoherent optical waves through supercontinuum generation in photonic crystal fibers, Phys. Rev. A 87 (2013) 035803.
[144] J. Garnier, M. Lisak, A. Picozzi, Toward a wave turbulence formulation of statistical nonlinear optics, J. Opt. Soc. Amer. B Opt. Phys. 29 (2012) 2229–2242.
[145] M. Peccianti, G. Assanto, Nematicons, Phys. Rep. 516 (2012) 147–208.
[146] C. Rotschild, O. Cohen, O. Manela, M. Segev, T. Carmon, Solitons in nonlinear media with an infinite range of nonlocality: first observation of coherent elliptic solitons and of vortex-ring solitons, Phys. Rev. Lett. 95 (2005) 213904.
[147] C. Conti, G. Ruocco, S. Trillo, Optical spatial solitons in soft matter, Phys. Rev. Lett. 95 (2005) 183902.
[148] V. Folli, C. Conti, Frustrated brownian motion of nonlocal solitary waves, Phys. Rev. Lett. 104 (2010) 193901.
[149] V. Folli, C. Conti, Anderson localization in nonlocal nonlinear media, Opt. Lett. 37 (2012) 332–334.
[150] C. Conti, Complex light: dynamic phase transitions of a light beam in a nonlinear nonlocal disordered medium, Phys. Rev. E 72 (2005) 066620.
[151] D. Brambila, A. Fratalocchi, Nonlinearly-enhanced energy transport in many dimensional quantum chaos, Scientific Reports 3 (2013) 2359.
[152] V. Babenko, B.Y. Zel'dovich, V. Malyshev, A.A. Sychev, Spectrum of a giant laser pulse under frequency self-modulation conditions, Quantum Electron. 3 (1973) 97–99.
[153] J.T. Manassah, Self-phase modulation of incoherent light revisited, Opt. Lett. 16 (1991) 1638.
[154] Y. Levin, R. Pakter, F.B. Rizzato, T.N. Teles, F.P. Benetti, Nonequilibrium statistical mechanics of systems with long-range interactions, Phys. Rep. 535 (2014) 1–60. Nonequilibrium statistical mechanics of systems with long-range interactions.
[155] B. Alfassi, C. Rotschild, M. Segev, Incoherent surface solitons in effectively instantaneous nonlocal nonlinear media, Phys. Rev. A 80 (2009) 041808.
[156] A. Vedenov, L. Rudakov, Interaction of waves in continuous media, in: Soviet Physics Doklady, vol. 9, 1965, p. 1073.
[157] A. Vedenov, A. Gordeev, L. Rudakov, Oscillations and instability of a weakly turbulent plasma, Plasma Phys. 9 (1967) 719.
[158] T. Hansson, D. Anderson, M. Lisak, V.E. Semenov, U. Österberg, Quasilinear evolution and saturation of the modulational instability of partially coherent optical waves, Phys. Rev. A 78 (2008) 011807.
[159] P.M. Bellan, Fundamentals of Plasma Physics, Cambridge University Press, Cambridge, 2006.
[160] D. Anderson, L. Helczynski-Wolf, M. Lisak, V. Semenov, Transverse modulational instability of partially incoherent soliton stripes, Phys. Rev. E 70 (2004) 026603.
[161] D. Anderson, L. Helczynski-Wolf, M. Lisak, V. Semenov, Features of modulational instability of partially coherent light: Importance of the incoherence spectrum, Phys. Rev. E 69 (2004) 025601.
[162] T. Hansson, D. Anderson, M. Lisak, Propagation of partially coherent solitons in saturable logarithmic media: A comparative analysis, Phys. Rev. A 80 (2009) 033819.
[163] M. Yu, G. Agrawal, C. McKinstrie, Pump-wave effects on the propagation of noisy signals in nonlinear dispersive media, J. Opt. Soc. Amer. 12 (1995) 1126.
[164] S.B. Cavalcanti, G.P. Agrawal, M. Yu, Noise amplification in dispersive nonlinear media, Phys. Rev. A 51 (1995) 4086.
[165] A. Sauter, S. Pitois, G. Millot, A. Picozzi, Incoherent modulation instability in instantaneous nonlinear Kerr media, Opt. Lett. 30 (2005) 2143–2145.
[166] A. Snyder, D. Mitchell, Big incoherent solitons, Phys. Rev. Lett. 80 (1998) 1422.
[167] C. Mouhot, C. Villani, On Landau damping, Acta Math. 207 (2011) 29.
[168] A. Antoniazzi, D. Fanelli, J. Barré, P.-H. Chavanis, T. Dauxois, S. Ruffo, Maximum entropy principle explains quasistationary states in systems with long-range interactions: The example of the Hamiltonian mean-field model, Phys. Rev. E 75 (2007) 011112.
[169] A. Antoniazzi, F. Califano, D. Fanelli, S. Ruffo, Exploring the thermodynamic limit of Hamiltonian models: Convergence to the vlasov equation, Phys. Rev. Lett. 98 (2007) 150602.
[170] C. Michel, B. Kibler, J. Garnier, A. Picozzi, Temporal incoherent solitons supported by a defocusing nonlinearity with anomalous dispersion, Phys. Rev. A 86 (2012) 041801.
[171] R. Boyd, Nonlinear Optics, third ed., Academic Press, 2008.
[172] A. Kompaneets, Sov. Phys.—JETP 4 (1957) 730.
[173] A. Galeev, V. Karpman, R. Sagdeev, One problem now under solution in the theory of plasma turbulence, in: Soviet Physics Doklady, vol. 9, 1965, p. 681.
[174] Y.B. Zel'dovich, E. Levich, Bose condensation and shock waves in photon spectra, Sov. Phys.—JETP 28 (1969) 1287–1290.
[175] J. Peyraud, Théorie cinétique des plasmas interaction mtiére-rayonnement. iii. Interaction entre un rayonnement intense et un plasma par effet compton induit, J. Phys. (Paris) 29 (1968) 872.
[176] V. Zakharov, Collapse of Langmuir waves, Sov. Phys.—JETP 35 (1972) 908.
[177] H. Dreicer, Kinetic theory of an electron–photon gas, Phys. Fluids 7 (1964) 735.
[178] Y. Zel'dovich, R. Syunyaev, Shock wave structure in the radiation spectrum during Bose condensation of bosons, Sov. Phys.—JETP 35 (1972) 81.

[179] Y. Zel'dovich, E. Levich, R. Syunyaev, Stimulated compton interaction between Maxwellian electrons and spectrally narrow radiation, Sov. Phys.—JETP 35 (1972) 733.
[180] S. Musher, A. Rubenchik, V. Zakharov, Weak Langmuir turbulence of an isothermal plasma, JETP 42 (1976) 80.
[181] C. Montes, Variability of intensity of interstellar maser lines due to induced compton scattering, Astrophys. J. 216 (1977) 329.
[182] C. Montes, Photon soliton and fine structure due to nonlinear compton scattering, Phys. Rev. A 20 (1979) 1081.
[183] C. Montes, J. Peyraud, M. Henon, One-dimensional boson soliton collisions, Phys. Fluids 22 (1979) 176.
[184] B. Barviau, B. Kibler, A. Kudlinski, A. Mussot, G. Millot, A. Picozzi, Experimental signature of optical wave thermalization through supercontinuum generation in photonic crystal fiber, Opt. Express 17 (2009) 7392.
[185] G. Xu, J. Garnier, S. Trillo, A. Picozzi, Spectral dynamics of incoherent waves with a noninstantaneous nonlinear response, Opt. Lett. 38 (2013) 2972–2975.
[186] A.E. Kaplan, Subfemtosecond pulses in mode-locked $2\pi$ solitons of the cascade stimulated Raman scattering, Phys. Rev. Lett. 73 (1994) 1243–1246.
[187] A. Kaplan, P. Shkolnikov, Subfemtosecond pulses in the multicascade stimulated Raman scattering, JOSA B 13 (1996) 347–354.
[188] G. McDonald, Ultrabroad-bandwidth multifrequency Raman soliton pulse trains, Opt. Lett. 20 (1995) 822–824.
[189] D.V. Skryabin, F. Biancalana, D.M. Bird, F. Benabid, Effective Kerr nonlinearity and two-color solitons in photonic band-gap fibers filled with a Raman active gas, Phys. Rev. Lett. 93 (2004) 143907.
[190] D.V. Skryabin, A.V. Yulin, Raman solitons with group velocity dispersion, Phys. Rev. E 74 (2006) 046616.
[191] D.V. Skryabin, A.V. Yulin, F. Biancalana, Nontopological Raman-Kerr self-induced transparency solitons in photonic crystal fibers, Phys. Rev. E 73 (2006) 045603.
[192] A. Gurevich, L. Pitaevskii, Nonstationary structure of a collisionless shock wave, Sov. Phys.—JETP 38 (1974) 291.
[193] R. Taylor, D. Baker, H. Ikezi, Observation of collisionless electrostatic shocks, Phys. Rev. Lett. 24 (1970) 206.
[194] M.A. Hoefer, M.J. Ablowitz, I. Coddington, E.A. Cornell, P. Engels, V. Schweikhard, Dispersive and classical shock waves in Bose–Einstein condensates and gas dynamics, Phys. Rev. A 74 (2006) 023623.
[195] J.J. Chang, P. Engels, M.A. Hoefer, Formation of dispersive shock waves by merging and splitting Bose–Einstein condensates, Phys. Rev. Lett. 101 (2008) 170404.
[196] R. Meppelink, S.B. Koller, J.M. Vogels, P. van der Straten, E.D. van Ooijen, N.R. Heckenberg, H. Rubinsztein-Dunlop, S.A. Haine, M.J. Davis, Observation of shock waves in a large Bose–Einstein condensate, Phys. Rev. A 80 (2009) 043606.
[197] M. Crosta, S. Trillo, A. Fratalocchi, Crossover dynamics of dispersive shocks in Bose–Einstein condensates characterized by two- and three-body interactions, Phys. Rev. A 85 (2012) 043607.
[198] J.E. Rothenberg, D. Grischkowsky, Observation of the formation of an optical intensity shock and wave breaking in the nonlinear propagation of pulses in optical fibers, Phys. Rev. Lett. 62 (1989) 531–534.
[199] W. Wan, S. Jia, J. Fleischer, Dispersive, superfluid-like shock waves in nonlinear optics, Nat. Phys. 3 (2007) 46.
[200] N. Ghofraniha, S. Gentilini, V. Folli, E. DelRe, C. Conti, Shock waves in disordered media, Phys. Rev. Lett. 109 (2012) 243902.
[201] N. Ghofraniha, L.S. Amato, V. Folli, S. Trillo, E. DelRe, C. Conti, Measurement of scaling laws for shock waves in thermal nonlocal media, Opt. Lett. 37 (2012) 2325–2327.
[202] A. Armaroli, S. Trillo, A. Fratalocchi, Suppression of transverse instabilities of dark solitons and their dispersive shock waves, Phys. Rev. A 80 (2009) 053803.
[203] S. Gentilini, N. Ghofraniha, E. DelRe, C. Conti, Shock waves in thermal lensing, Phys. Rev. A 87 (2013) 053811.
[204] M. Conforti, F. Baronio, S. Trillo, Competing wave-breaking mechanisms in quadratic media, Opt. Lett. 38 (2013) 1648–1650.
[205] M.F. Saleh, A. Marini, F. Biancalana, Shock-induced P-T-symmetric potentials in gas-filled photonic-crystal fibers, Phys. Rev. A 89 (2014) 023801.
[206] T. Roger, M.F. Saleh, S. Roy, F. Biancalana, C. Li, D. Faccio, High-energy, shock-front-assisted resonant radiation in the normal dispersion regime, Phys. Rev. A 88 (2013) 051801.
[207] N. Smyth, P. Holloway, J. Phys. Oceanogr. 18 (1988) 947.
[208] P. Lorenzoni, S. Paleari, Metastability and dispersive shock waves in the Fermi–Pasta–Ulam systems, Physica D 221 (2006) 110.
[209] A. Molinari, C. Daraio, Stationary shocks in periodic highly nonlinear granular chains, Phys. Rev. E 80 (2009) 056602.
[210] Y.C. Mo, R.A. Kishek, D. Feldman, I. Haber, B. Beaudoin, P.G. O'Shea, J.C.T. Thangaraj, Experimental observations of soliton wave trains in electron beams, Phys. Rev. Lett. 110 (2013) 084802.
[211] A. Fratalocchi, A. Armaroli, S. Trillo, Time-reversal focusing of an expanding soliton gas in disordered replicas, Phys. Rev. A 83 (2011) 053846.
[212] M.F. Saleh, W. Chang, J.C. Travers, P.S.J. Russell, F. Biancalana, Plasma-induced asymmetric self-phase modulation and modulational instability in gas-filled hollow-core photonic crystal fibers, Phys. Rev. Lett. 109 (2012) 113902.
[213] C. Conti, M.A. Schmidt, P.S.J. Russell, F. Biancalana, Highly noninstantaneous solitons in liquid-core photonic crystal fibers, Phys. Rev. Lett. 105 (2010) 263902.
[214] D. Skryabin, F. Luan, J. Knight, P. Russell, Soliton self-frequency shift cancellation in photonic crystal fibers, Science 301 (2003) 1705.
[215] G. Xu, J. Garnier, A. Picozzi, Spectral long-range interaction of temporal incoherent solitons, Opt. Lett. 39 (2014) 590–593.
[216] G. Fanjoux, J. Michaud, H. Maillotte, T. Sylvestre, Slow-light spatial solitons, Phys. Rev. Lett. 100 (2008) 013908.
[217] C. Conti, M.A. Schmidt, P.S.J. Russell, F. Biancalana, Highly noninstantaneous solitons in liquid-core photonic crystal fibers, Phys. Rev. Lett. 105 (2010) 263902.
[218] C. Conti, S. Stark, P.S.J. Russell, F. Biancalana, Multiple hydrodynamical shocks induced by the Raman effect in photonic crystal fibers, Phys. Rev. A 82 (2010) 013838.
[219] M.F. Saleh, W. Chang, P. Hölzer, A. Nazarkin, J.C. Travers, N.Y. Joly, P.S.J. Russell, F. Biancalana, Theory of photoionization-induced blueshift of ultrashort solitons in gas-filled hollow-core photonic crystal fibers, Phys. Rev. Lett. 107 (2011) 203902.
[220] M.F. Saleh, F. Biancalana, Understanding the dynamics of photoionization-induced nonlinear effects and solitons in gas-filled hollow-core photonic crystal fibers, Phys. Rev. A 84 (2011) 063838.
[221] P. Hölzer, W. Chang, J.C. Travers, A. Nazarkin, J. Nold, N.Y. Joly, M.F. Saleh, F. Biancalana, P.S.J. Russell, Femtosecond nonlinear fiber optics in the ionization regime, Phys. Rev. Lett. 107 (2011) 203901.
[222] M. Conforti, G. Della Valle, Derivation of third-order nonlinear susceptibility of thin metal films as a delayed optical response, Phys. Rev. B 85 (2012) 245423.
[223] C. Brée, A. Demircan, G. Steinmeyer, Kramers–Kronig relations and high-order nonlinear susceptibilities, Phys. Rev. A 85 (2012) 033806.
[224] A. Marini, M. Conforti, G. Della Valle, H. Lee, T.X. Tran, W. Chang, M. Schmidt, S. Longhi, P.S. J. Russell, F. Biancalana, Ultrafast nonlinear dynamics of surface plasmon polaritons in gold nanowires due to the intrinsic nonlinearity of metals, New J. Phys. 15 (2013) 013033.
[225] V.V. Shkunov, D.Z. Anderson, Radiation transfer model of self-trapping spatially incoherent radiation by nonlinear media, Phys. Rev. Lett. 81 (1998) 2683.
[226] T. Hansson, M. Lisak, D. Anderson, Integrability and conservation laws for the nonlinear evolution equations of partially coherent waves in noninstantaneous Kerr media, Phys. Rev. Lett. 108 (2012) 063901.
[227] A. Ankiewicz, W. Krolikowski, N.N. Akhmediev, Partially coherent solitons of variable shape in a slow Kerr-like medium: exact solutions, Phys. Rev. E 59 (1999) 6079.
[228] T. Hansson, M. Lisak, D. Anderson, Generalized dressing method for nonlinear evolution equations describing partially coherent wave propagation in noninstantaneous Kerr media, Phys. Rev. E 84 (2011) 056601.
[229] W. Krolikowski, D. Edmundson, O. Bang, Unified model for partially coherent solitons in logarithmically nonlinear media, Phys. Rev. E 61 (2000) 3122.
[230] V. Semenov, M. Lisak, D. Anderson, T. Hansson, L. Helczynski-Wolf, U. Österberg, Mathematical basis for analysis of partially coherent wave propagation in nonlinear, non-instantaneous, Kerr media, J. Phys. A 41 (2008) 335207.

[231] L. Mandel, E. Wolf, Optical Coherence and Quantum Optics, Cambridge University Press, New York, 1995.
[232] T.H. Coskun, D.N. Christodoulides, M. Mitchell, Z. Chen, M. Segev, Dynamics of incoherent bright and dark self-trapped beams and their coherence properties in photorefractive crystals, Opt. Lett. 23 (1998) 418–420.
[233] D.N. Christodoulides, T.H. Coskun, R.I. Joseph, Incoherent spatial solitons in saturable nonlinear media, Opt. Lett. 22 (1997) 1080.
[234] O. Bang, D. Edmundson, W. Królikowski, Collapse of incoherent light beams in inertial bulk Kerr media, Phys. Rev. Lett. 83 (1999) 5479–5482.
[235] D.N. Christodoulides, T.H. Coskun, M. Mitchell, M. Segev, Multimode incoherent spatial solitons in logarithmically saturable nonlinear media, Phys. Rev. Lett. 80 (1998) 2310.
[236] M.I. Carvalho, T.H. Coskun, D.N. Christodoulides, M. Mitchell, M. Segev, Coherence properties of multimode incoherent spatial solitons in noninstantaneous Kerr media, Phys. Rev. E 59 (1999) 1193.
[237] S.A. Ponomarenko, N.M. Litchinitser, G.P. Agrawal, Theory of incoherent optical solitons: beyond the mean-field approximation, Phys. Rev. E 70 (2004) 015603.
[238] M. Lisak, B. Hall, D. Anderson, R. Fedele, V.E. Semenov, P.K. Shukla, A. Hasegawa, Nonlinear dynamics of partially incoherent optical waves based on the Wigner transform method, Phys. Scr. 2002 (2002) 12.
[239] L. Helczynski, D. Anderson, R. Fedele, B. Hall, M. Lisak, Propagation of partially incoherent light in nonlinear media via the Wigner transform method, IEEE J. Sel. Top. Quantum Electron. 8 (2002) 408.
[240] D. Kip, M. Soljačić, M. Segev, S.M. Sears, D.N. Christodoulides, 1+1-dimensional modulation instability of spatially incoherent light, J. Opt. Soc. Amer. B Opt. Phys. 19 (2002) 502–512.
[241] M. Lisak, D. Anderson, L. Helczynski-Wolf, P. Berczynski, R. Fedele, V. Semenov, Quasi-linear evolution of the modulational instability in the presence of partial incoherence, Phys. Scr. 2004 (2004) 56.
[242] M. Segev, D.N. Christodoulides, Incoherent solitons, Opt. Photonics News 13 (2002) 70–76.
[243] N. Akhmediev, A. Ankiewicz, Partially coherent solitons on a finite background, Phys. Rev. Lett. 82 (1999) 2661.
[244] T.H. Coskun, D.N. Christodoulides, Y.-R. Kim, Z. Chen, M. Soljacic, M. Segev, Bright spatial solitons on a partially incoherent background, Phys. Rev. Lett. 84 (2000) 2374–2377.
[245] T. Hansson, D. Anderson, M. Lisak, V.E. Semenov, U. Österberg, Propagation of partially coherent light beams with parabolic intensity distribution in noninstantaneous nonlinear Kerr media, JOSA B 25 (2008) 1780–1785.
[246] W. Królikowski, O. Bang, J. Wyller, Nonlocal incoherent solitons, Phys. Rev. E 70 (2004) 036617.
[247] K.G. Makris, H. Sarkissian, D.N. Christodoulides, G. Assanto, Nonlocal incoherent spatial solitons in liquid crystals, JOSA B 22 (2005) 1371–1377.
[248] A. Barak, C. Rotschild, B. Alfassi, M. Segev, D.N. Christodoulides, Random-phase surface-wave solitons in nonlocal nonlinear media, Opt. Lett. 32 (2007) 2450–2452.
[249] H. Buljan, M. Segev, M. Soljačić, N.K. Efremidis, D.N. Christodoulides, White-light solitons, Opt. Lett. 28 (2003) 1239–1241.
[250] H. Buljan, A. Šiber, M. Soljačić, T. Schwartz, M. Segev, D.N. Christodoulides, Incoherent white light solitons in logarithmically saturable noninstantaneous nonlinear media, Phys. Rev. E 68 (2003) 036607.
[251] H. Buljan, A. Šiber, M. Soljačić, M. Segev, Propagation of incoherent white light and modulation instability in noninstantaneous nonlinear media, Phys. Rev. E 66 (2002) 035601.
[252] T. Schwartz, T. Carmon, H. Buljan, M. Segev, Spontaneous pattern formation with incoherent white light, Phys. Rev. Lett. 93 (2004) 223901.
[253] F. Lederer, G.I. Stegeman, D.N. Christodoulides, G. Assanto, M. Segev, Y. Silberberg, Discrete solitons in optics, Phys. Rep. 463 (2008) 1–126.
[254] Y.V. Kartashov, B.A. Malomed, L. Torner, Solitons in nonlinear lattices, Rev. Modern Phys. 83 (2011) 247–305.
[255] D.N. Christodoulides, R.I. Joseph, Discrete self-focusing in nonlinear arrays of coupled waveguides, Opt. Lett. 13 (1988) 794–796.
[256] K. Motzek, A. Sukhorukov, F. Kaiser, Y. Kivshar, Incoherent multi-gap optical solitons in nonlinear photonic lattices, Opt. Express 13 (2005) 2916–2923.
[257] R. Pezer, H. Buljan, J. Fleischer, G. Bartal, O. Cohen, M. Segev, Gap random-phase lattice solitons, Opt. Express 13 (2005) 5013–5023.
[258] G. Bartal, O. Cohen, O. Manela, M. Segev, J.W. Fleischer, R. Pezer, H. Buljan, Observation of random-phase gap solitons in photonic lattices, Opt. Lett. 31 (2006) 483–485.
[259] R. Pezer, H. Buljan, G. Bartal, M. Segev, J.W. Fleischer, Incoherent white-light solitons in nonlinear periodic lattices, Phys. Rev. E 73 (2006) 056608.
[260] M. Jablan, H. Buljan, O. Manela, G. Bartal, M. Segev, Incoherent modulation instability in a nonlinear photonic lattice, Opt. Express 15 (2007) 4623–4633.
[261] H. Buljan, M. Soljačić, T. Carmon, M. Segev, Cavity pattern formation with incoherent light, Phys. Rev. E 68 (2003) 016616.
[262] T. Carmon, M. Soljačić, M. Segev, Pattern formation in a cavity longer than the coherence length of the light in it, Phys. Rev. Lett. 89 (2002) 183902.
[263] T. Schwartz, J.W. Fleischer, O. Cohen, H. Buljan, M. Segev, T. Carmon, Pattern formation in a ring cavity with temporally incoherent feedback, J. Opt. Soc. Amer. B Opt. Phys. 21 (2004) 2197–2205.
[264] T. Carmon, H. Buljan, M. Segev, Spontaneous pattern formation in a cavity with incoherent light, Opt. Express 12 (2004) 3481–3487.
[265] S. Barland, J.R. Tredicce, M. Brambilla, L.A. Lugiato, S. Balle, M. Giudici, T. Maggipinto, L. Spinelli, G. Tissoni, T. Knödl, et al., Cavity solitons as pixels in semiconductor microcavities, Nature 419 (2002) 699–702.
[266] F. Leo, S. Coen, P. Kockaert, S.-P. Gorza, P. Emplit, M. Haelterman, Temporal cavity solitons in one-dimensional Kerr media as bits in an all-optical buffer, Nature Photonics 4 (2010) 471.
[267] N. Akhmediev, W. Krolikowski, A.W. Snyder, Partially coherent solitons of variable shape, Phys. Rev. Lett. 81 (1998) 4632.
[268] S.V. Manakov, On the theory of two-dimensional stationary self-focusing of electromagnetic waves, Soviet J. Exp. Theor. Phys. 38 (1974) 248–253.
[269] W. Krolikowski, N. Akhmediev, B. Luther-Davies, Collision-induced shape transformations of partially coherent solitons, Phys. Rev. E 59 (1999) 4654–4658.
[270] D. Anderson, M. Lisak, Bandwidth limits due to incoherent soliton interaction in optical-fiber communication systems, Phys. Rev. A 32 (1985) 2270–2274.
[271] G.I. Stegeman, M. Segev, Optical spatial solitons and their interactions: universality and diversity, Science 286 (1999) 1518–1523.
[272] T.-S. Ku, M.-F. Shih, A.A. Sukhorukov, Y.S. Kivshar, Coherence controlled soliton interactions, Phys. Rev. Lett. 94 (2005) 063904.
[273] D. Anderson, L. Helczynski-Wolf, M. Lisak, V. Semenov, Interaction between two partially incoherent soliton stripes, Opt. Commun. 281 (2008) 3919–3923.
[274] C.-F. Huang, Q. Guo, Interaction of nonlocal incoherent spatial solitons, Opt. Commun. 277 (2007) 414–422.
[275] C.-F. Huang, R. Guo, S.-M. Liu, Z.-H. Liu, Interaction of incoherent white-light solitons, Opt. Commun. 269 (2007) 174–178.
[276] E.D. Eugenieva, D.N. Christodoulides, M. Segev, Elliptic incoherent solitons in saturable nonlinear media, Opt. Lett. 25 (2000) 972–974.
[277] O. Katz, T. Carmon, T. Schwartz, M. Segev, D.N. Christodoulides, Observation of elliptic incoherent spatial solitons, Opt. Lett. 29 (2004) 1248–1250.
[278] M. Peccianti, C. Conti, E. Alberici, G. Assanto, Spatially incoherent modulational instability in a non local medium, Laser Phys. Lett. 2 (2005) 25.
[279] T.H. Coskun, D.N. Christodoulides, M. Mitchell, Z. Chen, M. Segev, Dynamics of incoherent bright and dark self-trapped beams and their coherence properties in photorefractive crystals, Opt. Lett. 23 (1998) 418–420.
[280] Z. Chen, M. Segev, D. N. Christodoulides, R.S. Feigelson, Waveguides formed by incoherent dark solitons, Opt. Lett. 24 (1999) 1160–1162.
[281] T.H. Coskun, A.G. Grandpierre, D.N. Christodoulides, M. Segev, Coherence enhancement of spatially incoherent light beams through soliton interactions, Opt. Lett. 25 (2000) 826–828.
[282] T.H. Coskun, D.N. Christodoulides, Z. Chen, M. Segev, Dark incoherent soliton splitting and "phase-memory" effects: theory and experiment, Phys. Rev. E 59 (1999) R4777–R4780.
[283] Y.S. Kivshar, B. Luther-Davies, Dark optical solitons: physics and applications, Phys. Rep. 298 (1998) 81–197.
[284] J. Klinger, H. Martin, Z. Chen, Experiments on induced modulational instability of an incoherent opticalbeam, Opt. Lett. 26 (2001) 271–273.
[285] J.P. Torres, C. Anastassiou, M. Segev, M. Soljačic, D.N. Christodoulides, Transverse instability of incoherent solitons in Kerr media, Phys. Rev. E 65 (2001) 015601.

[286] C. Anastassiou, M. Soljačić, M. Segev, E.D. Eugenieva, D.N. Christodoulides, D. Kip, Z.H. Musslimani, J.P. Torres, Eliminating the transverse instabilities of Kerr solitons, Phys. Rev. Lett. 85 (2000) 4888–4891.
[287] Y.S. Kivshar, V.V. Afanasjev, Dark optical solitons with reverse-sign amplitude, Phys. Rev. A 44 (1991) R1446–R1449.
[288] N. Bélanger, P.-A. Bélanger, Bright solitons on a cw background, Opt. Commun. 124 (1996) 301–308.
[289] D. Frantzeskakis, K. Hizanidis, B. Malomed, C. Polymilis, Stable anti-dark light bullets supported by the third-order dispersion, Phys. Lett. A 248 (1998) 203–207.
[290] P. Aschieri, J. Garnier, C. Michel, V. Doya, A. Picozzi, Condensation and thermalization of classsical optical waves in a waveguide, Phys. Rev. A 83 (2011) 033838.
[291] A. Leggett, Quantum Liquids, Oxford University Press, 2006.
[292] S. Pitaevskii, L. Stringari, Bose–Einstein Condensation, Oxford Science Publications, 2003.
[293] Y.S. Kivshar, T.J. Alexander, S.K. Turitsyn, Nonlinear modes of a macroscopic quantum oscillator, Phys. Lett. A 278 (2001) 225–230.
[294] S.K. Turitsyn, T. Schäfer, V.K. Mezentsev, Self-similar core and oscillatory tails of a path-averaged chirped dispersion-managed optical pulse, Opt. Lett. 23 (1998) 1351–1353.
[295] S. Turitsyn, V. Mezentsev, Dynamics of self-similar dispersion-managed soliton presented in the basis of chirped Gauss–Hermite functions, J. Exp. Theor. Phys. Lett. 67 (1998) 640–646.
[296] K. Huang, Statistical Mechanics, Wiley, 1963.
[297] C. Conti, S. Trillo, P. Di Trapani, G. Valiulis, A. Piskarskas, O. Jedrkiewicz, J. Trull, Nonlinear electromagnetic X-waves, Phys. Rev. Lett. 90 (2003) 170406.
[298] P. Di Trapani, G. Valiulis, A. Piskarskas, O. Jedrkiewicz, J. Trull, C. Conti, S. Trillo, Spontaneously generated X-shaped light bullets, Phys. Rev. Lett. 91 (2003) 093904.
[299] J. Trull, O. Jedrkiewicz, P. Di Trapani, A. Matijosius, A. Varanavicius, G. Valiulis, R. Danielius, E. Kucinskas, A. Piskarskas, S. Trillo, Spatiotemporal three-dimensional mapping of nonlinear X waves, Phys. Rev. E 69 (2004) 026607.
[300] C. Conti, S. Trillo, Nonspreading wave packets in three dimensions formed by an ultracold Bose gas in an optical lattice, Phys. Rev. Lett. 92 (2004) 120404.
[301] P.V. Larsen, M.P. Sørensen, O. Bang, W.Z. Królikowski, S. Trillo, Nonlocal description of X-waves in quadratic nonlinear materials, Phys. Rev. E 73 (2006) 036614.
[302] F. Devaux, E. Lantz, Spatial and temporal properties of parametric fluorescence around degeneracy in a type i LBO crystal, Eur. Phys. J. D 8 (2000) 117–124.
[303] O. Jedrkiewicz, A. Picozzi, M. Clerici, D. Faccio, P. Di Trapani, Emergence of X-shaped spatiotemporal coherence in optical waves, Phys. Rev. Lett. 97 (2006) 243903.
[304] O. Jedrkiewicz, M. Clerici, A. Picozzi, D. Faccio, P. Di Trapani, X-shaped space–time coherence in optical parametric generation, Phys. Rev. A 76 (2007) 033823.
[305] A. Picozzi, M. Haelterman, Hidden coherence along space–time trajectories in parametric wave mixing, Phys. Rev. Lett. 88 (2002) 083901.
[306] S. Lagrange, H.R. Jauslin, A. Picozzi, Thermalization of the dispersive three-wave interaction, Europhys. Lett. 79 (2007) 64001.
[307] A. Picozzi, Towards a nonequilibrium thermodynamic description of incoherent nonlinear optics, Opt. Express 15 (2007) 9063.
[308] V. Zakharov, Weak turbulence spectrum in a plasma without a magnetic field, Sov. Phts. JETP 24 (1967) 455.
[309] S.Y. Annenkov, V.I. Shrira, Evolution of wave turbulence under gusty forcing, Phys. Rev. Lett. 107 (2011) 114502.
[310] S.Y. Annenkov, V.I. Shrira, Fast nonlinear evolution in wave turbulence, Phys. Rev. Lett. 102 (2009) 024502.
[311] G.Z. Forristall, Measurements of a saturated range in ocean wave spectra, J. Geophys. Res.: Oceans (1978–2012) 86 (1981) 8075–8084.
[312] V. L'Vov, Wave turbulence under parametric excitation, Springer Verlag, 1994.
[313] E. Henry, P. Alstrom, M. Levinsen, Prevalence of weak turbulence in strongly driven surface ripples, Europhys. Lett. 52 (2000) 27.
[314] G. Düring, C. Falcón, Symmetry induced four-wave capillary wave turbulence, Phys. Rev. Lett. 103 (2009) 174503.
[315] C. Falcon, E. Falcon, U. Bortolozzo, S. Fauve, Capillary wave turbulence on a spherical fluid surface in low gravity, Europhys. Lett. 86 (2009) 14002.
[316] G. Düring, C. Josserand, S. Rica, Weak turbulence for a vibrating plate: can one hear a Kolmogorov spectrum? Phys. Rev. Lett. 97 (2006) 025503.
[317] B. Miquel, N. Mordant, Nonstationary wave turbulence in an elastic plate, Phys. Rev. Lett. 107 (2011) 034501.
[318] P. Cobelli, P. Petitjeans, A. Maurel, V. Pagneux, N. Mordant, Space–time resolved wave turbulence in a vibrating plate, Phys. Rev. Lett. 103 (2009) 204301.
[319] C. Connaughton, A.C. Newell, Y. Pomeau, Non–stationary spectra of local wave turbulence, Physica D 184 (2003) 64–85. Complexity and Nonlinearity in Physical Systems—A Special Issue to Honor Alan Newell.
[320] R. Lacaze, P. Lallemand, Y. Pomeau, S. Rica, Dynamical formation of a Bose–Einstein condensate, Physica D 152 (2001) 779.
[321] M. Escobedo, M.A. Valle, Instability of the Rayleigh–Jeans spectrum in weak wave turbulence theory, Phys. Rev. E 79 (2009) 061122.
[322] L. Bergé, Wave collapse in physics: principles and applications to light and plasma waves, Phys. Rep. 303 (1998) 259–370.
[323] A. Picozzi, S. Rica, Condensation of classical optical waves beyond the cubic nonlinear Schrödinger equation, Opt. Commun. 285 (2012) 5440.
[324] E. Assémat, A. Picozzi, H.R. Jauslin, D. Sugny, Instabilities of optical solitons and Hamiltonian singular solutions in a medium of finite extension, Phys. Rev. A 84 (2011) 013809.
[325] P. Kirton, J. Keeling, Nonequilibrium model of photon condensation, Phys. Rev. Lett. 111 (2013) 100404.
[326] D.N. Sob'yanin, Bose–Einstein condensation of light: general theory, Phys. Rev. E 88 (2013) 022132.
[327] B. Fischer, R. Weill, When does single-mode lasing become a condensation phenomenon? Opt. Express 20 (2012) 26704–26713.
[328] T. Dauxois, M. Peyrard, Energy localization in nonlinear lattices, Phys. Rev. Lett. 70 (1993) 3935.
[329] T. Cretegny, T. Dauxois, S. Ruffo, A. Torcini, Localization and equipartition of energy in the $\beta$-FPU chain: Chaotic breathers, Physica D 121 (1998) 109–126.
[330] O. Bang, M. Peyrard, High order breather solutions to a discrete nonlinear Klein–Gordon model, Physica D 81 (1995) 9–22.
[331] O. Bang, M. Peyrard, Generation of high-energy localized vibrational modes in nonlinear Klein–Gordon lattices, Phys. Rev. E 53 (1996) 4143.
[332] B. Rumpf, A.C. Newell, V.E. Zakharov, Turbulent transfer of energy by radiating pulses, Phys. Rev. Lett. 103 (2009) 074502.
[333] J. Fuchs, C. Labaune, H. Bandulet, P. Michel, S. Depierreux, H. Baldis, Reduction of the coherence time of an intense laser pulse propagating through a plasma, Phys. Rev. Lett. 88 (2002) 195003.
[334] J. Garnier, J.P. Fouque, L. Videau, C. Gouédard, A. Migus, Amplification of broadband incoherent light in homogeneously broadened media in the presence of Kerr nonlinearity, J. Opt. Soc. Amer. B Opt. Phys. 14 (1997) 2563–2569.
[335] J. Garnier, L. Videau, C. Gouédard, A. Migus, Propagation and amplification of incoherent pulses in dispersive and nonlinear media, J. Opt. Soc. Amer. B Opt. Phys. 15 (1998) 2773–2781.
[336] A. Dyachenko, G. Falkovich, Condensate turbulence in two dimensions, Phys. Rev. E 54 (1996) 5095–5099.
[337] N.G. Berloff, B.V. Svistunov, Scenario of strongly nonequilibrated Bose–Einstein condensation, Phys. Rev. A 66 (2002) 013603.
[338] S. Nazarenko, M. Onorato, Wave turbulence and vortices in Bose–Einstein condensation, Physica D 219 (2006) 1.
[339] S. Nazarenko, M. Onorato, Freely decaying turbulence and Bose–Einstein condensation in Gross–Pitaevskii model, J. Low Temp. Phys. 146 (2007) 31.
[340] M. Kobayashi, M. Tsubota, Kolmogorov spectrum of superfluid turbulence: Numerical analysis of the Gross–Pitaevskii equation with a small-scale dissipation, Phys. Rev. Lett. 94 (2005) 065302.
[341] D. Proment, S. Nazarenko, M. Onorato, Sustained turbulence in the three-dimensional Gross–Pitaevskii model, Physica D 241 (2012) 304–314.
[342] N. Vladimirova, S. Derevyanko, G. Falkovich, Phase transitions in wave turbulence, Phys. Rev. E 85 (2012) 010101.
[343] P. Miller, N. Vladimirova, G. Falkovich, Oscillations in a turbulence-condensate system, Phys. Rev. E 87 (2013) 065202.
[344] S. Pitois, S. Lagrange, H.R. Jauslin, A. Picozzi, Velocity locking of incoherent nonlinear wave packets, Phys. Rev. Lett. 97 (2006) 033902.
[345] B. Barviau, B. Kibler, A. Picozzi, Wave turbulence description of supercontinuum generation: influence of self-steepening and higher-order dispersion, Phys. Rev. A 79 (2009) 063840.

[346] L. Landau, E. Lifchitz, Statistical Physics, Pergamon Press, New York, 1980, Part 1.
[347] G. Genty, S. Coen, J. Dudley, Fiber supercontinuum sources, J. Opt. Soc. Amer. B Opt. Phys. 24 (2007) 1771.
[348] D. Skryabin, A. Gorbach, Colloquium: looking at a soliton through the prism of optical supercontinuum, Rev. Modern Phys. 82 (2010) 1287.
[349] M. Kolesik, E.M. Wright, J.V. Moloney, Dynamic nonlinear X-waves for femtosecond pulse propagation in water, Phys. Rev. Lett. 92 (2004) 253901.
[350] M. Kolesik, L. Tartara, J.V. Moloney, Effective three-wave-mixing picture and first born approximation for femtosecond supercontinua from microstructured fibers, Phys. Rev. A 82 (2010) 045802.
[351] G. Genty, M. Surakka, J. Turunen, A.T. Friberg, Second-order coherence of supercontinuum light, Opt. Lett. 35 (2010) 3057–3059.
[352] G. Genty, M. Surakka, J. Turunen, A. Friberg, Complete characterization of supercontinuum coherence, J. Opt. Soc. Amer. B Opt. Phys. 28 (2011) 2301.
[353] M. Erkintalo, M. Surakka, J. Turunen, A.T. Friberg, G. Genty, Coherent-mode representation of supercontinuum, Opt. Lett. 37 (2012) 169–171.
[354] M. Korhonen, A.T. Friberg, J. Turunen, G. Genty, Elementary field representation of supercontinuum, J. Opt. Soc. Amer. B Opt. Phys. 30 (2013) 21–26.
[355] A. Mussot, M. Beaugeois, M. Bouazaoui, T. Sylvestre, Tailoring cw supercontinuum generation in microstructured fibers with two-zero dispersion wavelengths, Opt. Express 15 (2007) 11553–11563.
[356] S. Martin-Lopez, L. Abrardi, P. Corredera, M.G. Herraez, A. Mussot, Spectrally-bounded continuous-wave supercontinuum generation in a fiber with two zero-dispersion wavelengths, Opt. Express 16 (2008) 6745–6755.
[357] B.A. Cumberland, J.C. Travers, S.V. Popov, J.R. Taylor, 29 W high power cw supercontinuum source, Opt. Express 16 (2008) 5954–5962.
[358] W. Wadsworth, N. Joly, J. Knight, T. Birks, F. Biancalana, P. Russell, Supercontinuum and four-wave mixing with Q-switched pulses in endlessly single-mode photonic crystal fibres, Opt. Express 12 (2004) 299–309.
[359] B. Barviau, B. Kibler, S. Coen, A. Picozzi, Towards a thermodynamic description of supercontinuum generation, Opt. Lett. 33 (2008) 2833.
[360] B. Kibler, J. Dudley, S. Coen, Supercontinuum generation and nonlinear pulse propagation in photonic crystal fiber: influence of the frequency-dependent effective mode area, Appl. Phys. B 81 (2005) 337.
[361] D.B.S. Soh, J.P. Koplow, S.W. Moore, K.L. Schroder, W.L. Hsu, The effect of dispersion on spectral broadening of incoherent continuous-wave light in optical fibers, Opt. Express 18 (2010) 22393–22405.
[362] M. Taki, A. Mussot, A. Kudlinski, E. Louvergneaux, M. Kolobov, M. Douay, Third-order dispersion for generating optical rogue solitons, Phys. Lett. A 374 (2010) 691.
[363] K. Hammani, B. Kibler, C. Finot, A. Picozzi, Emergence of rogue waves from optical turbulence, Phys. Lett. A 374 (2010) 3585.
[364] B. Kibler, K. Hammani, C. Finot, A. Picozzi, Rogue waves, rational solitons and wave turbulence theory, Phys. Lett. A 375 (2011) 3149.
[365] B. Kibler, C. Michel, B. Barviau, G. Millot, A. Picozzi, Thermodynamic approach of supercontinuum generation, Opt. Fiber Technol. 18 (2012) 257.
[366] D.J. Kaup, A.C. Newell, An exact solution for a derivative nonlinear Schrödinger equation, J. Math. Phys. 19 (1978) 798.
[367] T. Kawata, H. Inoue, Exact solutions of the derivative nonlinear Schrödinger equation under the nonvanishing conditions, J. Phys. Soc. Japan 44 (1978) 1968–1976.
[368] M. Wadati, K. Konno, Y.-H. Ichikawa, A generalization of inverse scattering method, J. Phys. Soc. Japan 46 (1979) 1965–1966.
[369] Y.H. Ichikawa, K. Konno, M. Wadati, H. Sanuki, Spiky soliton in circular polarized Alfvén wave, J. Phys. Soc. Japan 48 (1980) 279–286.
[370] A.C. Newell, J.V. Moloney, Nonlinear Optics, Addison-Wesley Publ. Comp., 1992.
[371] C. Sun, S. Jia, C. Barsi, S. Rica, A. Picozzi, J.W. Fleischer, Observation of the kinetic condensation of classical waves, Nat. Phys. 8 (2012) 470–474.
[372] J.W. Goodman, Introduction to Fourier Optics, third ed., Roberts & Co, 2005.
[373] P. Suret, S. Randoux, Far field measurement in the focal plane of a lens : a cautionary note, arXiv:1307.5034, 2013.
[374] L. Deike, M. Berhanu, E. Falcon, Decay of capillary wave turbulence, Phys. Rev. E 85 (2012) 066311.
[375] B. Gershgorin, Y.V. Lvov, D. Cai, Renormalized waves and discrete breathers in $\beta$-Fermi–Pasta–Ulam chains, Phys. Rev. Lett. 95 (2005) 264302.
[376] Y. Silberberg, Y. Lahini, Y. Bromberg, E. Small, R. Morandotti, Universal correlations in a nonlinear periodic 1d system, Phys. Rev. Lett. 102 (2009) 233904.
[377] E. Small, R. Pugatch, Y. Silberberg, Berezinskii–Kosterlitz–Thouless crossover in a photonic lattice, Phys. Rev. A 83 (2011) 013806.
[378] J.C. Travers, A.B. Rulkov, B.A. Cumberland, S.V. Popov, J.R. Taylor, Visible supercontinuum generation in photonic crystal fibers with a 400 W continuous wave fiber laser, Opt. Express 16 (2008) 14435–14447.
[379] A. Mussot, A. Kudlinski, M. Kolobov, E. Louvergneaux, M. Douay, M. Taki, Observation of extreme temporal events in cw-pumped supercontinuum, Opt. Express 17 (2009) 17010–17015.
[380] V. Zakharov, E. Schulman, Degenerative dispersion laws, motion invariants and kinetic equations, Physica 4D (1980) 192.
[381] V. Zakharov, E. Schulman, To the integrability of the system of two coupled nonlinear Schrödinger equations, Physica 4D (1982) 270.
[382] V. Zakharov, E. Schulman, On additional motion invariants of classical Hamiltonian wave systems, Physica 29D (1988) 283.
[383] A. Balk, E. Ferapontov, in: V. Zakharov (Ed.), Nonlinear Waves and Weak Turbulence, Amer. Math. Soc. Transl., 1998.
[384] C. Michel, J. Garnier, P. Suret, S. Randoux, A. Picozzi, Kinetic description of random optical waves and anomalous thermalization of a nearly integrable wave system, Lett. Math. Phys. 96 (2011) 415–447.
[385] L. Biven, S. Nazarenko, A. Newell, Breakdown of wave turbulence and the onset of intermittency, Phys. Lett. A 280 (2001) 28.
[386] B. Barviau, S. Randoux, P. Suret, Spectral broadening of a multimode continuous-wave optical field propagating in the normal dispersion regime of a fiber, Opt. Lett. 31 (2006) 1696–1698.
[387] M. Ablowitz, H. Segur, Solitons and the inverse scattering transform, in: SIAM, Society for Industrial and Applied Mathematics, 1981.
[388] G. El, A. Kamchatnov, Kinetic equation for a dense soliton gas, Phys. Rev. Lett. 95 (2005) 204101.
[389] M. Tabor, Chaos and Integrability in Nonlinear Dynamics, Wiley, 1989.
[390] V. Zakharov, Turbulence in integrable systems, Stud. Appl. Math. 122 (2009) 219.
[391] P. Janssen, Nonlinear four-wave interactions and freak waves, J. Phys. Oceanogr. 33 (2003) 864.
[392] S.Y. Annenkov, V.I. Shrira, Role of non-resonant interactions in the evolution of nonlinear random water wave fields, J. Fluid Mech. 561 (2006) 181–207.
[393] S.K. Turitsyn, S.A. Derevyanko, Soliton-based discriminator of noncoherent optical pulses, Phys. Rev. A 78 (2008) 063819.
[394] S.A. Derevyanko, J.E. Prilepsky, Random input problem for the nonlinear Schrödinger equation, Phys. Rev. E 78 (2008) 046610.
[395] S.A. Derevyanko, Appearance of bound states in random potentials with applications to soliton theory, Phys. Rev. E 84 (2011) 016601.
[396] Y. Bromberg, Y. Lahini, E. Small, Y. Silberberg, Hanbury Brown and Twiss interferometry with interacting photons, Nat. Photon. 4 (2010) 721.
[397] S. Derevyanko, E. Small, Nonlinear propagation of an optical speckle field, Phys. Rev. A 85 (2012) 053816.
[398] T. Arecchi, S. Boccalettic, P. Ramazza, Pattern formation and competition in nonlinear optics, Phys. Rep. 318 (1999) 1.
[399] H. Haken, Synergetics: An Introduction, Springer-Verlag, Berlin, 1977.
[400] J. Kasprzak, M. Richard, S. Kundermann, A. Baas, P. Jeambrun, J. Keeling, M. FM Marchetti, et al., Bose–Einstein condensation of exciton polaritons, Nature 443 (2006) 409–414.
[401] R. Balili, V. Hartwell, D. Snoke, L. Pfeiffer, K. West, Bose–Einstein condensation of microcavity polaritons in a trap, Science 316 (2007) 1007–1010.
[402] H. Deng, H. Haug, Y. Yamamoto, Exciton-polariton Bose–Einstein condensation, Rev. Modern Phys. 82 (2010) 1489–1537.
[403] G. Nardin, G. Grosso, Y. Léger, B. Pietka, F. Morier-Genoud, B. Deveaud-Plédran, Hydrodynamic nucleation of quantized vortex pairs in a polariton quantum fluid, Nature Phys. 7 (2011) 635.
[404] J. Scheuer, M. Orenstein, Optical vortices crystals: spontaneous generation in nonlinear semiconductor microcavities, Science 285 (1999) 230–233.
[405] J. Klaers, F. Vewinger, M. Weitz, Thermalization of a two-dimensional photonic gas in a white wall photon box, Nat. Phys. 6 (2010) 512–515.
[406] J. Klaers, J. Schmitt, T. Damm, F. Vewinger, M. Weitz, Statistical physics of Bose–Einstein-condensed light in a dye microcavity, Phys. Rev. Lett. 108 (2012) 160403.
[407] R. Weill, B. Levit, A. Bekker, O. Gat, B. Fischer, Laser light condensate: experimental demonstration of light-mode condensation in actively mode locked laser, Opt. Express 18 (2010) 16520–16525.
[408] A. Gordon, B. Fischer, Phase transition theory of many-mode ordering and pulse formation in lasers, Phys. Rev. Lett. 89 (2002) 103901.

[409] R. Weill, A. Rosen, A. Gordon, O. Gat, B. Fischer, Critical behavior of light in mode-locked lasers, Phys. Rev. Lett. 95 (2005) 013903.
[410] S.A. Babin, D.V. Churkin, A.E. Ismagulov, S.I. Kablukov, E.V. Podivilov, Four-wave-mixing-induced turbulent spectral broadening in a long Raman fiber laser, J. Opt. Soc. Amer. B Opt. Phys. 24 (2007) 1729.
[411] D.J. Dougherty, F.X. Kärtner, H.A. Haus, E. Ippen, Measurement of the Raman gain spectreum of optical fibers, Opt. Lett. 20 (1995) 31.
[412] J.W. Nicholson, M.F. Yan, P. Wisk, J. Fleming, F. DiMarcello, E. Monberg, T. Taunay, C. Headley, D.J. DiGiovanni, Raman fiber laser with 81 W output power at 1480 nm, Opt. Lett. 35 (2010) 3069–3071.
[413] V.I. Karpov, E.M. Dianov, V.M. Paramonov, O.I. Medvedkov, M.M. Bubnov, S.L. Semyonov, S.A. Vasiliev, V.N. Protopopov, O.N. Egorova, V.F. Hopin, A.N. Guryanov, M.P. Bachynski, W.R.L. Clements, Laser-diode-pumped phosphosilicate-fiber Raman laser with an output power of 1 W at 1.48 μm, Opt. Lett. 24 (1999) 887–889.
[414] P.S. Westbrook, K.S. Abedin, J.W. Nicholson, T. Kremp, J. Porque, Raman fiber distributed feedback lasers, Opt. Lett. 36 (2011) 2895–2897.
[415] J.D. Ania-Castañón, V. Karalekas, P. Harper, S.K. Turitsyn, Simultaneous spatial and spectral transparency in ultralong fiber lasers, Phys. Rev. Lett. 101 (2008) 123903.
[416] S.K. Turitsyn, J.D. Ania-Castañón, S.A. Babin, V. Karalekas, P. Harper, D. Churkin, S.I. Kablukov, A.E. El-Taher, E.V. Podivilov, V.K. Mezentsev, 270-km ultralong Raman fiber laser, Phys. Rev. Lett. 103 (2009) 133901.
[417] S.A. Babin, D.V. Churkin, E.V. Podivilov, Intensity interactions in cascades of a two-stage Raman fiber laser, Opt. Commun. 226 (2003) 329.
[418] P. Suret, S. Randoux, Influence of spectral broadening on steady characteristics of Raman fiber lasers: from experiments to questions about validity of usual models, Opt. Commun. 237 (2004) 201.
[419] J.C. Bouteiller, Spectral modeling of Raman fiber laser, IEEE Photon. Technol. Lett. 15 (2003) 1698.
[420] J. Hagen, R. Engelbrecht, O. Welzel, A. Siekiera, B. Schmauss, Numerical modeling of intracavity spectral broadening of Raman fiber lasers, IEEE Photon. Technol. Lett. 19 (2007) 1759.
[421] N. Dalloz, S. Randoux, P. Suret, Influence of dispersion of fiber Bragg grating mirrors on formation of optical power spectrum in Raman fiber lasers, Opt. Lett. 35 (2010) 2505–2507.
[422] S.A. Babin, V. Karalekas, P. Harper, E.V. Podivilov, V.K. Mezentsev, J.D. Ania-Castanon, S.K. Turitsyn, Experimental demonstration of mode structure in ultralong Raman fiber lasers, Opt. Lett. 32 (2007) 1135–1137.
[423] S. Randoux, N. Dalloz, P. Suret, Intracavity changes in the field statistics of Raman fiber lasers, Opt. Lett. 36 (2011) 790–792.
[424] E.G. Turitsyna, S.K. Turitsyn, V.K. Mezentsev, Numerical investigation of the impact of reflectors on spectral performance of Raman fibre laser, Opt. Express 18 (2010) 4469.
[425] D.V. Churkin, S.V. Smirnov, E.V. Podivilov, Statistical properties of partially coherent cw fiber lasers, Opt. Lett. 35 (2010) 3288–3290.
[426] D.V. Churkin, O.A. Gorbunov, S.V. Smirnov, Extreme value statistics in Raman fiber lasers, Opt. Lett. 36 (2011) 3617–3619.
[427] S. Randoux, P. Suret, Experimental evidence of extreme value statistics in Raman fiber lasers, Opt. Lett. 37 (2012) 500–502.
[428] S. Coen, M. Haelterman, Modulational instability induced by cavity boundary conditions in a normally dispersive optical fiber, Phys. Rev. Lett. 79 (1997) 4139–4142.
[429] L.A. Lugiato, R. Lefever, Spatial dissipative structures in passive optical systems, Phys. Rev. Lett. 58 (1987) 2209–2211.
[430] M. Haelterman, S. Trillo, S. Wabnitz, Additive-modulation-instability ring laser in the normal dispersion regime of a fiber, Opt. Lett. 17 (1992) 745–747.
[431] A. Picozzi, S. Rica, Coherence absorption and condensation induced by the thermalization of incoherent fields, Europhys. Lett. 84 (2008) 34004.
[432] A. Majda, D. McLaughlin, E. Tabak, A one-dimensional model for dispersive wave turbulence, J. Nonlinear Sci. 7 (1997) 9–44.
[433] D. Cai, D.W. McLaughlin, Chaotic and turbulent behavior of unstable one-dimensional nonlinear dispersive waves, J. Math. Phys. 41 (2000) 4125–4153.
[434] D. Cai, A.J. Majda, D. W. McLaughlin, E.G. Tabak, Dispersive wave turbulence in one dimension, Physica D 152 (2001) 551–572.
[435] C. Barenghi, R. Donnelly, W.E. Vinen, Quantized Vortex Dynamics and Superfluid Turbulence, Springer-Verlag, Berlin and Heidelberg, 2010.
[436] Z. Hadzibabic, P. Krüger, M. Cheneau, B. Battelier, J. Dalibard, Berezinskii–Kosterlitz–Thouless crossover in a trapped atomic gas, Nature 441 (2006) 013806.
[437] Z. Hadzibabic, J. Dalibard, Two-dimensional Bose fluids: an atomic physics perspective, Riv. Nuovo Cimento 34 (2011) 389.
[438] T.P. Simula, P.B. Blakie, Thermal activation of vortex-antivortex pairs in quasi-two-dimensional Bose–Einstein condensates, Phys. Rev. Lett. 96 (2006) 020404.
[439] C.J. Foster, P.B. Blakie, M.J. Davis, Vortex pairing in two-dimensional Bose gases, Phys. Rev. A 81 (2010) 023623.
[440] A. Picozzi, C. Montes, M. Haelterman, Coherence properties of the parametric three-wave interaction driven from an incoherent pump, Phys. Rev. E 66 (2002) 056605.
[441] A. Picozzi, P. Aschieri, Influence of dispersion on the resonant interaction between three incoherent waves, Phys. Rev. E 72 (2005) 046606.
[442] C. Montes, A. Picozzi, K. Gallo, Ultra-coherent signal output from an incoherent cw-pumped singly resonant optical parametric oscillator, Opt. Commun. 237 (2004) 437–449.
[443] S. Wabnitz, A. Picozzi, A. Tonello, D. Modotto, G. Millot, Control of signal coherence in parametric frequency mixing with incoherent pumps: narrowband mid-infrared light generation by downconversion of broadband amplified spontaneous emission source at 1550 nm, J. Opt. Soc. Amer. B Opt. Phys. 29 (2012) 3128–3135.
[444] C. Montes, W. Grundkötter, H. Suche, W. Sohler, Coherent signal from incoherently cw-pumped singly resonant $TiLiNbO_3$ integrated optical parametric oscillators, J. Opt. Soc. Amer. B Opt. Phys. 24 (2007) 2796–2806.
[445] C. Montes, A. Mikhailov, A. Picozzi, F. Ginovart, Dissipative three-wave structures in stimulated backscattering. I. A subluminous solitary attractor, Phys. Rev. E 55 (1997) 1086–1091.
[446] C. Montes, A. Picozzi, D. Bahloul, Dissipative three-wave structures in stimulated backscattering. II. Superluminous and subluminous solitons, Phys. Rev. E 55 (1997) 1092–1105.
[447] A. Picozzi, M. Haelterman, Spontaneous formation of symbiotic solitary waves in a backward quasi-phase-matched parametric oscillator, Opt. Lett. 23 (1998) 1808–1810.
[448] A. Picozzi, M. Haelterman, Condensation in Hamiltonian parametric wave interaction, Phys. Rev. Lett. 92 (2004) 103901.
[449] A. Piskarskas, V. Smilgevicius, A. Stabinis, Optical parametric oscillation excited by an incoherent conical beam, Opt. Commun. 143 (1997) 72.
[450] A. Marcinkevicius, A. Piskarskas, V. Smilgevicius, A. Stabinis, Parametric superfluorescence excited in a nonlinear crystal by two uncorrelated pump beams, Opt. Commun. 158 (1998) 101.
[451] A. Dubietis, R. Danielius, G. Tamošauskas, A. Piskarskas, Combining effect in a multiple-beam-pumped optical parametric amplifier, J. Opt. Soc. Amer. B Opt. Phys. 15 (1998) 1135–1139.
[452] A. Piskarskas, V. Smilgevičius, A. Stabinis, V. Vaičaitis, Spatially cumulative phenomena and output patterns in optical parametric oscillators and generators pumped by conical beams, J. Opt. Soc. Amer. B Opt. Phys. 16 (1999) 1566–1578.
[453] G. Tamosauskas, A. Dubietis, G. Valiulis, A. Piskarkas, Optical parametric amplifier pumped by two mutually incoherent laser beams, Appl. Phys. B 91 (2008) 305.
[454] Y. Yan, C. Yang, Coherent light wave generated from incoherent pump light in nonlinear Kerr medium, J. Opt. Soc. Amer. B Opt. Phys. 26 (2009) 2059–2063.
[455] A. Piskarskas, V. Pyragaite, A. Stabinis, Generation of coherent waves by frequency up-conversion and down-conversion of incoherent light, Phys. Rev. A 82 (2010) 053817.
[456] A. Stabinis, V. Pyragaite, G. Tamošauskas, A. Piskarskas, Spectrum of second-harmonic radiation generated from incoherent light, Phys. Rev. A 84 (2011) 043813.
[457] V. Pyragaite, A. Stabinis, A. Piskarskas, Frequency spectrum of second-harmonic radiation excited by a Gaussian Schell-model beam, Phys. Rev. A 86 (2012) 033812.

[458] G. Strömqvist, V. Pasiskevicius, C. Canalias, P. Aschieri, A. Picozzi, C. Montes, Temporal coherence in mirrorless optical parametric oscillators, J. Opt. Soc. Amer. B Opt. Phys. 29 (2012) 1194–1202.
[459] V. Pyragaite, A. Stabinis, A. Piskarskas, V. Smilgevičius, Parametric amplification in the field of incoherent light, Phys. Rev. A 87 (2013) 063809.
[460] S.A. Ponomarenko, G.P. Agrawal, Asymmetric incoherent vector solitons, Phys. Rev. E 69 (2004) 036604.
[461] A. Picozzi, Spontaneous polarization induced by natural thermalization of incoherent light, Opt. Express 16 (2008) 17171.
[462] H. Salman, N. Berloff, Condensation of classical nonlinear waves in a two-component system, Physica D 238 (2009) 1482.
[463] T. Hansson, E. Wallin, G. Brodin, M. Marklund, Scalar Wigner theory for polarized light in nonlinear Kerr media, J. Opt. Soc. Amer. B Opt. Phys. 30 (2013) 1765–1769.
[464] J. Heebner, R. Bennink, R. Boyd, R. Fisher, Conversion of unpolarized light to polarized light with greater than 50% efficiency by photorefractive two-beam coupling, Opt. Lett. 25 (2000) 257.
[465] S. Pitois, A. Picozzi, G. Millot, H.R. Jauslin, M. Haelterman, Polarization and modal attactors in conservative counterpropagating four-wave interaction, Europhys. Lett. 70 (2005) 88.
[466] B. Crosignani, B. Daino, P. Di Porto, Depolarization of light due to the optical Kerr effect in low-birefringence single-mode fibers, J. Opt. Soc. Amer. B Opt. Phys. 3 (1986) 1120.
[467] V.E. Chernov, B.A. Zon, Depolarization of laser radiation in a nonlinear medium, J. Opt. Soc. Amer. B Opt. Phys. 10 (1993) 210–212.
[468] Y.P. Svirko, N.I. Zheludev, Propagation of partially polarized light, Phys. Rev. A 50 (1994) 709.
[469] Y.P. Svirko, N.I. Zheludev, Polarization of Light in Nonlinear Optics, Wiley & Sons, 2000.
[470] A. Picozzi, Entropy and degree of polarization for nonlinear optical waves, Opt. Lett. 29 (2004) 1653.
[471] H. Prakash, D. Singh, Change in coherence properties and degree of polarization of light propagating in a lossless isotropic nonlinear Kerr medium, J. Phys. B: At. Mol. Opt. Phys. 41 (2008) 045401.
[472] J. Sorrentini, M. Zerrad, G. Soriano, C. Amra, Enpolarization of light by scattering media, Opt. Express 19 (2011) 21313–21320.
[473] M. Zerrad, G. Soriano, A. Ghabbach, C. Amra, Light enpolarization by disordered media under partial polarized illumination: the role of cross-scattering coefficients, Opt. Express 21 (2013) 2787–2794.
[474] D. Sugny, A. Picozzi, S. Lagrange, H. Jauslin, Role of singular tori in the dynamics of spatiotemporal nonlinear wave systems, Phys. Rev. Lett. 103 (2009) 034102.
[475] S. Lagrange, D. Sugny, A. Picozzi, H.R. Jauslin, Singular tori as attractors of four-wave-interaction systems, Phys. Rev. E 81 (2010) 016202.
[476] E. Assémat, S. Lagrange, A. Picozzi, H.R. Jauslin, D. Sugny, Complete nonlinear polarization control in an optical fiber system, Opt. Lett. 35 (2010) 2025–2027.
[477] V.V. Kozlov, S. Wabnitz, Theoretical study of polarization attraction in high-birefringence and spun fibers, Opt. Lett. 35 (2010) 3949–3951.
[478] V.V. Kozlov, J. Nuno, S. Wabnitz, Theory of lossless polarization attraction in telecommunication fibers, J. Opt. Soc. Amer. B Opt. Phys. 28 (2011) 100–108.
[479] E. Assémat, D. Dargent, A. Picozzi, H.-R. Jauslin, D. Sugny, Polarization control in spun and telecommunication optical fibers, Opt. Lett. 36 (2011) 4038–4040.
[480] E. Assémat, C. Michel, A. Picozzi, H.R. Jauslin, D. Sugny, Manifestation of Hamiltonian monodromy in nonlinear wave systems, Phys. Rev. Lett. 106 (2011) 014101.
[481] M. Guasoni, V.V. Kozlov, S. Wabnitz, Theory of polarization attraction in parametric amplifiers based on telecommunication fibers, J. Opt. Soc. Amer. B Opt. Phys. 29 (2012) 2710–2720.
[482] M. Guasoni, V.V. Kozlov, S. Wabnitz, Theory of modal attraction in bimodal birefringent optical fibers, Opt. Lett. 38 (2013) 2029–2031.
[483] S. Pitois, J. Fatome, G. Millot, Polarization attraction using counter-propagating waves in optical fiber at telecommunication wavelengths, Opt. Express 16 (2008) 6646–6651.
[484] J. Fatome, S. Pitois, P. Morin, G. Millot, Observation of light-by-light polarization control and stabilization in optical fibre for telecommunication applications, Opt. Express 18 (2010) 15311–15317.
[485] V.V. Kozlov, J. Fatome, P. Morin, S. Pitois, G. Millot, S. Wabnitz, Nonlinear repolarization dynamics in optical fibers: transient polarization attraction, J. Opt. Soc. Amer. B Opt. Phys. 28 (2011) 1782–1791.
[486] B. Stiller, P. Morin, D. Nguyen, J. Fatome, S. Pitois, E. Lantz, H. Maillotte, C. Menyuk, T. Sylvestre, Demonstration of polarization pulling using a fiber-optic parametric amplifier, Optics express 20 (2012) 27248–27253.
[487] P.-Y. Bony, M. Guasoni, E. Assémat, S. Pitois, D. Sugny, A. Picozzi, H.R. Jauslin, J. Fatome, Optical flip-flop memory and data packet switching operation based on polarization bistability in a telecommunication optical fiber, J. Opt. Soc. Amer. B Opt. Phys. 30 (2013) 2318–2325.
[488] J. Fatome, S. Pitois, P. Morin, D. Sugny, E. Assemat, A. Picozzi, H. Jauslin, G. Millot, V. Kozlov, S. Wabnitz, A universal optical all-fiber omnipolarizer, Sci. Rep. 2 (2012) 938.
[489] V. Kozlov, S. Wabnitz, Instability of optical solitons in the boundary value problem for a medium of finite extension, Lett. Math. Phys. 96 (2011) 405.
[490] E. Assémat, A. Picozzi, H.-R. Jauslin, D. Sugny, Hamiltonian tools for the analysis of optical polarization control, J. Opt. Soc. Amer. B Opt. Phys. 29 (2012) 559–571.
[491] M. Guasoni, E. Assémat, P. Morin, A. Picozzi, J. Fatome, S. Pitois, H.R. Jauslin, G. Millot, D. Sugny, Line of polarization attraction in highly birefringent optical fibers, J. Opt. Soc. Amer. B Opt. Phys. 31 (2014) 572–580.
[492] B.A. Van Tiggelen, Localization of waves, in: Diffuse Waves in Complex Media, Springer, 1999, pp. 1–60.
[493] F. Evers, A.D. Mirlin, Anderson transitions, Rev. Modern Phys. 80 (2008) 1355–1417.
[494] A. Lagendijk, B. van Tiggelen, D.S. Wiersma, Fifty years of Anderson localization, Phys. Today 62 (2009) 24–29.
[495] F.M. Izrailev, A.A. Krokhin, N. Makarov, Anomalous localization in low-dimensional systems with correlated disorder, Phys. Rep. 512 (2012) 125–254.
[496] M. Segev, Y. Silberberg, D.N. Christodoulides, Anderson localization of light, Nat. Photon. 7 (2013) 197–204.
[497] G. Roati, C. D'Errico, L. Fallani, M. Fattori, C. Fort, M. Zaccanti, G. Modugno, M. Modugno, M. Inguscio, Anderson localization of a non-interacting Bose–Einstein condensate, Nature 453 (2008) 895.
[498] J. Billy, V. Josse, Z. Zuo, A. Bernard, B. Hambrecht, P. Lugan, D. Clement, L. Sanchez-Palencia, P. Bouyer, A. Aspect, Direct observation of Anderson localization of matter waves in a controlled disorder, Nature 453 (2008) 891.
[499] L. Sanchez-Palencia, M. Lewenstein, Disordered quantum gases under control, Nat. Phys. 6 (2010) 87.
[500] F. Manni, K.G. Lagoudakis, B. Pietka, L. Fontanesi, M. Wouters, V. Savona, R. André, B. Deveaud-Plédran, Polariton condensation in a one-dimensional disordered potential, Phys. Rev. Lett. 106 (2011) 176401.
[501] N. Akhmediev, A. Ankiewicz, M. Taki, Waves that appear from nowhere and disappear without a trace, Phys. Lett. A 373 (2009) 675–678.
[502] A. Osborne, Nonlinear Ocean Waves & the Inverse Scattering Transform, Academic Presss, San Diego, 2010.
[503] M. Onorato, A.R. Osborne, M. Serio, S. Bertone, Freak waves in random oceanic sea states, Phys. Rev. Lett. 86 (2001) 5831–5834.
[504] A. Dyachenko, V.E. Zakharov, On the formation of freak waves on the surface of deep water, JETP Lett. 88 (2008) 307–311.
[505] A. Chabchoub, N. Hoffmann, M. Onorato, G. Genty, J.M. Dudley, N. Akhmediev, Hydrodynamic supercontinuum, Phys. Rev. Lett. 111 (2013) 054104.
[506] A. Chabchoub, N. Hoffmann, M. Onorato, A. Slunyaev, A. Sergeeva, E. Pelinovsky, N. Akhmediev, Observation of a hierarchy of up to fifth-order rogue waves in a water tank, Phys. Rev. E 86 (2012) 056601.
[507] A. Montina, U. Bortolozzo, S. Residori, F. Arecchi, Non-Gaussian statistics and extreme waves in a nonlinear optical cavity, Phys. Rev. Lett. 103 (2009) 173901.
[508] J. Kasparian, P. Béjot, J.-P. Wolf, J.M. Dudley, Optical rogue wave statistics in laser filamentation, Opt. Express 17 (2009) 12070–12075.
[509] C. Bonatto, M. Feyereisen, S. Barland, M. Giudici, C. Masoller, J.R.R. Leite, J.R. Tredicce, Deterministic optical rogue waves, Phys. Rev. Lett. 107 (2011) 053901.
[510] K. Hammani, A. Picozzi, C. Finot, Extreme statistics in Raman fiber amplifiers: from analytical description to experiments, Opt. Commun. 284 (2011) 2594–2603.

[511] C. Lecaplain, P. Grelu, J.M. Soto-Crespo, N. Akhmediev, Dissipative rogue waves generated by chaotic pulse bunching in a mode-locked laser, Phys. Rev. Lett. 108 (2012) 233901.
[512] S. Birkholz, E.T.J. Nibbering, C. Brée, S. Skupin, A. Demircan, G. Genty, G. Steinmeyer, Spatiotemporal rogue events in optical multiple filamentation, Phys. Rev. Lett. 111 (2013) 243903.
[513] M. Shats, H. Punzmann, H. Xia, Capillary rogue waves, Phys. Rev. Lett. 104 (2010) 104503.
[514] A.N. Ganshin, V.B. Efimov, G.V. Kolmakov, L.P. Mezhov-Deglin, P.V.E. McClintock, Observation of an inverse energy cascade in developed acoustic turbulence in superfluid helium, Phys. Rev. Lett. 101 (2008) 065303.
[515] L. Stenflo, M. Marklund, Rogue waves in the atmosphere, J. Plasma Phys. 76 (2010) 293.
[516] R. Höhmann, U. Kuhl, H.-J. Stöckmann, L. Kaplan, E. Heller, Freak waves in the linear regime: a microwave study, Phys. Rev. Lett. 104 (2010) 093901.
[517] E. Kuznetsov, Solitons in a parametrically unstable plasma, in: Akademiia Nauk SSSR Doklady, vol. 236, 1977, pp. 575–577.
[518] N. Akhmediev, V.M. Eleonskii, N.E. Kulagin, Exact first-order solutions of the nonlinear Schrödinger equation, Theor. Math. Phys. 72 (1987) 809–818.
[519] N. Akhmediev, J. Soto-Crespo, A. Ankiewicz, Extreme waves that appear from nowhere: on the nature of rogue waves, Phys. Lett. A 373 (2009) 2137–2145.
[520] K. Henderson, D. Peregrine, J. Dold, Unsteady water wave modulations: fully nonlinear solutions and comparison with the nonlinear Schrödinger equation, Wave motion 29 (1999) 341–361.
[521] N. Akhmediev, A. Ankiewicz, J.M. Soto-Crespo, Rogue waves and rational solutions of the nonlinear Schrödinger equation, Phys. Rev. E 80 (2009) 026601.
[522] D. Peregrine, Water waves, nonlinear Schrödinger equations and their solutions, J. Aust. Math. Soc. B 25 (1983) 16–43.
[523] B. Kibler, J. Fatome, C. Finot, G. Millot, F. Dias, G. Genty, N. Akhmediev, J.M. Dudley, The Peregrine soliton in nonlinear fibre optics, Nat. Phys. 6 (2010) 790–795.
[524] K. Hammani, B. Kibler, C. Finot, P. Morin, J. Fatome, J.M. Dudley, G. Millot, Peregrine soliton generation and breakup in standard telecommunications fiber, Opt. Lett. 36 (2011) 112–114.
[525] B. Kibler, J. Fatome, C. Finot, G. Millot, G. Genty, B. Wetzel, N. Akhmediev, F. Dias, J.M. Dudley, Observation of Kuznetsov–Ma soliton dynamics in optical fibre, Sci. Rep. 2 (2012) 463.
[526] B. Frisquet, B. Kibler, G. Millot, Collision of Akhmediev breathers in nonlinear fiber optics, Phys. Rev. X 3 (2013) 041032.
[527] M. Onorato, A. Osborne, M. Serio, L. Cavaleri, C. Brandini, C. Stansberg, Observation of strongly non-Gaussian statistics for random sea surface gravity waves in wave flume experiments, Phys. Rev. E 70 (2004) 067302.
[528] M. Onorato, A. Osborne, M. Serio, L. Cavaleri, Modulational instability and non-Gaussian statistics in experimental random water-wave trains, Phys. Fluids 17 (2005) 078101.
[529] M. Onorato, A. Osborne, M. Serio, L. Cavaleri, C. Brandini, C. Stansberg, Extreme waves, modulational instability and second order theory: wave flume experiments on irregular waves, Eur. J. Mech. B Fluids 25 (2006) 586–601.
[530] A. Ankiewicz, J. Soto-Crespo, N. Akhmediev, Rogue waves and rational solutions of the Hirota equation, Phys. Rev. E 81 (2010) 046602.
[531] C. Viotti, D. Dutykh, J.M. Dudley, F. Dias, Emergence of coherent wave groups in deep-water random sea, Phys. Rev. E 87 (2013) 063001.